Temperature dependence of magnetostriction of Gd/Tb alloys

Chaudhri, Muhammad Anwar

TEMPERATURE DEPENDENCE OF MAGNETOSTRICTION OF Gd/Tb ALLOYS

MUHAMMAD ANWAR CHAUDHRI

M.Sc. (Punjab); M.Phil (Islamabad)

Thesis submitted to the University of Durham, U.K. in candidature for the Degree of Doctor of Philosophy.

December 1983.

TO MY FATHER

ABSTRACT

The aim of the present study was to understand the mechanism responsible for the exceptionally high magnetostriction exhibited by the heavy rare earths. Magnetostriction constants $\lambda^{\gamma,2}$, $\lambda_2{}^{\alpha,2}$ and $\lambda_1{}^{\alpha,2}$ of order $\ell = 2$ for gadolinium, terbium and their alloys were measured using a resistive strain gauge technique. The temperature dependence of these magnetostriction constants was observed from liquid helium temperature to close to their Curie temperatures for Gd, 90%Gd-10%Tb, 70%Gd-30%Tb, 50%Gd-50%Tb, 10%Gd-90%Tb and Tb. The adequacy of theoretical predictions of the temperature dependence was tested with the results of these measurements. The observed temperature dependence of $\lambda^{\gamma,2}$ over the entire range of temperature and alloy compositions except for pure Gd, was found to follow closely the variation predicted by a theory termed as a single-ion model. The same conclusion resulted from the measurements of $\lambda_2{}^{\alpha,2}$ and $\lambda_1{}^{\alpha,2}$ but with less reliability. The extrapolated values of the constants at OK for Gd and its experimental temperature dependence are consistent with results of other investigations on gadolinium. The magnetostriction constants of the alloys varied linearly with the terbium concentration, again showing that the single-ion magnetocrystalline interaction is principally responsible for the magnetostrictive effects due to terbium ions.

Some suggestions are included for improvements to experimental and analytical techniques and for the extension to other alloy systems.

ACKNOWLEDGEMENTS

Acknowledgement is made to the Government of Pakistan and the University of Agriculture, Faisalabad, whose financial support made this work possible.

I would also like to acknowledge gratefully the help and assistance of the following people:

I would like to thank Professor B.H. Bransden and Professor A.W. Wolfendale for making available to me the facilities of the Physics Department at the University of Durham.

My thanks are due to Dr. W.D. Corner for his excellent supervision, patience and continual inspiration throughout the research work and also making available magnetization and anisotropy data on Gd/Tb alloys.

I would like to thank Dr. B.K. Tanner for his help in the automation of the experiment and to Dr. S.R. Hoon who cordially extended his help all the time for all types of problems.

My thanks are due to Dr. M. Evans of the Botany Department for allowing me the use of the oven for heat treatment of the strain gauges.

I would like to thank Mr. K.G. Moulson, Mr. D. Jobling and his staff, Mr. T. Jackson and his staff, and Mr. T.W. Hogg and his staff for their help in the construction and modification of the equipment. The services of the late Mr. W. Leslie are gratefully acknowledged. My thanks are also due to Mr. S. Thompson, Mr. S. Jobson and Mr. P. Foley for their full cooperation.

I wish to thank Mr. J. Scott for his help in running the superconducting magnet, but the overnight running of the experiment for months was not possible without the help of Mr. S. Hawkes who stayed and assisted during the experiment. My special thanks are due to him.

The use of some of the equipment of British Gas is duly acknowledged. Thanks are due also to the SERC and the University of Durham, for funding for the purchase of liquid helium.

I would like to thank Dr. D.M. Paige and all the group members for their valuable help.

I wish to express my thanks to Mr. E.R. Wood who took keen interest in the improvement of the University accommodation for the overseas students, for his general cooperation towards family problems.

My thanks are due to my wife Rehana and my sons Nadeem, Waseem and Faheem for their cooperation and their tolerance of my absence.

Finally, I thank Miss K.L. Gittins for her help in drawing some of the diagrams, and Ms. M.A. Chipchase for typing this thesis.

CONTENTS

Page No.

Page No.

CHAPTER 1

MAGNETISM , SOME BASIC CONCEPTS

1.1 Introduction

Magnetism is a vast field of study and of interest to many scientists and technologists. Many particles, even some electrically neutral ones such as neutrons, possess elementary magnetic moments. Magnetic phenomena are encountered everywhere from the subatomic to the cosmological scales. The origin of magnetic forces, despite the fact that these were known from ancient times, remained obscure until quantum mechanics was developed at the turn of this century. Since then, continuous research and development has increased our understanding of magnetic properties and has led to a deeper insight into the fundamental structure of solids. This has enabled magnetic materials to find a wide range of applications. Indeed the scientific and technological applications of magnetism are now so extensive and diverse that the physics of magnetic phenomena has become one of the most important and rapidly developing branches of natural science.

The magnetic interaction between spatially separated materials is carried by the magnetic field. It is now firmly established that the main source of the magnetic field is due to the motion of charged particles, e.g. the spin of electrons.

A quantitative measure of the magnetism of a particle is its magnetic moment $\underline{\mu}$ which can be defined in terms of a current I flowing in an elementary closed loop as

$$\underline{\mu} = Ia\hat{n} \qquad (Am^2) \qquad 1.1$$

where a is the area of the loop and $\hat{n}$ is a unit vector perpendicular to the plane of the loop and whose direction is determined by the right hand rule.

The magnetic field $\underline{H}$ can also be defined in a similar way by the field inside a long solenoid carrying a current I as

$$\underline{H} = NI\hat{n} \qquad (Am^{-1}) \qquad 1.2$$

where N is the number of turns per meter.

The S.I. system of units is adopted in this thesis. Both $\underline{\mu}$ and $\underline{H}$ are the most basic quantities in magnetism. Another quantity of interest is the magnetization $\underline{M}$. This is defined as the magnetic moment per unit volume and has units A m^{-1}. In free space the magnetic field intensity $\underline{H}$ produces a magnetic induction or flux density $\underline{B}_0$ given by

$$\underline{B}_0 = \mu_o \underline{H} \qquad 1.3$$

where μ_o is the absolute permeability of free space and has a value of $4\pi .10^{-7}$ (Henry per meter) or (H m^{-1}).

If the space where $\underline{H}$ is acting is filled with any material then the flux density $\underline{B}$ is given by,

$$\underline{B} = \mu_o(\underline{H} + \underline{M}) \qquad 1.4$$

$$\underline{B}/\underline{H} = \mu_o(1 - \underline{M}/\underline{H}) \qquad 1.5$$

$$= \mu_o(1 + \kappa) \qquad 1.6$$

The quantity $\underline{B}/\underline{H} = \mu$ is known as the absolute permeability of the material and $\underline{M}/\underline{H} = \kappa$ is the absolute susceptibility of the material. The ratio of $\mu/\mu_o = \mu_r$ is the relative permeability. If a magnetic dipole possessing magnetization $\underline{M}$ is brought into a region of magnetic induction $\underline{B}_0$, it experiences a torque τ given by

$$\underline{\tau} = \underline{M} \wedge \underline{B}_0 \qquad 1.7$$

The magnetic potential energy density E_h, which is the work done on the magnet, is by convention taken to be zero for $\underline{M}$ and $\underline{B}_0$ perpendicular to each other. For other angles

$$E_h = \int_{\pi/2}^{\theta} \underline{M}\,\underline{B}_0 \sin\theta \, .d\theta \qquad 1.8$$

$$= -\underline{M} \cdot \underline{B}_0 \qquad 1.9$$

Subatomic particles such as electrons, protons and neutrons all possess magnetic moments. However, whilst the atoms of many elements have a magnetic moment, the free atoms of some elements have zero magnetic moment because the various orbital and spin components completely cancel each other. The complexity and diversity of atomic structure lead to a large variety of magnetic properties. The bulk magnetic properties of any material further depend upon temperature, that is, on the thermal energy and in solids on the complicated interatomic forces in the crystal.

The susceptibility of magnetic materials varies over a wide range from 10^{-6} to 10^{6} and may even have negative values. It is thus convenient to classify substances into a number of groups according to their principal properties. A brief description of some of the principal groups is given in the following sections.

1.2 Diamagnetism

The resultant magnetic moment of the atom is mainly due to incomplete electron shells. Atoms with closed shells such as inert gases, have zero magnetic moment. In ionic compounds, the transfer of electrons which occurs in the formation of the ions gives both positive and negative ions a closed shell structure. Covalent bonding may also lead to a similar state. Materials having no atomic or molecular magnetic moment have very small and negative susceptibilities. These substances, such as inert gases, copper, gold and many organic compounds, are grouped as diamagnetic materials. Each electron, on account of its orbital and spin motion possesses a magnetic moment. The application of a magnetic field produces a torque upon the system which causes the orbital and spin axes to precess about the field direction. This change, according to Lenz's law, is such that it opposes the cause which produces it. All the electrons of the material are affected in this way and produce a negative magnetization. Actually diamagnetism is present in all substances but in non-diamagnetic materials their relatively very large positive response dominates the diamagnetic effect.

The negative diamagnetic susceptibility is always very weak and is not very strongly temperature dependent. The induced magnetic moment as outlined by Kittel (1976) on the basis of Larmor's precession theorem is given by

$$\mu = - Z e^2 B / (4m) . \langle \rho^2 \rangle \qquad 1.10$$

where $\langle \rho^2 \rangle = \langle x^2 \rangle + \langle y^2 \rangle$ is the mean sqaure of the perpendicular distance of the electron from the field axis through the nucleus.

The diamagnetic susceptibility per unit volume is given by the classical Langevin equation, corrected for a numerical error by Pauli (1920) as

$$\kappa_{dia} = -\frac{NZe^2}{6m} \langle r^2 \rangle \qquad 1.11$$

where N is the number of electrons per unit volume.

The same formula is obtainable in quantum theory in which orbital electrical motions are considered.

1.3 Paramagnetism

Paramagnetic materials, unlike diamagnetic ones, possess an atomic or molecular magnetic moment. Their susceptibilities are positive and thus their relative permeabilities are slightly greater than unity. Langevin (1905) first gave a classical derivation for the calculation of paramagnetic susceptibility. He treated the atomic magnetic moments as being sufficiently far apart for particle interactions to be neglected so that the assembly behaved as a paramagnetic gas . He then applied Maxwell-Boltzmann statistics for perfect gases and derived the following expression.

$$M(T) = M(0)\ (\text{Coth } x - 1/x) \qquad 1.12$$

or $$m = \text{Coth } x - 1/x = \pounds(x) \qquad 1.13$$

where $x = \mu B/k_B T$, B is the magnetic induction, k_B is Boltzmann's constant, T is the temperature on the Kelvin scale, $m = M(T)/M(0)$ is the reduced magnetization, and $\pounds(x)$ is known as the Langevin function.

Brillouin (1931) considered paramagnetism quantum-mechanically. This imposes restrictions on the orientation of magnetic moments in applied magnetic fields whereas in the classical derivation all possible orientations are taken into account. The magnetic moment μ_J of each atom or molecule will precess about the field direction such that the resolved components of μ_J along the field direction are

$$\mu_M = gM\mu_B \qquad 1.14$$

where g is the Landé factor, M is the magnetic quantum number which has values:

$M = 0, \quad 1, \quad 2, \ldots\ldots J$ if J is an integer or

$= 1/2, 3/2, \ldots\ldots\ldots J/2$ if J is half integer

and $\mu_B = he/2m = 1.165 \times 10^{-29}$ Wb m and is known as the Bohr magnetron.

The total magnetic moment per atom is

$$\underline{\mu} = g\mu_B JB(J,\alpha) \qquad 1.15$$

where $B(J,\alpha) = \left(\frac{2J+1}{2J}\right) \text{Coth } \left(\frac{2J+1}{2J}\right)\alpha - \frac{1}{2J}\text{Coth } \left(\frac{\alpha}{2J}\right)$ 1.16

and is called the Brillouin function.

Here J is the total angular momentum quantum number

of the ion and

$$\alpha = gJ\mu_B B_0/kT \qquad 1.17$$

The classical situation is a particular limit of the quantum case with the hypothetical state of very large J and 2J + 1 allowed positions giving a virtually continuous distribution of orientations. In this case the Brillouin function $B(J, \alpha)$ reduces to the Langevin function $\pounds(\alpha)$. The volume susceptibility is given by

$$\chi = n g^2 J(J + 1)\mu_B^2/3kT = \frac{C}{T} \qquad 1.18$$

where n is the number of atoms per unit volume. Equation 1.18 is known as the Curie law and C is the Curie constant.

According to the Curie law, the paramagnetic susceptibility is inversely proportional to the temperature and does not depend upon the magnetic field. In ionic solids, Weiss (1907) proposed an aligning interaction between neighbouring ions giving rise to an equivalent magnetic field, known as the Weiss field. This field is proportional to the magnetization, and is superimposed upon the applied field. The presence of the Weiss field modifies Curie's law to

$$\chi = C/(T-\theta_p) \qquad 1.19$$

where θ_p is the paramagnetic Curie temperature.

It may have positive or negative values. This dependence of χ on the temperature is known as the Curie-Weiss law.

The characteristic magnetic susceptibilities of diamagnetic and paramagnetic substances is shown in Figure 1.1.

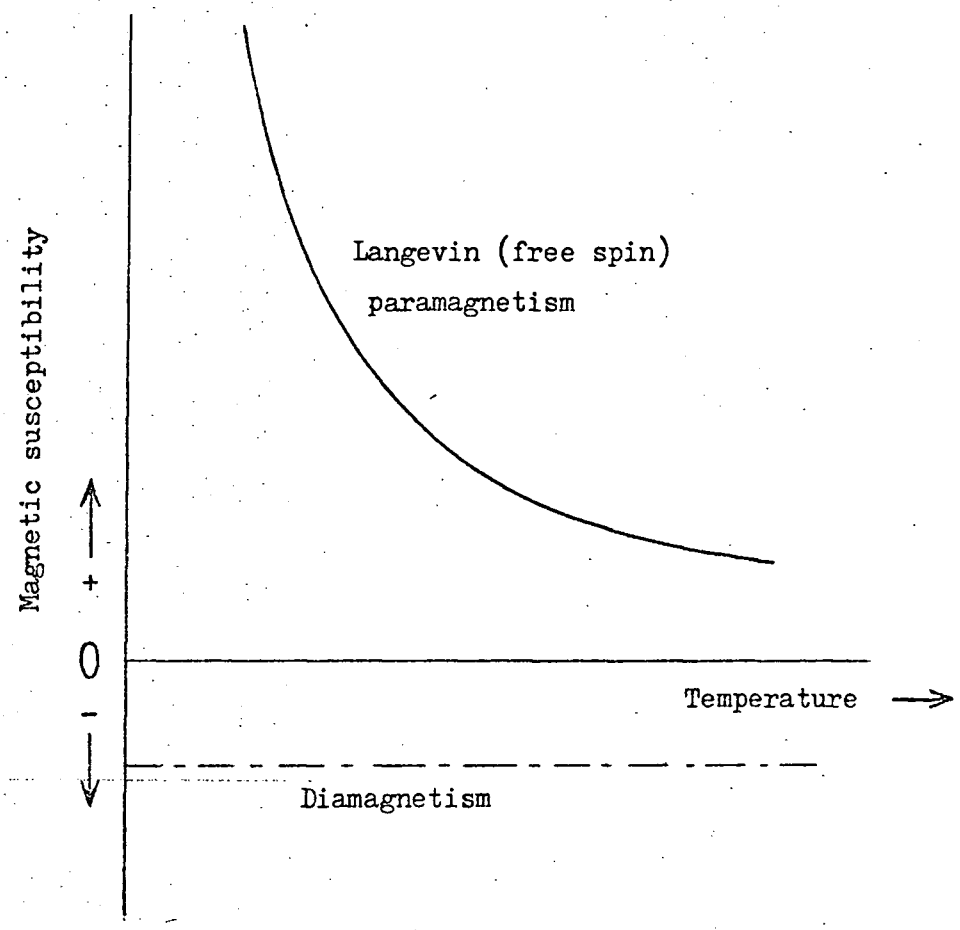

Fig. 1.1 Characteristic magnetic susceptibilities of diamagnetic and paramagnetic substances (after Kittel, 1976).

1.4 Ferromagnetism

In some materials, known as ferromagnetic, the atomic dipole moments tend to align themselves parallel to each other by a force now known as the exchange interaction; this results in spontaneous magnetization. This magnetization is present in the material even in the absence of an external field. Thermal agitation which increases with temperature, tends to disorder this alignment. Thus, above a characteristic temperature T_c, called the Curie temperature, the spontaneous magnetization disappears and the material exhibits paramagnetic behaviour and obeys the Curie-Weiss law. However, a ferromagnetic material in spite of its spontaneous magnetization may still have zero macroscopic magnetization in the absence of an external field. Weiss (1907) first explained this phenomenon satisfactorily by the domain hypothesis, that is small regions of atomic moment alignment oriented in various directions with a resultant zero magnetization. In ferromagnetic materials a small applied field produces a magnetization many orders of magnitude larger than in a paramagnetic substance. The ferromagnetic susceptibility is field dependent. The general behaviour of a ferromagnetic material is well described by the typical B-H curve shown in Figure 1.2. When the field applied to a demagnetized specimen is increased from zero, the OCD portion of the curve is irreversible. Magnetization increases with field and eventually approaches a saturation value M_S beyond which $\underline{B}$ varies linearly with applied field $\underline{H}$. The major magnetic hysteresis loop may have minor or subsidiary loops superimposed upon it,

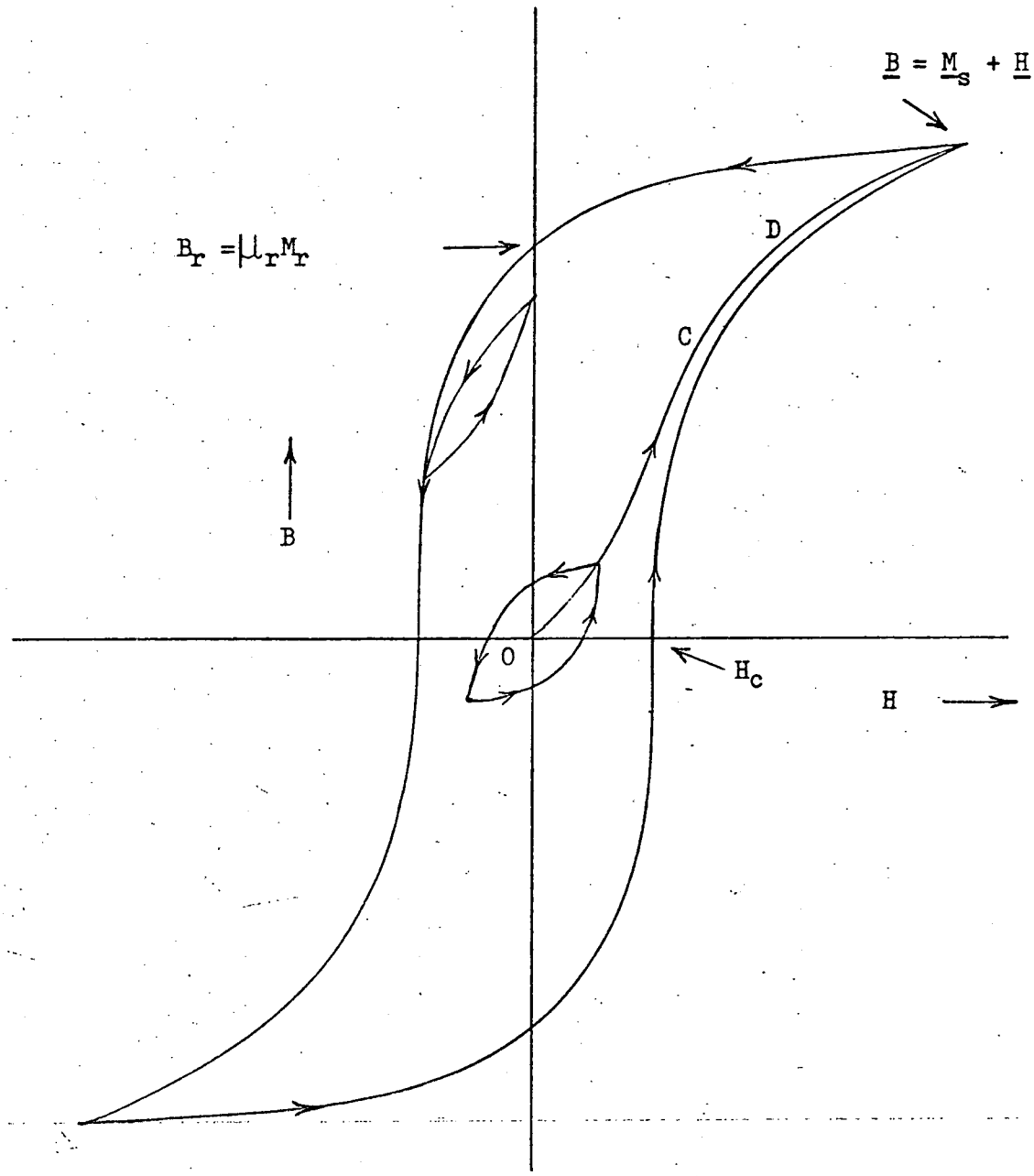

Fig. 1.2 Magnetic characteristics of ferromagnets.

depending on the way in which the applied field is varied. The magnetization $\underline{M}_r$ retained by the material when the field is brought to zero from saturation magnetization value is known as retentivity or remanence. The value of the magnetic field H_c required to destroy the retentivity is called the coercivity. The B-H curve is characteristic of the material. The temperature dependence of the spontaneous magnetization is shown in Figure 1.3.

1.5 Antiferromagnetism

In certain materials such as MnO, chromium and some rare earths, the exchange interaction is negative and thus the magnetic moments of the neighbouring atoms align antiparallel to each other. These substances are known as antiferromagnetic. They have zero net moment at temperatures below a certain ordering temperature T_n known as the Néel temperature. The Néel temperature is given by

$$T_N = \frac{J(J+1)ng^2\mu_B^2}{6k} N_w \qquad 1.20$$

where N_w is the Weiss constant.

The susceptibility is small at low temperatures because of strong exchange interaction, it increases with temperature and becomes a maximum at T_n as the thermal agitation weakens the exchange forces. At higher temperatures such substances assume paramagnetic behaviour and possess small susceptibility;

$$\chi = C/(T + \theta_n) \qquad 1.21$$

where θ_n is the extrapolated Curie temperature.

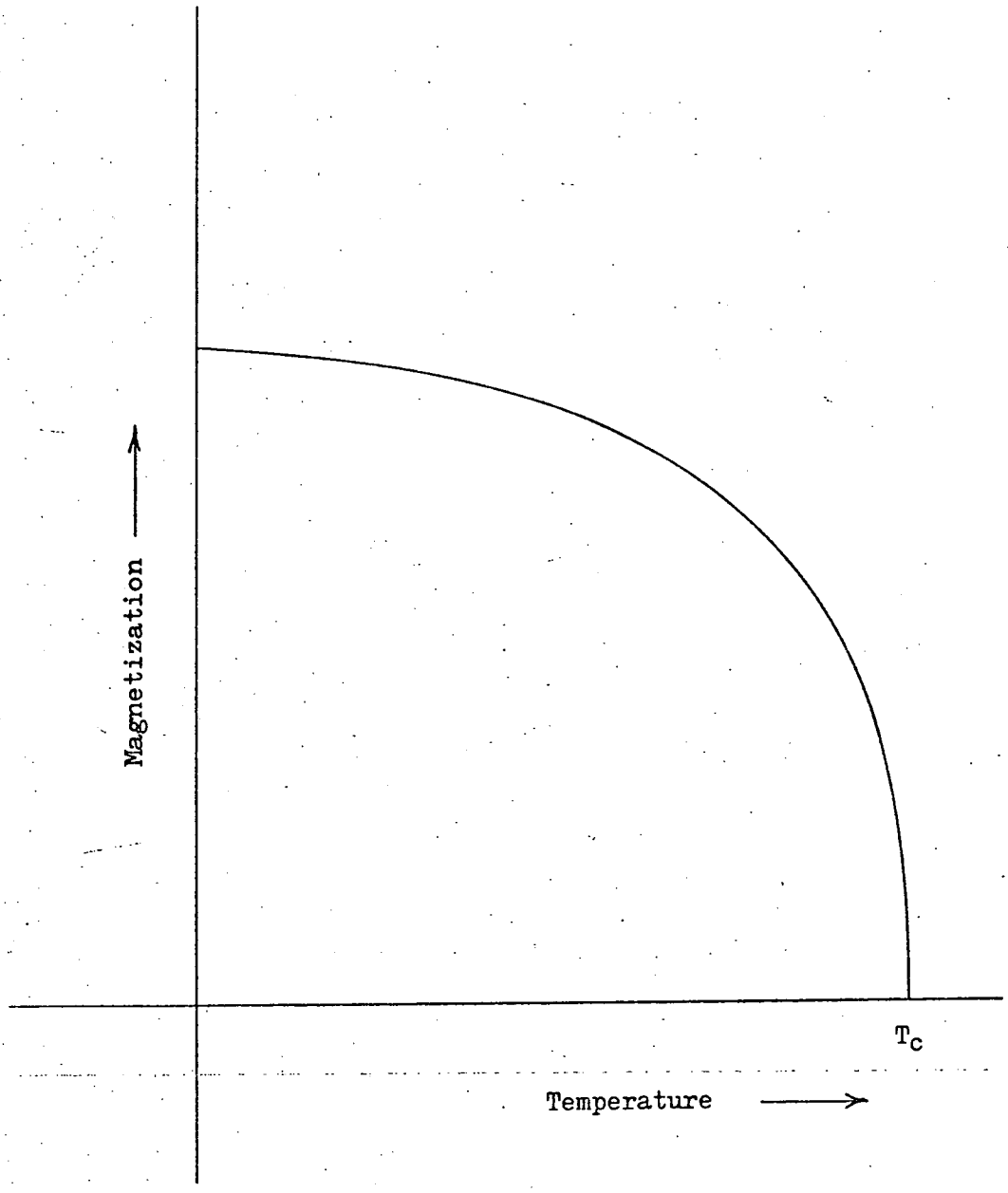

Fig. 1.3 A typical curve of temperature dependence of spontaneous magnetization.

There is yet another related class of magnetic ordering found in substances with negative exchange interaction like antiferromagnetics but with a net spontaneous magnetic moment. These materials are called ferrimagnetic although the phenomenon is also sometimes known as uncompensated antiferromagnetic ordering. Néel (1948) explained this phenomenon by the ordering of magnetic moments of unequal magnitudes at two different lattice sites antiparallel to each other. The temperature dependence of the magnetic susceptibilities of para-, ferro- and antiferro- magnetic materials is shown in Figure 1.4. Magnetic ordering and related phenomena are discussed in more detail in Chapter 2.

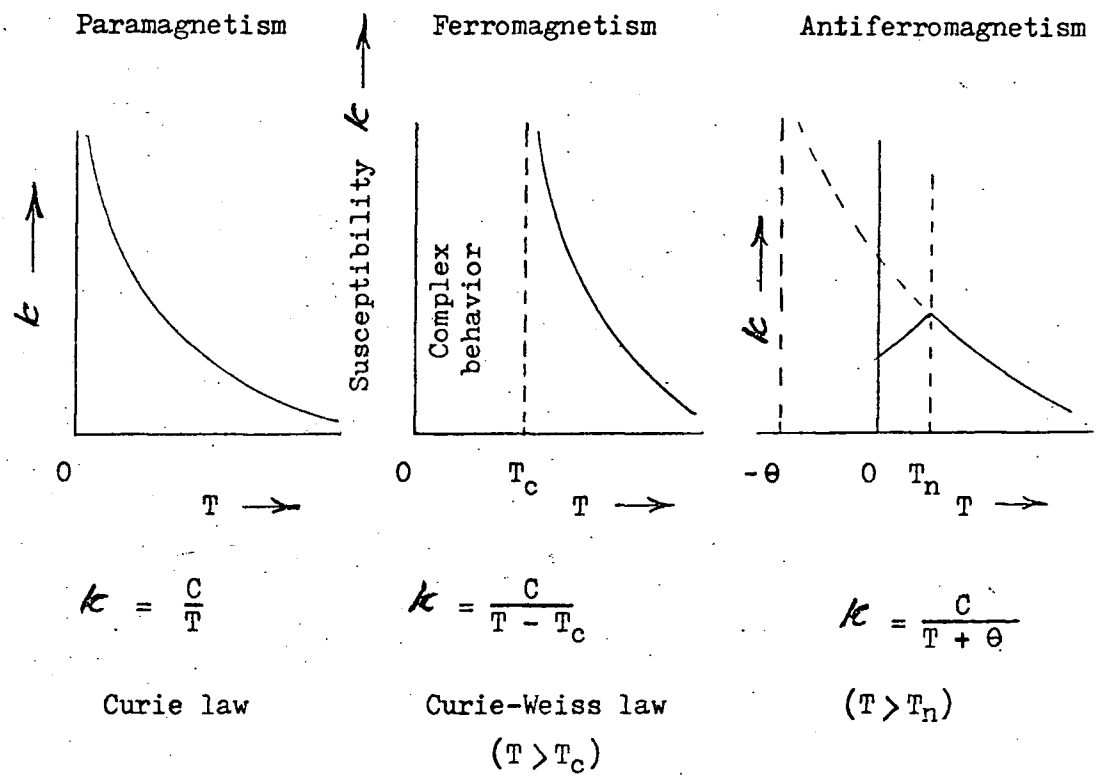

Fig. 1.4 Temperature dependence of magnetic susceptibility in paramagnets, ferromagnets, and antiferromagnets (after Kittel, 1976).

CHAPTER 2

MAGNETIC ORDER

2.1 Introduction

As mentioned in the previous chapter about the types of magnetism, in certain materials some sort of magnetic ordering exists below characteristic ordering temperatures. Ferromagnetism, antiferromagnetism and ferrimagnetism are the most common examples of magnetic ordering. In these materials the magnetic moments align themselves through various forms of exchange interaction and thus their magnetism may be classified as cooperative magnetism. Diamagnetism and ideal paramagnetism are examples of non-cooperative magnetism in which the individual magnetic moments (induced or spontaneous) are independent of each other. The characteristic ordering temperature below which an ordered magnetic structure with a net moment occurs is called the Curie temperature T_c in ferro- and ferrimagnetism. In antiferromagnetics ordering without a net moment takes place below the Neel temperature T_n and in spin glasses the transition to the spin glass state takes place at the spin glass temperature T_{SG}. In antiferromagnetics the change from para to antiferromagnetic occurs at T_n and that from antiferromagnetic to ferromagnetic (if it exists) at T_c.

2.2 Ferromagnetism and the Exchange Interaction

The existence of spontaneous magnetism in ferromagnets is due to (i) the presence of a magnetic moment associated with the total angular momentum of the electrons in the unfilled shell and (ii) the presence of an interaction

field between electron spins of neighbouring atoms aligning the spin moments parallel to each other. Types of alignment other than parallel are also possible and will be discussed later. When all the magnetic moments align themselves parallel to each other, which is the case of ferromagnetism at absolute zero temperature, the material then has maximum saturation magnetization. Thermal vibrations tend to disorder this magnetic structure. As the temperature is increased gradually, the thermal agitations become more energetic until at some stage the thermal energy becomes comparable with that due to the ordering forces. At a critical temperature T_c, known as the Curie temperature, there exists no magnetic order and so the spontaneous magnetization disappears. The material then behaves as paramagnetic above the Curie temperature and obeys the Curie-Weiss law. The Curie temperature thus reflects the magnitude of the force of the exchange interaction. Weiss explanation of the interaction on the basis of a molecular field $N_w M$ (the Weiss field) proportional to magnetization M is purely phenomenological and is simply a convenient device. In quantum mechanics, as pointed out by Heisenberg (1928), this ordering is the combination of coulomb forces and the application of the Pauli exclusion principle. These ordering forces are electrostatic and are several orders of magnitude greater than pure magnetostatic ones.

The state of an electron can be represented by its spin and orbital components. There are only two spin

states, parallel or antiparallel with respect to a certain direction - that of the external magnetic field; according to the Pauli principle no two electrons can be in the same quantum state. So electrons with the same spin state (symmetric spins) must have an antisymmetric spatial state if the other quantum numbers are identical and vice-versa. This leads to a force of repulsion between similar spins and a force of attraction between opposite spin electrons in the single spatial wave function. This force is known as the exchange force. On the other hand when two electrons approach each other, they give rise to a coulomb interaction W(1,2,a,b) where 1 and 2 are the electron positions and a and b those of their atoms respectively. W may be represented as

$$W = e^2/r_{12} + e^2/r_{ab} - e^2/r_{a2} - e^2/r_{b1} \qquad 2.1$$

where r_{ij} are the distances between positions i and j. Extending the concept to atoms with several electrons with arbitrary spin, Van Vleck (1945) derived the energy of the exchange interaction for a system of N atoms as

$$E = -\sum_{j=1}^{N}\sum_{i=1}^{N} J_{ij}\, \underline{S}_i \cdot \underline{S}_j \qquad 2.2$$

where J_{ij} is function of atomic distance r_{ij}, which varies exponentially with distance from the nucleus and is known as an exchange integral and S_i and S_j are the spins of i and j electrons respectively. The exchange integral is given by

$$J_{ab} = \tfrac{1}{2}\iint \psi_a^*(1)\psi_b^*(2)\mathcal{K}\psi_b(1)\psi_a(2)d\tau_1 d\tau_2 \qquad 2.3$$

where $\psi_a(1)$ and $\psi_b(2)$ are the wave functions for the electrons at positions 1 and 2 in their atoms a and b respectively, and $\mathcal{K}$ is a coulomb interaction Hamiltonian and is a function of inter-electron and electron nuclear distances. Thus the Pauli principle together with the coulomb interaction make the levels of the atomic spin system dependent on the relative orientations of the spins. Spins are parallel if J_{ij} is positive and anti-parallel if J_{ij} is negative. For direct inter-atomic exchange, J_{ij} can be positive or negative depending on the balance between coulomb and kinetic energies. The variation of the exchange integral with the ratio of nuclear separation to radius of active electron shell is shown in Figure 2.1.

In cases where the wave functions do not overlap or overlap only very little the exchange interaction may take place indirectly. In insulators the exchange interaction may be through diamagnetic ions, radicals or molecules. This comparatively long range indirect exchange interaction is known as superexchange (White and Geballe, 1979).

In rare earth metals where the incomplete 4f shell is an inner shell and screened by other shells the conduction electrons are polarized by direct exchange interaction with the 4f magnetic electrons and so couple the magnetic moments. This interaction is known as RKKY interaction after the first investigators Ruderman and Kittel (1954), Kasuya (1956) and Yosida (1957).

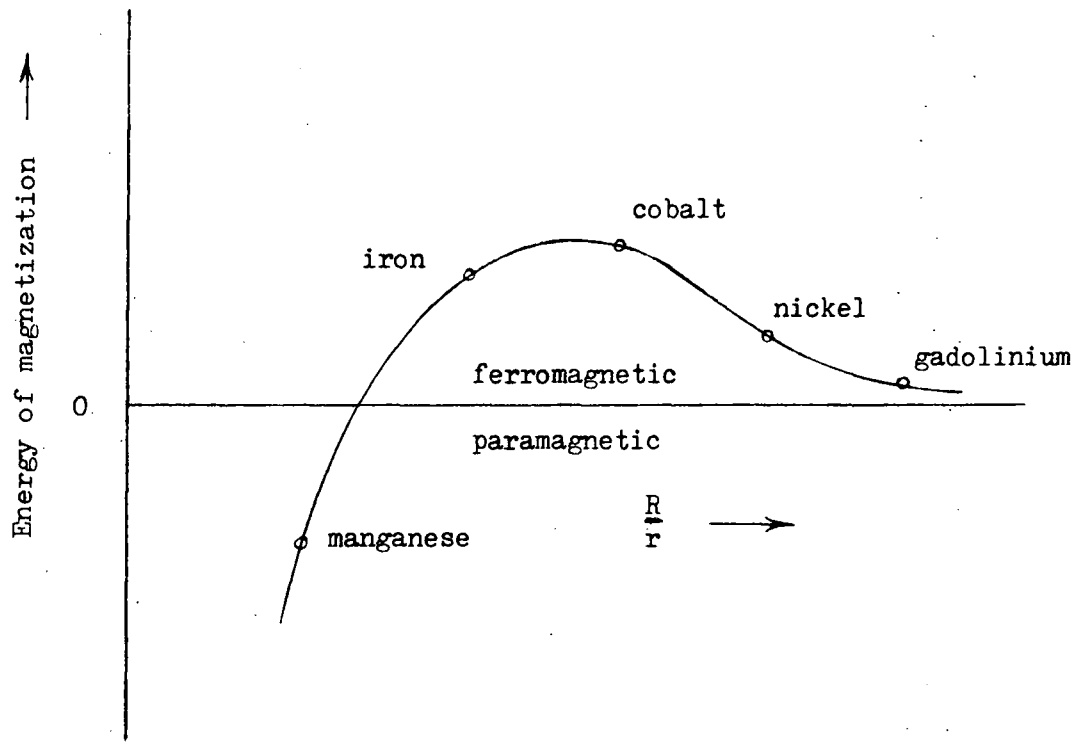

Fig. 2.1 Variation of the exchange energy of magnetization with the ratio of nuclear separation R to the radius of active electron shell r (after Bethe, 1933).

In the indirect exchange interaction J can be positive or negative as in superexchange in insulators or even oscillatory as in the RKKY interaction. In the RKKY interaction a magnetic ion induces an oscillatory spin polarization in the conduction electrons in its neighbourhood. The conduction electrons try to screen out the magnetic moment on the ion. The strength of this screening polarization decreases with increasing distance from the ion, but its effect is relatively long range. This modulation of spin polarization influences the magnetic moments of other ions within the range which leads to oscillatory indirect coupling. In disordered system the RKKY interaction can sometimes lead to positive and negative coupling which may cause a conflicting interaction known as frustration. In crystals, coupling between the magnetic ion and the crystal lattice also exists. The crystal lattice if anisotropic will cause an anisotropic electric field at the ion which leads to an anisotropic exchange interaction. Another source of anisotropy is spin-orbit coupling. In this interaction the effective magnetic field of an orbital motion of the electron acts on the electron's intrinsic moment which is associated with spin (Cullity, 1972, and Hurd, 1975). In ferromagnetic materials, every ion has an identical, spontaneous moment and occupies an identical crystallographic site. The exchange integral J is everywhere positive. The variation of spontaneous magnetization with temperature, and the reciprocal of the susceptibility above the Curie temperature T_c is shown in Figure 2.2.

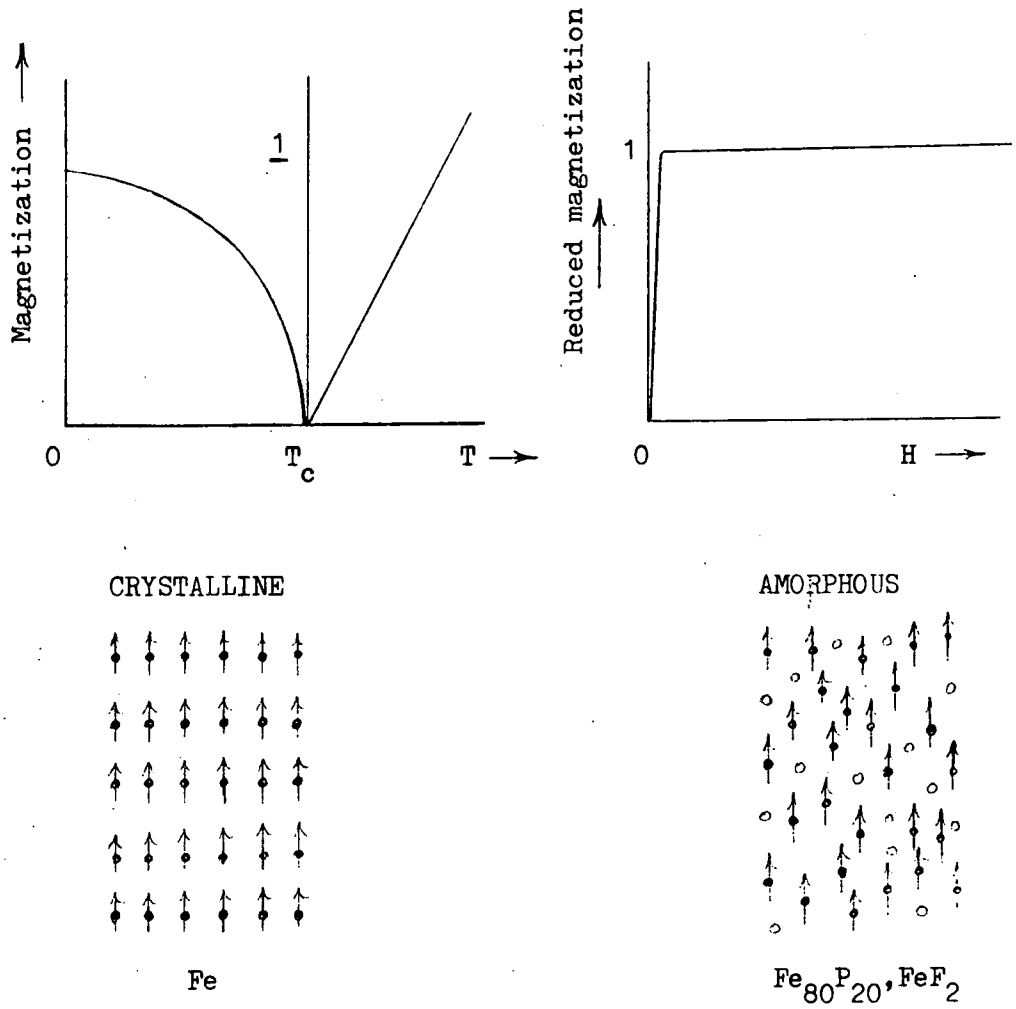

Fig. 2.2 Temperature dependence of spontaneous magnetization and reciprocal of susceptibility for ideal ferromagnetism (after Hurd, 1982).

At or near room temperature, iron, cobalt, nickel and gadolinium are examples of crystalline ferromagnetic elements and metal alloys which are of various compositions of Fe, Ni, Co and B can be amorphous ferromagnets when prepared by splat cooling (Cahn, 1980).

2.3 Antiferromagnetism

Antiferromagnetism like ferromagnetism is a cooperative phenomenon characterised by long range order among identical spontaneous moments. The exchange integral in antiferromagnetic substances like FeO, Mn and Sm is negative and thus there is no overall spontaneous magnetism. In some cases it is found that there are two sub-lattices each of which possess moments which lie parallel. Although the moments on the sub-lattices almost cancel they cannot do so exactly as they are not quite collinear (Yafet and Kittel 1952). The non-collinearity in antiferromagnets leads to weak ferromagnetism. The exchange energy operator for the sub-lattices, according to Heisenberg, has the form

$$\mathcal{H}_{ex} = \sum_{j\ k} |J_{jk}| \hat{\underline{S}}_j \cdot \hat{\underline{S}}_k \approx |J_{jk}| \sum_{<j,k>} \hat{S}_j \hat{S}_k \qquad 2.4$$

where J_{jk} is the exchange integral between nearest neighbours for the two magnetic sub-lattices and the sum is over all the adjacent pairs. It is generally the average value of clockwise or anticlockwise spins in the molecules as the exchange between clockwise and anticlockwise spins proceeds at a very high frequency, 10 kHz, and the average value is very nearly the same as the total spin of a sub-lattice (Anderson, 1951). Marshall (1955) introduced another term associated with the magnetic anisotropy in the Hamil-

tonian and wrote the Hamiltonian operator as

$$\mathcal{H}_k = k\left[\sum_j (S_{xj}^2 + S_{yj}^2) + \sum (S_{xk}^2 + S_{yk}^2)\right] \qquad 2.5$$

for the energy of magnetic anisotropy with axial symmetry. Here k is considered a convergent factor and is lower than the exchange integral J_{jk}.

In most antiferromagnets the magnetic coupling is by superexchange via non-magnetic ions etc. As the temperature increases, the increasing thermal energy as in the case of ferromagnets, leads to disorder in the magnetic coupling until at the Néel temperature T_n the material becomes paramagnetic and obeys the Curie-Weiss law (1.2). In some substances, e.g. the rare earths, cooling in zero field from T_c (the Curie temperature) results in a change from antiferromagnetism to ferromagnetism. Theoretical ideas were experimentally verified using neutron diffraction by Shull et al. (1951). The neutron possesses an intrinsic magnetic moment and is scattered by an ordered system of moments thus revealing information about both positional and magnetic ordering. Antiferromagnetic arrangements and neutron lines for MnF_2 after Erickson (1953) are shown in Figure 2.3.

A typical temperature dependence of the reciprocal susceptibility of antiferromagnetic substances is shown in Figure 2.4, where $\chi_{\parallel}$ and $\chi_{\perp}$ are susceptibilities when the field is applied parallel to and perpendicular to the spin axis respectively. When the field is perpendicular, the magnetization takes place by the rotation of each

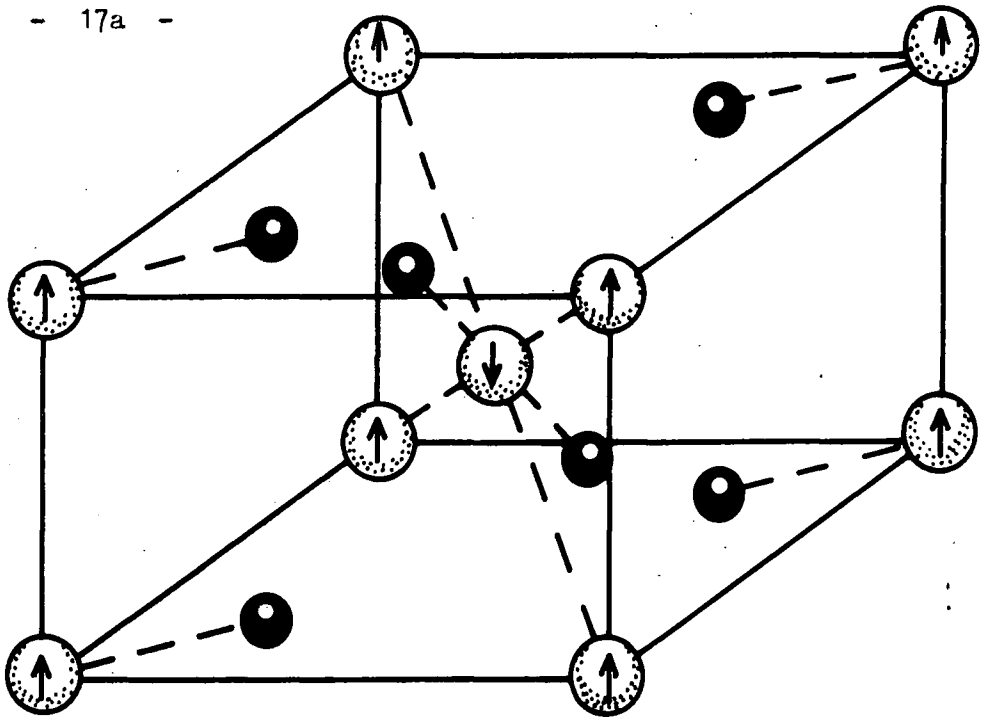

a

Fig. 2.3 (a) The antiferromagnetic arrangement of the magnetic ions for MnF_2, FeF_2, and CoF_2. The dark spheres represent the fluorine ions.

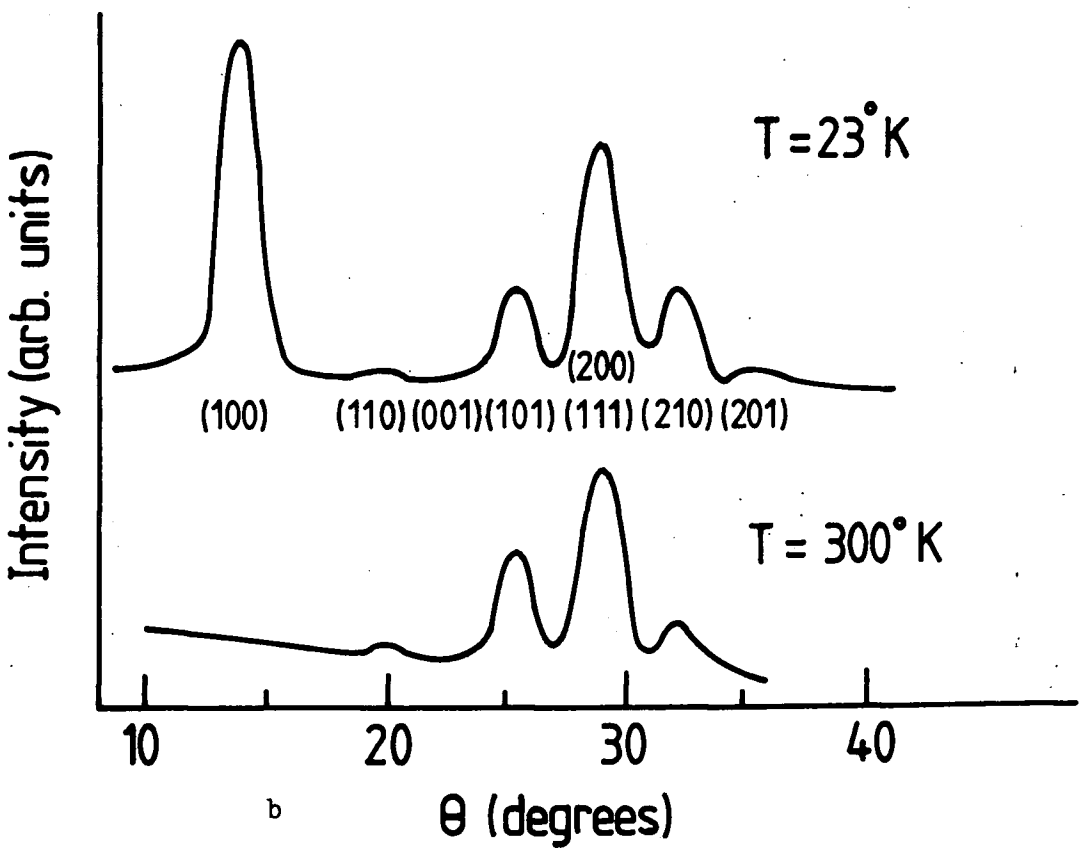

b

(b) Neutron diffraction pattern for MnF_2 below and above the Néel temperature.

(after Erickson, 1953).

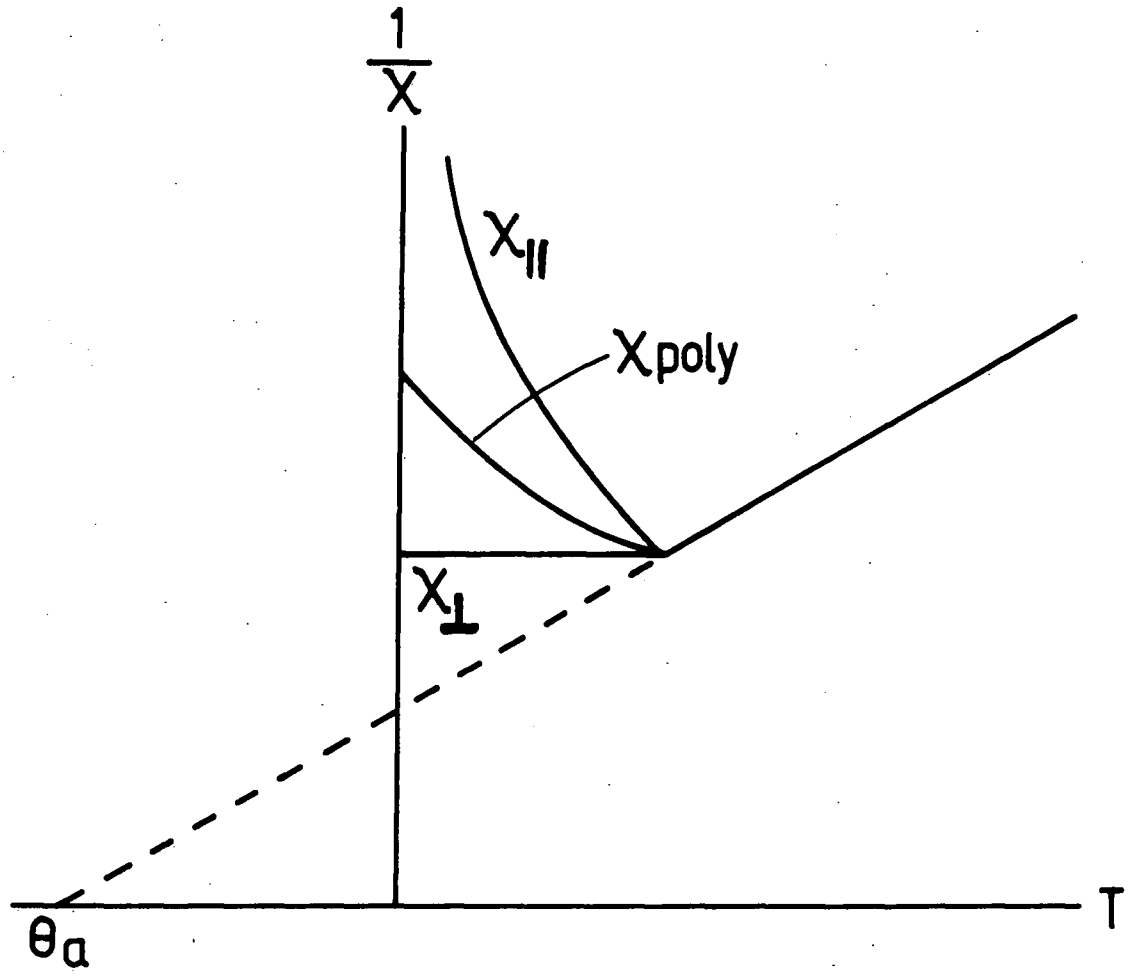

FIG. 2·4 Temperature dependence of the reciprocal susceptibility of an antiferromagnetic substance (after Chikazumi, 1964). θ_a is the asymptotic Curie temperature.

spin from the spin axis. In polycrystalline materials the susceptibility χ_{poly} is the average between the two cases. The intersection of $1/\chi$ with the abscissa is called the asymptotic Curie temperature. Spin rotation is shown in Figure 2.5. In some antiferromagnets, ferromagnetic behaviour may be induced below T_n by strong applied fields. This phenomenon is known as metamagnetism (Stryjewski and Giordano, 1977). A general phase diagram is shown in Figure 2.6.

2.4 Ferrimagnetism

This is again a magnetically ordered magnetism based on an indirect or superexchange interaction with a negative exchange integral. The magnetic moments are strongly coupled in various non-parallel arrangements. Ferrimagnetic materials unlike antiferromagnetic substance show spontaneous magnetism. In the simplest case, the magnetic moments of the ions at two magnetic sub-lattices are not equal so the difference of the two moments in antiparallel coupling give rise to spontaneous magnetism. The ions may be of the same element or of different magnetic species. Different numbers of ions at two sub-lattices with identical moments also lead to a similar state. Various possible ferromagnetic arrangements are shown in Figure 2.7.

Ferrimagnetism was first observed in ferrites. These are iron oxides with a divalent metal ion M and denoted by the general formula $MO.Fe_2O_3$. M may be Mn^{+2}, Fe^{+2}, Co^{+2}, Ni^{+2}, Cu^{+2}, Zn^{+2} or Gd^{+2}. Most of these compounds have the spinel structure. Antiferromagnetism

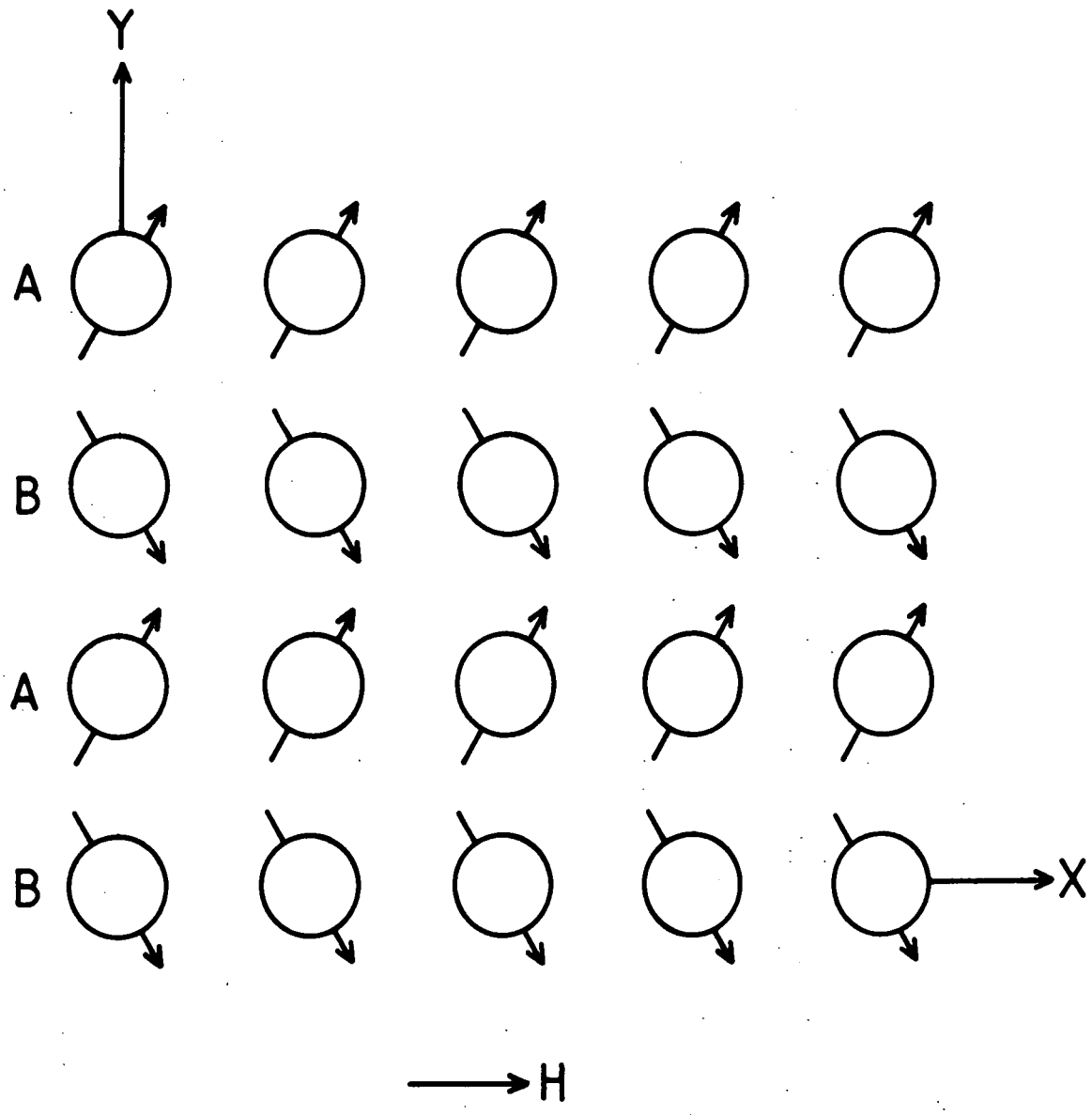

Fig. 2.5 Spin rotation in an antiferromagnetic substance (after Chikazumi, 1964).

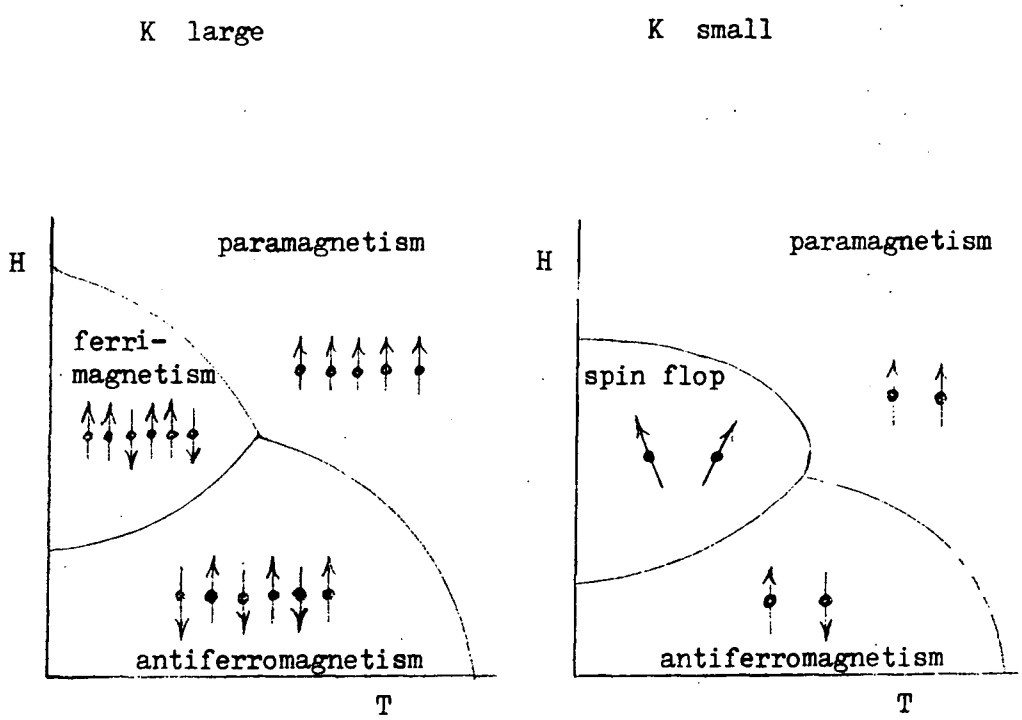

Fig. 2.6 A typical metamagnetic behaviour; field induced transitions (after Hurd, 1982).

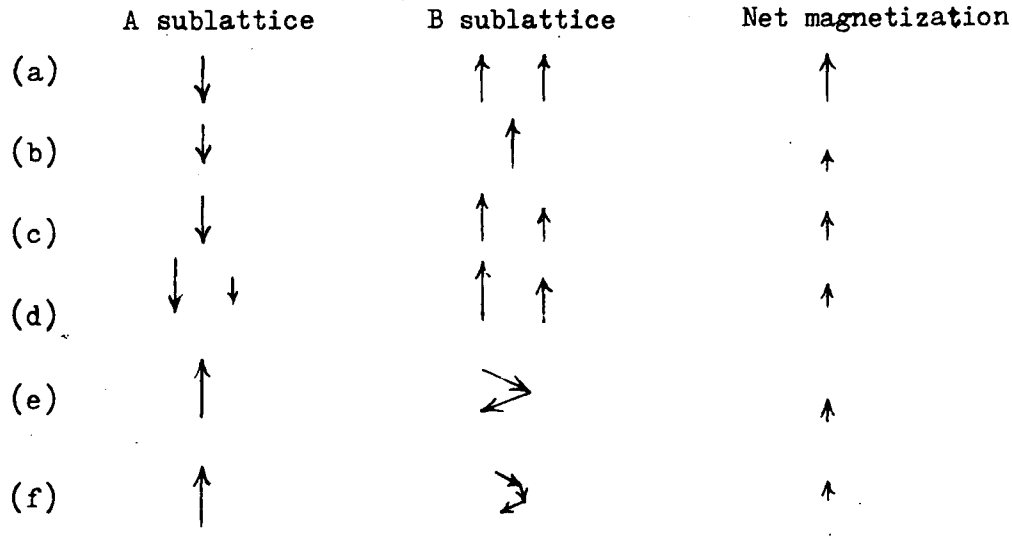

Fig. 2.7 Various possible ferrimagnetic arrangements for two sublattices (after Morrish, 1965).

is a special case of ferrimagnetism with identical anti-parallel moments on two sub-lattices. The temperature dependence of ferrimagnetism is qualitatively similar to that of ferromagnetism below the Curie temperature. Above the temperature T_c the paramagnetic subsceptibility does not exactly follow the Curie-Weiss law but has curvature particularly near T_c. Amorphous ferrimagnetism also exists, but in this case the sites in two sub-lattices have random positions e.g. alloys of the form $RE-Fe_2$. RE is a heavy rare earth like Tb or Gd. Fe-RE coupling is antiferromagnetic whereas Fe-Fe and RE-RE couplings are ferromagnetic.

2.5 Helimagnetism

In substances exhibiting helimagnetism the magnetic moments are so arranged that in layers perpendicular to some common axis they lie parallel but their direction in the plane varies in a progressive manner along the axis resulting in a helical moment arrangement. Helimagnetism was first observed in MnAu by neutron diffraction. In the heavy rare earths, because of the long and oscillatory nature of the RKKY exchange, various periodic structures such as ferro, helix, cone, antiphase etc. are frequently formed. These are shown in Figure 2.8 (after Crangle, 1977, page 87). The external magnetic field induces complex changes in the periodic magnetic structure of all the heavy rare earths except gadolinium which has a simple ferromagnetic nature. Magnetic order also changes from one arrangement to another with a change in temperature.

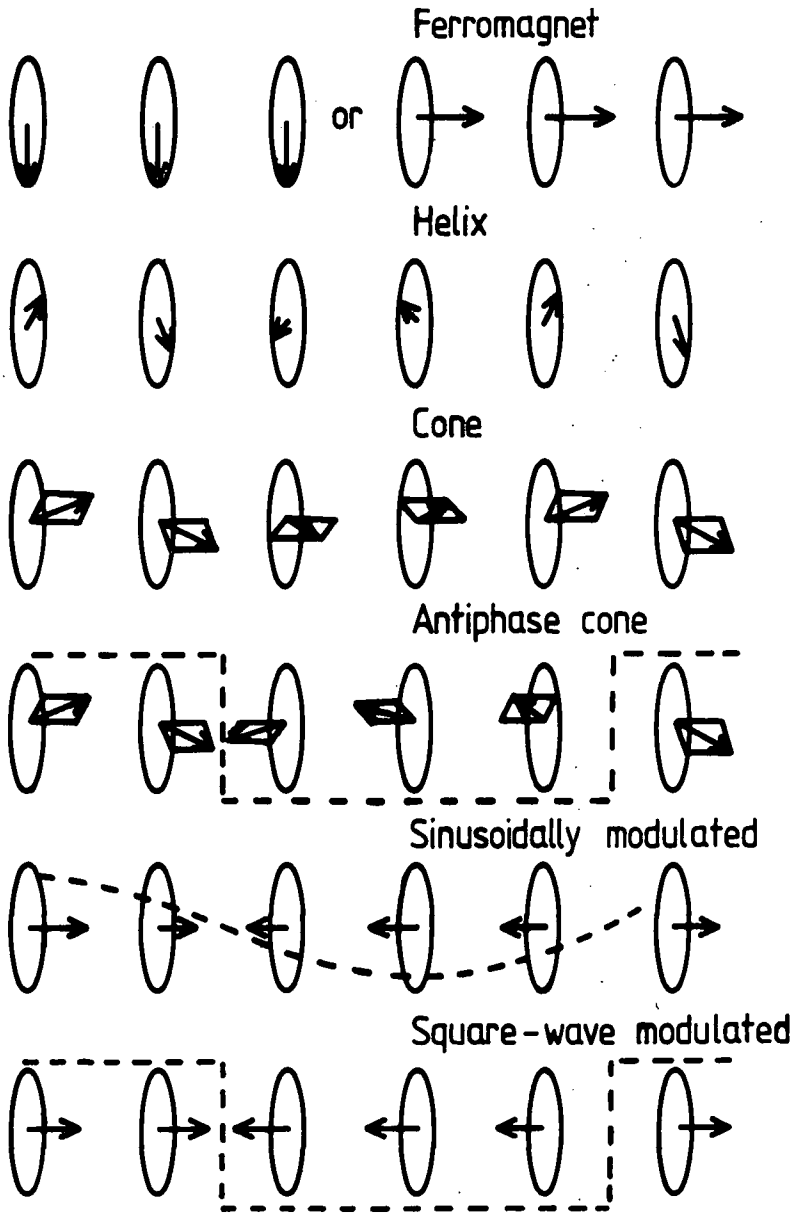

Fig. 2.8 Variety of magnetic structures found in the metallic heavy rare earths (after Crangle, 1977).

The magnetic structure and transitions of heavy rare earths are given in Table 2.1.

In general, ferromagnetic order at low temperatures changes to paramagnetism at high temperatures through various intermediary periodic arrangements.

2.6 Magnetic Anisotropy

It is commonly observed in ferromagnets that the magnetization takes up certain preferred crystallographic directions. This indicates that the internal energy function has minimum values in those particular directions. The dependence of internal energy on the direction of spontaneous magnetization is termed magnetic anisotropy. In a specimen of any shape other than a sphere the shape of the crystal causes the magnetic energy to depend on direction because of the demagnetization energy due to the formation of free poles leading to magnetic interaction. Similar effects are produced by applied or residual stress. This anisotropy is called shape anisotropy. Shape anisotropy disappears in the case of a sphere and has a maximum for the case of an infinite cylinder. In addition to the shape or stress effects, there is generally a magnetic anisotropy which depends on the crystal symmetry of the material and is known as crystal magnetic anisotropy or magnetocrystalline anisotropy. Preferred directions are called easy directions. In Ni these are the cube diagonals $\langle 111 \rangle$, in iron they are the cube edges $\langle 100 \rangle$ and in Co the easy direction is along the hexagonal axis

[0001]. However in the rare earths which also have hcp structure more complicated situations occur. For example, terbium has its basal plane $\hat{b}$-axis as the easy axis and gadolinium shows an easy cone. Magnetocrystalline energy is defined as the work required to magnetize the material along certain directions compared to an easy direction. This energy is actually a free energy if the work is performed at constant temperature. The existence of crystalline anisotropy may be demonstrated by the magnetization curves of single crystal specimens as shown in Figure 2.9.

2.7 Atomic Origin of Magnetocrystalline Anisotropy

In a crystal the electronic charge clouds of ions are distorted due to the crystalline lattice field. The spin-orbit coupling consequently makes the spin orientations anisotropic. There are two common models which are considered responsible for the electron charge alignment in the lattice. These are the single-ion model and the two-ion model. These two models are applicable to magnetic ions with localized moments. Materials in which the active electrons are itinerent also show anisotropy, but this cannot be discussed in terms of either of these simple models. The anisotropy models are discussed briefly in the following sections.

2.7.1 Single-Ion Model

In the single-ion model the crystalline electrostatic field which reflects the crystal symmetry is thought to distort the electronic charge of the ion. The electronic

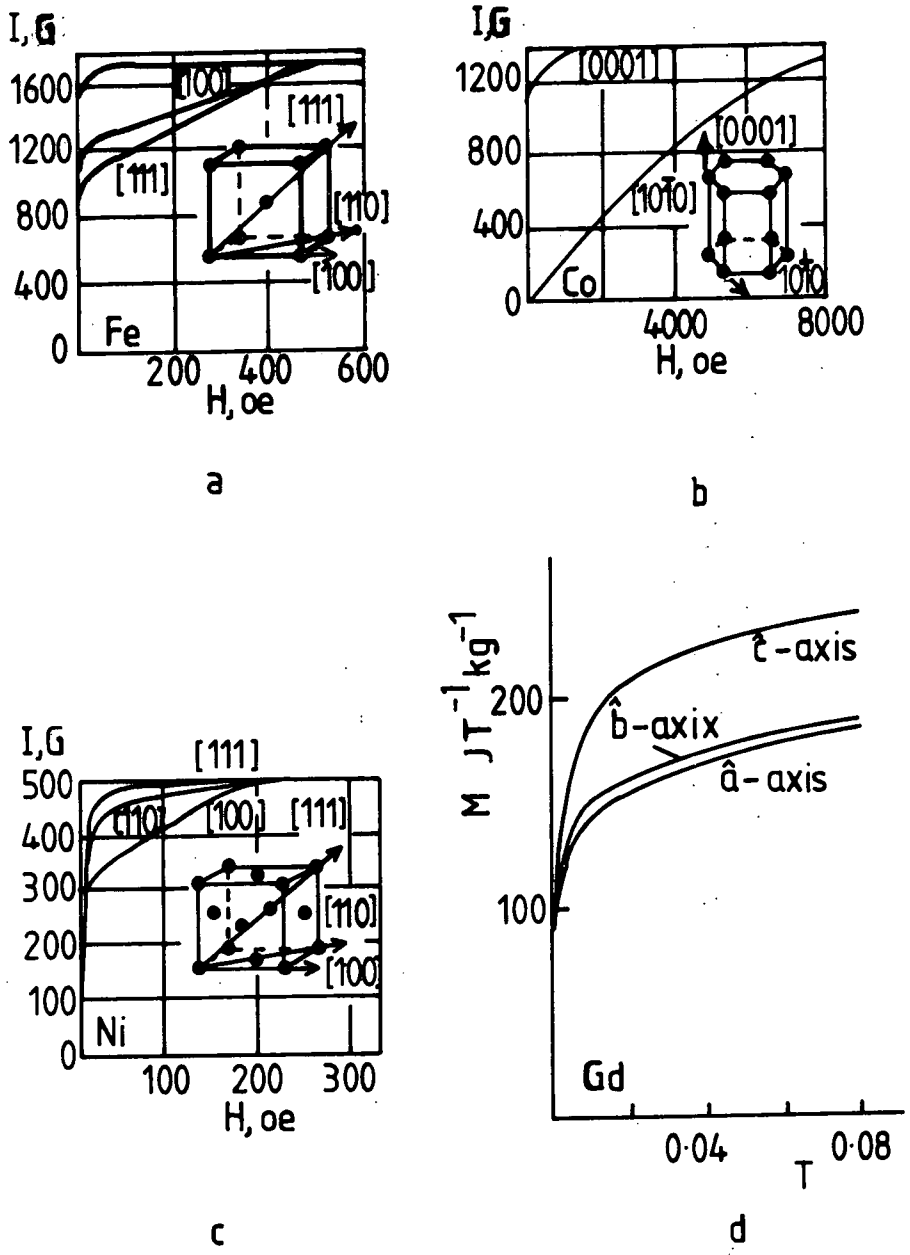

Fig. 2.9 Magnetization curves for single crystals of iron, nickel, cobalt, and gadolinium (a to c after Honda and Kaya, 1926 and d after Nigh et al. 1963).

charge distribution is governed by the orbital angular quantum numbers of the electrons. The spin-orbit interaction then links the spins to the crystal lattice. In this model, the active electrons are treated as localized to their ions as in the case of magnetic insulators. The inner, active electrons of the rare earths are also localised to their ions. The Hamiltonian expression for such a system is given by Darby and Isaac (1974) as

$$\mathcal{H} = g\mu_B \underline{B}_m \cdot \underline{S} + V_c(\underline{r}) + \mathcal{H}_{SL} + \mu_B \underline{B}_o \ (\underline{L} + 2\underline{S}) \qquad 2.6$$

where $\underline{B}_m$ is an effective molecular field representing the exchange interaction of the single-ion with its neighbours, $V_c(r)$ is the crystalline field potential, $\mathcal{H}_{SL}$ is the spin-orbital coupling and $\underline{B}_O$ is the external magnetic field. The terms $V_c(r)$ and $\mathcal{H}_{SL}$ in the above Hamiltonian give rise to magnetocrystalline anisotropy. The crystalline field $V_c(r)$ at position $\underline{r}$ can be expressed in terms of spherical harmonics representing crystal structures as

$$V_c(r) = \sum_{Lm} r^L \, A_L^m \, Y_L^m \, (\theta, \phi) \qquad 2.7$$

where the coefficients A_L^m depend on the inter-ionic separation and are thus temperature sensitive. The A_L^m can be experimentally determined by electron spin resonance studies (Abraham and Bleaney, 1970). The crystalline field can also be expressed in terms of convenient equivalent operators O_L^m which are polynomials in L or J and were introduced by Stevens (1952). Thus

$$V_c = \sum_{L,m}^{\infty} B_L^m \cdot O_L^m \qquad 2.8$$

where the coefficients B_L^m are given by

$$B_L^m = \langle r^L \rangle A_L^m \alpha_L \qquad 2.9$$

where α_L are constants known as Stevens factors and the averaging is performed over the ionic radial wave functions. The spin orbit interaction $\mathcal{H}_{SL}$ is given by

$$\mathcal{H}_{SL} = \sum \rho(r_i) \cdot \underline{S}_i \cdot \underline{L}_i \qquad 2.10$$

where

$$\rho(r_i) = h^2/(2m^2c^2).1/r_i.du/dr_i \qquad 2.11$$

and U is the central ionic potential.

In the calculation of the free energy of the system, V_c and $\mathcal{H}_{SL}$ are treated as perturbations on the exchange and Zeeman interactions with the quantization axis usually taken to be that of B_m. This gives the energy of a single-ion E_i as a function of alignment of B_m in the crystal. The partition function Z is written

$$Z = \sum_i \exp(E_i(\theta)/k_B T) \qquad 2.12$$

and the free energy E per ion is given by

$$E = -k_B T \log_e(Z) \qquad 2.13$$

The free energy thus obtained for a collection of such ions is a function of the direction of magnetization relative to the crystallographic axes.

In rare earth ions the spin-orbit interaction is strong compared to the crystal potential and the ionic

states are characterised by a total angular momentum J. Therefore, the anisotropy is determined solely by J. For a hexagonal system, the single-ion anisotropy Hamiltonian can be expressed according to Elliot and Stevens (1953) as

$$\mathcal{H}_A = \alpha A_2^o \langle r^2 \rangle Y_2^o(J) + \beta A_4^o r^4 Y_4^o(J) + \gamma A_6^o \langle r^6 \rangle Y_6^o(J) + \gamma A_6^6 \langle r^6 \rangle [Y_6^6(J) + Y_6^{-6}(J)] \quad 2.14$$

where A_i^m are crystal field potentials, α, β and γ are constants and $Y_1^m(J)$ are spherical harmonics.

2.7.2 Two-ion Model

Van Vleck (1937) first developed this model which takes account of the possibility that the anisotropy may also be due to the dependence of the interaction energy on the shape of the electronic charge cloud of the nearest-neighbour ions. It plays an important role in determining the anisotropy for materials such as Gd^{+3} which have no orbital moments particularly for spin S = 1/2 (Yosida, 1968, and Darby and Isaac, 1974). In the rare earths it is thought to contribute along with the single-ion model to the overall anisotropy. Van Vleck (1937) scaled by a function $C_{ij}(r_{ij})$ the classical electromagnetic coupling between two ionic spins which have too small anisotropic contribution by superimposing the spin orbital coupling on the exchange energy between the neighbouring spins in a second order perturbation to give

$$C_{ij}(r_{ij})(S_i.S_j - 3(S_i.R_{ij})(S_j.r_{ij})r_{ij}^{-2}) \quad 2.15$$

where

$$C_{ij} = g^2 \mu_B^2 / r_{ij}^3 \quad 2.16$$

The interaction between nearest-neighbour ions, called the pseudo-dipolar interaction, is often strong. The fourth order perturbation known as the pseudo-quadrupole interaction gives the correct magnitude of anisotropy in cubic materials. The pseudo-quadrupole interaction is given by

$$\sum_{j>i} \gamma_{ij} (S_i \cdot r_{ij})^2 (S_j \cdot r_{ij})^2 \qquad 2.17$$

The coulomb interaction $\mathcal{H}_c$ and exchange interaction $\mathcal{H}_{ex}$ yield anisotropy by fifth and third order perturbation calculations.

In rare earth metals the interaction is indirect via the RKKY interaction as mentioned earlier.

2.8 Magnetostriction

During the process of magnetization in ferromagnetic and ferrimagnetic crystals a change in the dimensions of the specimen is generally observed. This phenomenon is known as magnetostriction. The crystal anisotropy energy is dependent on the interatomic spacing of the lattice. Any change in the interatomic spacing causes a further contribution to the free energy of the system. The interaction between the magnetization and the lattice is the origin of magnetostriction. The interatomic energy can be expanded in Legendre polynomials as

$$W = g(h) + (\cos^2\phi - 1/3) + q(a)(\cos^4\phi - 6/7\cos^2\phi + 3/35) + .. \qquad 2.18$$

where ϕ is the angle between magnetization and the bond direction between the pair of magnetic atoms.

The first term is the exchange interaction term and is independent of magnetization direction and so does not contribute to magnetostriction during rotation of the magnetization vector in the crystal. It produces a change in the volume of the specimen at the onset of ferromagnetism. The volume change due to magnetization is known as volume magnetostriction. The alignment of a thermally agitated spin system by a strong applied field can also change the value of the first term. The volume change due to this phenomenon is known as forced magnetostriction. The third term which is due to the crystal anisotropy also contributes to volume magnetostriction but its value is small compared to that due to the second term. The shape of the specimen also affect the volume magnetostriction due to the formation of free poles or the magnetostatic energy, and the phenomenon is called the form effect. The volume magnetostriction is isotropic. It is the second term which plays a significant part in the magnetostriction during the magnetization process of ferromagnets due to the rotation of the magnetization vector in the crystal. This is the magnetostriction that forms the basis of the present study. The second term can be written in terms of α_i and β_i - the direction cosines of spontaneous magnetization and the lattice strain respectively (Chikazumi, 1964).

$$W = \ell(r)\left[\left(\sum_{i=1}^{3} \alpha_i \beta_i\right)^2 - \tfrac{1}{3}\right] \qquad 2.19$$

The energy thus expressed is called magnetoelastic energy

E_{magel}. Magnetoelastic energy is a linear function of strain tensor components and is counter-balanced by the elastic energy E_{el}. The minimization of the total energy $E = E_{magel} + E_{el}$, yields an expression for magnetostriction for a particular structure. A typical magnetostriction expression for a cubic crystal is

$$\frac{\delta \ell}{\ell} = \frac{3}{2}\lambda_{100}\left\{\sum_{i=1}^{3}\alpha_i\beta_i^2 - \frac{1}{3}\right\} + 3\lambda_{111}(\alpha_1\alpha_2\beta_1\beta_2 + \alpha_2\alpha_3\beta_2\beta_3 + \alpha_3\alpha_1\beta_3\beta_1) \qquad 2.20$$

where the β's are the direction cosines of the direction in which the strain is observed and λ_{100} and λ_{111} are the strains along the [100] and [111] directions respectively. The representation of magnetostriction will be discussed in Chapter 4.

Magnetostrictive strain increases with applied field and attains a maximum saturation value as shown in Figure 2.10. At first, on increasing the field from zero, a displacement of the 180 degree domain walls takes place in the demagnetized ferromagnet, in both cubic and uniaxial hcp crystals, which does not contribute towards strain. Domain structure is discussed in the next section. Then in the cubic system, the displacement of 90 degree walls also takes place during which strain may occur and finally the specimen becomes a single domain with the magnetization direction along the easy axis. Further increase in the field rotates the magnetization towards the external applied field direction. The saturation magnetostriction strain corresponds to the strain due to rotation of magnetization from easy directions to the field

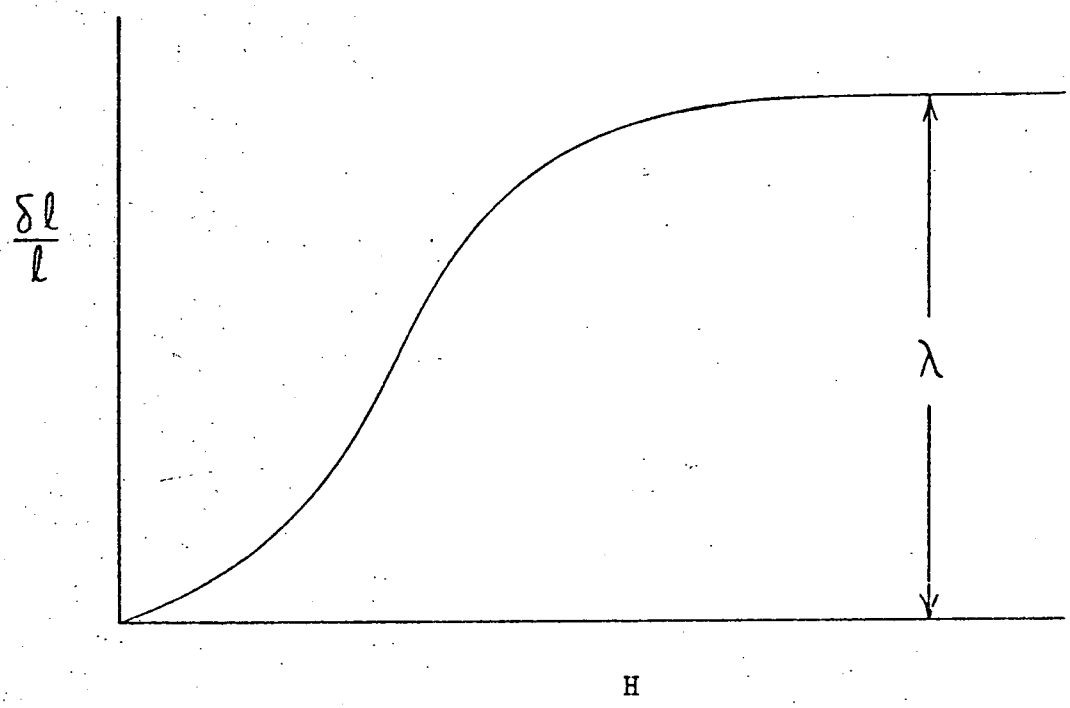

Fig. 2.10 Magnetostriction as a function of the field intensity (after Chikazumi, 1964).

direction.

2.9 Domains

Ferromagnetic and ferrimagnetic materials may be found in the demagnetized state despite the existence of spontaneous magnetization. Weiss (1907) explained the situation by assuming the existence of small regions, uniformly magnetized in the preferred direction and oriented in such a way as to give zero overall magnetization. These uniformly magnetized regions are known as domains. Domains are separated by thin layers in which the direction of magnetization gradually changes from the orientation in one domain to that in the other. The transitional boundary between the domains is called a domain boundary wall. Domains are formed to reduce the very high magnetostatic energy due to the formation of free poles at the surface which would occur if the specimen were magnetized in the same direction i.e. as in the single domain case. The sub-division of the specimen into smaller domains reduces the magnetization energy, yet the process is restricted by the other internal energies; the creation of the domain wall itself needs energy. The process of sub-division continues until the energy required to establish an additional boundary is greater than the reduction in magnetostatic energy gained by sub-division into further smaller domains. A domain wall must have a finite width. Abrupt change in the magnetization across a single atomic plane between the domains involves extremely high exchange energy. The rotation of the spin vector

takes place gradually in small steps over a number of atomic planes known as the wall thickness (Bloch, 1932). Figure 2.11 shows the transition in spin orientation for a 180 degree Bloch wall, i.e. a domain boundary between two domains with antiparallel magnetization where the rotation occurs about the wall normal. At the same time a domain wall cannot be infinitely thick due to the anisotropy energy which does not favour spins oriented away from the easy direction. Domain wall thicknesses and their energy were extensively treated by Lifshitz and Landau, (1935). The formation of free poles is often avoided by small secondary domains as shown in Figure 2.12. These domains prevent any leakage of magnetic flux and are known as closure domains. Magnetostriction may also influence the domain structure. A further term in the energy expression originates from the magnetostrictive strain and is known as the magnetoelastic energy. This must be included in any energy minimization. Domain structure is also modified around inclusions to avoid free poles. Various modified domain structures are shown in Figure 2.13. If the size of the crystal is reduced, the domain wall energy increases relatively until a stage is reached where the formation of the domain wall is energetically unfavoured and the specimen then behaves as a single domain. There is in fact a large variety of domain structure. Except in very simple systems, it is very difficult to predict the exact domain structure

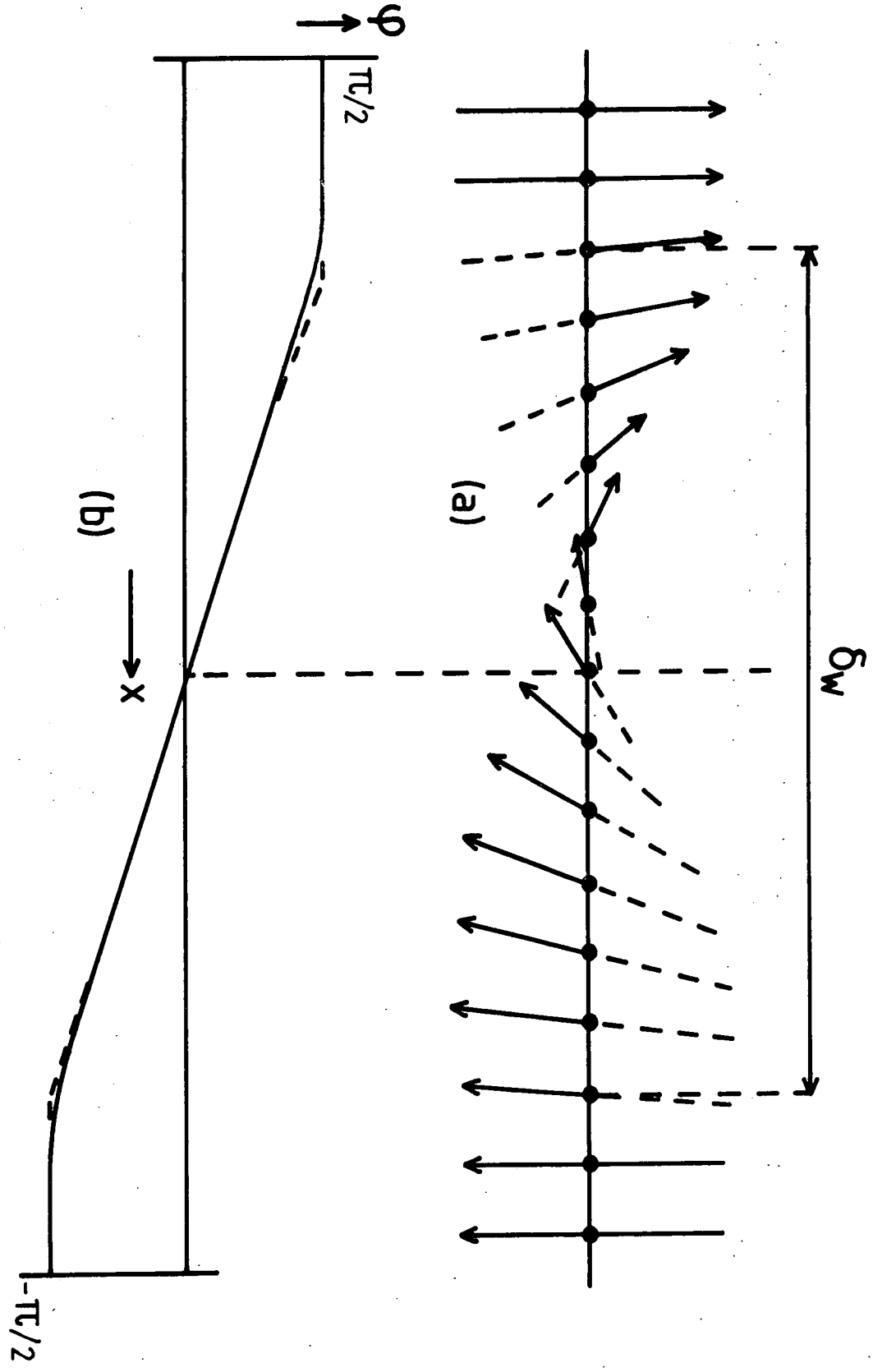

Fig. 2.11 (a) Spin configuration inside a Bloch wall
(b) Angle of deviation ϕ as a function of position (after Smit and Wijn, 1959).

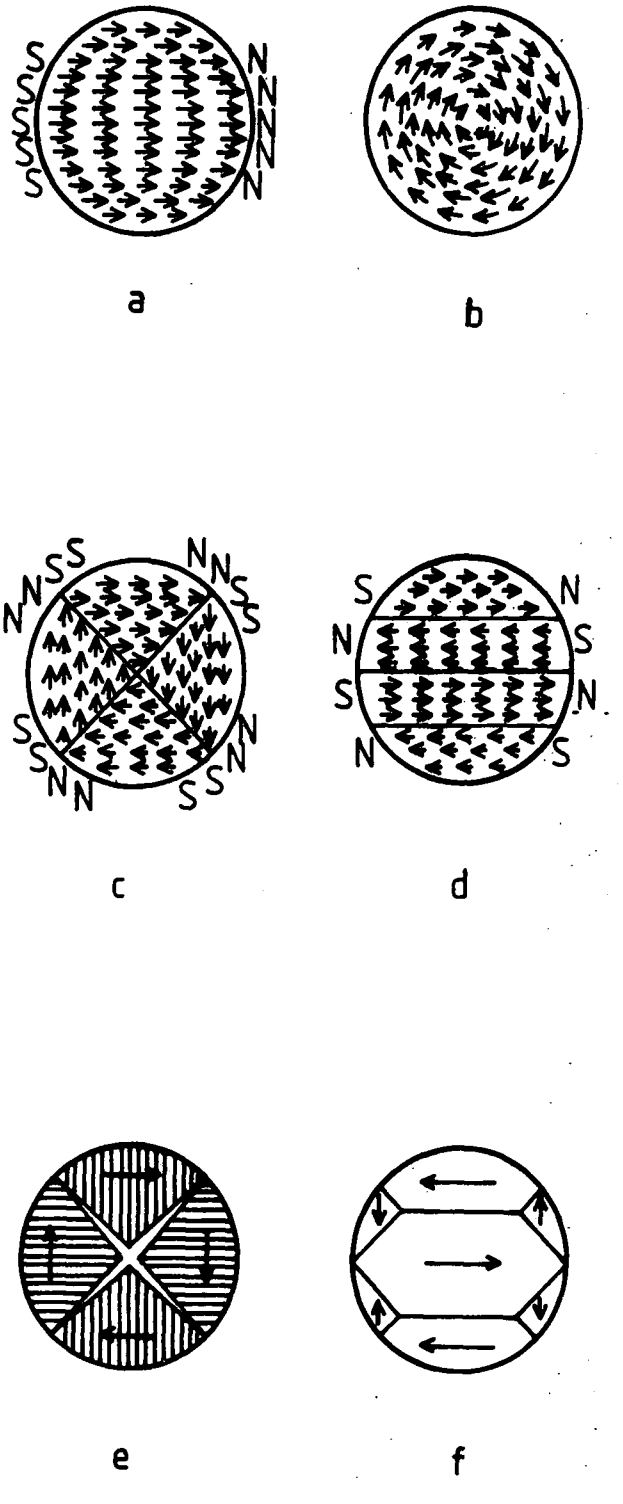

Fig. 2.12 Examples of Weiss domain configuration in which flux closure occurs (a) single domain structure, domain structure of a material with (b) small crystal anisotropy (c) large crystal anisotropy (d) uniaxial anisotropy (f) large magnetostriction, and (e) tendency of domain deformation for a material with positive magnetostriction (after Chikazumi, 1964).

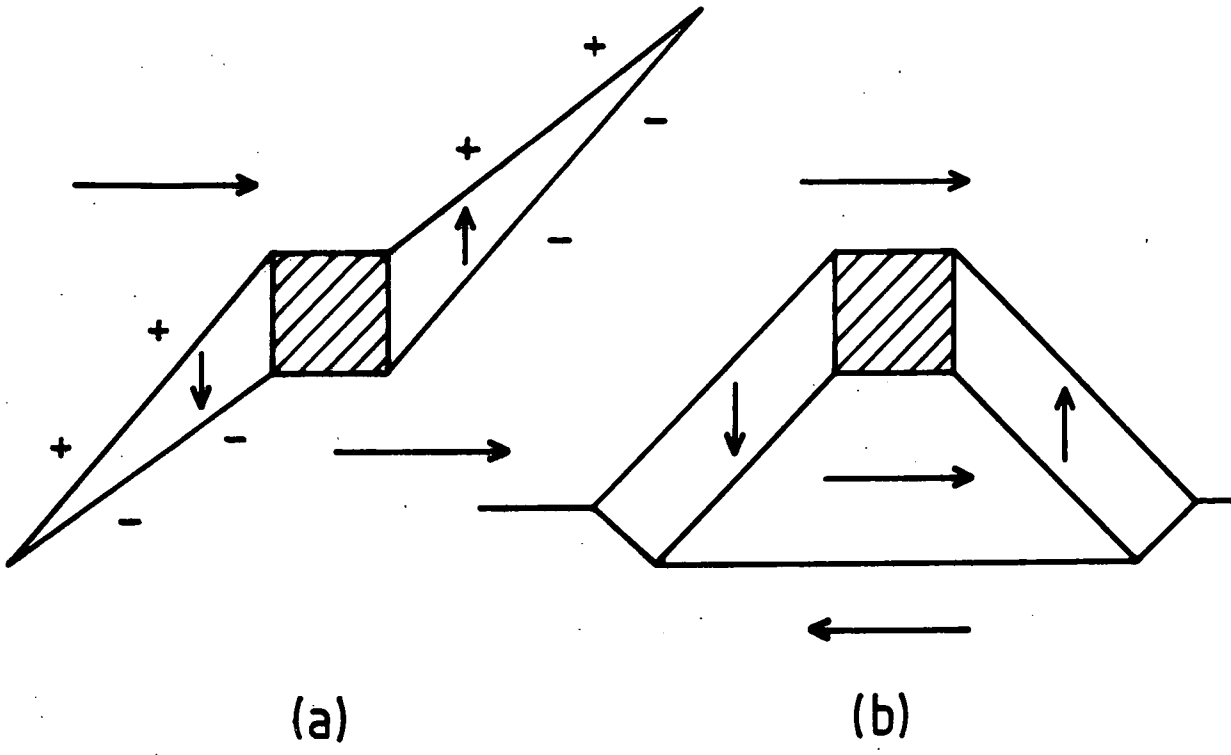

(a) around an isolated inclusion

(b) in the presence of a Bloch wall near the inclusion

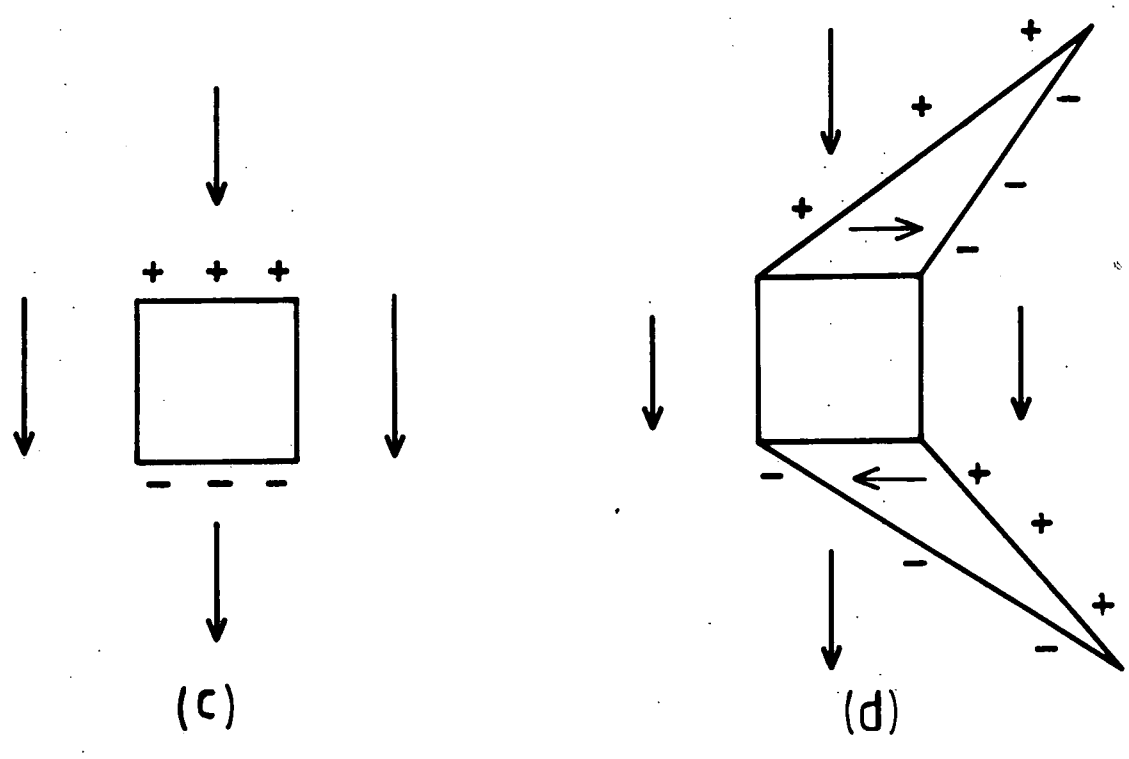

(c) the surface poles associated with a cavity lying within a domain

(d) the reduction of the surface pole density by a secondary domain structure

Fig. 2.13 Modification of the domains (a & b after Lifshitz and Landau, 1935, and c & d after Williams et al., 1949).

but observed structures can usually be understood on the basis of the minimization of the sum of the various energies of the magnetic system.

$$W = W_{ex} + W_k + W_\lambda + W_M + W_\gamma \qquad 2.21$$

where W_{ex} is the exchange, W_k is anisotropic, W_λ is magnetoelastic, W_M is magnetostatic and W_γ is the domain wall energy. The application of the field in the simplest case causes displacement of the domain walls such that the domain with magnetization direction close to the field grows at the cost of other domains, as shown in Figure 2.14. Finally the specimen becomes a single domain and possesses a technical saturation magnetization. A very small field only may be required for this process. Imperfections of one kind or another hinder the movement of domain walls and result in smaller initial permeabilities and large coercive forces. Further increase in the field rotates the domain magnetization towards the field direction. This process needs comparatively a much stronger field and indeed very high fields are needed in the case of strongly anisotropic materials to rotate the magnetization towards the hard direction. Domains can be experimentally observed by the Bitter method (1931) in which fine particles of magnetic powder are spread on the surface of the specimen. The magnetic field gradient near the domain boundaries attracts the particles towards the boundaries and reveals the domain configuration which can be photographed through

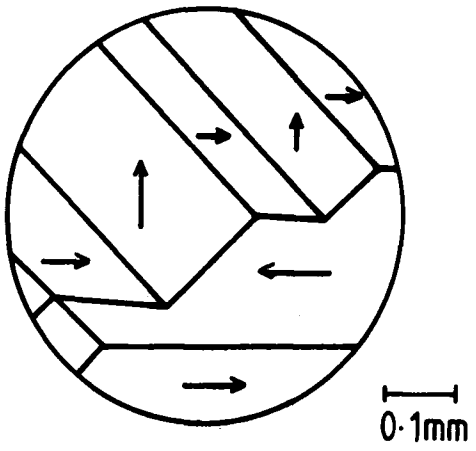

(a)

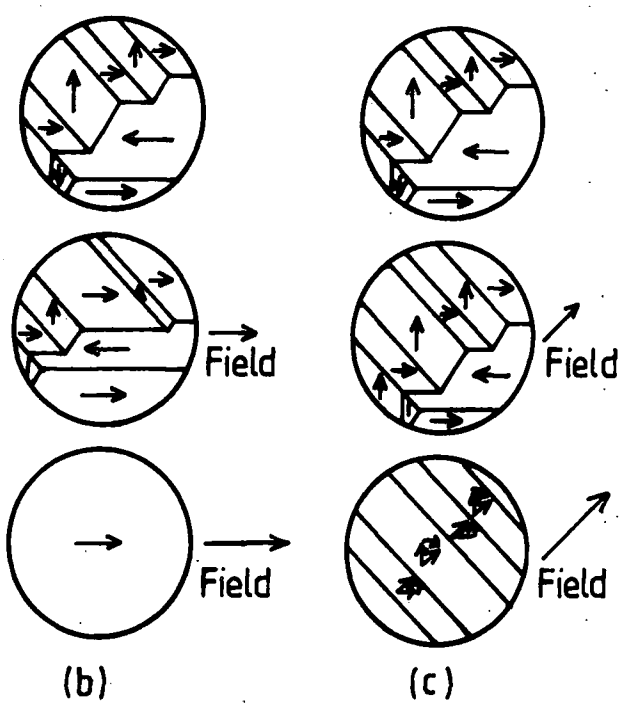

Fig. 2.14 Domain wall displacement and rotation of magnetization:
(a) initial configuration,
(b) magnetization in [100], and
(c) magnetization in [110] directions.
(after Chikazumi, 1964).

a microscope. The magnetic powder is usually in colloidal suspension in a liquid (a ferrofluid). Other techniques used for domain studies include the Kerr and Faraday methods based on rotation of the polarization of reflected or transmitted light, electron beam techniques and X-ray diffraction topography (Tanner, 1976).

TABLE 2.1

Magnetic structures and transition temperatures of the heavy earth metals (after Crangle, J., 1977).

Element	
Gd	ferromagnet $\xrightarrow[293]{}$ paramagnet
Tb	ferromagnet $\xrightarrow[220]{}$ helix $\xrightarrow[230]{}$ paramagnet
Dy	ferromagnet $\xrightarrow[85]{}$ helix $\xrightarrow[179]{}$ paramagnet
Ho	cone $\xrightarrow[20]{}$ helix $\xrightarrow[132]{}$ paramagnet
Er	cone $\xrightarrow[20]{}$ antiphase cone $\xrightarrow[53]{}$ sinusoidal collinear $\xrightarrow[85]{}$ paramagnet
Tm	square-wave collinear $\xrightarrow{\sim 35}$ sinusoidal collinear $\xrightarrow[58]{}$ paramagnet
Yb	paramagnet

CHAPTER 3

PHYSICAL AND MAGNETIC PROPERTIES OF RARE EARTHS

3.1 Introduction

The rare earths are a group of metallic elements consisting of scandium, yttrium, lanthanum and the lanthanides. The lanthanides are the fourteen elements lying between atomic numbers 57 and 71 of the periodic table. They are trivalent 4f shell transition metals. After element 57, electrons are gradually added to the inner 4f electronic shell of the atom as the atomic number increases, leaving the number of valence electrons undisturbed. The rare earth elements have very similar chemical properties. Their magnetic properties stem from unpaired electrons in the 4f shell. The rare earths are further subdivided into two groups; the light rare earths which are elements up to europium and the heavy rare earths, from gadolinium to lutetium. Almost all the rare earths crystallize in a hexagonal close packed structure. At room temperature, light rare earths have double hexagonal close packed structure with the exception of samarium which has rhombic and europium with bcc structure. The heavy rare earths have simple hexagonal close packed structure with the exception of yttrium which is fcc at room temperature but at low temperature is hcp. At higher temperature these elements undergo transitions in structure through fcc to bcc. Basic physical properties at room temperature of the rare earths are given in Table 3.1.

TABLE 3.1

Room temperature physical properties of the rare earth metals and their melting and boiling points*; dhcp = double-hexagonal close-packed, fcc = face-centered cubic, bcc = body-centered cubic, hcp = hexagonal close-packed

Rare earth metal	Z	Crystal structure	Lattice constants (Å) a_0	c_0	Metallic radius (Å)	Atomic volume** (cm^3/mol)	Density (g/cm^3)	Melting point (°C)	Boiling point (°C)
La	57	dhcp	3.7740	12.171	1.8791	22.603	6.145	918	3464
Ce	58	fcc	5.1610	—	1.8247	20.698	6.770	798	3433
Pr	59	dhcp	3.6721	11.8326	1.8279	20.804	6.773	931	3520
Nd	60	dhcp	3.6582	11.7966	1.8214	20.584	7.007	1021	3074
Pm	61	dhcp	3.65	11.65	1.811	20.248	7.260	1042	~ 3000
Sm	62	rhomb†	3.6290	26.207	1.8041	20.001	7.520	1074	1794
Eu	63	bcc	4.5827	—	2.0418	28.981	5.243	822	1529
Gd	64	hcp	3.6336	5.7810	1.8013	19.904	7.900	1313	3273
Tb	65	hcp	3.6055	5.6966	1.7833	19.312	8.229	1356	3230
Dy	66	hcp	3.5915	5.6501	1.7740	19.006	8.550	1412	2567
Ho	67	hcp	3.5778	5.6178	1.7661	18.753	8.795	1474	2700
Er	68	hcp	3.5592	5.5850	1.7566	18.450	9.066	1529	2868
Tm	69	hcp	3.5375	5.5540	1.7462	18.124	9.321	1545	1950
Yb	70	fcc††	5.4848	—	1.9392	24.843	6.965	819	1196
Lu	71	hcp	3.5052	5.5494	1.7349	17.781	9.840	1663	3402
Sc	21	hcp	3.3088	5.2680	1.6406	15.041	2.989	1541	2836
Y	39	hcp	3.6482	5.7318	1.8012	19.894	4.469	1522	3338

* After Beaudry and Gschneidner (1978).

** Data for coordination number 12.

† Rhombohedral is the primitive cell. The close-packed layer stacking is ABABCBCAC with symmetries chhchhchh in nine layers.

†† Low temperature form is hcp.

Table itself is after Legvold (1980).

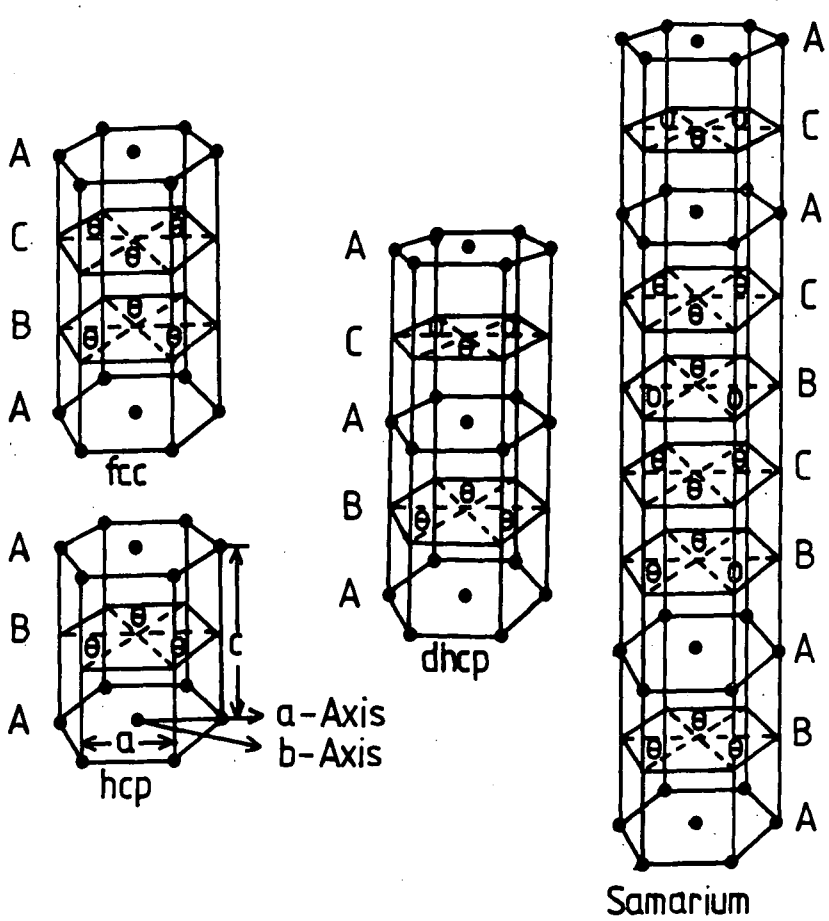

Fig. 3.1 Close packed stacking arrangements found in rare earth metals (after Legvold, 1980).

Eu, Er, Tm and Lu show no transitions. The several close packed atom stacking arrangements found in rare earths are shown in Figure 3.1.

3.2 Preparation and Purification of Rare Earths

Rare earths, with the exception of scandium, have not been found in nature in ores containing a single element alone. Natural deposits usually contain a mixture of various rare earth elements. Common deposits of minerals rich in rare earths are monazite, zenotime, bastnaesite, gadolinite and smarskite. Physical properties of the elements vary with impurity content. To study their intrinsic properties, high purity is very important. High purity in the rare earth is achieved by using starting materials and reducing agents as pure as possible and then purifying the product. Electrolytic methods for preparing rare earth metals produce reasonably pure metals. The other very successful method for producing highly pure rare earths is metallothermic reduction. In this technique the rare earth oxides from the minerals are converted to florides by anhydrous HF and 60% Ar. The rare earth floride is then reduced by Ca at temperatures above the melting point when the metals settle down and CaF_2 slag floats. Residual floride and other volatile impurities are removed by vacuum melting in which the metals are heated in vacuum to temperatures of between 500 to 1000 degrees Centigrade above the melting point.

Rare earth metals are further purified by distillation leaving behind the less volatile impurities. The highest

purity is achieved by the solid state electrotransport method. In this process a large d.c. current is passed through a rod made of the metal to be purified, at a temperature 100 to 200 degrees Centigrade below the melting point of the metal. The electric field transports the impurities to one end of the rod. The process is carried out under very high vacuum or in a pure inert gas and takes several weeks or even months. The rate of transport of impurities increases the greater the electric field but the maximum field is limited by the cooling rate of the rod. Only those rare earths which have low vapour pressures at the melting point can be purified by this method. Jordan (1974) reviewed the principle of this method while Peterson (1971) has discussed the experimental details. Peterson and Schmidt (1972) studied the electrotransport velocities of C, N, and O in gadolinium whilst Carlson et al. (1975) have studied their impurity concentration. Extensive studies are being made by Jones and co-workers at the University of Birmingham. Jordan et al. (1975) purified commercial Tb by the electrotransport method. Hukin and Jones (1976) refined Tb by zone melting in an atmosphere of pure argon with induction heating. Large grains are obtained if the samples purified by the electrotransport method are maintained at a high temperature for a long time. Other methods for growing single crystals include recrystallization, vapour deposition, Bridgeman and Czochralski and zone melting processes.

3.3 Electronic Structure of Rare Earths

The electronic configuration of the rare earths (lanthanides) has the Xenon structure ($1s^2 2s^2 2p^6 3s^2 3p^6 3d^{10} 4s^2 4p^6 4d^{10} 5s^2 5p^6$) with two or three outer valence electrons ($6s^2$ or $5d6s^2$) and a gradually filling electron shell $4f^N$, where N is a number from zero to fourteen. The 4f electrons are relatively closely bound to the nucleus and are shielded by the eight $5s^2$ $5p^6$ electrons. In salts the valence electrons are readily transferred to other ions while in metals they form the conduction band. Thus normally the rare earth ions are tripositive with all electrons in the closed shells except for the 4f electrons. With the exception of Eu and Yb, the mean ionic radius continuously decreases with increasing Z because of the further contraction of the 4f electrons shell caused by the greater positive charge Z of the nucleus as the atomic weight increases. This behaviour is known as lanthanide contraction and is shown in Figure 3.2. The total ionic angular momentum J is given by Hund's rules; (i) the lowest lying electronic state for the electrons in an incomplete shell having same n, ℓ quantum numbers has maximum multiplicity 2S + 1 within the constraint of Pauli's exclusion principle and (ii) the maximum orbital angular momentum consistent with this multiplicity, (iii) the total angular momentum J is given by J = L-S for less than half filled shell (light rare earth) and J = L+S for more than half filled shell (heavy rare earths). Strong spin-orbit

coupling of the 4f electrons results in low magnetic moments for the light rare earths and high magnetic moments for heavy rare earths. Theoretical saturation magnetic moments gJ in terms of the Bohr mangeton μ_B for tripositive rare earths are shown in Figure 3.3, g is the Landé factor. In energy band calculations of the rare earth metals the Hamiltonian for the many electrons in a solid can be written as

$$\mathcal{H}_{coul} = \sum_i \frac{P_i}{2m} - \sum_i \sum_\ell \frac{Ze^2}{|r_i - X_\ell|} + \sum_i \sum_{j \neq i} \frac{e^2}{r_i - r_j} \qquad 3.1$$

where r_i, P_i are the position and momentum of the ith electron, X_ℓ is the position of ℓth nucleus , m and e are the mass and charge of the electron and Z is the nuclear charge. The Hartree-Fock approximation is employed to transform this many body problem into a one body problem using the Slater determinant wave functions (Slater, 1965, 1967). This reduces the problem to an independent electron one, neglecting electron-electron correlation of opposite spin electrons. The electrons move in an average periodic potential due to the ions and all the other electrons. The exchange potential is

$$V_{xa} = -e^2 \sum_b \int \frac{\phi_b^*(r')\, \phi_a(r')\chi_b}{|r - r'|}\, dr'^3\, \frac{\phi_b(r)}{\phi_a(r)} \qquad 3.2$$

where $\phi_a(r)$ is the orbital part and χ is the spin part of the basis function Slater determinant.

In the augmented plane wave method, the wave functions for the Schrodinger equation are spherical waves inside

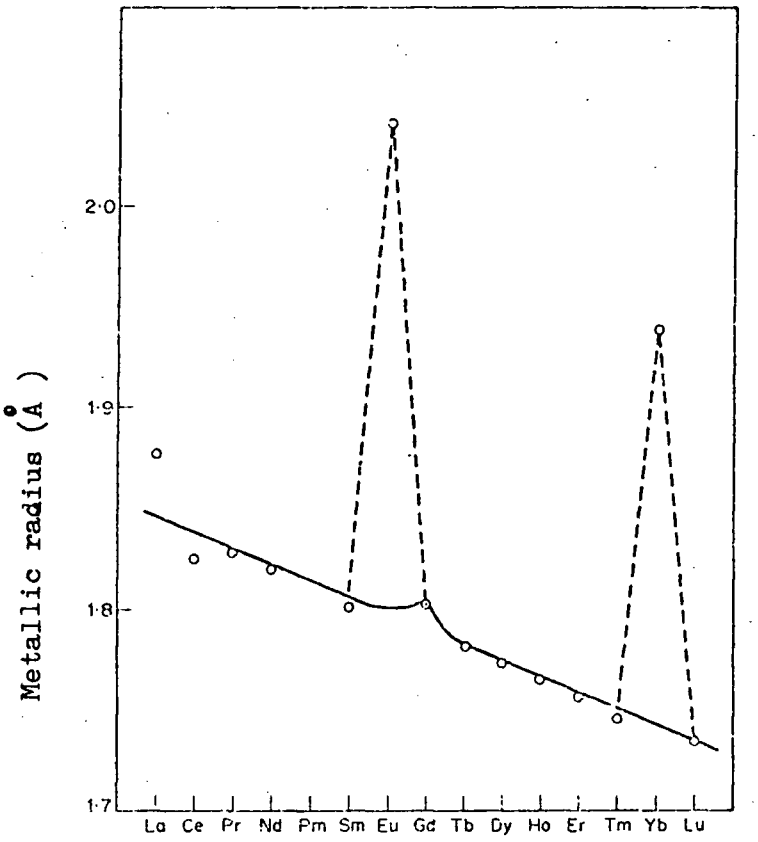

Fig. 3.2 Variation of the metallic radius of the rare earth elements, the Lanthanide contraction (after Taylor and Darby, 1972).

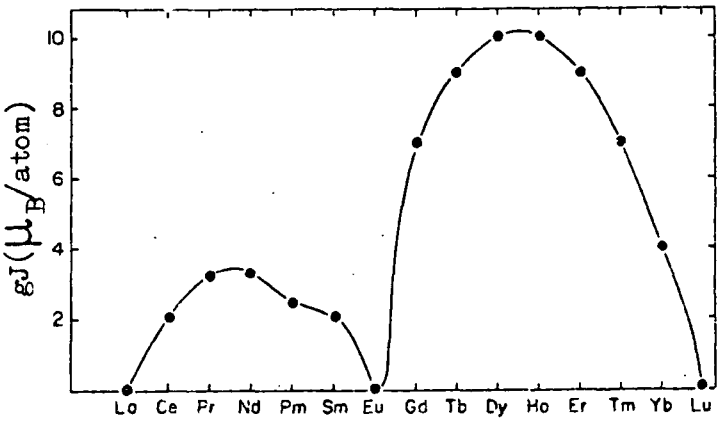

Fig. 3.3 Theoretical gJ saturation magnetic moments for tripositive rare earth ions in Bohr magnetons, μ_B, per atom (after Legvold, 1980).

the muffin tin (MT) sphere and are plane Bloch type waves outside the sphere. The wave function inside MT is

$$\psi_k^1(r) = \sum_{\ell,m} C_\ell^m R^\ell Y_\ell^m(r) \qquad 3.3$$

where A_ℓ^m are crystal field parameters and $Y_\ell^m(r)$ are the spherical harmonics, r is measured from the centre of the MT sphere. The function outside the MT sphere is

$$\psi_k^{11}(r) = \sum A_n \exp\,(i(k + k_n).r\,) \qquad 3.4$$

where k_n are reciprocal lattice vectors.

The two wave functions are matched at the surface of the MT spheres which gives linear relation between C_ℓ^m and A_n. Dimmock and Freeman (1964) calculated the paramagnetic bands for Gd which explains the observed anisotropy in the electrical resistivity.

3.4 Magnetic Properties

The 4f electron wave functions are confined close to the nucleus and are very localized. The direct Heisenberg exchange interaction does not occur. The magnetic order observed in rare earths is due to an indirect interaction (RKKY) via conduction electrons. The observed polarization of the conduction electrons supports this interaction. The RKKY interaction was discussed in Chapter 2 Section 2). Neutron diffraction studies reveal the magnetic structure. Koehler (1972) presents a review of this work. The magnetic structure of the heavy rare earths at various temperatures is shown in Figure 3.4. Gadolinium is a simple ferromagnet with a half filled

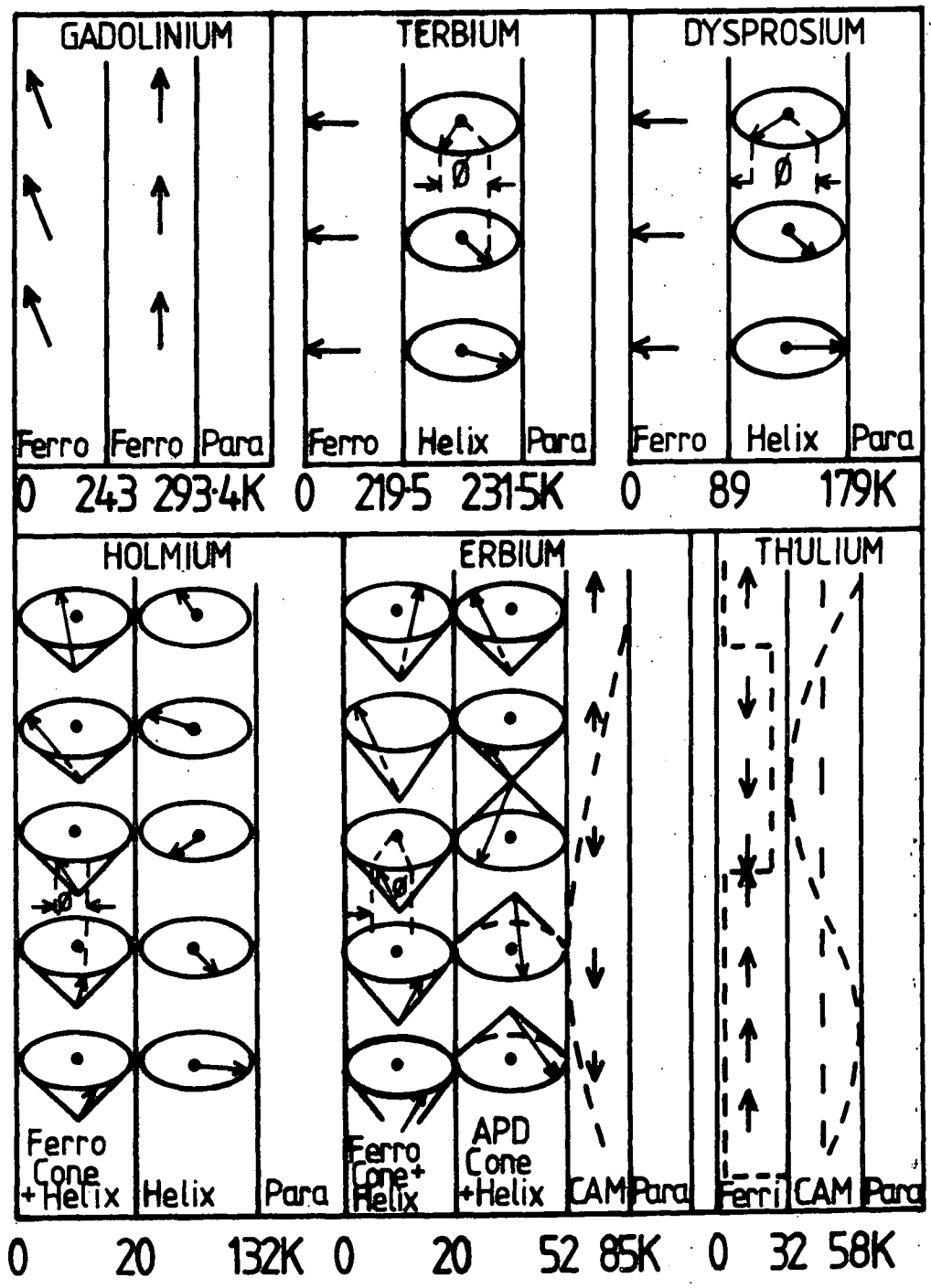

Fig. 3.4 Magnetic ordering in the heavy rare earths as found by neutron diffraction (after Legvold, 1980).

4f electron shell and has S = 7/2. The easy direction is along the $\hat{c}$-axis just below the Curie temperature T_c and moves away forming an easy cone around the $\hat{c}$-axis below 240K. Terbium has helical ordering between 230K to 219.5K. The magnetic moment lies in the basal plane. Below 219.5K it becomes ferromagnetic with the $\hat{b}$-axis as an easy direction. Dysprosium has similar magnetic ordering to terbium except that the $\hat{a}$-axis is easy. Dysprosium has helical structure below the Néel temperature 179K. The inter-layer turn angle is 43.2 degrees. The turn angle decreases with decreasing temperature and finally attains the value 26.5 degree at 89K - the Curie temperature T_c below which it is ferromagnetic (Wilkinson et al., 1961). The elements with Z higher than gadolinium have strong magnetic anisotropy due to the asymmetric charge distribution of 4f orbital electron wave functions. Holmium also has two magnetic transitions, its Néel temperature T_n is 133K and Curie temperature is 20K. The magnetic ordering between T_n and T_c is helical similar to terbium and dysprosium. In the ferromagnetic region it has a helical cone structure along the $\hat{c}$-axis with a cone angle of 80 degrees. It thus has a finite and constant component of magnetic moment along the $\hat{c}$-axis. The turn angle ϕ is 30degrees (Koehler et al., 1966). Erbium shows three magnetic transitions. At the Néel temperature, 85K, it undergoes a change from para to antiferromagnetic ordering. Below T_c = 20K it has the same magnetic structure

as of holmium in this temperature range. It has complex antiferromagnetic structure with another intermediate transition temperature T_H = 52K. Between T_n and T_H, it has a $\hat{c}$-axis modulated (CAM) magnetic structure. The magnetic moment in CA M remains along the $\hat{c}$-axis but its magnitude varies sinusoidally along the $\hat{c}$-axis. The period of oscillation is constant having 7 magnetic layers (Cable et al., 1965). Between an intermediate temperature T_H and T_c, there is another complex antiferromagnetic structure showing an antiphase domain cone plus a helix. Several layers have a constant magnetic moment pointing along the $\hat{c}$-axis followed by the same numbers of layers with the same magnetic moment pointing downwards. Thulium has the CAM magnetic structure between 58 and 32K and below 32K it has ferromagnetic structure. The magnetic moment always remains parallel to the $\hat{c}$-axis.

3.5 Gadolinium

This is the only rare earth element which is a simple ferromagnet. The magnetic moment rises sharply when it is cooled below its Curie temperature 293.4K (Wohlfarth, 1980) in the presence of a small magnetic field. The moment falls off and becomes a minimum at 170K due to the easy direction moving away from the $\hat{c}$-axis and then rises again on further cooling. Earlier measurements by Nigh et al. (1964) are found to be in agreement with the later neutron diffraction studies of Cable and Wollen (1968) and with the torque measurements on single crystals by Corner and Tanner, (1976). Their measurements are

shown in Figure 3.5 (a and b). Legvold et al. (1953) measured the electrical resistivity of polycrystalline Gd whilst Nigh et al. (1963) studied a single crystal of gadolinium. The temperature variation of the electrical resistivity ρ of Gd polycrystals and of Gd single crystals are shown in Figure 3.6 and 3.7 respectively. Nigh et al. (1963) showed that the saturation magnetization follows a $T^{3/2}$ law between 50 to 200 K and a $T^{2.2}$ law below 50K. Roeland et al. (1975a) and White et al. (1975) measured the saturation magnetization of gadolinium as $7.63\mu_B$ while the expected value would be $gJ\mu_B = 7\mu_B$. This slight increase in the measured value is thought to be due to the polarization of the 5d conduction electron band. The paramagnetic effective moment found by Nigh et al. was $7.98\mu_B$ which agrees with the expected value of $g\sqrt{S(S+1)} = 7.94\mu_B$. The paramagnetic Curie temperature of gadolinium is isotropic and equal to 317K both parallel and perpendicular to the $\hat{c}$-axis. ($\theta_{||} = \theta_{\perp} = \theta_p = 317K$). The specific heat measurements by Griffel et al. (1954), Voronel et al. (1966), Lewis (1970), Simons and Salamon (1974) and Wells et al. (1975) all show good correlation with the resistivity behaviour. The results of Griffel et al. (1954) along with those of Jennings et al. (1960) for lutetium (showing the phonon contribution) are given in Figure 3.8. The dashed curve represents the magnetic specific heat.

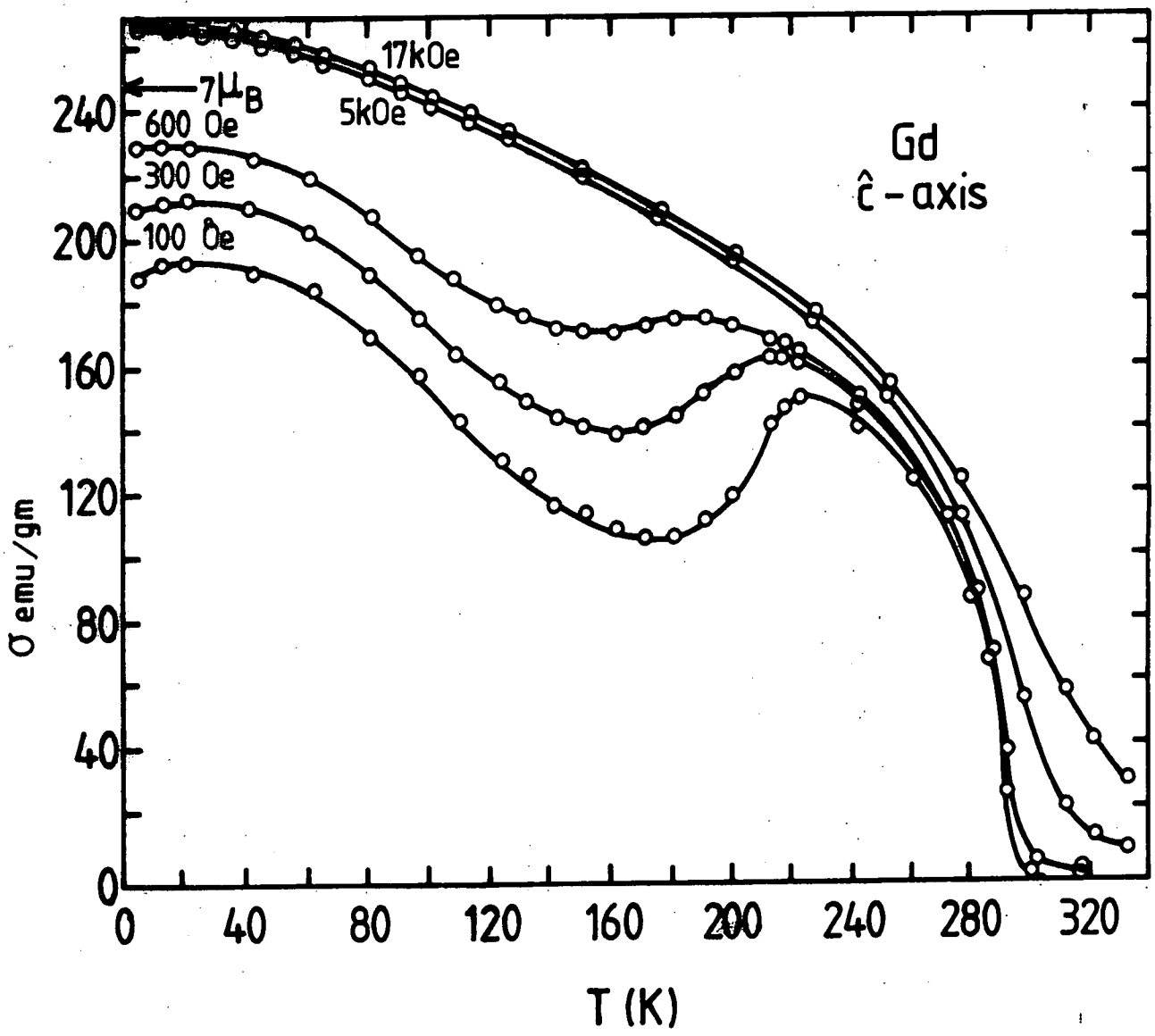

Fig.3.5 (a) Isofield magnetization data for Gd in the $\hat{c}$-axis direction found by Nigh et al., 1963).

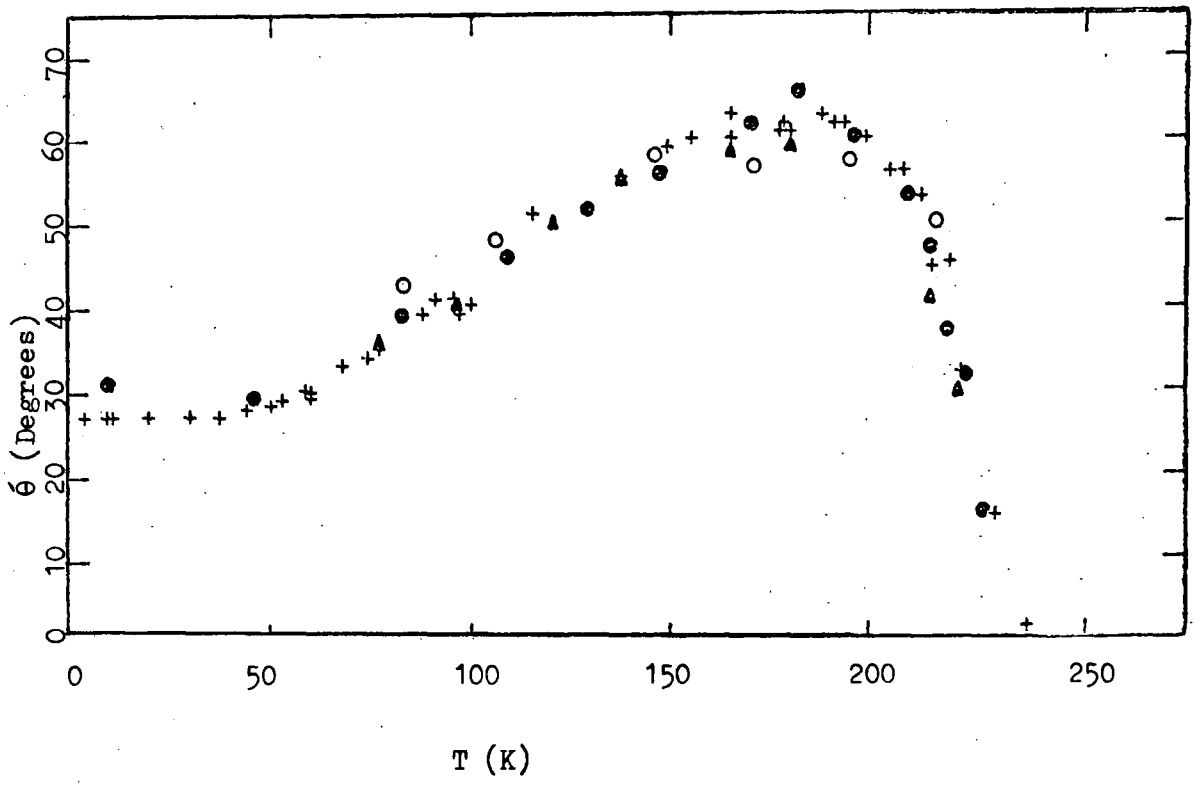

Fig. 3.5 (b) The temperature dependence of the angle of easy cone in Gd,
• (002) reflection, o (100) reflection
from neutron diffraction measurements of
Cable and Wollan,(1968).
+ 0·85 T, infinite field extrapolation
torque magnetometer measurements and the figure
itself are from the work of Corner and Tanner (1976).

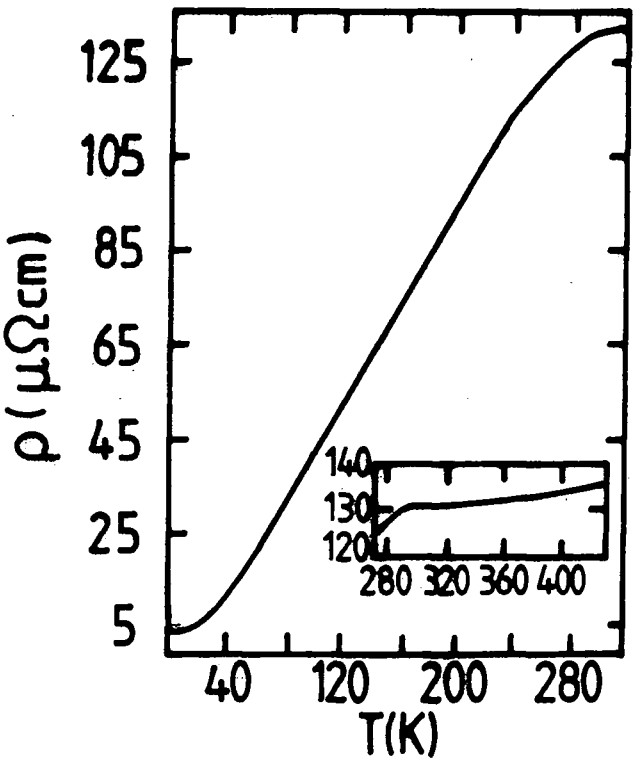

FIG. 3·6 Thermal dependence of the resistivity of gadolinium polycrystals (after Colvin et al., 1960).

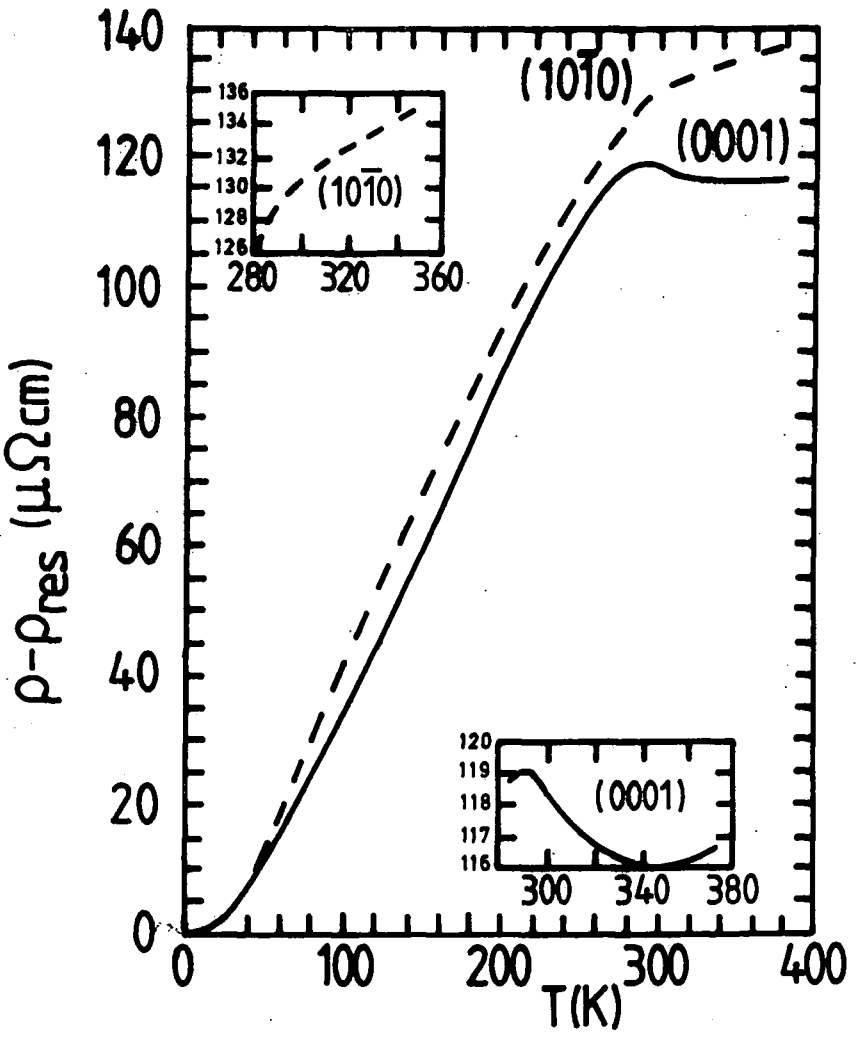

FIG. 3·7 Thermal dependence of the resistivity of Gd single crystals along the $\hat{b}$- and $\hat{c}$-axes. The residual resistivity is subtracted (after Nigh et al., 1963).

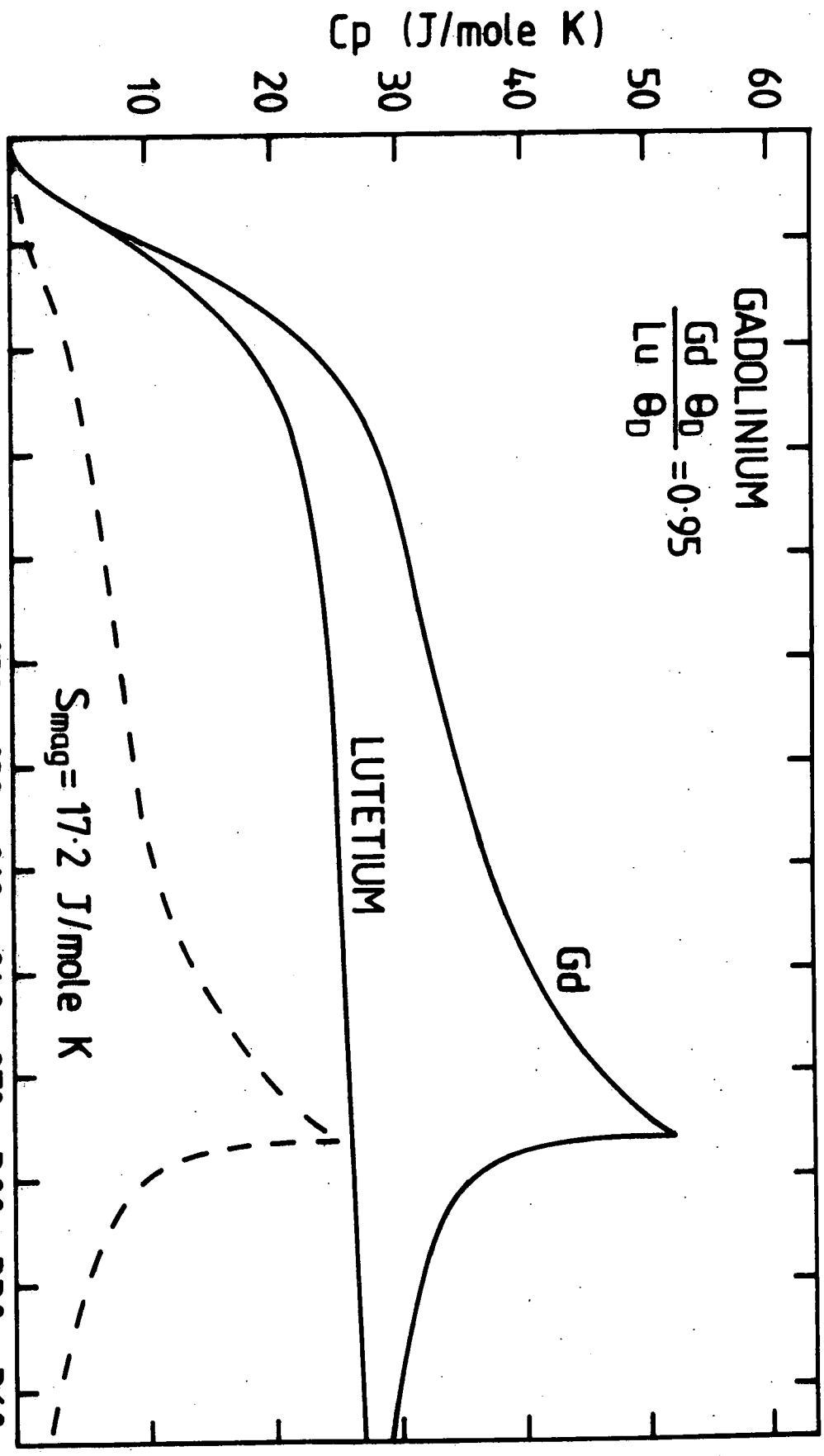

Fig. 3.8 Specific heat of Gd and of Lu. The dashed curve is the magnetic contribution to the specific heat of Gd (Gd after Griffel et al., 1954 and Lu after Jennings et al., 1960).

3.6 Terbium

This has two magnetic transitions like the other heavy rare earths. The turn angle in the helical structure between 219.5K to 230K decreases slightly with temperature from 20 degrees just below the Néel point to 18 degrees before rising again at the Curie temperature. Terbium is a strong basal plane anisotropic element. It requires a very high magnetic field to magnetize it along the $\hat{c}$-axis and it is even possible that in this attempt at magnetization it might suffer sudden recrystallization. The other heavy rare earths also show similar behaviour. The helical phase can be suppressed by an external field of 0.8 Tesla. The saturation magnetic moment found by the high field - low temperature extrapolation method is 9.34 μ_B against an expected value of gJ = 9.0μ_B (Roeland et al., 1975a). The surplus 0.34μ_B is a lot less than the 0.63μ_B of Gd and it is assumed that the addition of the 4f orbital moment causes a decrease in the overlap of the 5d conduction electrons and 4f wave functions. The paramagnetic susceptibility of Tb is anisotropic, higher in the basal plane than along the $\hat{c}$-axis. The paramagnetic Curie temperature along the $\hat{c}$-axis θ_p is equal to 195K and in the basal plane θ_p = 239K. These results of Hegland et al. (1963) are shown in figure 3.9. Kasuya (1966) attributed this anisotropy to the crystal field. The electrical resistivity measurements of Hegland et al. (1963) are shown in Figure 3.10. The spin disorder resistivity part, after subtraction of the phonon contribution is shown by the dotted curve.

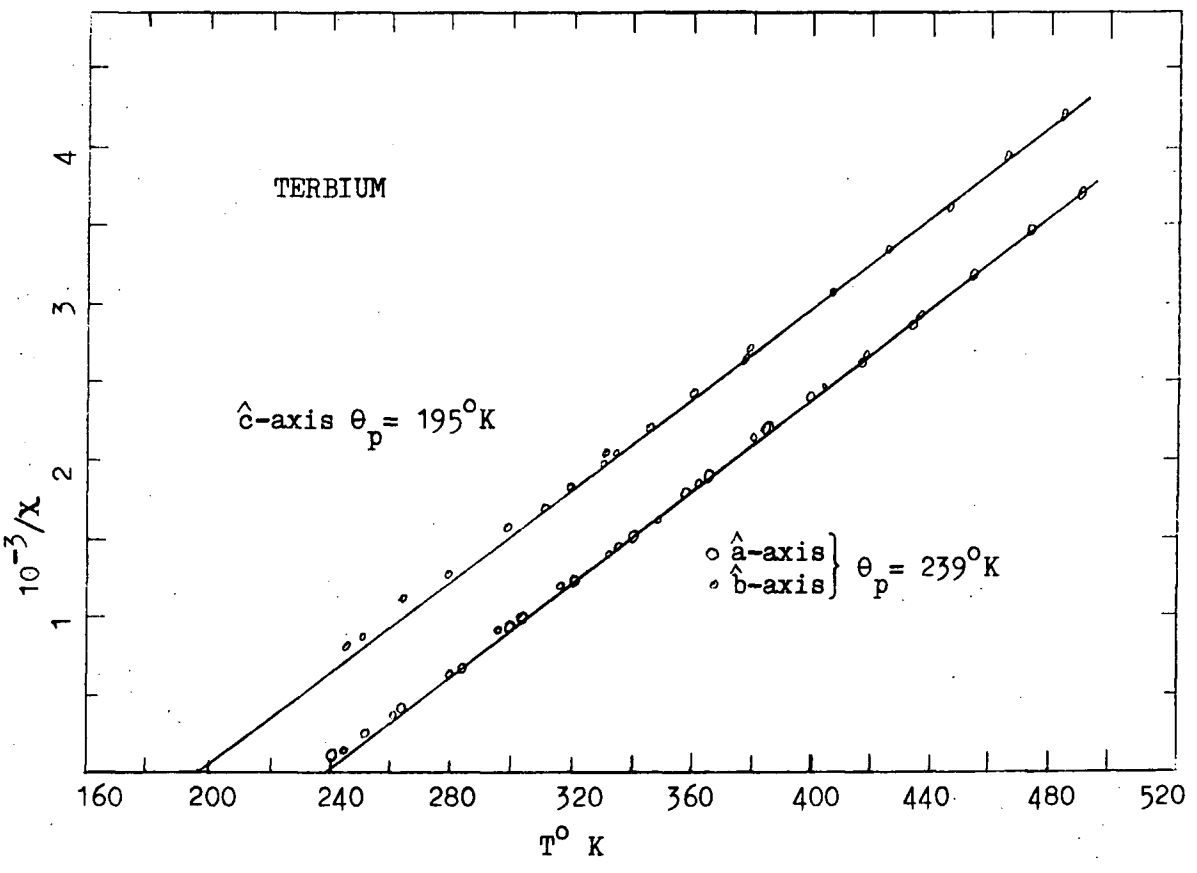

Fig. 3.9 The reciprocal of the paramagnetic susceptibility of $\hat{a}$-, $\hat{b}$-, and $\hat{c}$-axis samples of Tb versus temperature (after Hegland et al., 1963).

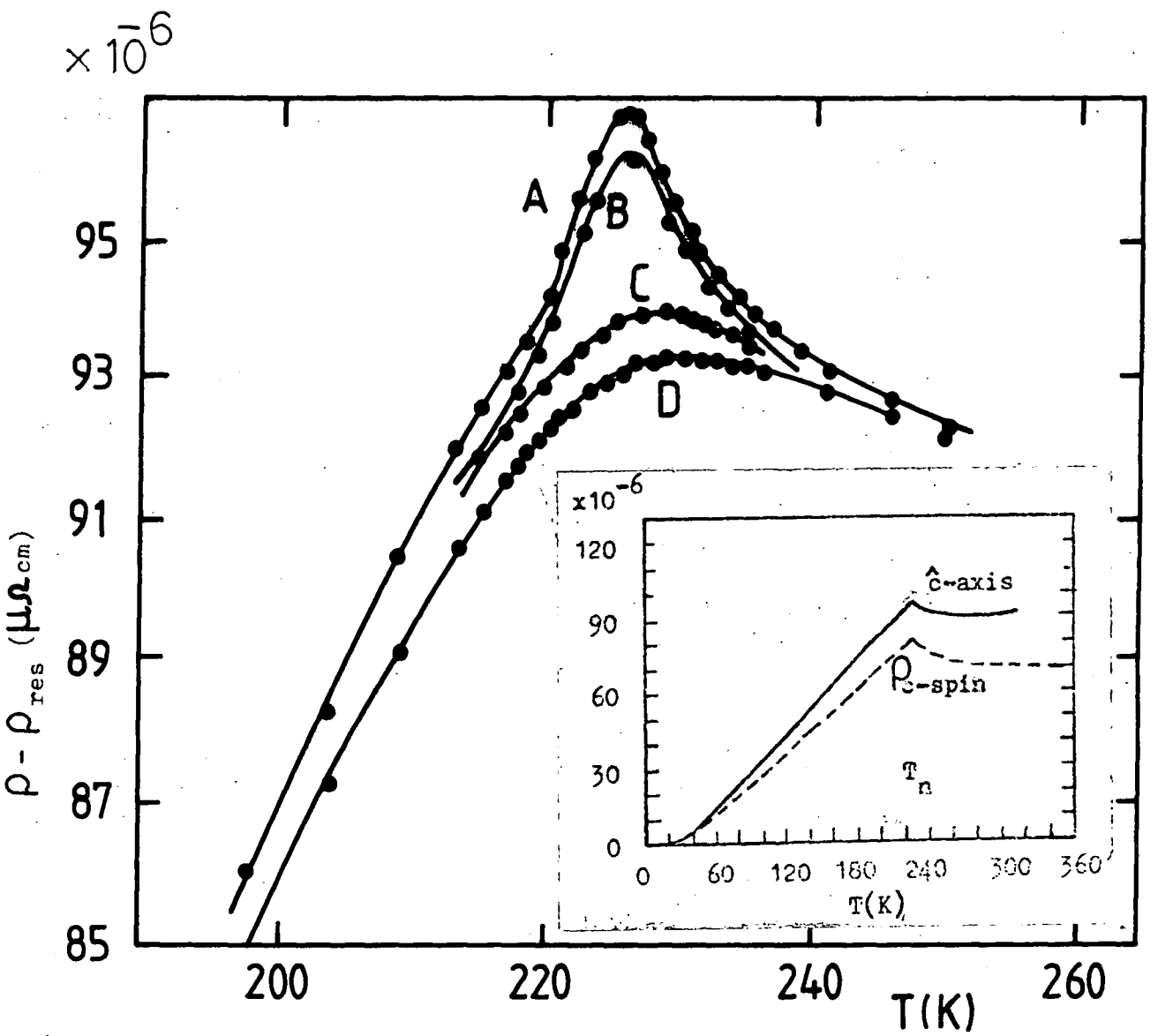

Fig. 3.10 The electrical resistivity of Tb along $\hat{c}$-axis versus temperature for various magnetic fields along $\hat{b}$-axis. The residual resistivity ρ_{res} is subtracted. The curves A, B, C, and D correspond to fields of 0, 858, 6700, and 11350 Oe respectively (after Hegland et al., 1963).

An external field suppresses the helical phase and results in broadening of the peak at T_n. Later resistivity measurements by Sze et al. (1969), Nellis and Legvold (1969) confirmed the spin wave energy gap of width 1.9Mev. Jennings et al. (1957) measured the specific heat of terbium over a wide range of temperature and their results are shown in Figure 3.11. A slight kink at 219.5K correspond to θ_c while the sharp peak at 228K coincides with the Néel temperature. Again the dotted curve shows the magnetic part of the specific heat after subtraction of the phonon and electron parts.

3.7 Binary Rare Earth Alloys

Rare earths form solid solutions with each other with the exception of Eu and Yb. The alloying of a heavy rare earth metal with a lightrare earth causes competition between the two crystal structures hcp and dhcp favoured by heavy and light rare earths respectively. Around the middle concentration of heavy and light rare earth alloys the samarium structure is observed. Legvold et al. (1977a) observed that the saturation magnetic moment of alloys of gadolinium with Sc, Y, La, Mg, Yb and Th correlated with the c/a ratio of the sample but the drop in the ordering temperature showed a linear relationship with residual resistivity and not with c/a. Fujiwara et al. (1977) studied a large number of intra-heavy rare earth alloys. Legvold (1978a) plotted ordering temperature versus average spin factor $C_1S_1(S_1 + 1) + C_2S_2(S_2 + 1)$ which followed the straight line established by the pure

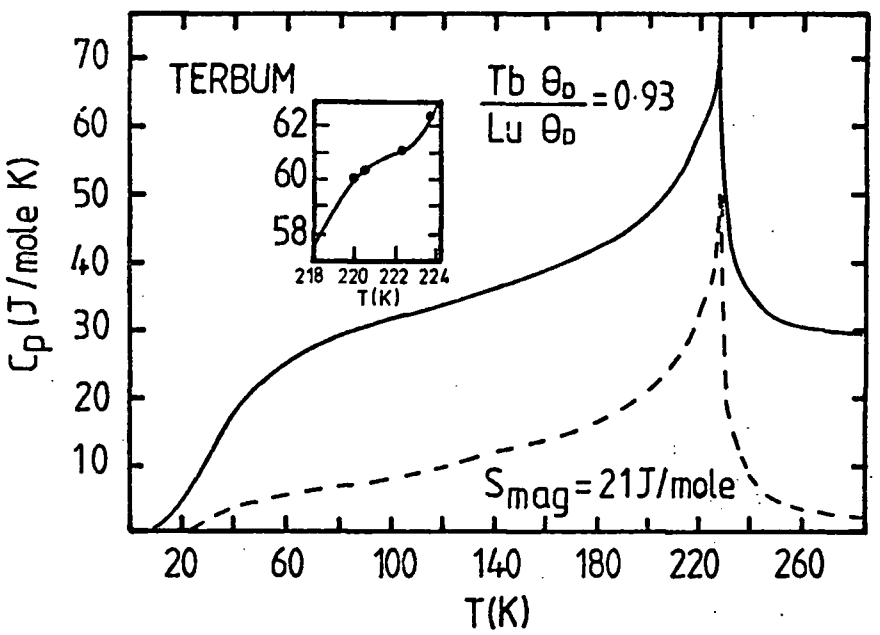

Fig. 3.11 Specific heat of terbium versus temperature. Dashed curve gives the magnetic contribution. (after Jennings et al., 1957).

elements. Here C_1 and C_2 are the atomic concentration of the alloy components. Legvold et al. (1979a) measured the residual resistivity of one atomic percent of heavy rare earths in thorium and found that the atomic volume difference between the host and solute was a major contributor to the residual resistivity. On adjusting the spin only resistivity data of Makintosh and Smidh (1962) for the volume effect, the resistivity was found to be proportional to $S(S + 1)$. Earlier Bozorth (1967) observed that the magnetic ordering temperatures were proportional to the two third power of the average de Gennes factor G of the alloys. Ordering temperatures observed by Fujiwara et al. (1977) are shown in table 3.2.

3.8 Gadolinium Based Alloys

The alloys which have de Gennes factor $G > 11.5$ remain ferromagnetic without any intermediate antiferromagnetic phase. Gadolinium is the only metal which has $G > 11.5$. The gadolinium based alloys can be ferromagnetic at all temperatures in the magnetically ordered region. The magnetization versus temperature curve is continuously decreasing for a ferromagnetic phase only. If an antiferromagnetic phase exists, a peak occurs at the Néel temperature. Thoburn et al. (1958) studied Y-Gd alloys. Their results showed that Y-Gd alloys have only the ferromagnetic phase for gadolinium concentrations of 70% or more, only the antiferromagnetic type for gadolinium concentration of less than 60% and two types of magnetic ordering in the intermediate region for 60 to 70 percent gadolinium. The

TABLE 3.2

Pressure effect on magnetism of heavy rare earth alloys. After Fujiwara et al. (1977)

	$\langle S(S+1)\rangle$	T_c	T_t	T_N	θ_p	$\frac{\Delta T_c}{\Delta P}$	$\frac{\Delta T_t}{\Delta P}$	$\frac{\Delta T_N}{\Delta P}$	$\frac{\Delta \theta_p}{\Delta P}$	n_{eff}	$\frac{1}{n_{eff}}\frac{\Delta n_{eff}}{\Delta P}$	Magnetic structure†
		(K)				(10^{-3} deg bar^{-1})					(10^{-6} bar^{-1})	
Gd	15.8	292.6			304	−1.56			−1.46	8.1		
Gd–50% Tb	13.9	262.4			270	−1.30				9.0		
Tb*	12			230.0	230			−0.86	−0.75	9.7	−0.96	HS
Gd–25% Dy	14	265.0			274	−1.10				8.8		
Gd–50% Dy	12.3	233.0			240	−1.00				9.5		
Gd–75% Dy	10.55		155.2	203.0	203		−1.06	−0.66	−0.51	10.2	−0.50	HS
Dy*	8.8		87.6	178.0	148		−1.28	−0.44	−0.17	10.7	−0.62	HS
Gd–25% Ho	13.35	253.8			265	−1.20				8.7		
Gd–25% Ho	10.9		172.0	206.7	213		−0.84	−0.76	−0.83	9.5	0.55	HS
Gd–75% Ho	8.95			168.6	158			−0.54	−0.40	10.1	−0.10	HS
Ho*	6.0			125.0	87			−0.40	−0.39	11.0	0.06	HS
Gd–25% Er	12.8	247.3			255	−1.05				8.4		
Gd–50% Er	9.8		171.0	184.8	200		−0.48	−0.66	−0.68	8.4	0.40	CAM
Gd–75% Er	6.8			131.8	111			−0.46	−0.72	9.4	0.60	CAM
Er*	3.8			82.0	39			−0.24	−0.53	10.2	0.34	CAM
Tb–50% Dy	10.4		150.8	204.4	201		−0.96	−0.61	−0.46	10.2	−0.80	HS
Dy–25% Ho	8.1			166.5	143			−0.42	−0.09	11.0	−0.50	HS
Dy–50% Ho	7.4			154.7	126			−0.40	−0.12	11.0	−0.30	HS
Dy–75% Ho	6.7			141.5	108			−0.40	−0.26	11.0	−0.05	HS
Dy–25% Er	7.55			156.5	126			−0.41	−0.20	10.8	−0.38	HS
Dy–50% Er	6.3			132.2	94			−0.38	−0.32	10.6	−0.05	HS
Dy–75% Er	5.05			103.4	63			−0.30	−0.48	10.4	0.15	HS
Ho–25% Er	5.45			113.5	73			−0.35	−0.46	10.9	0.15	HS
Ho–50% Er	4.9			98.6	54			−0.34	−0.56	10.7	0.28	HS
Ho–75% Er	4.35			84.6	42			−0.28	−0.55	10.4	0.30	HS
Tm	2.0			58	−17					9.9		CAM

† HS = Helical screw structure, CAM = c-axis modulated.

* H. Fuji, 1969, J. Sci. Hiroshima University, ser. A-II 33, 43.

plot of Néel temperature T_n, the Curie temperature T_c and the paramagnetic Curie temperature θ_p for Y-Gd is given in Figure 3.12. The magnetic moment values per gadolinium atom in Gd-Y alloys were larger than the theoretical ones of tripositive Gd in both ferromagnetic and paramagnetic states. The values of ordering temperatures and magnetic moments after Thoburn et al. (1958) are given in Table 3.3. The hyperfine studies of Dreyfus et al. (1967) show that gadolinium remains in the normal trivalent state. The later neutron studies by Child and Cable (1969) showed that the Néel temperature of Gd-Y alloys follows reasonably well the mean curves of the Gd-R alloys as shown in Figure 3.13. The turn angle varies from 50 degrees for very small G to zero degrees for G = 11. Bagguley et al. (1980a) obtained the same results from magnetization and microwave studies.

In Gd-Lu alloys, the helical structure changes to ferromagnetic only in high magnetic fields for alloys containing more than 45% Lu while gadolinium rich alloys are only ferromagnetic (80% Gd or more), (Bozorth and Gambino, 1966). In 50% Gd-Lu alloys the helical phase changes into 'fan' structure 'FM1' at a crical field H_c and then to ferromagnetic 'FM2' above a higher magnetic field H_x. The magnetic moments are always larger than the theoretical $7\mu_B$ value, $0.55\mu_B$ excess for pure gadolinium to more than $1\mu_B$ in some alloys. A summary of Néel temperatures and Curie temperatures for various Gd-RE alloys as given

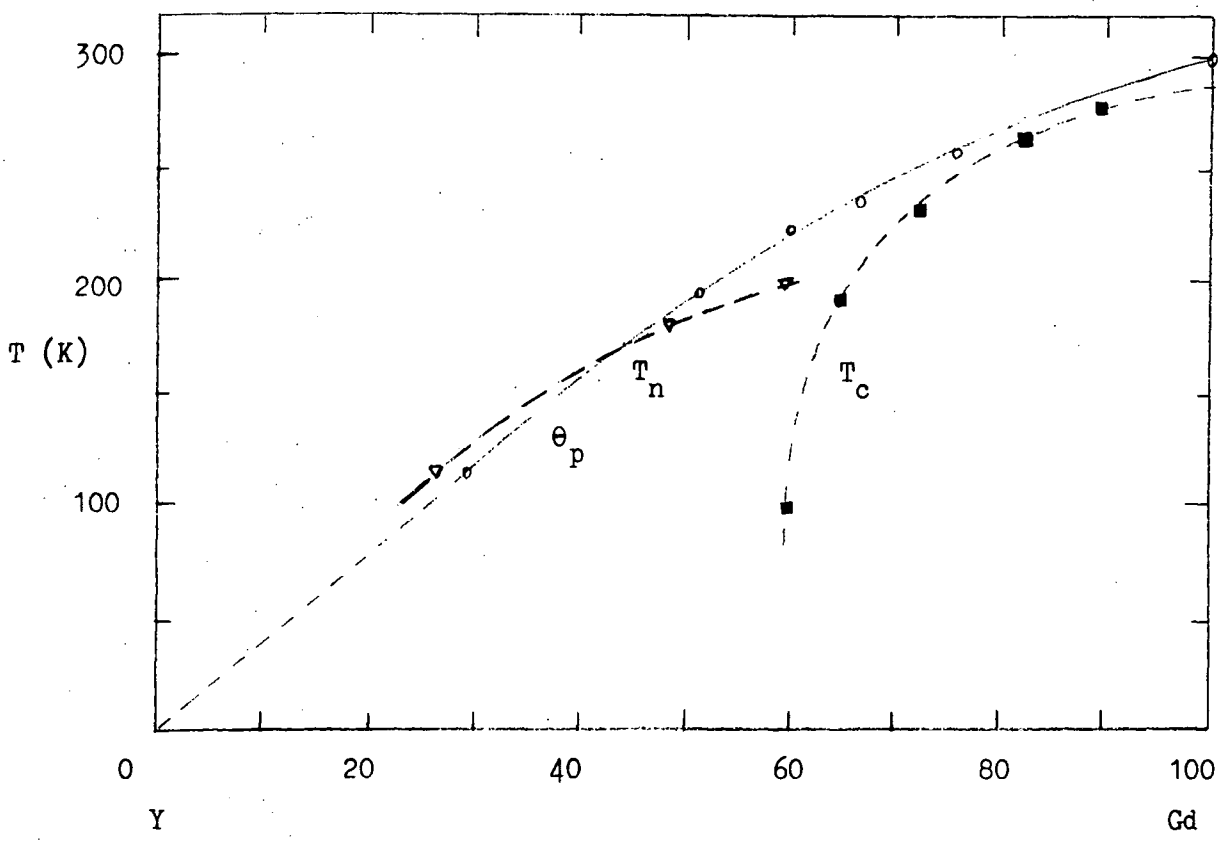

Fig. 3.12 Plot of the Néel temperature T_n, the ferromagnetic Curie temperature T_c (■), and the paramagnetic Curie temperature θ_p(o) in the Y-Gd system (after Thoburn et al., 1958).

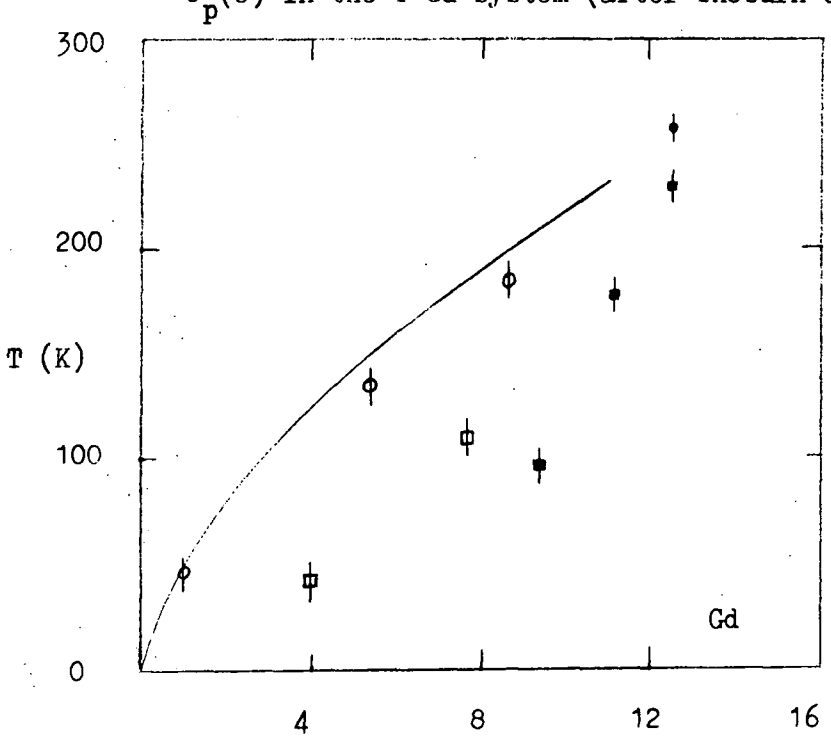

Fig. 3.13 The ordering temperatures versus de Gennes factor: T_n of Gd-Y (o) and Gd-Sc (□), and T_c of Gd-Y (●) and Gd-Sc (■). The full line represents the mean curve of T_n for Y-RE alloys. (after Child and Cable, 1969).

by Bozorth and Gambino (1966) is plotted in Figure 3.14. Bozorth and Suits (1964) observed T_n and T_c for Gd-Dy alloys by magnetization and resistivity measurements. The difference between T_n and T_c for 50% or more gadolinium concentration is shown in Figure 3.15. The magnetic behaviour of gadolinium alloys with Ho, Er or Tm is very close to Gd-Dy alloys (Bozorth and Gambino, 1966). In general gadolinium rich alloys are ferromagnetic while gadolinium weak alloys have at least one anti-ferromagnetic phase and T_n follows a universal law:

$$T_n = 46.7\ G^{2/3} \qquad 3.5$$

3.9 Terbium Based Alloys

Terbium alloys differ from those based on gadolinium because terbium has a Néel temperature T_n at 230K and ferromagnetic T_c at 219.5K. The helical structure disappears for 14% Nd, 6% Pr (Curry and Taylor, 1976), 5% La (Burgardt, 1976) and 2% Th (Burgardt and Legvold, 1975). At higher concentrations of light rare earths with terbium, the crystal structure changes to Sm type and causes large changes in the magnetic properties. The magnetic ordering temperature of terbium alloys with non magnetic Y, Lu (after Child et al., (1965) from neutron diffraction measurements) and Sc (after Child and Koehler, 1966) are shown in Figure 3.16. The magnetic phase diagram for terbium alloys with heavy rare earths, Dy, Ho, Er and Tm is shown in Figure 3.17. T_n and T_c for Tb-Dy varies linearly with alloy concentration (Fujiwara et

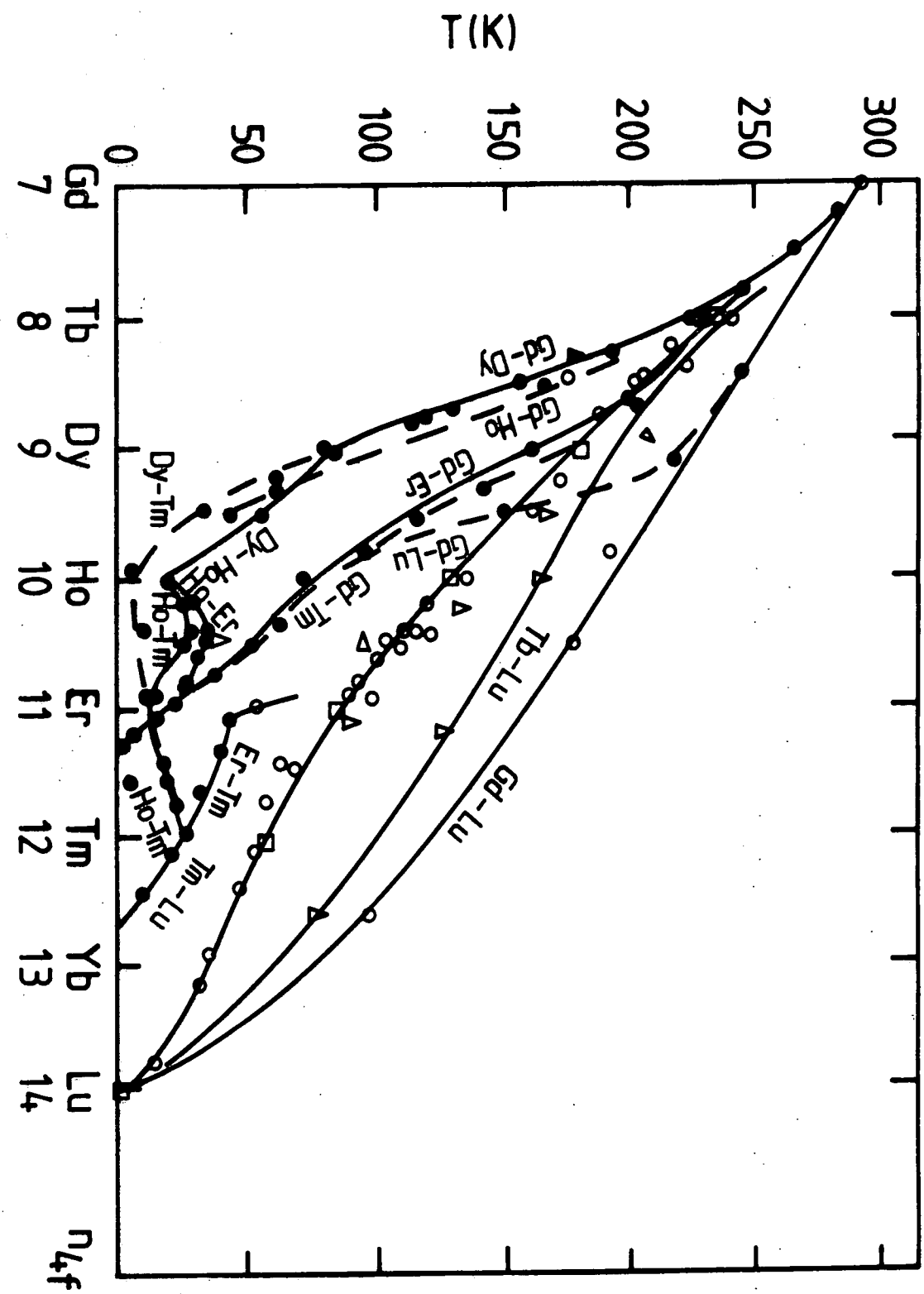

FIG 3·14 Plot of the Néel temperature of different alloys versus the number n of 4f electrons. The open symbols represent T_n and full T_C . (after Bozorth and Gambino, 1966).

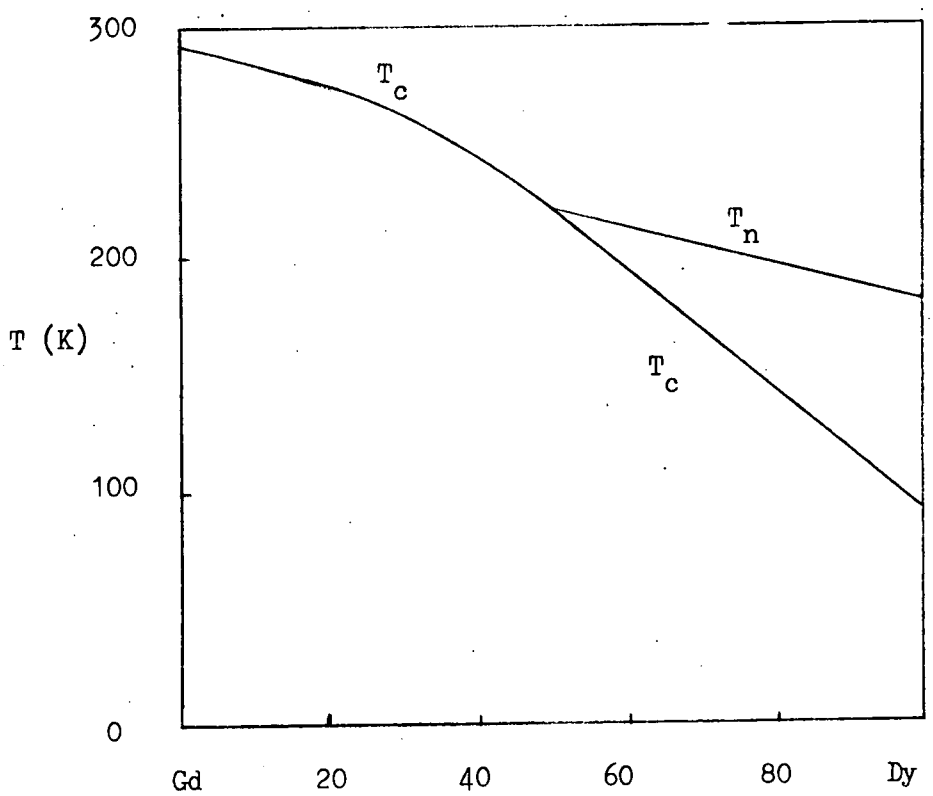

Fig. 3.15 The Néel temperature T_n and the Curie temperature T_c in the Gd-Dy system (after Bozorth and Suits, 1964).

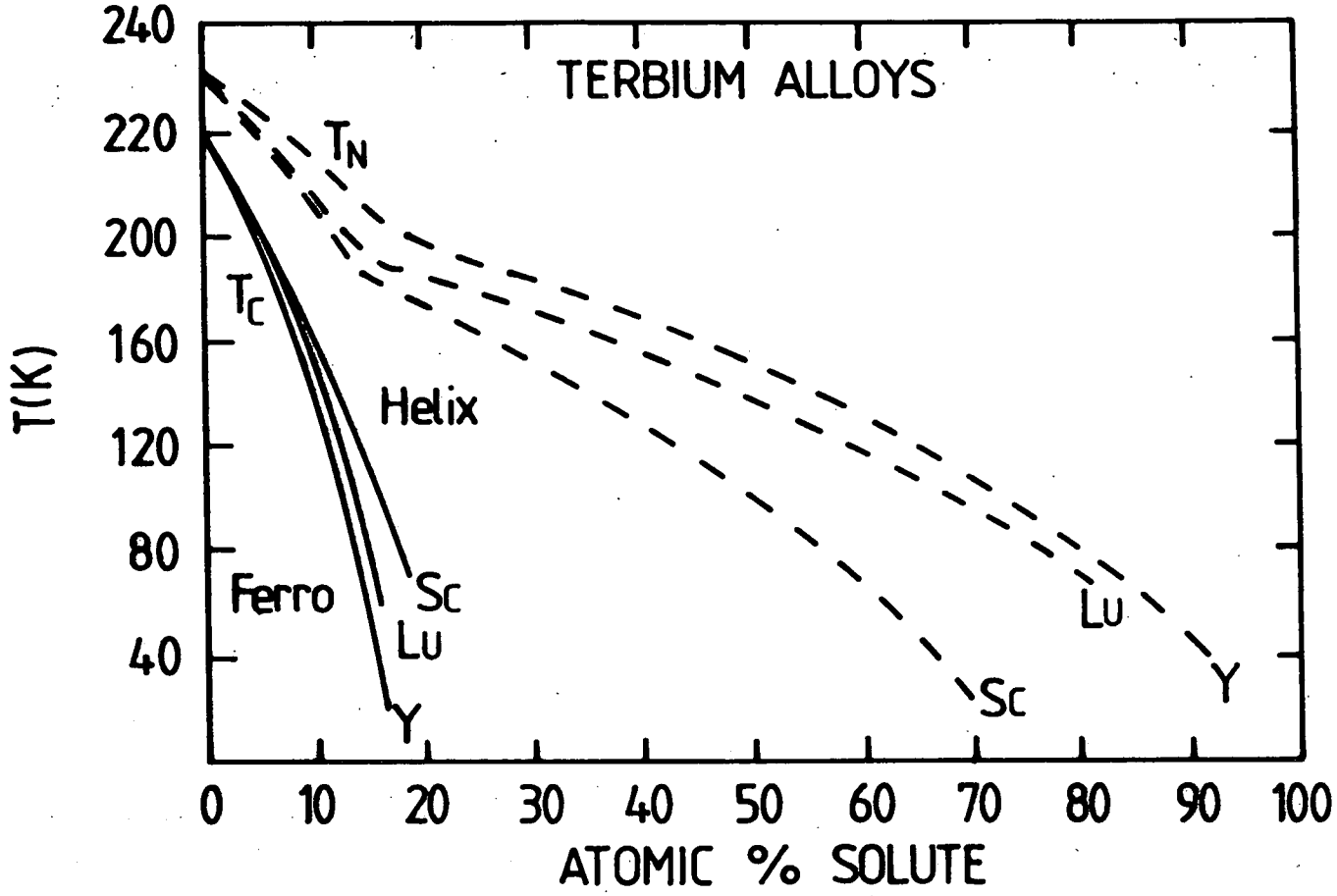

FIG. 3·16 Magnetic phase diagrams for Tb alloyed with Y, Lu, and Sc (after Child et al., 1965 and Child and Koehler, 1966).

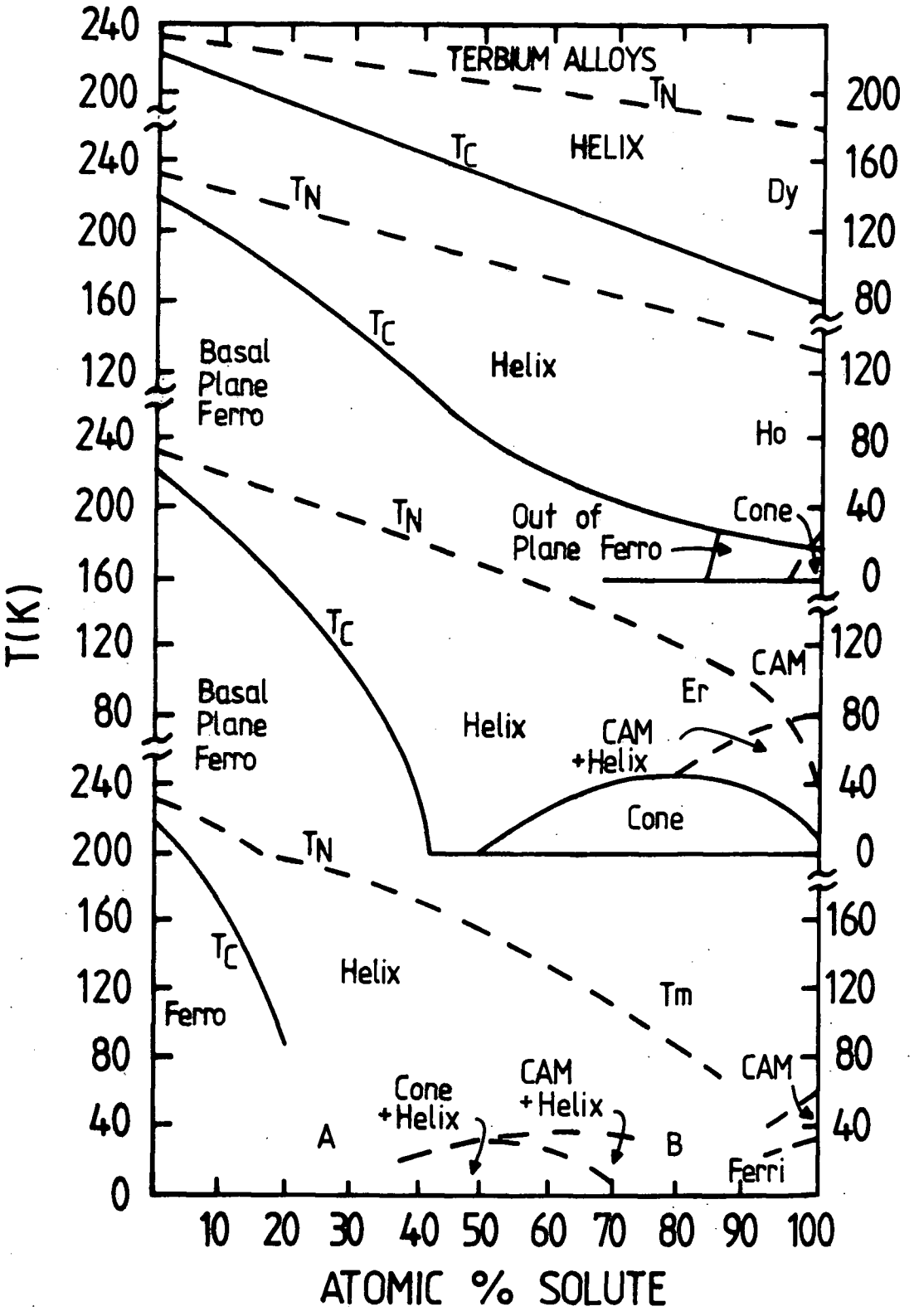

FIG. 3.17 Magnetic phase diagrams for Tb alloyed with Dy, Ho, Er, and Tm. After Koehler (1972) for Tb alloyed with Dy, Ho and Er. After Hansen and Lebech (1976) for Tb-Tm alloys.

al., 1977). For Tb-Ho only T_n is linear (Koehler, 1972). The situation is more complicated in the case of Tb-Er due to the difference in 4f charge densities. T_n varies smoothly until 90% Er concentration (Koehler, 1972). The T_n and T_c variation of Tb-Tm alloys shown in Figure 3.17 are after Hansen and Lebech, (1976). It was difficult to determine the ordering temperatures at the positions marked A and B.

TABLE 3.3

Magnetic moments and ordering temperatures in the Y-Gd system (after Thoburn et al., 1958).

Gadolinium percentage	T_n(K)	T_c(K)	θ_p(K)	$\mu_{sat}(\mu_B)$	$\mu_{eff}(\mu_B)$
25	111		102		8.66
50	182		186		8.49
60	197	95	217	7.79	8.63
66.7		211	229	7.63	8.84
75		241	252	7.63	8.84
83.3		262	266	7.55	8.72
90		281	280	7.47	8.84
100(Gd)		289	302.7	7.12	7.93

CHAPTER 4

FORMAL REPRESENTATION OF MAGNETIC ANISOTROPY AND MAGNETOSTRICTION

4.1 Magnetocrystalline Anisotropy

Magnetocrystalline energy, i.e. the energy required to magnetize a crystal in a specific direction with respect to crystallographic axes is given by

$$E_{k/V} = \int_{o}^{M_s} \underline{B}_o . d\underline{M} \qquad 4.1$$

where V is the volume of the crystal and $\underline{M}_s$ is saturation magnetization.

In a cubic system this energy is assumed to be a function of the direction cosines α_1, α_2 and α_3 of the magnetization vector $\underline{M}$, with respect to the crystallographic axes and can be expressed in an infinite power series in the direction cosines (Akulov, 1931). The function must have the symmetry of the crystal, e.g. it must be independent of a change in sign of any α_i and therefore odd powers and cross terms such as $\alpha_1\alpha_2$ will not appear in it. Further the condition that it must be invariant with respect to an interchange of any two α's, requires in the second-degree term $c_1\alpha_1^2 + c_2\alpha_2^2 + c_3\alpha_3^2$ that

$$c_1 = c_2 = c_3 \qquad 4.2$$

and as

$$\alpha_1^2 + \alpha_2^2 + \alpha_3^2 = 1 \qquad 4.3$$

no anisotropy results from this term. The allowable fourth-

degree terms are $\alpha_1^4 + \alpha_2^4 + \alpha_3^4$ and $\alpha_1^2\alpha_2^2 + \alpha_2^2\alpha_3^2 + \alpha_3^2\alpha_1^2$ but these can be expressed linearly in terms of one another by the relation

$$\alpha_1^2\alpha_2^2 + \alpha_2^2\alpha_3^2 + \alpha_3^2\alpha_1^2 = \tfrac{1}{2} - \tfrac{1}{2}(\alpha_1^4 + \alpha_2^4 + \alpha_3^4). \qquad 4.4$$

Thus the first non-vanishing non-constant term may be taken as $K_1(\alpha_1^2\alpha_2^2 + \alpha_2^2\alpha_3^2 + \alpha_3^2\alpha_1^2)$ where K_1 is a parameter dependent on temperature. The next term of sixth degree, on similar reasoning, may be written as $K_2\alpha_1^2\alpha_2^2\alpha_3^2$. It is found experimentally that the first two terms are usually sufficient to represent the crystal anisotropy. Hence for a cubic crystal, the expression is

$$E_{k/V} = K_1(\alpha_1^2\alpha_2^2 + \alpha_2^2\alpha_3^2 + \alpha_3^2\alpha_1^2) + K_2\alpha_1^2\alpha_2^2\alpha_3^2 + \ldots \qquad 4.5$$

For crystals of symmetry lower than cubic, various expressions for crystal anisotropy energy are used of which a few have become conventional. For example in crystals of hexagonal symmetry, anisotropy can be expressed in powers of sin θ, where θ is the angle between the magnetization $\underline{M}$ and the hexagonal axis [0001] as (Mason, 1954).

$$E_{k/V} = K_o + K_1\sin^2\theta + K_2\sin^4\theta + K_3\sin^6\theta + K_4\sin^6\theta \cdot \cos 6\phi \qquad 4.6$$

where ϕ is the angle between the projection of the magnetization vector on the basal plane and an $\hat{a}$-axis $[11\bar{2}0]$ and K_n are temperature dependent anisotropy constants. The $\cos 6\phi$ term represents a six fold symmetric basal plane anisotropy. Generally the second-degree term is of major importance and usually in practice second-

and fourth-degree terms are sufficient to express the actual anisotropy energy. The expression may be written in terms of sin nθ which is a convenient form for Fourier analysis (Pearson, 1979). However, in theoretical models anisotropy is usually expressed in terms of spherical harmonics as

$$E_{k/V} = \sum_{\ell=o}^{\infty} \sum_{m-\ell}^{+\ell} K_{\ell}^{'m} Y_{\ell}^{m} (\theta,\phi) \qquad 4.7$$

where K_{ℓ}^{m} are anisotropy constants and Y_{ℓ}^{m} (θ,ϕ) are spherical harmonics

$$Y_{\ell}^{m} (\theta,\phi) = (-1)^{m} \sqrt{\frac{(2\ell+1)(\ell-m)!}{4\pi (\ell+m)!}} P_{\ell}^{m}(\cos\theta) \exp(i|m|\phi) \qquad 4.8$$

where $P_{\ell}^{m}(\cos\theta)$ are associated Legendre polynomials;

$$P_{\ell}^{m} \cos\theta = (-1)^{m} \frac{(2\ell - 2m)!}{2^{\ell} m!(\ell - m)!(\ell - 2m)!} (\cos\theta)^{\ell-2m} \qquad 4.9$$

Due to orthogonality of spherical harmonics, truncation of the series of Equations 4-7 does not affect the accuracy of the lower order coefficients. This expression is also convenient when comparing experimental results with theoretical predictions (Birss & Keeler, 1974). The expression for a hexagonal system is (Coqblin, 1977);

$$E_{k/V} = K_{o}^{o} + K_{2}^{'o}Y_{2}^{o}(\theta) + K_{4}^{'o}Y_{4}^{o}(\theta) + K_{6}^{'o}Y_{6}^{o}(\theta) + K_{6}^{'6}Y_{6}^{6}(\theta,\phi) + \cdots \qquad 4.10$$

where Y_{ℓ}^{o} stands for spherical harmonic $Y^{o}(\theta,\phi)$ of and

$m = 0$ values, because $Y_\ell^o(\theta,\phi)$ does not depend on ϕ.

More commonly magnetocrystalline anisotropy is expressed using the Legendre polynomials, $P(\cos\theta)$ as

$$E_{k/V} = K_o^o + K_2^o P_2(\cos\theta) + K_4^o P_4(\cos\theta) + K_6^o P_6(\cos\theta) + K_6^6 \sin^6\theta \cos 6\phi + \ldots \quad 4.11$$

Volkov et al. (1981) considering reduction as well as transformation of symmetries, gave another form of the expression namely

$$E_{k/V} = K_1''(3\cos^2\theta - 1) + K_2''(35\cos^4\theta - 30\cos^2\theta + 3) + K_3''(231\cos^6\theta - 315\cos^4\theta + 105\cos^2\theta - 5) + K_4'' \sin^6\theta \cos 6\phi + \ldots \quad 4.12$$

where the K_m'' are anisotropy constants and the terms are orthogonal. The K's are related to each other in Appendix I.

4.2 Temperature Dependence of Anisotropy

The anisotropy is usually a sensitive function of temperature. It is found experimentally that it drops more rapidly with increasing temperature than the spin-orbit interaction indicated by the "g" Landé factor of an ion (ratio of the total angular moment J to the magnetic moment) and much faster than magnetization. The main cause of its rapid fall with temperature is thermal agitation. Thermal vibrations produce a spread of spin direction about the hard and easy directions and so lower the average energy in the hard direction and increase it along the easy axis. Consequently, the anisotropy decreases with narrowing energy gap due to loss of parallelism between individual spins (Akulov, 1936).

In determining anisotropy, the average energy of all the spins is required. As magnetization is the average of the projection of all the spins on the magnetization vector, the ratio of magnetization at temperature T, M(T), to the magnetization at $0^{o}K$, M(0), with all spins parallel is a good parameter to describe the spin distributions. This ratio is known as reduced magnetization m(T);

$$m(T) = \frac{M(T)}{M(0)} \qquad 4.13$$

The temperature dependence of anisotropy is frequently expressed empirically as a power law in terms of reduced magnetization

$$\frac{K(T)}{K(0)} = (m(T))^{n} \qquad 4.14$$

where K(T) and K(0) are anisotropy constants at temperature T and 0 K respectively. Akulov (1936) theoretically predicted that in a cubic system the variation of K_1 should obey a tenth power law which is in good agreement with the experimental data for iron at low temperature. Ni was found to follow a fifteenth power law. Birss and Wallis (1968) showed that the power is reduced to 10 if thermal expansion effects are removed.

Anisotropy energy associated with each ionic spin at absolute zero temperature can be written;

$$E(S) = \frac{1}{N} \sum_{\ell} K_{\ell}(0) \rho_{\ell}(S) \qquad 4.15$$

where N is number of spins per unit volume, $K_{\ell}(0)$ is the ℓ^{th} order anisotropy constant at $0^{o}K$ and $\rho_{\ell}(S)$ is

a normalized polynomial in spin operators or a unit vector along the spin axis expressible in spherical harmonics suiting the crystal symmetry.

This equation also applies to individual spins in a single-ion model which are under the influence of the crystalline field and are disoriented by thermal agitation. The anisotropy energy per unit volume for a spin distribution may be written (Callen and Callen, 1966);

$$E/V = \sum_{\ell} K_{\ell}(0) \langle Y_{\ell}^{o}(\hat{s}') \rangle \mathcal{S}_{\ell}(\hat{\alpha}) \qquad 4.16$$

where $\hat{s}'$ is a spin unit vector and $\hat{\alpha}$ is a unit vector along the magnetization. The spin distribution is given by Callen and Shtrikman (1965);

$$P_{M'} = \frac{\exp(xM')}{\sum_{M=-S}^{+S} \exp(xM')} \qquad 4.17$$

where $P_{M'}$ is the probability of $S' \cdot \alpha = M'$ and x is some function of temperature. The averages are given by

$$\langle Y_{\ell}^{o}(\hat{s}') \rangle = \langle Y_{\ell}^{o}(M') \rangle \qquad 4.18$$

$$= \frac{\int_{-1}^{+1} Y_{\ell}^{o}(M') \exp(xM')dM'}{\int_{-1}^{+1} \exp(xM')dM'} \qquad 4.19$$

The integral can be expressed in terms of hyperbolic Bessel functions (Keffer, 1955);

$$\int_{-1}^{+1} Y_{\ell}^{o}(M') \exp(xM')dM' = I_{\ell+\frac{1}{2}}(x) \qquad 4.20$$

and

$$\int_{-1}^{+1} \exp(xM')dM' = \int_{-1}^{+1} Y_o^o(M')\exp(xM')dM' = I_{\frac{1}{2}}(x) \qquad 4.21$$

where $I_n(x)$ are hyperbolic Bessel functions of order n. The theoretical temperature dependence of anisotropy constants may be written as

$$\frac{K_\ell(T)}{K_\ell(0)} = \frac{\langle Y_\ell^o(S')\rangle_T}{\langle Y_\ell^o(S')\rangle_o} = \frac{I_{\ell+\frac{1}{2}}(x)}{I_{\frac{1}{2}}(x)} = \hat{I}_{\ell+\frac{1}{2}}(x) \qquad 4.22$$

where $\hat{I}_{\ell+\frac{1}{2}}$ is the reduced hyperbolic Bessel function of order $\ell+\frac{1}{2}$, x is related to the reduced magnetization m :

$$m(T) = \langle \cos\Theta' \rangle = £(x) = \hat{I}_{3/2}(x) \qquad 4.23$$

where £(x) is the familiar Langevin function:

$$£(x) = \coth(x) - \frac{1}{x} . \qquad 4.24$$

Thus the most general form of the temperature dependence may be written as

$$\frac{K_\ell(T)}{K_\ell(0)} = I_{\ell+\frac{1}{2}}(£^{-1}(m(T))). \qquad 4.25$$

At low temperatures this equation reduces to a $\ell(\ell+1)/2$ power law

$$K_\ell(T) = K_\ell(0)(m(T))^{\ell(\ell+1)/2} \qquad 4.26$$

which is in good agreement with the Akulov and Van Vleck results. At higher temperature it has the form

$$K_\ell(T) = K_\ell(0)\,(m(T))^{\ell} . \qquad 4.27$$

Brenner (1957) used the Boltzmann distribution and obtained the following temperature dependence

$$K_1(T)/K_1(O) = 1 - 10/3\ t + 35/9(1-t)t^2(m(T))^{-2} \qquad 4.28$$

where $t = T/T_c$ and the reduced magnetization m(T) is as given by the Langevin-Weiss formula

$$m(T) = \coth(3m(T)/t) - t/(3m(T)) \qquad 4.29$$

At low temperature the equation reduces to the 10th power law but gives an increased power at higher temperature. An equivalent expression for hexagonal crystals is given by Carr (1958);

$$K_1(T) = (K_1(O) + {}^8/_7K_2(O))(m(T))^3 - {}^8/_7K_2(O)(m(T))^{10} + \qquad 4.30$$

or $$K_1(T) \simeq K_1(O)(m(T))^3$$

and also $$K_2(T) = K_2(O)(m(T))^{10} + \qquad 4.31$$

The K_2 dependence was consistent with the 10th-power law but equation 4.30 could not explain the change in sign of $K_1(T)$ for Cobalt at about 500K and this was possibly due to thermal expansion effects. Temperature dependences were derived on the basis of spin-wave theories, treating the misorientation of single spins in proximity to others as part of a cooperative temperature dependent excitation by Pal (1954), Keffer (1955), Turov and Mitsek (1960) and Hausmann (1970). These formulae show the standard 10th power law and do not make any real change in the theoretical predictions. Cooper (1968) gives a review of these spin-waves calculations.

The above theories are based on cylindrical symmetry of the spin direction about the magnetization axis. Brooks (1969) suggested that the enormous anisotropy in some of the rare-earths, e.g. terbium and dysprosium which have their easy axes in the basal plane, effects axial symmetry of the spin distribution. In this case spin precession is compressed into the easy basal plane which increases the power fall-off of the basal plane anisotropy and reduces the basal plane anisotropy. Egami (1972) and Brooks and Egami (1973, 1974) following a spin-wave theory, obtained a temperature dependence of anisotropy:

$$K_\ell^o(T)/K_\ell^o(0) = (m(T))^{\ell(\ell+1)/2}\Big/(1-b(T))^{(\ell(\ell+1)-4)/2} \qquad 4.32$$

and

$$K_\ell^o(T)/K_\ell^o(0) = (m(T))^{\ell(\ell+1)/2}\Big/(1+b(T))^{\ell(\ell-1)/2} \qquad 4.33$$

where b(T) is termed the ellipticity parameter and is related to the spin

$$b(T) = \frac{S_y^2 - S_x^2}{2S^2} \qquad 4.34$$

where S_y and S_x are the transverse components of spin $\underline{S}$.

At higher temperatures the spin precession becomes more symmetrical and a normal power law is restored. In terbium at lower temperatures, (1-b(T)) is proportional to m(T) and leads to

$$\frac{K_2^o(T)}{K_2^o(0)} \propto (m(T))^2 \qquad 4.35$$

and $$\frac{K_6^6(T)}{K_6^6(0)} \propto (m(T))^{36} \qquad 4.36$$

These power laws are theoretical and according to Coqblin (1977), there is no definite experimental evidence for them. In cubic crystals, K_1 requires 4th order perturbation calculations by the spin orbit coupling of the unperturbed energy bands. Large contributions to K_1 are expected where there is band degeneracy which are rapidly reduced by raising the temperature. The temperature dependence is thus not immediately related to a power law but needs to be computed by the direct methods of perturbation theory with the effect of temperature included by the use of Fermi statistics. The Fermi distribution is smeared out by alloying which introduces a mean free path effect (Wohlfarth,1980). Generally, magnetostrictive effects are excluded from the theoretical analysis while actual measurements involve magnetostrictive contributions.

Rhyne and McGuire (1972) considered magnetoelastic effects in the anisotropy and obtained, in a single-ion model,

$$\frac{K_6^6(T)}{K_6^6(0)} = \hat{I}_{9/2} \cdot \hat{I}_{5/2} \qquad 4.37$$

In a two-ion model, Callen and Callen (1965) have shown that the temperature dependence has the general power

law variation as given in equation 4.26. Van Vleck (1937) showed that K_2^o depended upon a power of m(T) varying from 2 to 4 as temperature increases for a pseudo-dipole interaction. In the pseudo-quadrupole interaction for cubic materials for K_4^o the power decreases from 6 to 5 at higher temperatures. Considering the molecular field along with pseudo-quadrupole interaction, a power law of 10 decreasing to about 5 is found and is the same as in equation 4.27.

Yang (1971), combined single- and two-ion models and obtained expressions for K_1 and K_2 hexagonal anisotropy constants:

$$K_1(T)/K_1(O) = f_1''\hat{I}_{5/2} + f_2''\hat{I}_{9/2} + g_1''(m(T))^2 + g_2''(\hat{I}_{5/2})^2 \qquad 4.38$$

and

$$K_2(T)/K_2(O) = h_1''\hat{I}_{9/2} + h_2''(\hat{I}_{5/2})^2 \qquad 4.39$$

The coefficients f_2'' and h_1'' are derived from the one-ion model while g_1'', g_2'' and h_2'' are from the two-ion model and f_1'' from a combination of both. These relations are claimed to be in agreement with the experimental data of cobalt and gadolinium, but the significance of this is not so convincing with the large number of disposable parameters available.

4.3 Magnetostriction

The magnetostriction of a material is a result of the interaction between the magnetic anisotropy and exchange energy and the elastic energy. Equation 2.20 gives the

expression for cubic crystals. A more precise expression taking into account higher order terms is

$$\begin{aligned}\delta\ell/\ell = {} & h_1(\alpha_1^2\beta_1^2 + \alpha_2^2\beta_2^2 + \alpha_3^2\beta_3^2 - \tfrac{1}{3}) \\ & + h_2(2\alpha_1\alpha_2\beta_1\beta_2 + 2\alpha_2\alpha_3\beta_2\beta_3 + 2\alpha_3\alpha_1\beta_3\beta_1) + h_3(S - \tfrac{1}{3}) \\ & + h_4(\alpha_1^4\beta_1^2 + \alpha_2^4\beta_2^2 + \alpha_3^4\beta_3^2 - \tfrac{2}{3}S - \tfrac{1}{3}) \\ & + h_5(2\alpha_1\alpha_2\alpha_3^2\beta_1\beta_2 + 2\alpha_2\alpha_3\alpha_1^2\beta_2\beta_3 + 2\alpha_3\alpha_1\alpha_2^2\beta_3\beta_1)\end{aligned} \qquad 4.40$$

where α and β are the direction cosines of the magnetization and the direction in which strain is observed respectively as defined earlier, and $S = \alpha_1^2\alpha_2^2 + \alpha_2^2\alpha_3^2 + \alpha_3^2\alpha_1^2$. For anisotropy K_1 negative, $\frac{1}{3}$ in the h_3 term is omitted (Chikazumi, 1964). Mason (1954) obtained an expression for the magnetostriction in the hexagonal materials.

$$\begin{aligned}\Delta\ell/\ell = {} & A(2\alpha_1\alpha_2\beta_1 + (\alpha_1^2 - \alpha_2^2)\beta_2)^2 \\ & + B_3^2\,(\alpha_1\beta_1 + \alpha_2\beta_2)^2 - (\alpha_1\beta_2 - \alpha_2\beta_1)^2 \\ & + C\,(\alpha_1\beta_1 + \alpha_2\beta_2)^2 - (\alpha_1\beta_2 - \alpha_2\beta_1)^2) + D(1-\alpha_3^2)(1-\beta_3^2)^2 \\ & + E\alpha_3^2\beta_3^2(1-\alpha_3^2) + F\alpha_3^2(1-\alpha_3^2) + G\beta_3^2(1-\alpha_3^2) + H\alpha_3\beta_3(\alpha_1\beta_1 + \alpha_2\beta_2) \\ & + I(\alpha_3^2\beta_3(\alpha_1\beta_1 + \alpha_2\beta_2) + J\alpha_3^2(1-\beta_3^2) + K\alpha_3^2\beta_3^2\end{aligned} \qquad 4.41$$

The contribution from the coefficients J and K is negligible in the case of cobalt but they are necessary for terbium. The free energy of the system, to first order perturbation, is of the form (Callen and Callen, 1965);

$$F = F_m + H_e + \langle H_{me} \rangle + \langle H_a \rangle \qquad 4.42$$

where F_m is the unperturbed free energy of the spins system H_e is the elastic energy associated with homogeneous strain components $\varepsilon_{xx}, \varepsilon_{yy}, \varepsilon_{xy}, \varepsilon_{yz}$ and ε_{zx} and the average of magnetoelastic energy H_{me} and magnetocrystalline anisotropy

energy H_a are carried out in the unperturbed density operator of the spin system. Equilibrium strains are obtained by minimizing the free energy.

The elastic energy may be written as

$$H_e = \sum_{\Gamma} \sum_{j,j'} \tfrac{1}{2} C^{\Gamma}_{jj'} \sum_{i} \varepsilon_i^{\Gamma,j} \varepsilon_i^{\Gamma,j'} \qquad 4.43$$

where Γ is a sub-group of the chemical point group for the n-dimensions and $\varepsilon_i^{\Gamma,j}$ are the strain functions ($i = 1,2,\ldots n$); j in the superscript represents two such sets.

Most complete results, on the basis of the group theoretical representations for the allowed strain, have been obtained in a series of papers by Callen and Callen (1963, 1965 and 1966). Magnetoelastic energy may be written in terms of one- and two- ion magnetoelastic coupling constants B^{Γ}_{ij} and D^{Γ}_{jj}:

$$H_{me} = -\sum_{f} \sum_{\Gamma} \sum_{jj'} B^{\Gamma}_{ij'}(f)\, \varepsilon_i^{\Gamma,j} K_i^{\Gamma,j'}(f) - \sum_{(f,g)} \sum_{\Gamma} \sum_{jj'} D^{\Gamma}_{jj'}(f,g) \sum_{i} \varepsilon_i^{\Gamma,j} K_i^{\Gamma,j'}(f,g) \qquad 4.44$$

where $\varepsilon_i^{\Gamma,j}$ are irreducible hexagonal strains. $K_i^{\Gamma,j}(S_f)$ and $K_i^{\Gamma,j}(S_f,S_g)$ the basis functions are one- and two- ion spin polynomials of order ℓ. Superscripts Γ,j label the irreducible representation of the crystal group and i labels the basis function while f and g are lattice sites.

Minimization of this free energy with respect to

strain yielded the magnetostriction expression of order $\ell=2$ for hexagonal substances;

$$\frac{\Delta\ell}{\ell}=\lambda=\lambda_1^{\alpha,0}(1-\beta_z^2)+\lambda_2^{\alpha,0}\beta_z^2+\lambda_1^{\alpha,2}(1-\beta_z^2)(\alpha_z^2-\tfrac{1}{3})$$
$$+\lambda_2^{\alpha,2}\beta_z^2(\alpha_z^2-\tfrac{1}{3})+\lambda^{\gamma,2}(\tfrac{1}{2}(\beta_x^2-\beta_y^2)(\alpha_x^2-\alpha_y^2)+2\beta_x\beta_y\alpha_x\alpha_y)$$
$$+2\lambda^{\epsilon,2}(\beta_x\alpha_x+\beta_y\alpha_y)\beta_z\alpha_z \qquad 4.45$$

where $\lambda_1^{\alpha,0}$ and $\lambda_2^{\alpha,0}$ contain only two-ion coefficients, are related to the anomalous thermal expansion and are independent of magnetization direction. $\lambda_1^{\alpha,0}$ is the basal plane strain while $\lambda_2^{\alpha,0}$ is along the $\hat{c}$-axis and they are the same type of strain as of corresponding $\ell=2$ modes. $\lambda^{\alpha,0}$ strains vary only with the magnitude of the magnetization. α, γ and ϵ are the strain modes, α is dilation in the basal plane ($\lambda_1^{\alpha,2}$) and along $\hat{c}$-axis ($\lambda_2^{\alpha,2}$) preserving the hexagonal symmetry, γ is the distortion of the hexagonal symmetry into orthohombic (circle to ellipse in order 2) and ϵ is $\hat{c}$-axis shear. These modes are illustrated in Figure 4.1 after Clark et al. (1965). The six magnetostriction constants are experimentally determined quantities. The equation 4.45 of Clark et al. and corrected by Callen(1968) has been used to measure the magnetostriction constant in the present work.

Callen and Callen (1965) also gave an expression for magnetostriction in slightly differently defined temperature and field dependent magnetostriction constants $\lambda_{j,k}^{\mu}$ as

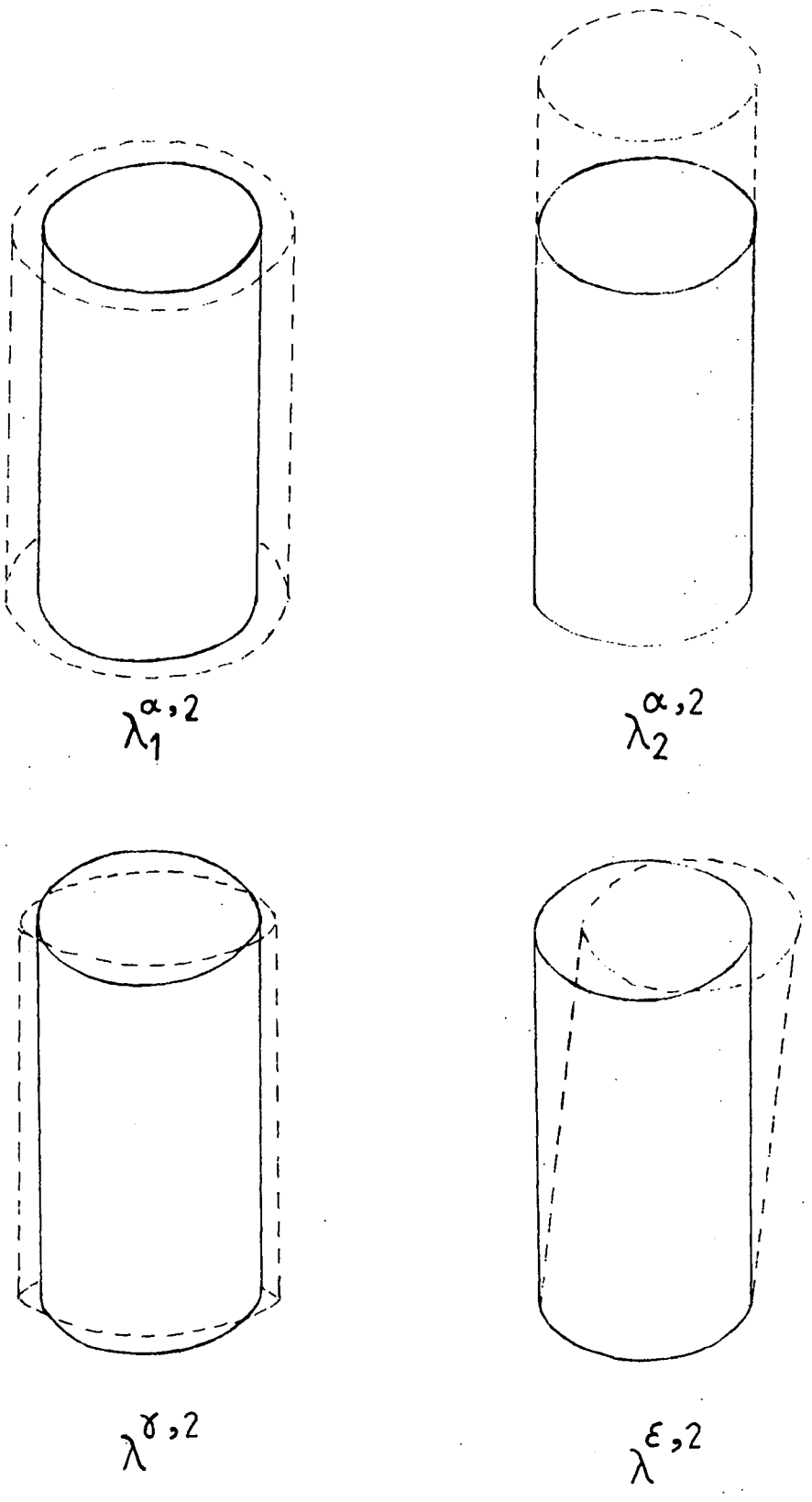

Fig. 4.1 The four possible magnetostriction strain modes in $\ell = 2$ order for hexagonal symmetry arising from α, γ, and ε representations (after Clark et al., 1965).

$$\lambda = \frac{1}{3}\lambda_{11}^{\alpha} + \frac{1}{2\sqrt{3}}\lambda_{12}^{\alpha}(\alpha_z^2 - \frac{1}{3}) + 2\lambda_{21}(\beta_z^2 - \frac{1}{3}) + \sqrt{3}\lambda_{22}^{\alpha}(\alpha_z^2 - \frac{1}{3})(\beta_z^2 - \frac{1}{3})$$

$$+ 2\lambda^{\gamma}(\tfrac{1}{4}(\alpha_z^2 - \alpha_y^2)(\beta_z^2 - \beta_y^2) + \alpha_x\alpha_y\beta_x\beta_y) + 2\lambda^{\epsilon}(\alpha_y\alpha_z\beta_y\beta_z + \alpha_x\alpha_z\beta_x\beta_z)$$

4.46

Callen and Callen(1965) related $\lambda_{j,k}^{\mu}$ magnetostriction to equilibrium strains and to the stiffness constants.

The magnetostriction constants of Callen and Callen (1965) and those of Clark and Callen (equation 4.45) were shown by Coqblin (1977) to be related by the following expressions;

$$\lambda_1^{\alpha,0} = \frac{1}{3}(\lambda_{11}^{\alpha} - \sqrt{3}\lambda_{21}^{\alpha}) \qquad 4.47$$

$$\lambda_2^{\alpha,0} = \frac{1}{3}(\lambda_{11}^{\alpha} + 2\sqrt{3}\lambda_{21}^{\alpha}) \qquad 4.48$$

$$\lambda_1^{\alpha,2} = \frac{1}{2\ 3}(\lambda_{12}^{\alpha} - \sqrt{3}\lambda_{22}^{\alpha}) \qquad 4.49$$

$$\lambda_2^{\alpha,2} = \frac{1}{2\ 3}(\lambda_{12} + 2\sqrt{3}\lambda_{22}) \qquad 4.50$$

$$\lambda^{\gamma,2} = \lambda^{\gamma} \qquad 4.51$$

$$\lambda^{\epsilon,2} = \lambda^{\epsilon} \qquad 4.52$$

Mishiama et al. (1976) derived a higher order formula up to ℓ=4 which adds the following terms to equation 4.45

$$\lambda_1^{\alpha,4}(1-\beta_z^2)(7\alpha_z^4 - 6\alpha_z^2 + {}^3/5) + \lambda_2^{\alpha,4}\beta_z^2(7\alpha_z^4 - 6\alpha_z^2 + {}^3/5)$$

$$+ \lambda^{\gamma,4}(\tfrac{1}{2}(\beta_x^2 - \beta_y^2)(\alpha_x^2 - \alpha_y^2) + 2\beta_x\beta_y\alpha_x\alpha_y)(7\alpha_z^2 - 1)$$

$$+ 2\lambda^{\epsilon,4}(\beta_x\alpha_x + \beta_y\alpha_y)(\beta_z\alpha_z)(7\alpha_z^2 - 3)$$

$$+ \lambda^{\delta,4}(8\beta_x\beta_y\alpha_x\alpha_y(\alpha_x^2 - \alpha_y^2) - (\beta_x^2 - \beta_y^2)(\alpha_x^4 + \alpha_y^4 - 6\alpha_x^2\alpha_y^2)$$

4.53

The magnetostriction constants given in Clark and Callen (Eq 4.45) and in the extended higher order expression (Eq. 4.53) (Mishima et al., 1976) are related to the magnetostriction constants of Mason's expression 4.41 as:

$$A = \frac{4}{3}\lambda^{\delta,4} \quad , B = -\lambda_1^{\alpha,0} - \frac{2}{3}\lambda_1^{\alpha,2} - \frac{43}{5}\lambda_1^{\alpha,4} + \frac{7}{2}\lambda^{\gamma,4} + \frac{2}{3}\lambda^{\delta,4}$$

$$C = \tfrac{1}{2}(\lambda^{\gamma,2} - \lambda^{\gamma,4}), \quad D = \lambda_1^{\alpha,0} - \frac{1}{3}\lambda_1^{\alpha,2} + \frac{3}{5}\lambda_1^{\alpha,4} - \frac{2}{3}\lambda^{\delta,4}$$

$$E = -\lambda_1^{\alpha,0} - \frac{2}{3}\lambda_1^{\alpha,2} - \frac{8}{5}\lambda_1^{\alpha,4} + 7\lambda_2^{\alpha,4} - \frac{1}{3}\lambda^{\delta,4}$$

$$F = \lambda_1^{\alpha,0} + \frac{2}{3}\lambda_1^{\alpha,2} + \frac{8}{5}\lambda_1^{\alpha,4} - \frac{1}{3}\lambda^{\delta,4}$$

$$G = \lambda_2^{\epsilon,0} - \frac{1}{3}\lambda_2^{\alpha,2} - \frac{7}{80}\lambda_2^{\alpha,4}, \quad H = 2\lambda^{\epsilon,2} + \frac{11}{4}\lambda^{\delta,4}$$

$$I = \frac{11}{3}\lambda^{\epsilon,4}, \quad J = \lambda_1^{\alpha,0} + \frac{2}{3}\lambda_1^{\alpha,2} + \frac{29}{16}\lambda_1^{\epsilon,4} + \frac{1}{3}\lambda^{\delta,4}$$

$$K = \lambda_2^{\alpha,0} + \frac{2}{3}\lambda_2^{\alpha,2} + \frac{73}{80}\lambda_2^{\alpha,4} \qquad 4.54$$

Alstad and Legvold (1964) and Bozorth and Wakiyma (1963) used a simplified magnetostriction expression given by Bozorth (1954) to represent the magnetostriction of gadolinium. The expresion is given as

$$\begin{aligned}\delta\ell/\ell = {} & \lambda_A((\alpha_x\beta_x + \alpha_y\beta_y)^2 - \alpha_z\beta_z(\alpha_x\beta_x + \alpha_y\beta_y)) \\ & + \lambda_B((1-\alpha_z^2)(1-\beta_z^2) - (\alpha_x\beta_x + \alpha_y\beta_y)^2) \\ & + \lambda_C((1-\alpha_z^2)\beta_z^2 - \alpha_z\beta_z(\alpha_x\beta_x + \alpha_y\beta_y)) \\ & + 4\lambda_D\alpha_z\beta_z(\alpha_x\beta_x + \alpha_y\beta_y)\end{aligned} \qquad 4.55$$

The constants in 4.55 are related to those of Clark and Callen used in equation 4.45 by Rhyne (1972) by

$$\lambda^{\gamma,2} = \lambda_A - \lambda_B$$

$$\lambda_1^{\alpha,2} = -\tfrac{1}{2}(\lambda_A + \lambda_B)$$

$$\lambda_2^{\alpha,2} = -\lambda_C$$

$$\lambda^{\epsilon,2} = 2\lambda_D - \tfrac{1}{2}(\lambda_A + \lambda_C) \qquad 4.56$$

Birss (1959) gave another expresion for magnetostriction:

$$\lambda = R_o + R_1\beta_z^2 + (R_2 + R_3\beta_z^2)(1 - \alpha_z^2) + (R_4\alpha_z\beta_z + R_5(\alpha_x\beta_x + \alpha_y\beta_y))(\alpha_x\beta_x + \alpha_y\beta_y) \qquad 4.57$$

Its magnetostriction constants are related to those of Bozorth (1954) by Coleman and Pavlovic (1965) by

$$R_2 = \lambda_B$$

$$R_3 = \lambda_C - \lambda_B$$

$$R_4 = 4\lambda_D - \lambda_C - \lambda_A$$

and

$$R_5 = \lambda_{\bar{A}} - \lambda_B \qquad 4.58$$

4.4 Temperature Dependence of Magnetostriction

The temperature dependence of all magnetostriction constants is characterized entirely by (i) the one-ion $\mathcal{L}_f(T,H)$, (ii) the two-ion $\mathcal{L}_{fg}(T,H)$ and (iii) the isotropic $\mathcal{J}_{fg}(T,H)$ correlation functions (Coqblin, 1977). These functions have been discussed in detail by Callen and Callen (1965). Callen and Strikman (1965) have shown that for all the renormalized collective excitation theories the one-ion averages are the same functions of magnetization and

so one-ion magnetostriction coefficients can be expressed as functions of magnetization. Callen and Callen (1965) obtained a temperature dependence of the magnetostriction constants of order ℓ in the one ion model as

$$\lambda(T) = \lambda(0)\, \hat{I}_{(\ell+\frac{1}{2})} (\mathcal{L}^{-1} m(T)) \qquad 4.59$$

In the paramagnetic region

$$\hat{I}_{\ell+\frac{1}{2}}(x) \longrightarrow m^{\ell}(T,H) \qquad 4.60$$

where $x = \mathcal{L}^{-1} m(T)$.

The notation used in this section is the same as that defined in Section 4.2.

At low temperatures

$$\hat{I}_{\ell+\frac{1}{2}}(x) = 1 - \left[\ell(\ell+1)/2x\right] + \cdots \qquad 4.61$$

and $m = \hat{I}_{3/2} = 1 - \frac{1}{x}$ 4.62

Hence $\hat{I}_{\ell+\frac{1}{2}}(x) = 1 - (\ell(\ell+1)/2)(1-m) + \ldots \simeq m^{\frac{\ell(\ell+1)}{2}}$ 4.63

The theoretical temperature variation is in good agreement with the experimental measurements of constants $\lambda^{\gamma,2}$ and $\lambda^{\epsilon,2}$ for dysprosium by Clark et al. (1965). Their results along with the theoretical temperature dependence are shown in Figure 4.2.

The two-ion longitudinal correlation function in the theory of mangetostriction which arises from the modulation by the strain of spin interaction energies, such as dipolar, pseudodipolar and exchange energies, is

$$\mathcal{L}_{fg}(T,H) \sim \left\langle S_f z\, S_g z - \tfrac{1}{3}\, \underline{S}_f \cdot \underline{S}_g \right\rangle \qquad 4.64$$

where $\underline{S}_f$ and $\underline{S}_g$ are spins of electrons in ion f and g respectively. At sufficiently low temperature and

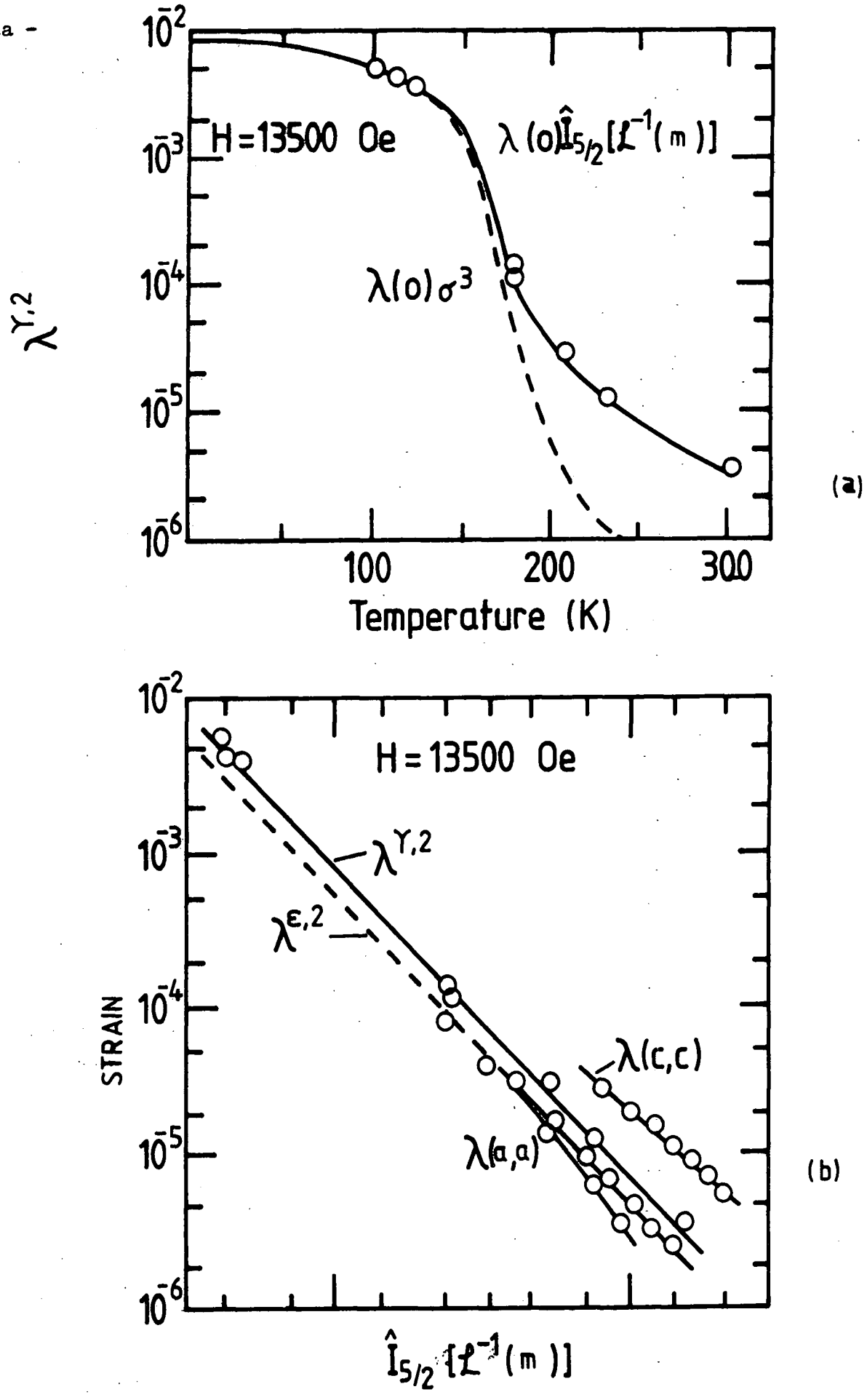

Fig. 4.2 The magnetostriction coefficients of dysprosium of Clark et al., 1965 compared with the theory of Callen and Callen, 1965.

when f and g ions are close enough to be strongly correlated, this function satisfies the $\frac{1}{2}\ell(\ell+1)$ - power law, whence

$$(\frac{3}{2}\ S^2)\ \langle S_f z\ S_g z - \frac{1}{3}\underline{S}_f \cdot \underline{S}_g \rangle = m^3(T,H) \qquad 4.65$$

When ions f and g are sufficiently far apart, the spins are independent, then the power 3 of reduced magnetization in equation 4.65 becomes 2. The $m^2(T,H)$ temperature dependence is valid for almost all temperatures while the $m^3(T,H)$ dependence holds only at low temperatures for near neighbours.

CHAPTER 5

PREVIOUS STUDIES ON MAGNETOCRYSTALLINE ANISOTROPY AND MAGNETOSTRICTION OF Gd, Tb AND THEIR ALLOYS

5.1 Introduction

The availability of high purity rare earth crystals led to extensive systematic investigations into the properties of these materials. The magnetic properties result from an interplay of forces of comparable magnitude, e.g. indirect RKKY exchange interaction, single-ion crystal-field anisotropy , magnetoelastic effects and two-ion anisotropy. One of the most interesting properties of Tb, like most other rare earth ferromagnets, is the huge magnetic anisotropy compared to the ferromagnets of the iron group. The theoretical temperature dependence of magnetic anisotropy involves values of magnetization. The magnetization of gadolinium has been studied by Elliot et al. (1953), Graham (1963), Nigh et al. (1963), and Feron and Pauthenet (1969). Magnetization measurements on terbium have been made by Hegland et al. (1963), Rhyne et al. (1968), Feron (1969), Roeland et al. (1975) and Bagguley et al. (1980a,b). The values for gadolinium and terbium alloys have been given by Nikitin et al. (1977) and Bagguley et al. (1980a,b). Very recently Corner et al.(1983a) measured the magnetization of high purity Gd, Tb and their alloys at Genoble, France and his results are very close to those of Bagguley et al. (1980a,b). The values used in the analysis of present work are those of Corner et al. and are given in Table 5.1. The derivation of magnetostriction constants of the ac and bc-plane

TABLE 5.1

Temperature variation of the specific magnetization σ_s (emu/gm) of Gd/Tb alloys (after Corner et al., 1983a).

Pure Gd		90% Gd		70% Gd		50% Gd		10% Gd		Pure Tb	
Temp. K	σ	T(K)	σ	T(K)	σ	T(K)	σ	T(K)	σ	T(K)	σ
4.2	271	4.2	277.0	4.2	289.2	4.2	302.2	4.2	320.7	4.2	329.0
25.6	270.1	25.5	276.0	25.6	288.1	25.6	301.0	20.3	320.3	25.6	327.5
50.0	265.8	50.1	271.4	50.1	283	50.1	295.6	50.1	313.5	50.1	320.3
74.8	257.0	74.7	263.5	74.7	274.5	74.7	286.1	74.7	301.5	74.7	308.9
100.1	248.0	100.1	253.0	100.0	263.7	100.1	274.7	100.0	289.5	100.1	297.7
125.1	236.0	125.1	242.3			125.1	261.0	150.0	255.8	125.0	280.7
150.0	224.0	150.0	229.5	150.0	237.0	150.0	246.0	200.0	195.0	150.4	232.8
175.0	210.0	175.0	215.0			175.0	228.0	220.0	150.0	200.0	196.5
200.0	196.0	200.0	198.8	200.0	202.5	200.0	205.5	240.0	0	210.0	171.9
225.1	176.5	225.0	178.5	220.0	183.6	220.0	181.2	260.0	0	220.0	136.5
250.1	148.5	250.1	150.0	240.8	158.6	240.1	148.2			230.0	0
275.1	110.0	275.1	100.1	260.0	118.2	260.1	69.8				
300.1	0			280.0	0	280.0	0				

crystals of the present work is based on the magnetocrystalline anisotropy constants. The unspecified use of "anisotropy" would refer to magnetocrystalline anisotropy. The terbium and gadolinium binary alloys provides an insight into the interactions responsible for anisotropic behaviour in terbium. Gadolinium pure metal has a very small anisotropy compared to the very high anisotropy energy density of terbium metal. The crystalline fields of gadolinium and terbium are almost identical and the elements form continuous solid solutions. The presence of gadolinium in terbium would not be expected to change the single ion contribution to the terbium anisotropy because of unchanged crystalline environment for each terbium ion. Thus gadolinium acts as an ideal diluent for terbium.

5.2 Magnetocrystalline Anisotropy of Gadolinium

The magnetocrystalline anisotropy of gadolinium has been studied by Corner et al. (1962), Graham (1962, 1963, 1967), Darby and Taylor (1964), Birss and Wallis (1964), Belov et al. (1968), Tajima (1971), Tohyama and Chikazumi (1973), Corner and Tanner (1976) and Mihai and Franse (1976) by torque methods and from magnetization curves by Feron and Pauthenet (1969) and Feron et al. (1970a,b). More recently Smith et al. (1978), using high purity single crystals produced results which may be regarded as the most reliable currently available. The disagreement between previous measurements of uniaxial anisotropy is attributed to the impurities particularly the oxygen content. Smith et al. (1977) found that

inclusions of non-magnetic impurities affected the measurements of the first anisotropy constant and the easy direction of magnetization significantly in gadolinium. The temperature dependence of the first three magnetocrystalline anisotropy constants for gadolinium as defined in equation 4.6 is shown in Figure 5.1. The anisotropy energy surface, constructed on the basis of equation 4.6 at various temperatures is shown in Figure 5.2a and b. The temperature dependence of anisotropy constant K, was found to be associated with single- and two-ion mechanisms, K_2 on single-ion mechanism only and K_4 followed the 21st-power law with respect to reduced magnetization.

5.3 Magnetocrystalline Anisotropy of Terbium

Measurements of magnetocrystalline anisotropy of Tb are extensive and have been made by Rhyne and Clark (1967), Bly et al. (1968), Rhyne et al. (1968), Du Plessis (1969), Feron (1969), Wagner and Stanford (1969), Feron et al. (1970a,b), Shepherd (1976), Birss et al. (1977a,b), Nikitin and Arutyunian (1979), Birss et al. (1981) and Corner (1983b). The various techniques used to determine magnetic anisotropy constants include torque magnetometry, analysis of magnetization curves and magnetostriction co-efficients, rotating sample magnetometry and ferromagnetic resonance. The table 5.2 shows the quoted values of magnetocrystalline anisotropy of Tb along with the method used to obtain them.

The temperature dependence of the first anisotropy constant K_2^o studied by Rhyne and Clark by torque

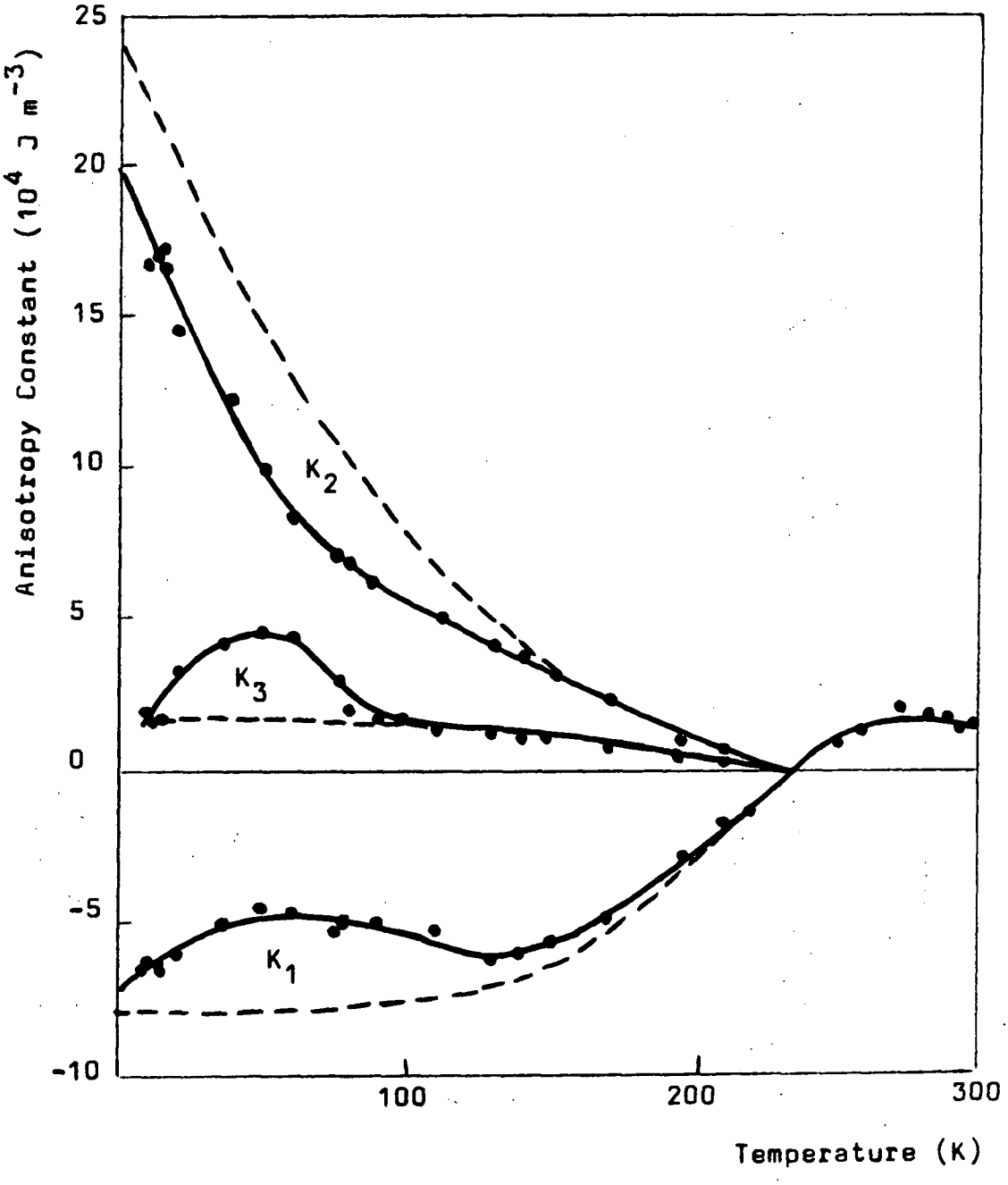

Fig. 5.1 The first three anisotropy constants of gadolinium (after Smith (1978)). Experimental points were measured at 1·01 tesla, and the dashed lines represent "infinite-field" values.

Coeff.	Temp. (K)	Method	Value ($J\ m^{-3}$)	Author(s)	Date
K_2^0	0	Torque	$5{\cdot}5 \times 10^7$	Rhyne & Clark	1967
,,	80	,,	$4{\cdot}6 \times 10^7$	,,	,,
,,	4·2	Magnetisation	$4{\cdot}5 \times 10^7$	Rhyne et al.	1968
,,	0	Torque (Paramagnetic Extrapol'n)	$2{\cdot}7 \times 10^7$	DuPlessis	1969
,,	0	Magnetisation	$(5{\cdot}65 \pm 1{\cdot}10) \times 10^7$	Féron	,,
,,	80	,,	$3{\cdot}5 \times 10^7$	,,	,,
,,	0	Ferromagnetic Resonance	$3{\cdot}1 \times 10^7$	Wagner & Stanford	,,
,,	0	Magnetisation	$3{\cdot}5 \times 10^7$	Nikitin & Arutyunian	1979
K_4^0	0	,,	$(0{\cdot}46 \pm 0{\cdot}12) \times 10^7$	Féron	1969
,,	80	,,	$0{\cdot}25 \times 10^7$	,,	,,
K_6^6	0	Magnetostriction	$2{\cdot}42 \times 10^5$	Rhyne & Clark	1967
,,	80	,,	$0{\cdot}69 \times 10^5$	,,	,,
,,	0	Torque	$2{\cdot}44 \times 10^5$	Bly et al.	1968
,,	80	,,	$1{\cdot}0 \times 10^5$	,,	,,
,,	0	,,	$2{\cdot}9 \times 10^5$	DuPlessis	1969
,,	0	Magnetisation	$(1{\cdot}85 \pm 0{\cdot}18) \times 10^5$	Féron	,,
,,	80	,,	$1{\cdot}0 \times 10^5$	,,	,,
,,	0	R.S.M.	$2{\cdot}96 \times 10^5$	Birss et al.	1977
,,	80	,,	$0{\cdot}9 \times 10^5$	,,	,,
,,	4·2	Torque	$3{\cdot}5 \times 10^5$	Nikitin & Arutyunian	1979
,,	78	,,	$0{\cdot}92 \times 10^5$	,,	,,

Table 5.2. Values of the Anisotropy Coefficients of Terbium.

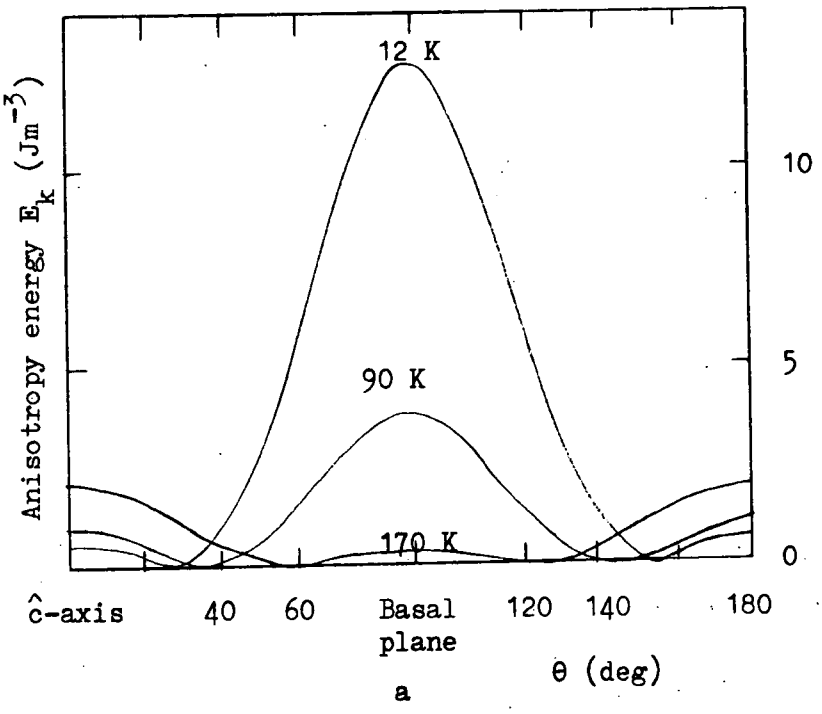

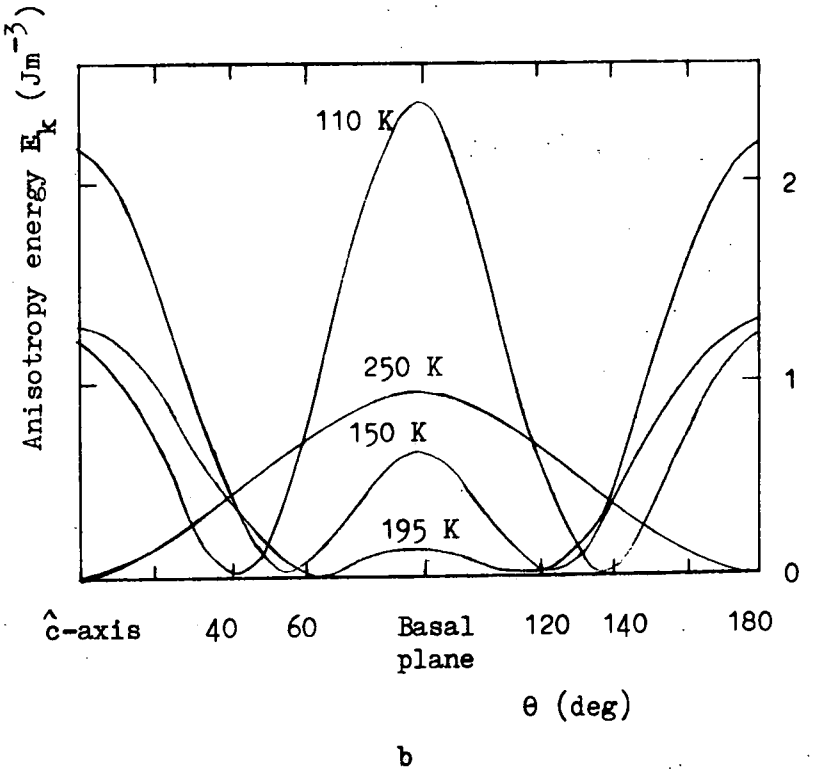

Fig. 5.2 The anisotropy energy surface of gadolinium at temperatures
(a) 12, 90, and 170 K
(b) 110, 150, 195, and 250 K
(after Smith et al., 1978).

magnetometry follows the $\hat{I}_{5/2}$ single-ion variation as predicted by Callen & Callen (1966). The results of Feron from magnetization curves also fit very well with the single-ion model. There is discrepancy between the temperature dependent behaviour of $K_6^6 = K_4$ as reported by different authors. The results of Feron, Rhyne and Clark (1967) and Bly et al. (1968) follow a $\hat{I}_{9/2}$ $\hat{I}_{5/2}$ dependence which is purely of magnetoelastic origin on the model of Rhyne and McGuire (1972), while those of Birss et al. (1977a,b) are in good agreement with a single-ion model and follow an $\hat{I}_{13/2}$ law. These results are shown in Figure 5.3A and B.

5.4 Magnetocrystalline Anisotropy of Gd/Tb Alloys

Magnetocrystalline anisotropy constants of various Gd/Tb alloy compositions have been measured by Tajima and Chikazumi (1967b), and Tajima (1971), Nikitin and Arutyunian (1979), Bagguley et al. (1980a,b), Hawkins (1982), Corner (1983b)and Paige (1983). Bagguley et al. used a different method, microwave resonance techniques, to determine the anisotropy constants. The anisotropy was measured during an oscillation of local magnetization vectors in an effective field. The dynamic nature of the technique resulted in fundamentally different anisotropy values in some cases. Corner derived the anisotropy constants K_2^o from the magnetization curves assuming that K_4^o and higher coefficients in the uniaxial anisotropy expression are zero. Nikitin and Arutyunian also found higher order constants negligibly small. The comparison

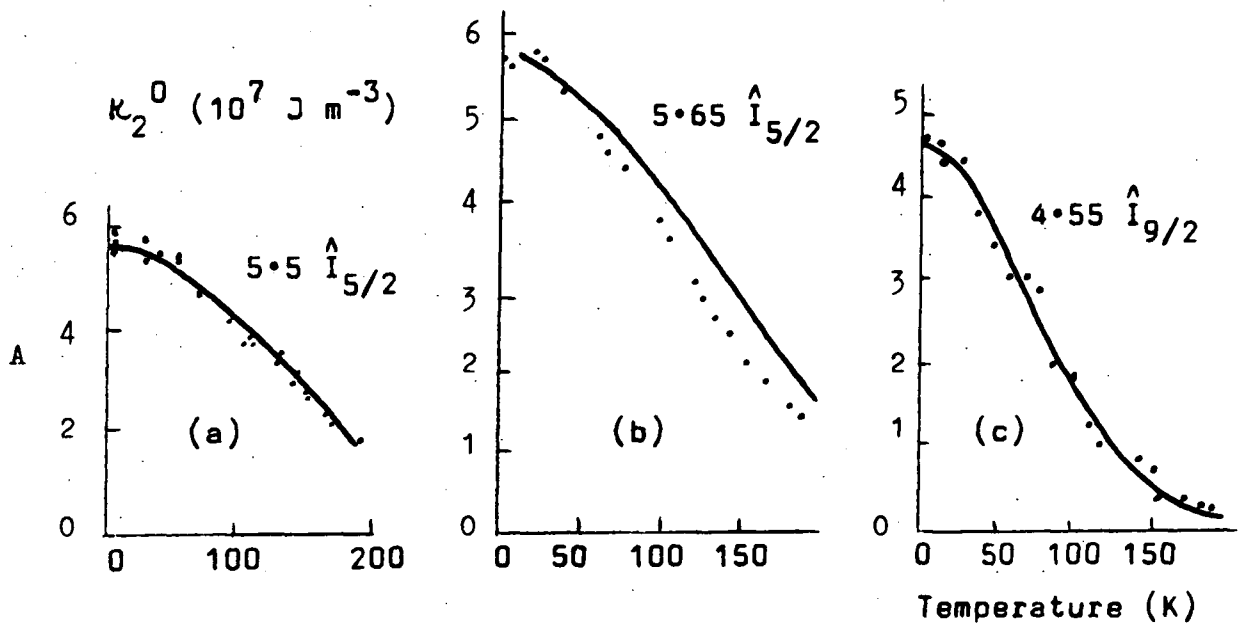

Fig. 5.3A The temperature dependence of (a) the K_2^0 coefficient of terbium after Rhyne and Clark (1967), (b) and (c) the K_2^0 and K_4^0 coefficients after Féron (1969).

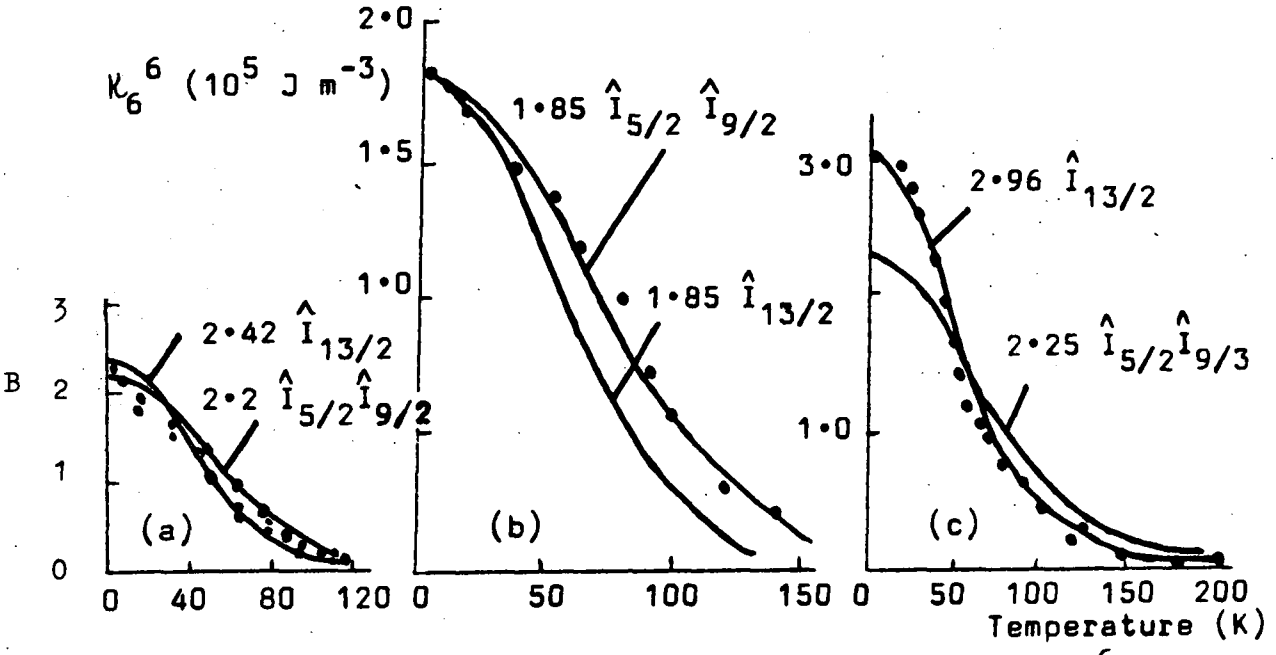

Fig. 5.3B The temperature dependence of the K_6^6 coefficient of terbium (a) after Rhyne and Clark (1967) and Bly et al. (1968), (b) after Féron et al. (1970a, b), (c) after Birss et al. (1977a, b).

between the existing data is illustrated in Figures 5.4, 5.5 and 5.6. The values of the constants are expressed in a single convention for direct comparison. Some of the differences in the results may be due to different techniques. Tajima accounted for the differences in his values and those of Rhyne and Clark (1967) by a combination of three effects, (i) that his inclusion of K_4^o and K_6^o constants (which were ignored by others) could reduce the pure Tb results by 10%, (ii) that the values of the $^c/_a$ lattice parameter ratio are different in pure Tb and in its alloys, and (iii) higher magnetostrictive effects in pure Tb than in the alloys. The results of Feron (1969) disagree with the first reason as he included K_4^o in the calculations; this is consistent with the orthagonal nature of the constants. The coefficients of the anisotropy of terbium would be expected to be linear with the Tb concentration in the Gd/Tb alloys if the origin of the anisotropy of Tb is of a single-ion nature. The recent work of Corner (1983b) shows a fair agreement with the single-ion model. The temperature dependence of K_2^o for 90% Gd/Tb follows $\hat{I}_{5/2}$ (single-ion) while K_6^6 for the same alloy includes a fraction of two-ion contributions in addition to the $\hat{I}_{13/2}$ single-ion variation. K_2^o for 79% Gd/Tb seem to follow an m^3 power law while for 25% Gd/Tb an m^4 power law is found. The temperature variations of K_2^o for Gd, Tb and their alloys is given in Table 5.3. These are the values used in

TABLE 5.3

Temperature variation of the Magnetocrystalline anisotropy constant K_2^o (10^7 J m^{-3}) for Gd/Tb alloys (after Corner 1983b).

90% Gd		70% Gd		50% Gd		10% Gd		Pure Tb	
T(K)	K_2^o	T(K)	K_2^o	T(K)	K_2^o	T(K)	K_2^o	T(K)	K_2^o
0.0	.258	0	0.97	0	2.1	0	5.0	0	5.87
20.0	.256	4.2	0.966	20	2.08	4.2	4.9	4.2	5.86
40.0	.249	25.5	0.934	50	1.94	20.4	5.03	25.7	5.83
50.0	.241	50.1	0.878	70	1.78	50.1	4.66	50.1	5.33
70.0	.223	70.0	0.80	100	1.50	74.7	3.92	74.7	4.6
100.0	.196	100.0	0.66	120	1.40	100.4	3.33	100.1	3.96
120.0	.176	120.0	.57	150	1.00	125.0	2.74	125.1	3.16
150.0	.144	150.0	.43	170	0.81	150.0	2.08	150.0	2.27
175.0	.124	175.0	.33	190	0.62	175.0	1.51	175.0	1.55
200.0	.096	200.0	.23	200	0.52	200.0	0.92	200.0	0.84
220.0	.074	220.0	.15	240	0.16	220.0	0.86	220.0	0.38
250.0	.04								

the calculation of the bc and ac plane magnetostriction constants. The temperature variation of the existing data of anisotropy constants for Gd, Tb and their alloys is, over all, in favour of the single-ion nature of the anomalously high anisotropy of Tb.

5.5 Magnetostriction of Gadolinium

Gadolinium has L=0, so there is no total orbital momentum contribution to the total moment. The magnetization curves are characteristic of its almost isotropic ferromagnetic behaviour. It has the lowest saturation magnetization value at absolute zero, 268.2 emu/gm = $7.55\mu_B$, in the series Gd-Er due to the s-state character of the ion. The s-state character also rules out a single-ion anisotropic contribution to magnetostriction. Its magnetostriction is small compared to the other rare earths with large single-ion contribution. The two-ion origin of the magnetostriction of Gd makes it difficult to predict theoretically its temperature dependence. The magnetostriction of Gd has been studied by Belov et al. (1961), Bozorth and Wakiyama (1963), Alstad and Legvold (1964), Coleman (1964), Coleman and Pavlovic (1964), Belov et al. (1968), Bartholin and Bloch (1969), Bartholin (1970) and Mishima et al. (1976). The lattice parameters of Gd were studied by Banister et al. (1954), Darnell (1963a), and Darnell and Cloud (1964). Bozorth and Wakiyama and Alstad and Legvold used the simplified expression for magnetostriction (4-55) with only four independent constants $\lambda_A, \lambda_B, \lambda_C$ and λ_D of order $\ell = 2$ and determined these constants by the strain

Fig 5.4 K_1 AND K_4 VS COMPOSITION AT 0 K FOR Tb_xGd_{1-x} ALLOYS; COMPARISON

(AFTER PAIGE, 1983)

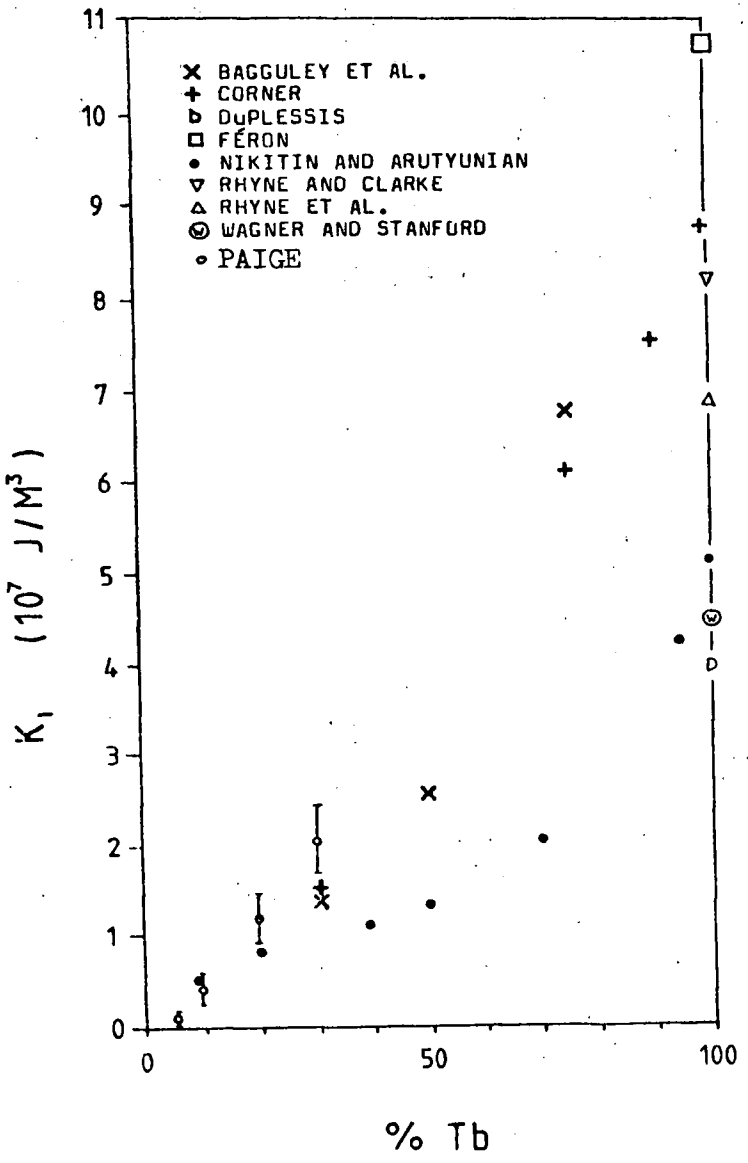

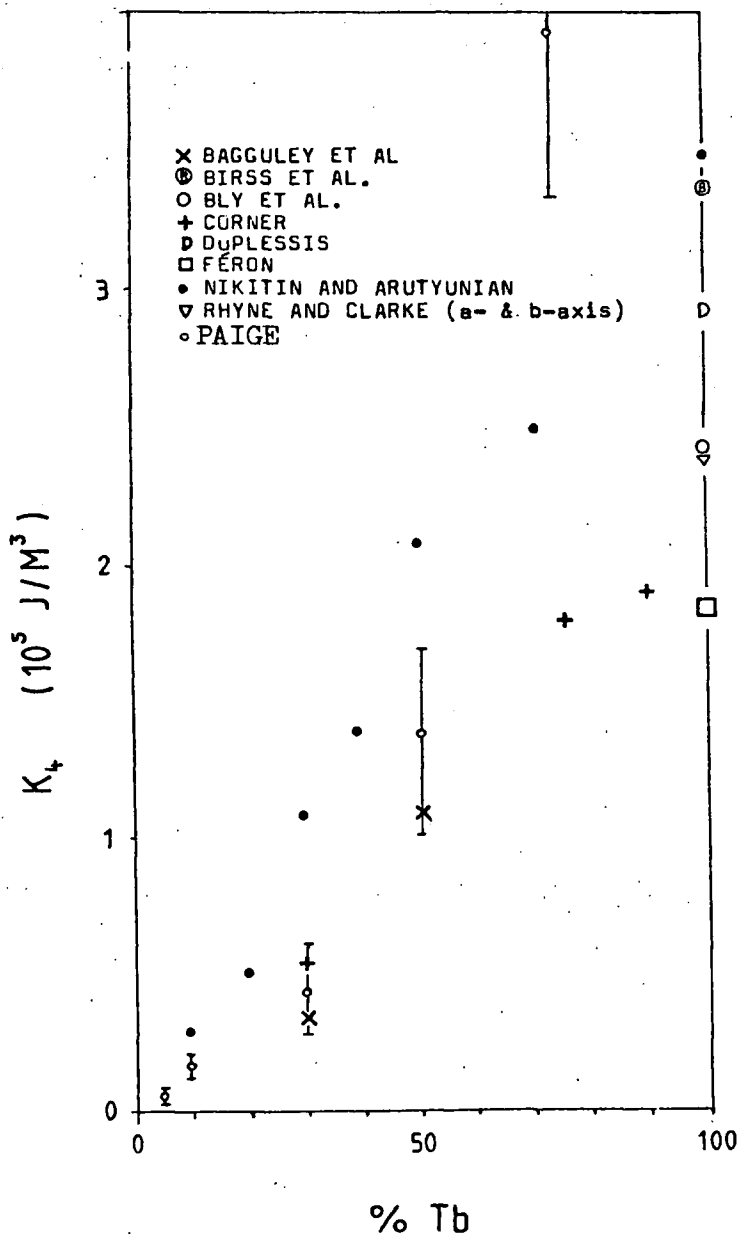

FIG.5.5 K_1 VS TEMPERATURE FOR Tb_xGd_{1-x} ALLOYS; AFTER PAIGE (1983)

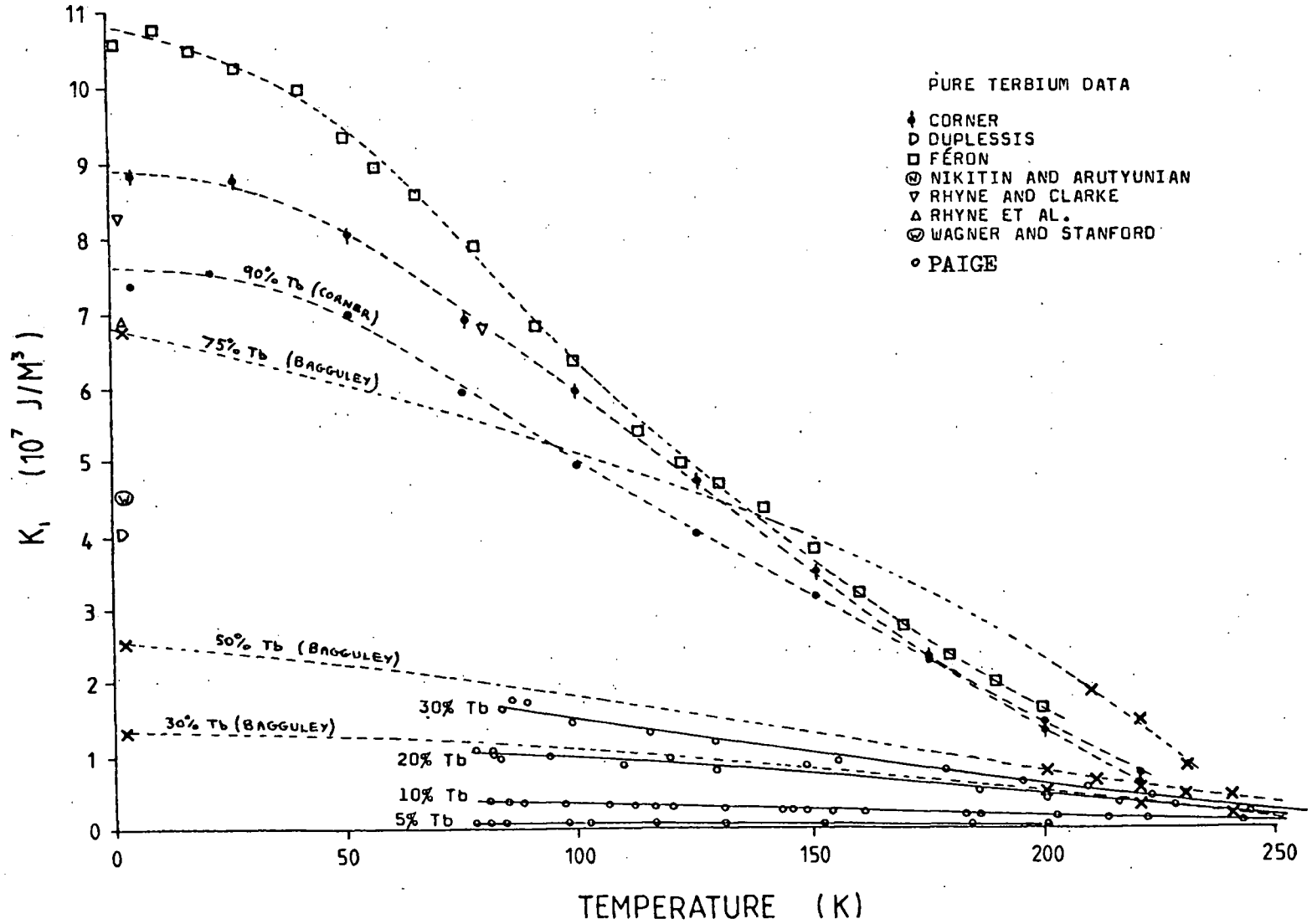

K_4 VS TEMPERATURE FOR Tb_xGd_{1-x} ALLOYS;

(AFTER PAIGE, 1983)

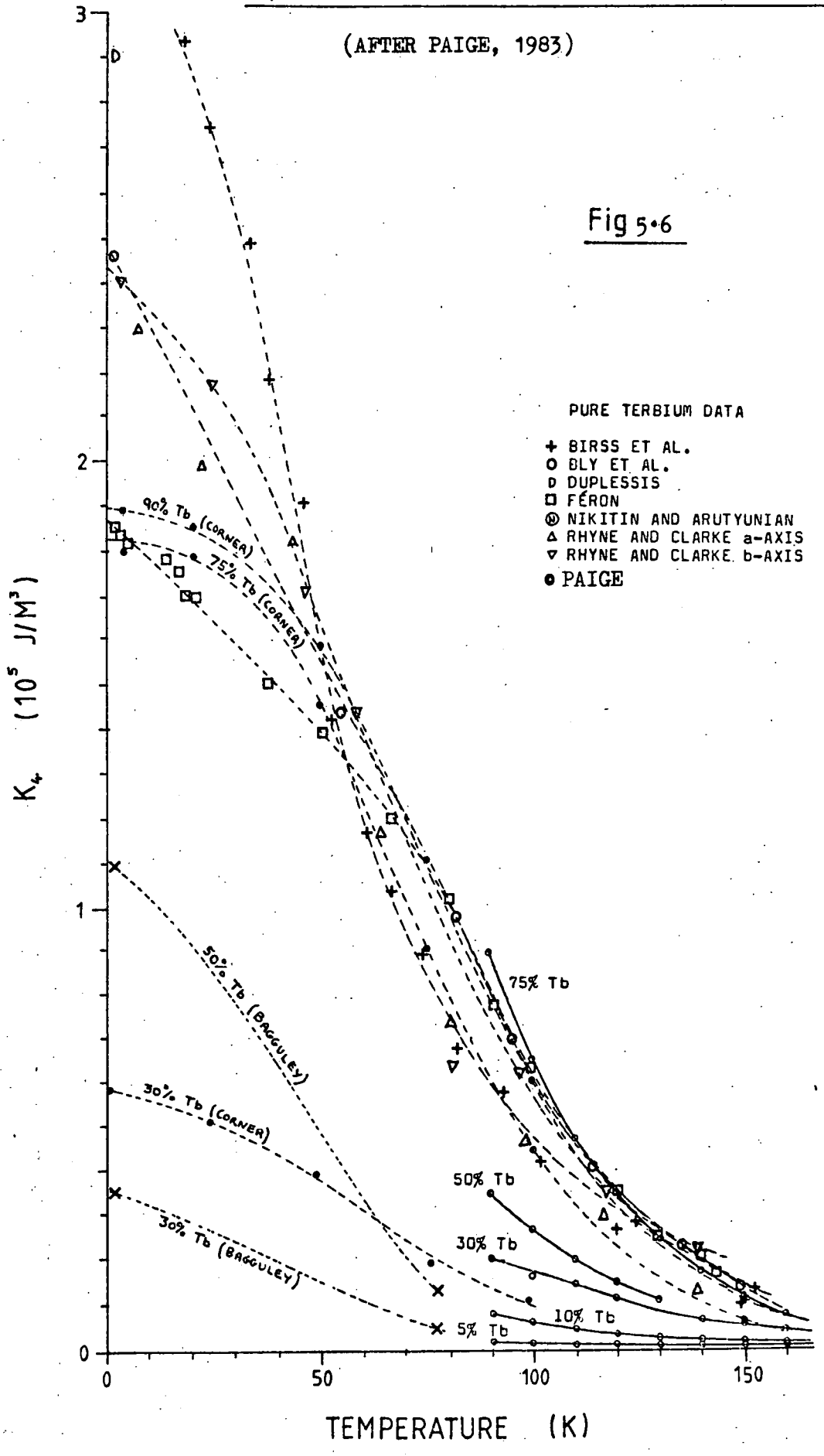

Fig 5·6

gauge technique. These four magnetostriction constants are related to those of Clark and Callen's expression (4.45) by the equation 4.56. The results of Alstad and Legvold (1964) are shown in Figure 5.7. The results of Bozorth and Wakiyama are very similar to these. A marked change in slope of λ_A was observed where the easy direction of magnetization tilts away from $\hat{c}$-axis. The temperature dependence is different from that of the single-ion model. The change in sign in $(\lambda_A - \lambda_B) = \lambda^{\gamma}$ is an effect of two-ion origin. This reversal of sign in λ^{γ} before vanishing is in agreement with the measurements of other authors. Coleman and Pavlovic (1965) have also studied the temperature dependence of magnetostriction using another magnetostriction expression (4.57) in terms of exchange magnetostriction constants which are independent of magnetization direction and depend only on the magnitude of magnetization. These constants are related to those of Bozorth (1954) by equations 4.58. Callen and Callen (1965) have fitted the experimental values of λ^{γ} determined by Coleman (1964) by an expression having single-ion and two-ion contributions

$$\lambda^{\gamma} = 351 \times 10^{-5} \hat{I}_{5/2}(\mathcal{L}^{-1}(m)) - 243 \times 10^{-6} m^2 \qquad 5.1$$

where the symbols have their usual meaning as defined in equation 4.22. The fit is remarkable for the entire range of temperature.

The results of the measurements of forced magneto-

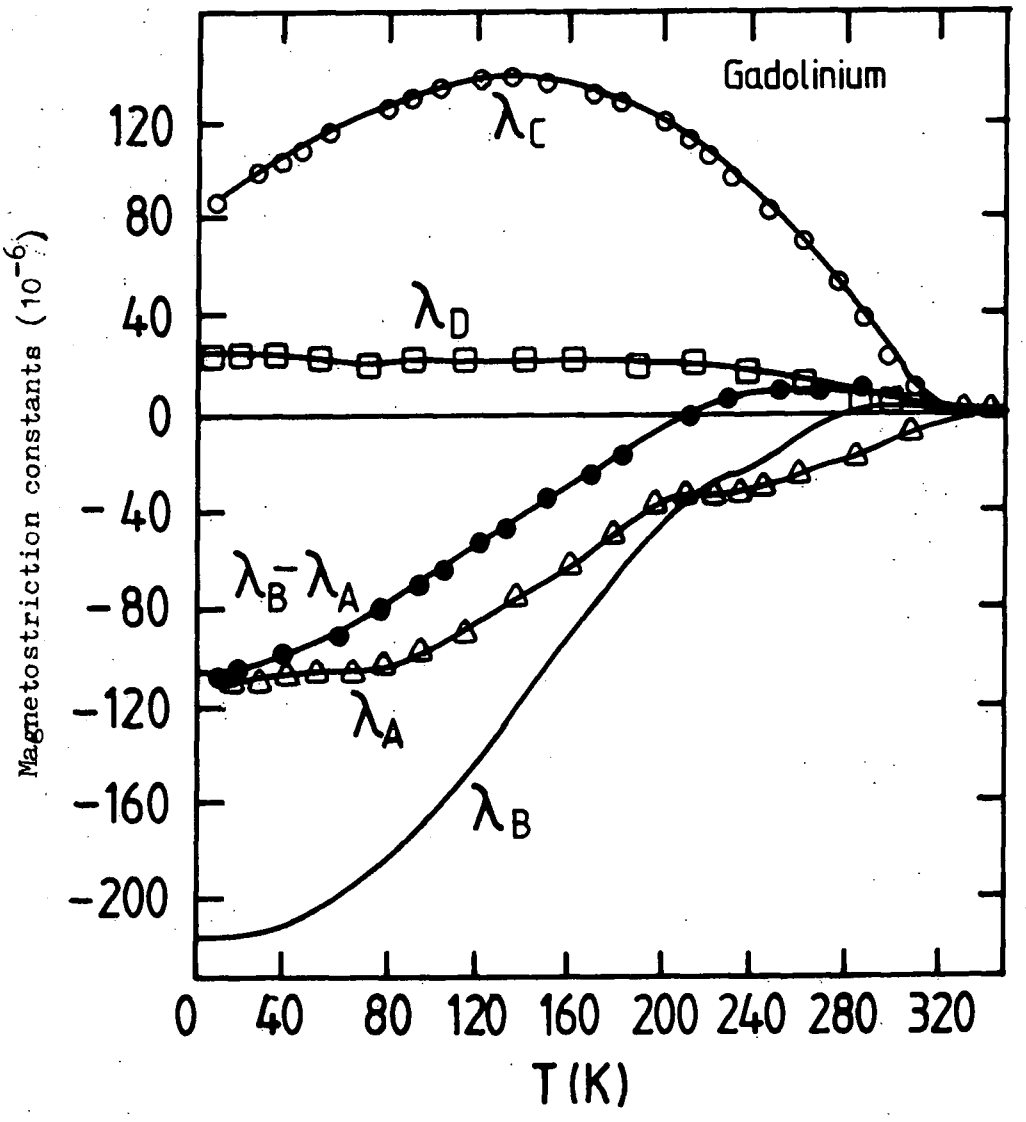

Fig. 5.7 Temperature dependence of the four $l = 2$ order anisotropic magnetostriction contants for gadolinium (after Alstad and Legvold, 1964).

striction by Bozorth and Wakiyama (1963), and Coleman and Pavlovic (1965) along with the theoretical estimations of Tonegawa (1964) based on the model of Yosida and Watabe (1962) are shown in Figure 5.8. The forced magnetostriction is approximately linear to the field strength and is independent of magnetization direction. The results in field strengths above 10 kOe, free from ordinary anisotropic magnetostriction (λ_A, λ_C), show that expansion $\lambda_{||}$ measured parallel to the $\hat{c}$-axis is about 20 times the contraction $\lambda_{\perp}$ measured perpendicular to the $\hat{c}$-axis.

Saturation magnetostriction measurements by Mishiama et al. (1976) are shown in Figure 5.9. They determined the constants by Fourier analysis of the saturation magnetostriction and included higher order terms up to order 8 in $\lambda_i^{\alpha,\ell}$ to explain the experimental results. Their quoted values are given in table 5.4.

5.6 Magnetostriction of Terbium

Terbium has total orbital moment L = 3, spin S = 3 and J = L + S = 6. It has basal plane anisotropy, the $\hat{b}$-axis being the easy axis, the $\hat{a}$-axis is a hard axis in the basal plane and the $\hat{c}$-axis is the hardest axis. The single-ion interaction leads to phenomenally high magnetic anisotropy and giant magnetostriction. The field required to magnetize terbium along the $\hat{c}$-axis is of the order of 100 tesla (Legvold, 1980). Magnetostriction measurements on Tb in magnetic fields up to 15 kOe for temperatures above 80 K were first reported by Nikitin (1962). Darnell (1963a,b) measured the lattice

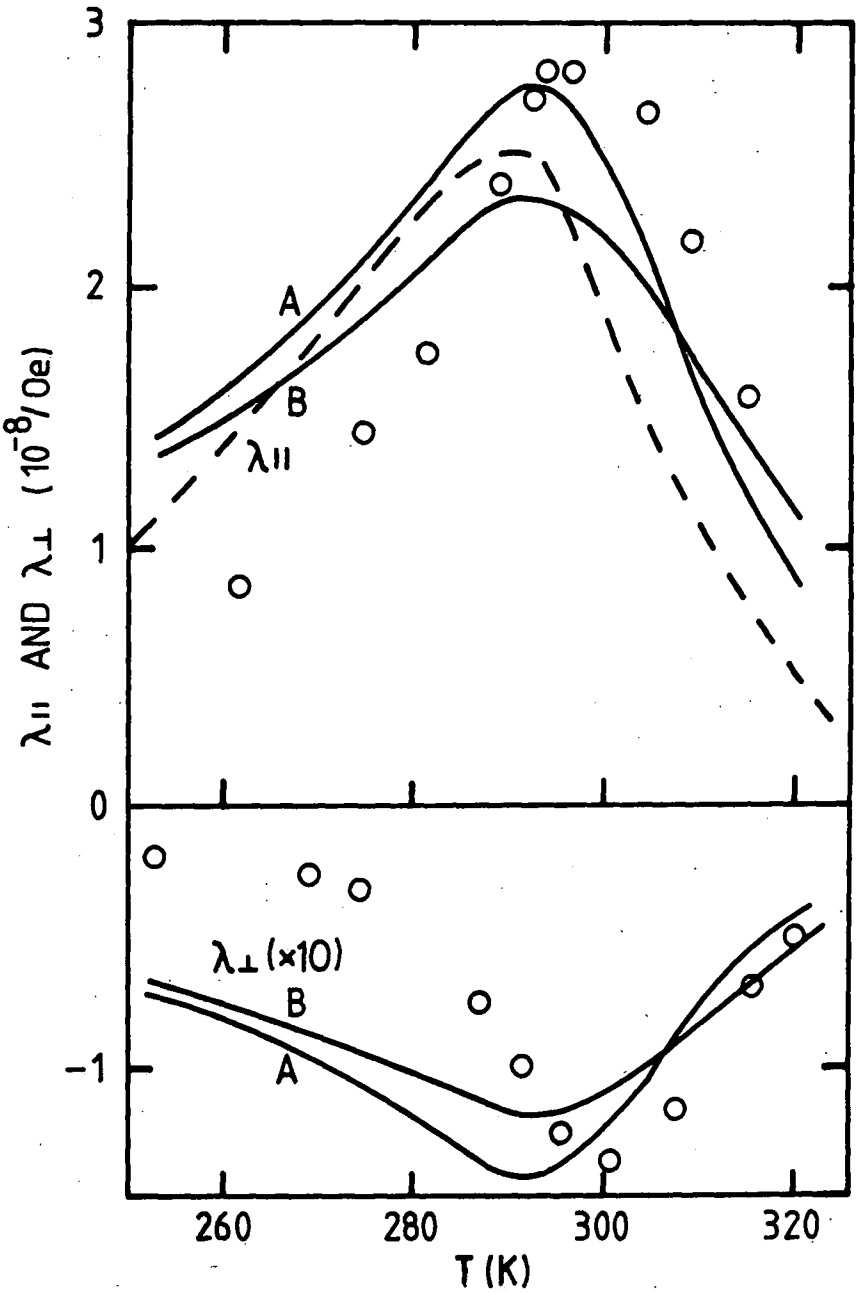

Fig. 5.8 The temperature dependence of the forced magnetostriction coefficients of Gd, λ_{11} and $\lambda_{\perp}$, parallel and perpendicular to the $\hat{c}$-axis respectively, o represents the results by Bozorth and Wakiyama (1963), —— by calculation of Tonegawa (1964), and --- those by Coleman and Pavlovic (1965).

TABLE 5.4

Magnetostriction coefficients at zero Kelvin in units of 10^{-3} (after Legvold, 1980).

Element	$\lambda_1^{\alpha,2}$	$\lambda_2^{\alpha,2}$	$\lambda^{\gamma,2}$	$\lambda^{\epsilon,2}$	$\lambda_1^{\alpha,0}-\frac{1}{3}\lambda_1^{\alpha,2}$	$\lambda_2^{\alpha,0}-\frac{1}{3}\lambda_2^{\alpha,2}$	$\lambda^{\gamma,4}$
Gadolinium[a]	0.14	-0.13	0.11	0.02	-	-	-
Terbium[b]	-2.6[c]	9.0[c]	8.7	15.0[c]	-0.8	4.3	-2.1
Dysprosium[b]	-	-	9.4	5.5	-2.0	7.3	1.5
Holmium[b]	-	-	2.5[c]	-	-3.9	7.1	-
Erbium[b]	-	-	-5.1[c]	-	+0.3	6.2	-

TABLE 5.5

Magnetostriction constants of Gd/Tb alloys at OK in units of 10^{-4} (after Joraide, 1980).

	$\lambda^{\gamma,2}$	$\lambda_1^{\alpha,2}$	$\lambda_2^{\alpha,2}$	$\lambda^{\epsilon,2}$
95%Gd - 5% Tb	3.22		1.55	2.8
80%Gd - 20%Tb	5.5	- 3.6	0.65	6.4
50%Gd - 50%Tb	14.4	- 10.7	1.15	
25%Gd - 70%Tb	25.3	- 16.6	27.6	

(a) After Mishima et al. (1976).

(b) After Rhyne (1972).

(c) Extrapolated from paramagnetic range using single-ion theory.

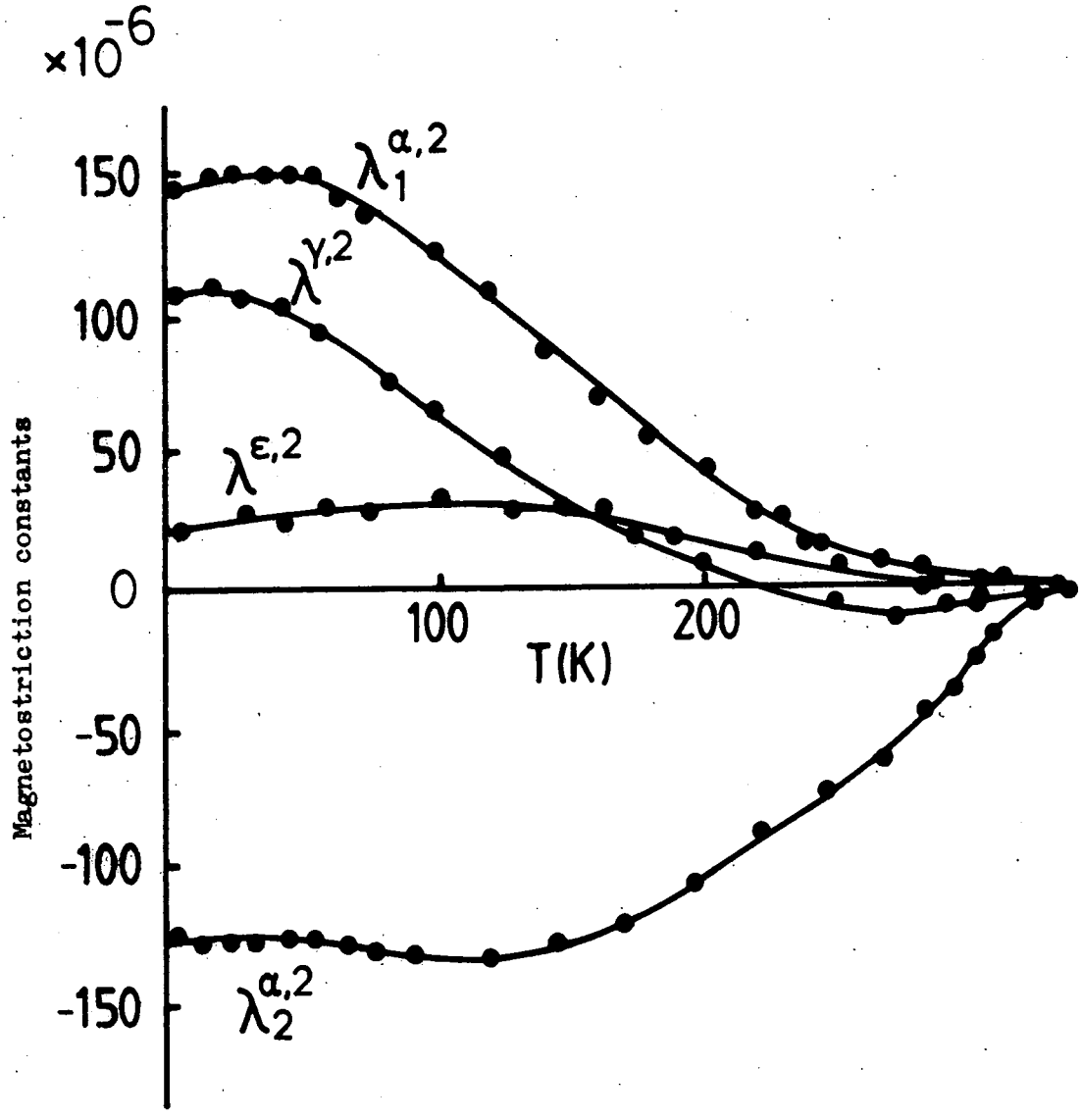

Fig. 5.9 Magnetostriction constants of gadolinium as functions of temperature (after Mishima et al., 1976).

parameters of Tb by X-ray techniques and deduced the thermal dependence of the magnetostriction coefficients between 77K and room temperature. Magnetostriction and forced magnetostriction for the same temperature range have been measured by Du Plessis (1969a,b) and Du Plessis and Alberts (1965, 1968). Rhyne and Legvold (1965) have measured the magnetostriction of Tb over the whole range of temperature of magnetic ordering in applied fields up to 30kOe by strain gauge methods. Darnell (1963) and Rhyne and Legvold (1965) used the expression for magnetostriction (4.41) derived by Mason for a hexagonal system with the assumption that the magnetic moment remains in the basal plane. The coefficients A,B,E,F and J in this expression correspond to order $\ell = 4$, while the other coefficients correspond to $\ell = 0$ and $\ell = 2$. The most complete and accurate measurements of coefficients A and C by Rhyne and Legvold (1965) are shown in Figure 5.10. The temperature dependence fits very well with the theoretical temperature variations predicted by Callen and Callen (1963) given in equations 4.59 i.e. A follows $\hat{I}_{9/2}$ $(\pounds^{-1}(m))$ and C follows $\hat{I}_{5/2}$ $(\pounds^{-1}(m))$. The temperature dependence of forced magnetostriction, which is a field dependence of linear magnetostriction expressed as $(\delta\ell/\ell)/\delta H$, in the $\hat{a}$, $\hat{b}$ and $\hat{c}$ directions for Tb in magnetic fields up to 30kOe parallel to the $\hat{b}$-axis is shown in Figure 5.11. It shows maxima around the Néel temperature. The values near the Curie temperature are field dependent and do not represent true saturation forced magnetostriction.

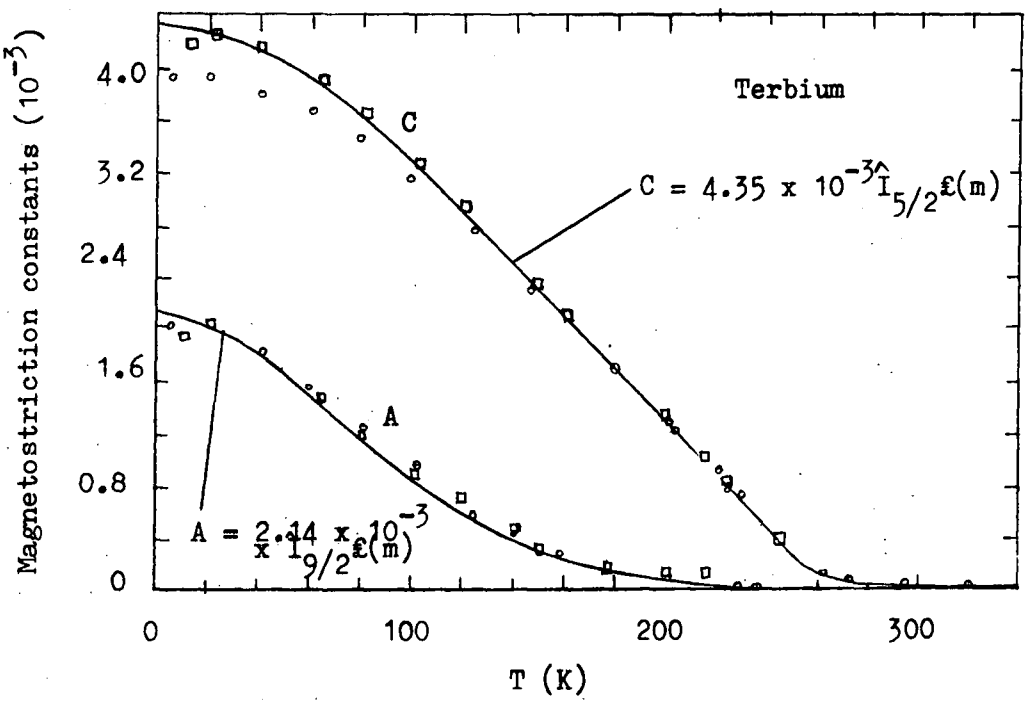

Fig. 5.10 Temperature dependence of the magnetostriction constants A and C at 30 kOe, □ $\hat{a}$-axis and ○ $\hat{b}$-axis strains.

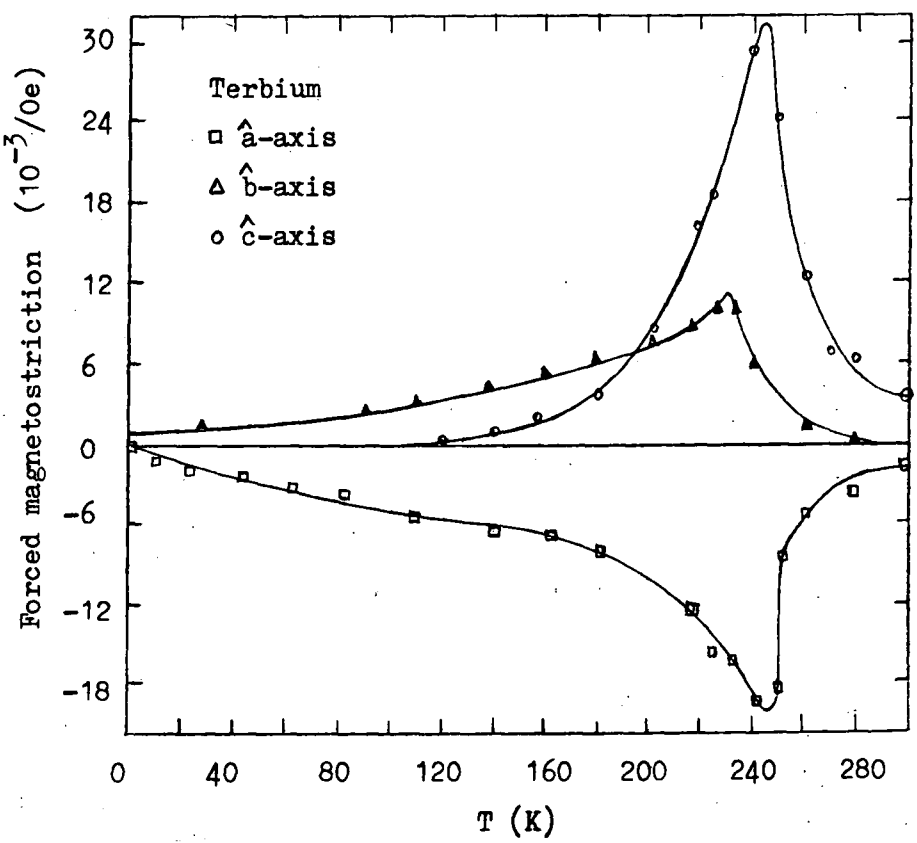

Fig. 5.11 Temperature dependence of forced magnetostriction of Tb, field parallel to the $\hat{b}$-axis .

(Both figures are after Rhyne and Legvold, 1965)

Du Plessis used the Clark and Callen expression (4.45) to determine the magnetostriction constants. The temperature dependence of $\lambda^{\gamma,2}, \lambda_2{}^{\alpha,2}$ and $\lambda^{\epsilon,2}$ observed by Du Plessis fits very well with $\hat{I}_{5/2}(\mathcal{L}^{-1}(m))$ over the whole temperature range except for $\lambda^{\epsilon,2}$ near the Curie temperature for measured values smaller than 2×10^{-4}. His results, which are similar to those of Rhyne and Legvold are shown in Figure 5.12 a,b. Bartholin et al. (1970, 1971) calculated the spontaneous magnetostriction which fits better with Rhyne and Legvold than Darnell. Finkel and Belovol (1973, 1974) also investigated strains of polycrystalline Tb and Dy with X-ray diffraction techniques and the changes in the a and b directions are directly comparable with the results of Rhyne and Legvold. Their applied field of 3T was insufficient to produce a single domain in Tb below 40k due to basal plane anisotropy of Tb. Martin reanalysed the results of Rhyne and Legvold to allow for the multidomain nature of the samples. As a result the values of A and C changed slightly and are in reasonable agreement with measurements of Keeler and Pearson (1978) in a field of 4T using a capacitance technique. Houmann et al. (1975) found that C follows $m^{2.42 \pm .04}$ while A follows $m^{7.5 \pm .15}$ with temperature. The difference between the expressions and the larger power of reduced magnetization is suggested to indicate the two-ion contributions. The extrapolated values of various magnetostriction constants at OK for Tb after different authors are given in Table 5.4 along with those of Gd.

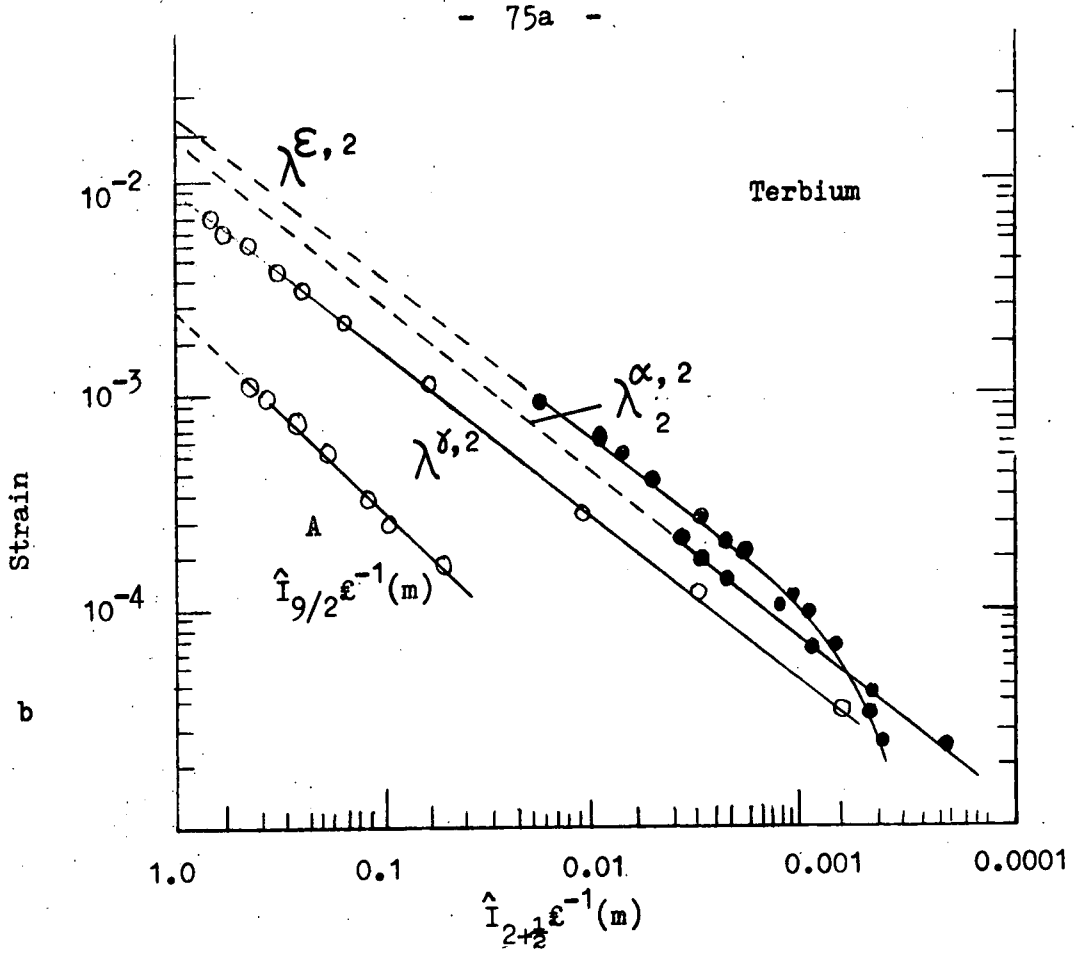

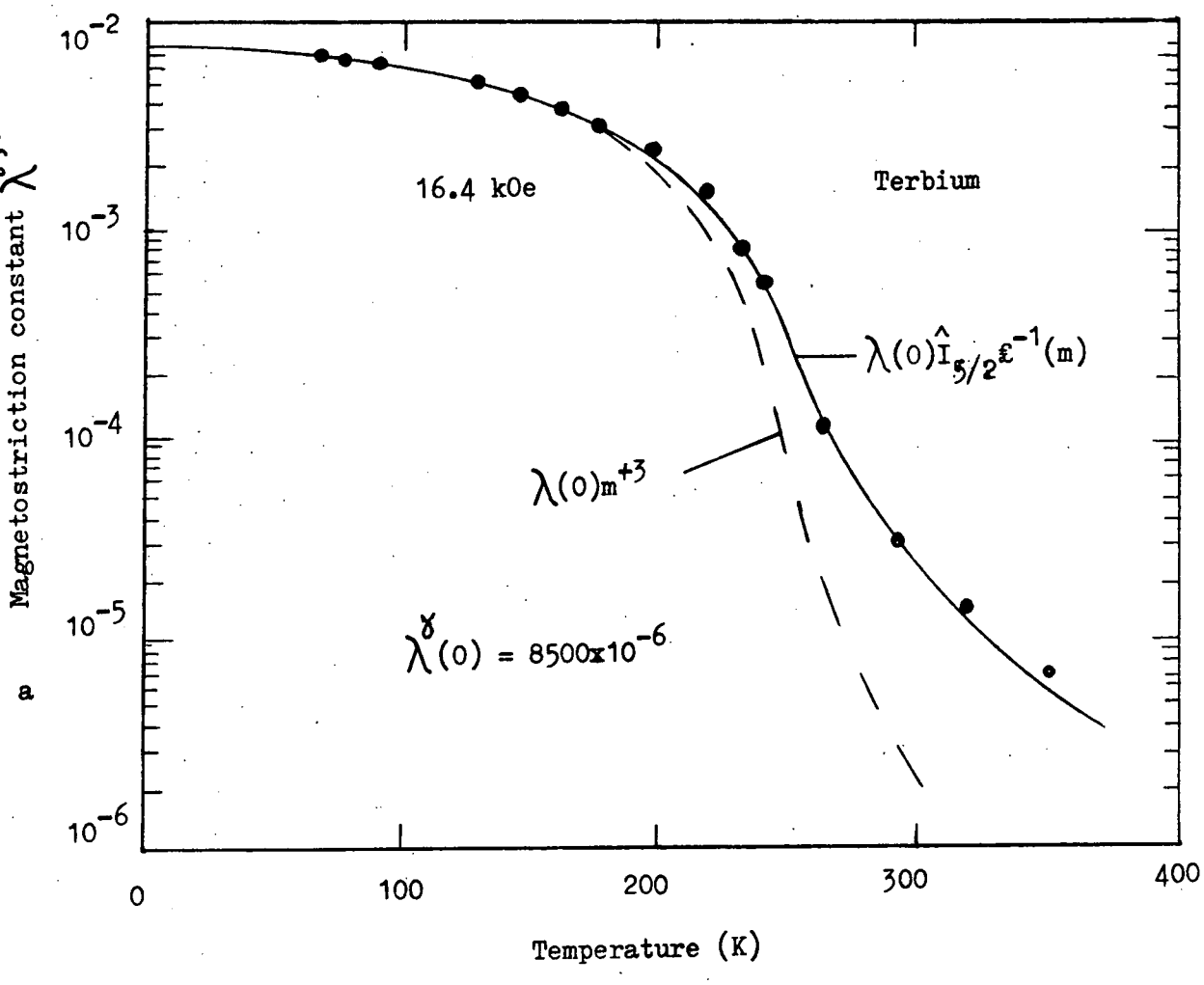

Fig. 5.12 (a) Temperature variation of $\lambda^{\gamma,2}$
(b) 'A' strain is versus $\hat{I}_{9/2}$ (after du Plessis, 1968).

5.7 Magnetostriction of Gadolinium and Terbium Alloys

Terbium is an f-state element exhibiting strong anisotropy and high magnetostriction. On the other hand gadolinium being an s-state element has weak anistropy and magnetostriction. Gadolinium and terbium form continuous solid solution with each other with hexagonal closed packed structure. The Tb-Gd alloys have an antiferro-magnetic helixphase between the para- and ferromagnetic phases only for Gd concentration less than 6 at. %, and show a direct transition from the paramagnetic to the ferromagnetic phase for the remainder of the alloy series (Fujiwara et al., 1977). The fermi surfaces of Tb and Gd are quite close in their structure (Taylor and Darby 1972). Gadolinium thus acts as an ideal diluent to study the single- and or two-ion behaviour of Tb metal. The magnetic properties of the rare earths have been studied extensively, but there are not many magnetostriction measurements on particular Gd-Tb alloys. Nikitin et al. (1977) investigated magnetic, magnetostrictive and electric properties of single crystal terbium-gadolinium alloys. They measured the spontaneous magnetostriction deformations λ_{oc} along the $\hat{c}$-axis and λ_{ob} along the $\hat{b}$-axis using strain gauges by subtracting the phonon part of the thermal expansion $(\Delta\ell/\ell)_{ph}$ from the experimental $(\Delta\ell/\ell)^{\parallel}$ and $(\Delta\ell/\ell)^{\perp}$ curves measured in the magnetic field along the easy axis of magnetization. The phonon part for each alloy was obtained from the thermal expansion curves of non-magnetic lutetium with correction for the

change of Debye temperature assuming that the largest elongation $(\Delta\ell/\ell)_{ph}$ is a universal function of T/θ_D, where θ_D is the Debye temperature. $\lambda^{\gamma,2}$ was obtained from the difference between the longitudinal and the transverse magnetostrictions in the basal plane. The constants $\lambda^{\gamma,2}$ and λ_{ob} decrease linearly with increasing gadolinium concentration as would be expected for a single-ion model. The constant λ_{oc} varies differently with change in concentration. With increasing gadolinium concentration, it remains constant up to about 50% gadolinium, then decreases, has a minimum in the region 60-70% Gd and finally increases rapidly afterwards. Their results are shown in Figure 5.13. These magnetostriction constants used by Nikitin et al. are linear functions of those of Clark and Callen's (Nikitin et al. (1976)) as follows:

$$\begin{aligned}\lambda_a &= \lambda_1^{\alpha,o} - \tfrac{1}{3}\lambda_1^{\alpha,2} + \tfrac{1}{2}\lambda^{\gamma,2} \\ \lambda_b &= \lambda_1^{\alpha,o} - \tfrac{1}{3}\lambda_1^{\alpha,2} - \tfrac{1}{2}\lambda^{\gamma,2} \\ \lambda_c &= \lambda_2^{\alpha,o} - \tfrac{1}{3}\lambda_2^{\alpha,2}\end{aligned} \qquad 5.2$$

Measurements of various magnetostriction constants for terbium gadolinium alloys were also made by Joraide, (1980) by rotating magnetization with respect to crystallographic axes using resistive strain gauges, at the University of Durham. The magnetostriction constants of order $\ell = 2$ of the Clark and Callen expression 4-45 were measured for four alloy compositions in magnetic fields up to 13 Tesla in temperatures ranging from liquid helium to room temperature. The observed temperature variation of $\lambda^{\gamma,2}$ for the alloys is shown in Figure 5.14.

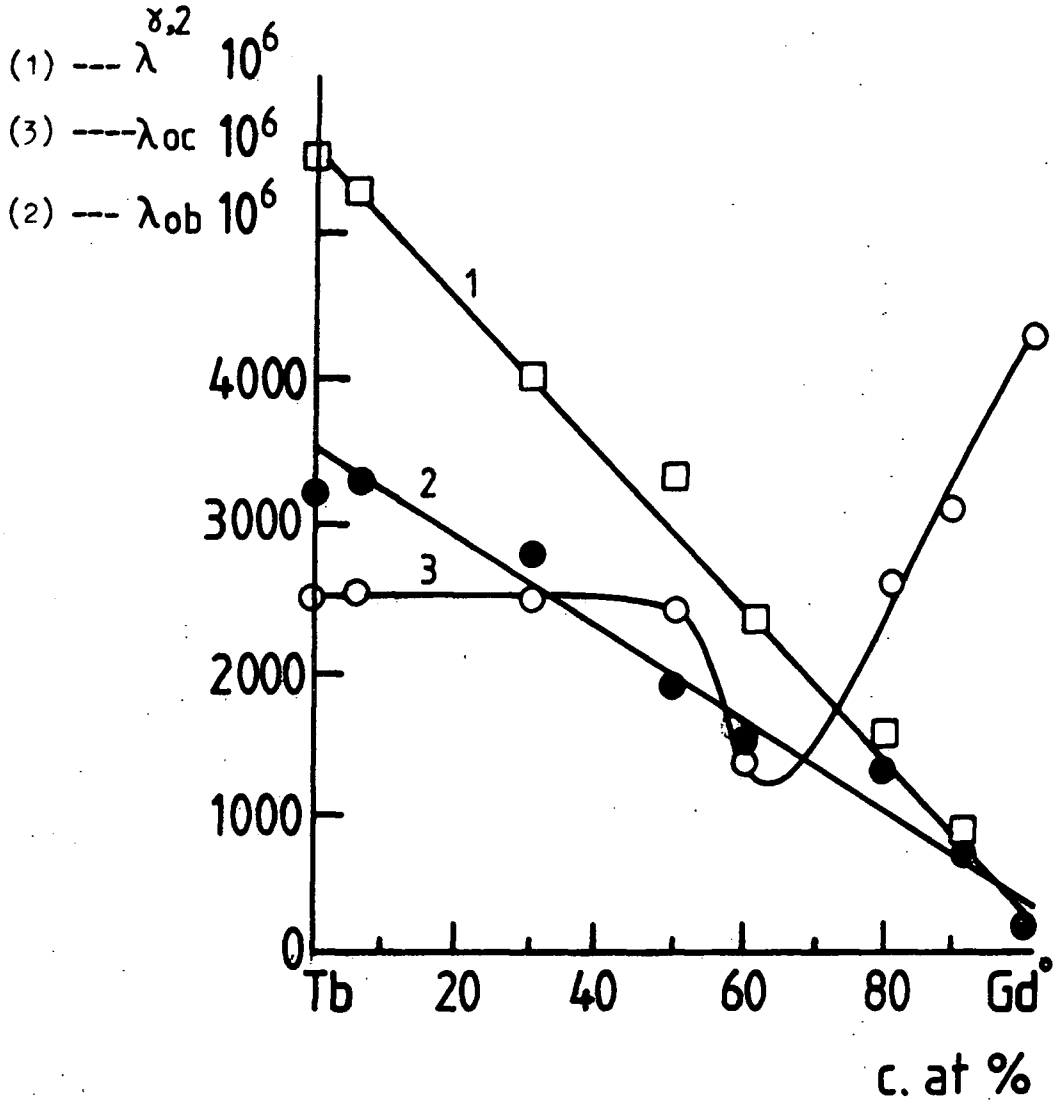

Fig. 5.13 Temperature variation of magnetostriction constants, curve 2 and 3 represent spontaneous magnetostriction along b and c axis respectively (after Nikitin et al., 1977a).

The magnetization values used were obtained from the interpolated curves between magnetization of Tb after Hegland et al. (1963) and Gd after Nigh et al. (1963). The temperature dependence of $\lambda^{\gamma,2}$ does not seem to follow a single-ion variation particularly at lower Tb concentrations. The fit with a single-ion mechanism does improve towards the Tb rich end but does not cover the entire temperature range even at 75% of Tb. The coefficient $\lambda_2^{\alpha,2}$ does not increase much up to 50% of Tb but quite significantly for 75% of Tb. The temperature variation does seem to follow the single-ion dependence very well but for 75% of Tb the fit is excellent. The temperature dependence of $\lambda_2^{\alpha,2}$ for alloys is shown in Figure 5.15. Similar curves for $\lambda_1^{\alpha,2}$ and $\lambda^{\epsilon,2}$ are shown in Figure 5.16 and 5.17 respectively. The value of $\lambda_1^{\alpha,2}$ was observed to vary linearly with the alloy composition while the other constants varied in a roughly exponential manner. The temperature variation of $\lambda_2^{\alpha,2}$, $\lambda_1^{\alpha,2}$ and $\lambda^{\epsilon,2}$ was not capable of being well represented by any simple theoretical model. The alloy containing 50% Tb showed a better fit with a model containing contributions from both single- and two-ion mechanisms. The temperature dependence of $\lambda^{\epsilon,2}$ does not fit to any theoretical models for 5% of Tb alloy but for 20% of Tb the fit is reasonable with the model containing both single- and two-ion contributions. The extrapolated values for these constants at 0 K are given in Table 5.5.

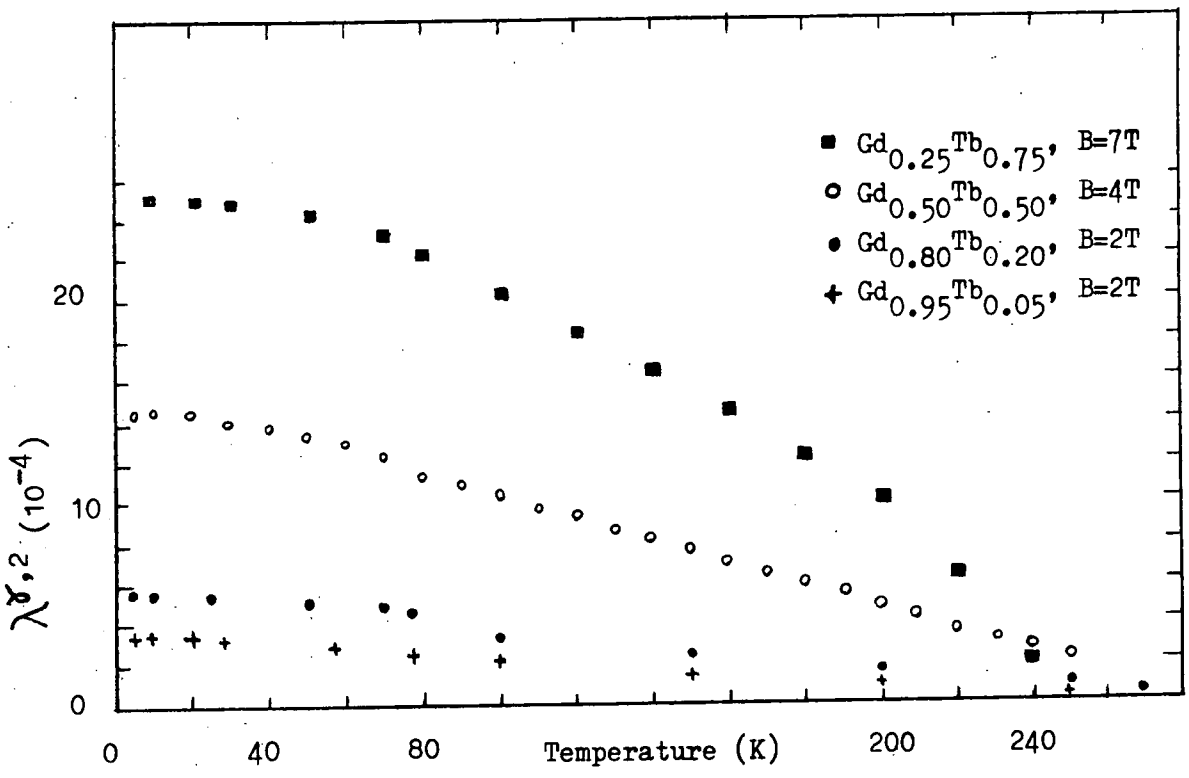

Fig. 5.14 Temperature variation of $\lambda^{\gamma,2}$ (after Joraide, 1980).

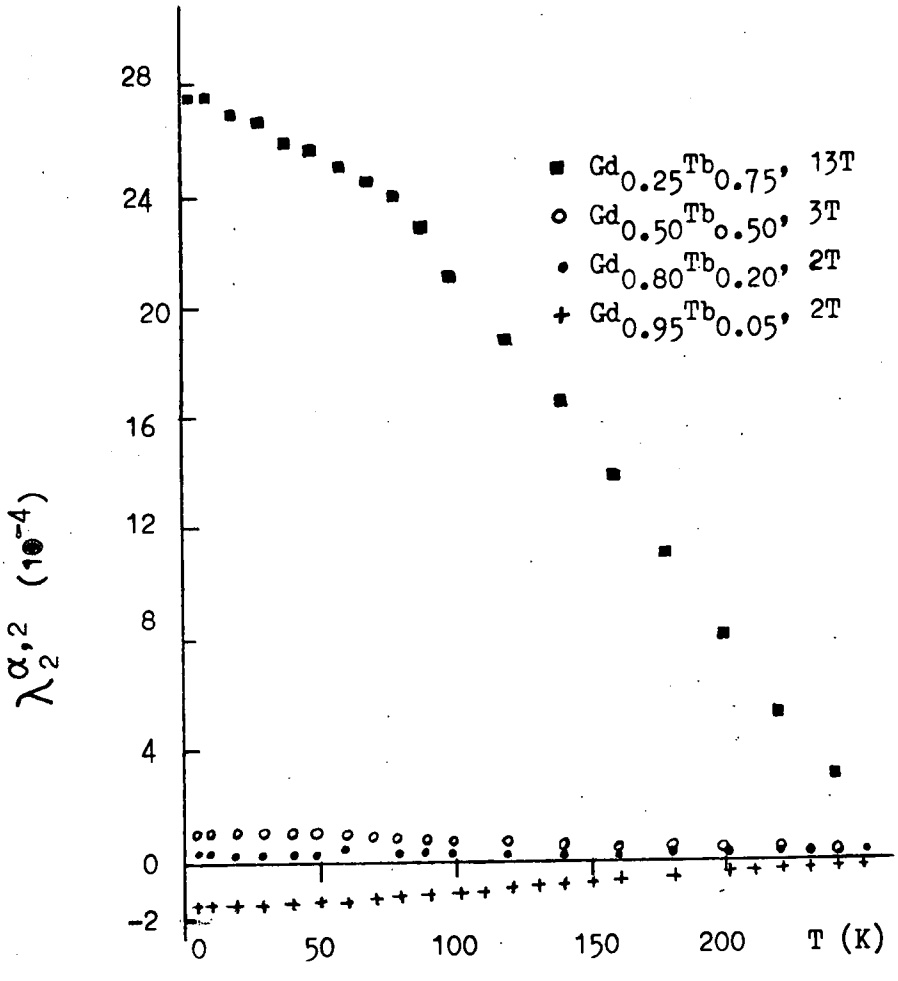

Fig. 5.15 Temperature variation of $\lambda_2^{\alpha,2}$ (after Joraide, 1980).

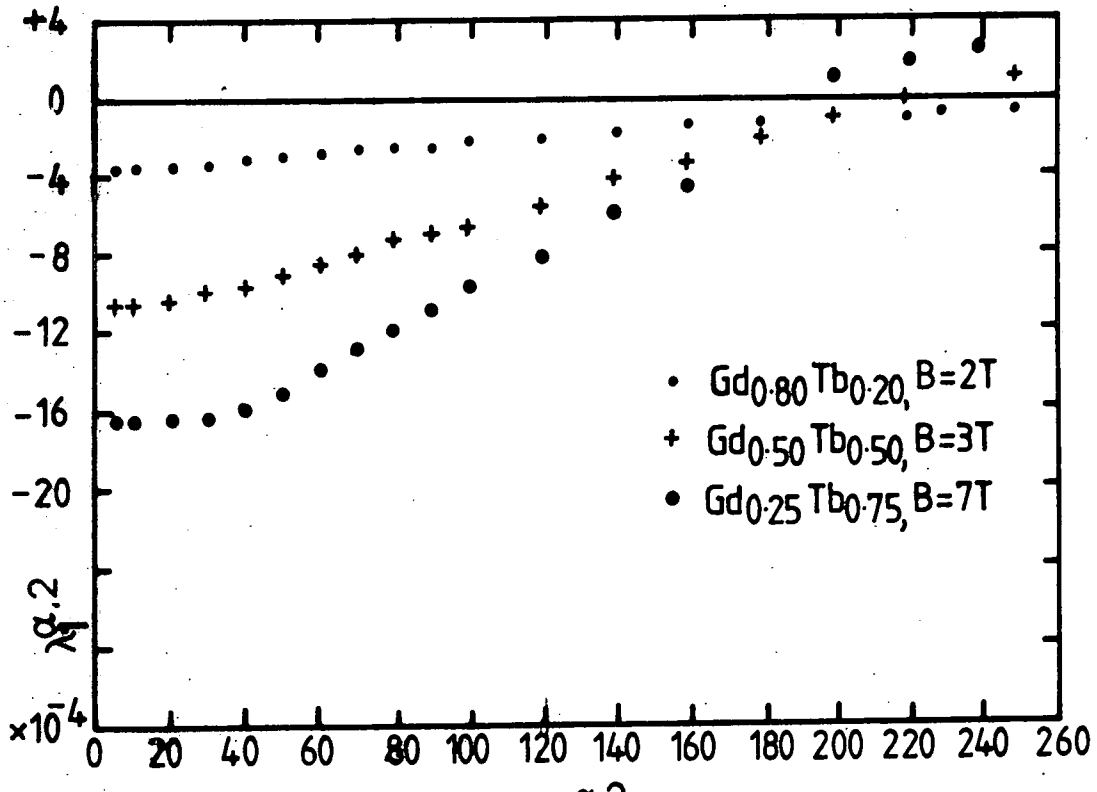

Fig.5.16 Temperature dependence of $\lambda^{\alpha,2}$ for Gd/Tb alloys, after Joraide (1980).

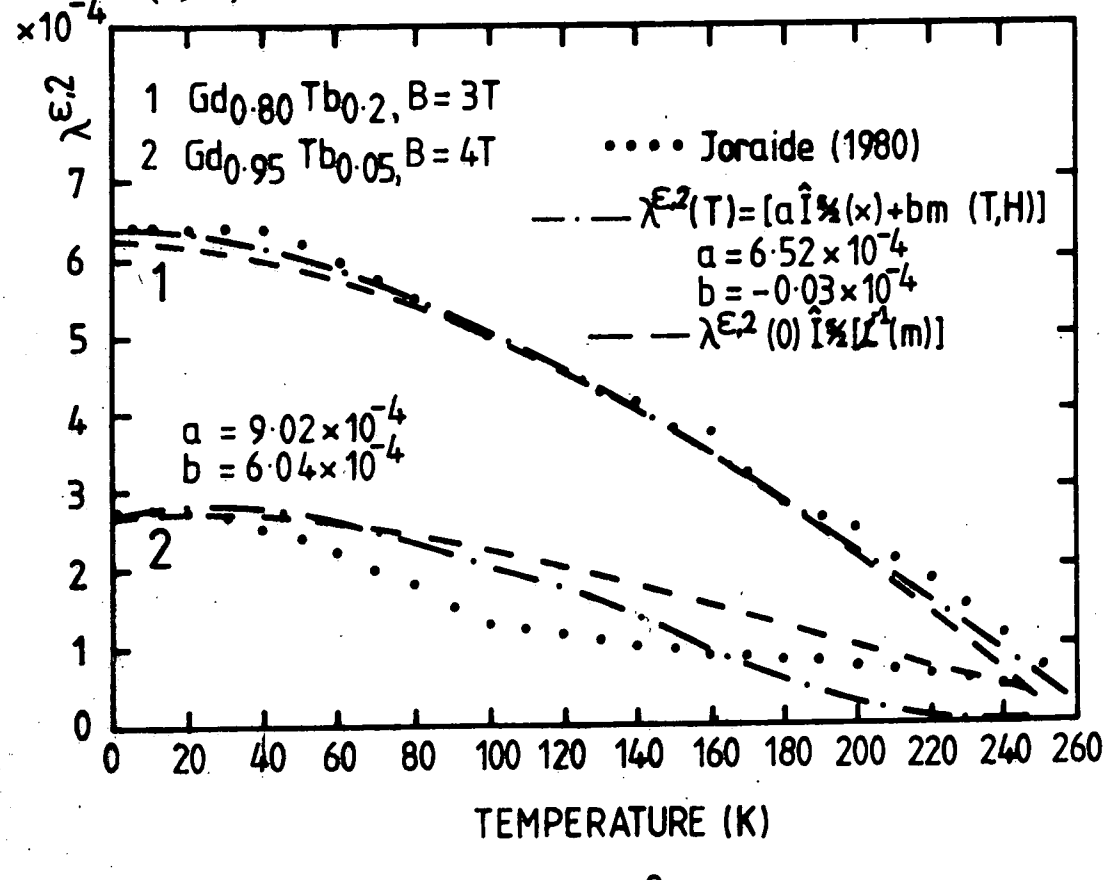

Fig. 5.17 Temperature dependence of $\lambda^{\varepsilon,2}$ for Gd/Tb alloys (after Joraide, 1980).

In the model for the determination of the above magnetostriction constants Joraide (1980) assumed, from the saturation observed for these constants against increasing applied field, that the magnetization was following the external field and was continuously rotated through 180°. This made the derivation of the constants possible from the amplitude measurements of the peak to peak variation of the strain observed. The assumption that the magnetization follows the field closely is reasonable in the case of the $\lambda^{\gamma,2}$ constant where rotation is confined to the basal plane. The very high anisotropy of the terbium gives cause for justifiable doubts about the validity for rotation in planes containing the $\hat{c}$-axis. The calculation of magnetization angle with respect to the applied field from the anisotropy values shows that the magnetization is only pulled a few degrees out of the basal plane for alloys close to the terbium rich end and it never passes through the $\hat{c}$-axis for the available fields. The saturation observed might be due to anchoring of the magnetization after a few degrees rotation from the easy axis and the increase in the strength of the field was not enough to cause further rotation.

To understand the real mechanism of the interaction of the terbium ions leading to the giant magnetic anisotropy and magnetostriction it is important to study the temperature dependence of these phenomena. Magnetic anisotropy has been very recently and extensively investigated by Hawkins (1982), Paige (1983) and Corner (1983b) at Durham

in addition to previous work by the other researchers.

The magnetostriction measuremenets made by Joraide (1980) do not cover the entire range of alloy composition. In the study of the temperature dependence, the terbium ions should be gradually diluted with gadolinium ions in order to differentiate between the various possible theoretical interactions. The temperature dependence of magnetostriction $\lambda^{(T)}/\lambda_{(o)}$ of Tb-Gd alloys has not been established by Nikitin et al. over the entire range of the alloy composition. It was thought desirable to complete the study over the whole range of alloy composition. It was also thought necessary to remeasure the $\lambda_1^{\alpha,2}$ and $\lambda_2{}^{\alpha,2}$ constants using magnetization directions rather than applied field ones for the reasons pointed out earlier. Study of the 90% Gd - 10% Tb, the intermediate composition, was also needed to investigate further the anomalous behaviour of $\lambda_2{}^{\alpha,2}$ constant reported by Joraide for the 80% Gd - 20% Tb specimen.

CHAPTER 6

EXPERIMENTAL TECHNIQUES AND APPARATUS

6.1 Determination of Magnetostriction Constants

The magnetostriction constants of order $\ell = 2$ were measured using the expression of Clark and Callen (4.45):

$$\frac{\delta \ell}{\ell} = \lambda_1^{\alpha,0}(1-\beta_z^2) + \lambda_2^{\alpha,0}\beta_z^2 + \lambda_1^{\alpha,2}(1-\beta_z^2)(\alpha_z^2 - \tfrac{1}{3}) + \lambda_2^{\alpha,2}\beta_z^2(\alpha_z^2 - \tfrac{1}{3})$$
$$\lambda^{\gamma,2}\left[\tfrac{1}{2}(\beta_x^2-\beta_y^2)(\alpha_x^2-\alpha_y^2) + 2\beta_x\beta_y\alpha_x\alpha_y\right] + 2\lambda^{\epsilon,2}(\beta_x\alpha_x + \beta_y\alpha_y)\beta_z\alpha_z$$

where the α's and β's are the direction cosines of magnetization and of strain respectively.

6.1.1 The Constant $\lambda^{\gamma,2}$

To find the $\lambda^{\gamma,2}$ constant, strain was measured along the $\hat{b}$-axis of the basal plane crystals. The direction cosines then have the following values when the magnetization lies at an angle of θ to the $\hat{b}$-axis,

$$\begin{aligned} \alpha_x &= \sin\theta & \beta_x &= 0 \\ \alpha_y &= \cos\theta \quad \text{and} & \beta_y &= 1 \\ \alpha_z &= 0 & \beta_z &= 0 \end{aligned} \qquad 6.1$$

Substituting first β's and then α's in equation 4.45, yields equations:

$$\lambda_b = \lambda_1^{\alpha,0} + \lambda_1^{\alpha,2}(\alpha_z^2 - \tfrac{1}{3}) - \tfrac{1}{2}\lambda^{\gamma,2}(\alpha_x^2 - \alpha_y^2) \qquad 6.2$$

and

$$\begin{aligned} \lambda_b &= \lambda_1^{\alpha,0} - \tfrac{1}{3}\lambda_1^{\alpha,2} - \tfrac{1}{2}\lambda^{\gamma,2}(\sin^2\theta - \cos^2\theta) \\ &= \lambda_1^{\alpha,0} - \tfrac{1}{3}\lambda_1^{\alpha,2} + \cos 2\theta \,. \end{aligned} \qquad 6.3$$

Now if the magnetization is rotated from the $\hat{b}$-axis to the orthogonal $\hat{a}$-axis, i.e. from $\theta = 0$ to $\theta = 90°$, then

the constant $\lambda^{\gamma,2}$ can be derived from the difference of the strains

$$\lambda_b^{\theta=o} - \lambda_b^{\theta=90} = \lambda^{\gamma,2} \qquad 6.4$$

6.1.2 The Constant $\lambda_1^{\alpha,2}$

If the strain is measured along the $\hat{a}$-axis of a crystal with the disc plane perpendicular to the $\hat{b}$-axis, then the strain direction cosines are:

$$\begin{aligned} \beta_x &= 1 \\ \beta_y &= 0 \\ \beta_z &= 0 \end{aligned} \qquad 6.5$$

and we get:

$$\lambda_a = \lambda_1^{\alpha,0} + \lambda_1^{\alpha,2}(\alpha_z^2 - \tfrac{1}{3}) + \tfrac{1}{2}\lambda^{\gamma,2}(\alpha_x^2 - \alpha_y^2) \quad . \qquad 6.6$$

The magnetization in specimens, other than the basal plane ones, does not remain in one plane throughout the rotation process. If the initial applied field lies along the $\hat{a}$-axis and is strong enough, the magnetization will lie along the $\hat{a}$-axis. If this field is now rotated towards the $\hat{c}$-axis its component in the $\hat{a}$-axis direction will decrease. The sample will split into two sets of domains in each of which the magnetization vector will rotate in the basal plane towards the immediately adjacent $\hat{b}$-axes at 30° on both sides of the original $\hat{a}$-axis because of the large basal plane anisotropy. There will also be a rotation of the magnetization towards the $\hat{c}$-axis, indeed both changes will take place simultaneously, but

their relative importance will depend upon the terbium concentration, the temperature and the applied field. The shape anisotropy makes the alignment of magnetization along the $\hat{b}$-axis perpendicular to the plane at the disc energetically unfavourable. We assume that the magnetization lies along an arbitrary direction making an angle θ with the $\hat{c}$-axis and that its basal plane projection makes an angle ϕ with the $\hat{a}$-axis. The direction cosines of magnetization are, then;

$$\begin{aligned} \alpha_x &= \sin\theta \cos\phi \\ \alpha_y &= \sin\theta \sin\phi \\ \alpha_z &= \cos\theta \end{aligned} \qquad 6.7$$

The substitution of α's gives an expression which can yield $\lambda_2^{\alpha,2}$ by observing the change in strain for rotation of magnetization from an angle of 90° to the $\hat{c}$-axis to an angle θ:

$$\lambda_a = \lambda_1^{\alpha,0} + \lambda_1^{\alpha,2}(\cos^2\theta - \tfrac{1}{3}) + \tfrac{1}{2}\lambda^{\gamma,2}\sin^2\theta(\cos^2\phi - \sin^2\phi) \qquad 6.8$$

For $\underline{B}_o$ along $\hat{a}$-axis, $\theta = 90°$, $\phi = 0$ and for $\underline{B}_o$ parallel to the $\hat{c}$-axis, $\phi = 30$ and $\underline{M}$ makes an angle θ with the $\hat{c}$-axis. Hence

$$\lambda_a^{\theta=90} - \lambda_a^{\theta} = -\lambda_1^{\alpha,2}\cos^2\theta + \lambda^{\gamma,2}(\tfrac{1}{2} - \tfrac{1}{4}\sin^2\theta) \qquad 6.9$$

6.1.3 The Constant $\lambda_2^{\alpha,2}$

This constant is determined in a similar way to constant $\lambda_2^{\alpha,2}$ but measuring the strain along the $\hat{c}$-axis for the bc or ac plane crystals. Then the direction cosines of the strain are,

$$\begin{aligned} \beta_x &= 0 \\ \beta_y &= 0 \\ \beta_z &= 1 \end{aligned} \qquad 6.10$$

and the magnetostriction expression becomes

$$\lambda_c = \lambda_2^{\alpha,0} + \lambda_2^{\alpha,2}(\alpha_z^2 - \tfrac{1}{3}) \ . \qquad 6.11$$

Substituting the direction cosines of magnetization as given in 6.7, we have

$$\lambda_c = \lambda_2^{\alpha,0} + \lambda_2^{\alpha,2}(\cos^2\theta - \tfrac{1}{3}) \ . \qquad 6.12$$

Hence for the rotation of magnetization from an angle of 90° to an angle θ with the $\hat{c}$-axis

$$\lambda_c^{90} - \lambda_c^{\theta} = -\lambda_2^{\alpha,2}\cos^2\theta \qquad 6.13$$

where θ is the angle of magnetization with the $\hat{c}$-axis. $\underline{M}$ is along the applied field $\underline{B}_o$. A detailed discussion for the case when $\underline{M}$ does not lie along $\underline{B}_o$ follows in Chapter 8, in the derivation of constants $\lambda_1^{\alpha,2}$ and $\lambda_2^{\alpha,2}$.

6.2 Method of Measuring Strains

The deformation of the crystal can be measured by a variety of means. The most commonly used methods include X-ray diffraction, resistive strain gauges and capacitative transducers. Measurement techniques at very low temperature and in high magnetic fields are usually limited by space. Bulky X-ray equipment cannot be used conveniently and the capacitance method also has operational difficulties at low temperature. A method using resistive strain gauges seemed the most appropriate technique for

the present work. It is simple to use and has been very commonly employed to measure magnetostriction since it was introduced by Goldman (1947). This method also has some inherent sources of errors, (i) the magnetoresistance effect; this effect has been reduced to a negligible limit by the use of Karma gauges, (ii) misalignment of the gauge with respect to the desired direction; with a little skill and careful fixing of the gauge it was found possible to achieve an accuracy of alignment within one degree, (iii) the uncertainty in the gauge factor, the value of the gauge factor quoted by the manufacturer was previously checked by Joraide (1980) and was found reasonably accurate. Moreover the uncertainty in the gauge factor is very small and causes no significant error in the measurement of very large magnetostriction like that of Tb, (iv) it is an indirect method and depends upon the bond of the adhesive between the gauge and the specimen, (v) the adhesive used to hold the specimen causes some restriction to the free magnetostrictive deformation of the specimen. Its effect is minimized by the use of cotton wool pads placed on both sides of the specimen.

6.3 Specimen

The specimens were produced at the Centre for Material Science, University of Birmingham. The Gd and Tb metals were purified by the solid state electrotransport technique. The single crystals of various alloy compositions were then grown by melting the parent metals in the desired ratio. Suitable grains were selected in the ingot and

the single crystals in the form of discs about 5mm dia. and 1mm thick were cut with disc planes perpendicular to $\hat{a}$-, $\hat{b}$- and $\hat{c}$-axes by electrospark errosion under paraffin.

6.3.1 Specimen Preparation

The specimens were polished mechanically with grade 6M3 diamond lapping compound for about half an hour followed by polishing with grade 1M¼ compound using dialap fluid for the same length of time. The specimen holder assembly of the polisher was degreased with ethanol before changing to a lapping wheel carrying 1M¼ compound. The specimens were then chemically polished in 50% nitric acid and 50% acetic acid for 2 to 4 minutes. The chemical reagent was kept stirred throughout the polishing and the specimen was immediately given a thorough wash in dry acetone.

6.3.2 Specimen Orientation

The back reflection Laue method was used to find the orientation of the crystallographic axes of the specimen. The polished specimen was fixed on a brass holder (Figure 6.29) with Durofix and was mounted on a two circle goniometer. The position of the edges of the brass specimen holder were noted with respect to the vertical axis of the goniometer with the help of a travelling microscope. White X-rays from the Mo anode tube which have minimum absorption coefficient for Gd and Tb were used. The series of Laue spots from the X-rays reflected by the specimen were photographed by a simple polaroid cassette camera with an intensifying fluorescent screen. The camera was placed

between the radiation source and the specimen. The film used was a 57 high speed polaroid film. The distance of the film from the specimen was kept at 3 cm. A preliminary picture was taken with 25mA and 40kV setting of the X-rays generator with exposure time of 10 minutes. The centre of symmetry was brought to coincide with the centre of the incident beam by turning the crystal about vertical axis and tilting the disc plane towards or away from the beam so that the axis perpendicular to the disc plane was parallel to the incident radiation. The final Laue pattern was recorded with 25mA and 30kV settings for 20 to 30 minutes exposure time. The crystallographic axes in the disc plane were recognized by comparison with a computed transparent print-out of the Laue spots from a hexagonal crystal with the same film to specimen distance. The angle of the axes with respect to the vertical was measured on the film using a protractor.

6.4 Fixing of Strain Gauge on the Crystal

Modified Karma gauges (M = M, Micro-Measurements of type WK-06-050- AR-350) were used. Karma alloys have an approximate composition, 80% of Ni, 20% of Cr with small quantities of Al and Fe and have very low magneto-resistance, even at liquid helium temperature (Greenough and Underhill, 1976). These gauges are fully encapsulated with high endurance leads, can be used over a wide range of temperature and have the most extreme environmental capability of a general purpose gauge when self-temperature compensation is required. These gauges can be used in

a wide range of temperature from 4K to 563K. The gauge factor is 2.04 $\pm$ .02 at 297k. Its variation with temperature is shown in Figure 6.1 as supplied by the manufacturer. The recommended Micro-Measurements M-Band 610 high-temperature epoxy adhesive suitable for this temperature range with WK-gauges was used. The brass specimen holder was fixed using Durafix adhesive on a turn-table of a microscope calibrated in degrees. The cross-wire of the microscope was aligned with the reference edge of the holder and then the turntable was rotated by an appropriate amount so that the desired crystallographic axes became parallel to the cross-wires. Thin layers of M-Bond 610 were coated on the cleaned crystal surface and the strain gauge was allowed to dry for 30 minutes. The strain gauge was then placed along the chosen axis. The specimen was covered with a thin sheet of teflon, placed in another brass holder shown in Figure 6.2b or c and was spring clamped to ensure even pressure during heat treatment. The clamped specimen was placed in an oven at room temperature and then the temperature was raised slowly about 8 degrees perminute to 150°C and was kept constant for two hours before cooling it down slowly to room temperature. This form of heat treatment followed the recommendations of the manufacturer as shown in Figure 6.3. In basal plane samples, one strain gauge was fixed along the $\hat{b}$-axis only and two gauges were fixed on ac or bc plane crystals along both principal axes in the disc plane. The second gauge

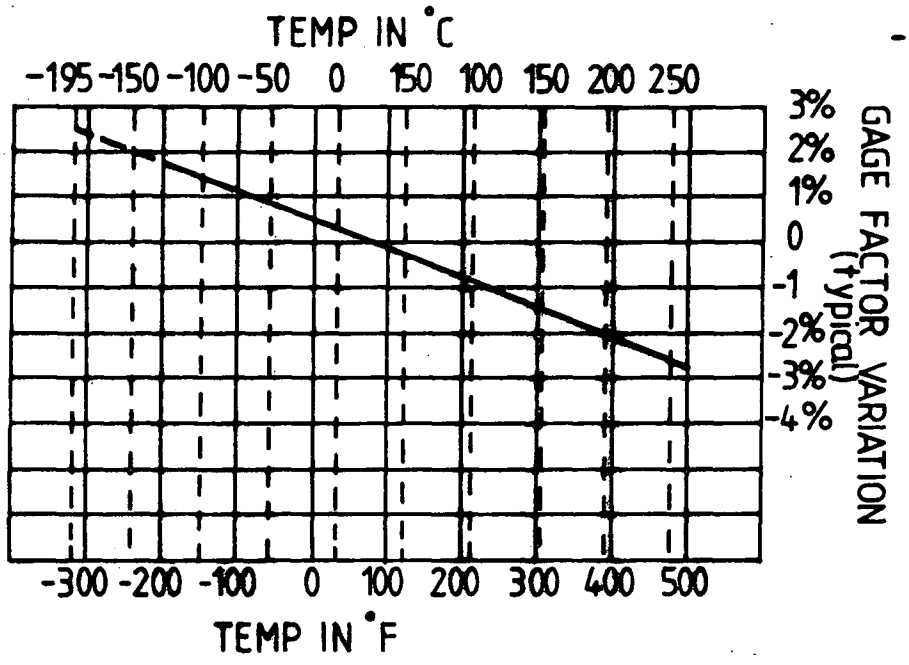

Fig. 6.1 The thermal dependence of the gauge factor as supplied by the manufacturer.

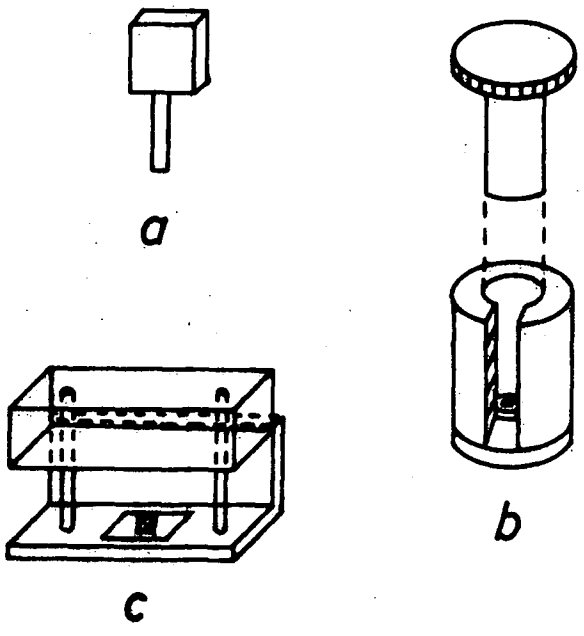

Fig. 6.2 The hoiders for crystal mounting and its heat treatment.

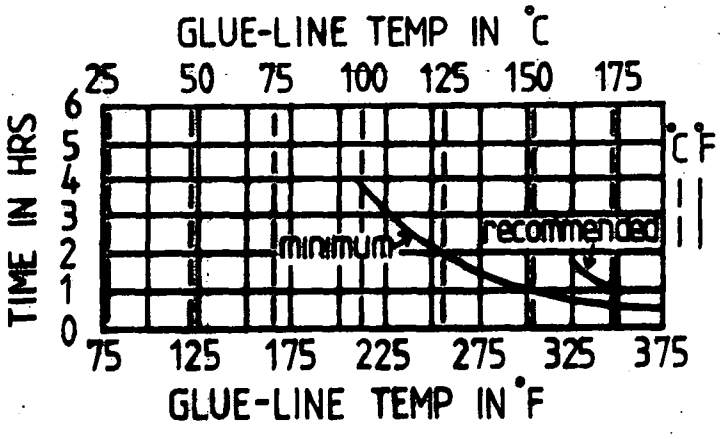

Fig. 6.3 The time versus temperature manufacturer's recommendation for curing M-Bond 610 adhesive.

was fixed when the first was heat cured, on the other side of the crystal at right angles to the previous one and was heat treated in the same way as before using the holding device (6.2c).

6.5 Measurements of Magnetostriction

The resistance of a wire depends upon the dimensions of the wire as

$$R = \rho \ell / a \qquad 6.14$$

where ρ is the resistivity of the material of the wire, ℓ - the length and an the area of cross section. The resistance of the strain gauge thus changes with the deformation of the crystal to which it is attached. The gauge sensitivity K, also known as the gauge factor, is defined as the ratio of the change in gauge resistance to the strain

$$K = \left(\frac{\Delta R}{R}\right) / \left(\Delta \ell / \ell\right) \qquad 6.15$$

The gauge factor is also expressed after Brophy (1977):

$$K = 1 + 2\sigma + \ell \frac{d\rho}{d\ell} \qquad 6.16$$

where σ is Poisson's ratio and ρ the resistivity for the gauge material. The change in resistivity with strain represented by the third term in equation 6.16 is negligible in the case of Karma alloys. The value of Poisson's ratio is close to 0.5, so the value of the gauge factor K is approximately 2. The actual value supplied by the manufacturer is $2.04 \pm .02$.

The resistance changes of the gauge were measured

with a Wheatstone bridge shown in Figure 6.4. Another strain gauge called a dummy was cemented on a commercial polycrystalline copper disc and placed close to the active strain gauge on the test specimen so that both gauges are in the same temperature and magnetic field environment. The strain gauges were connected in the adjacent arms of the bridge. The dummy gauge is used to compensate the magneto and thermal resistive effects. Using a detector system of high input impedance compared to the bridge resistance, the small change in the resistance of a bridge arm can be observed.

When the resistances in each arm of the bridge are the same then A and B are at the same potential and there is no output signal. For a small change in the resistance of active gauge, i.e. from R to $R + \Delta R$, V_1 and V_2 have the following values.

$$V_1 = \frac{V}{2R} .R = \frac{V}{2}$$

and

$$V_2 = \frac{V(R + \Delta R)}{2R + \Delta R}$$

$$= \frac{V\ (1 + \Delta R/R)}{2\ (1 + \Delta R/2R)}$$

where V is the bridge voltage for $\Delta R \ll R$

$$V_2 \simeq \frac{V}{2}\ (1 + \frac{\Delta R}{R})\ (1 - \frac{\Delta R}{2R})$$

$$= \frac{V}{2}\ (1 + \frac{\Delta R}{2R})$$

So the output voltage e is

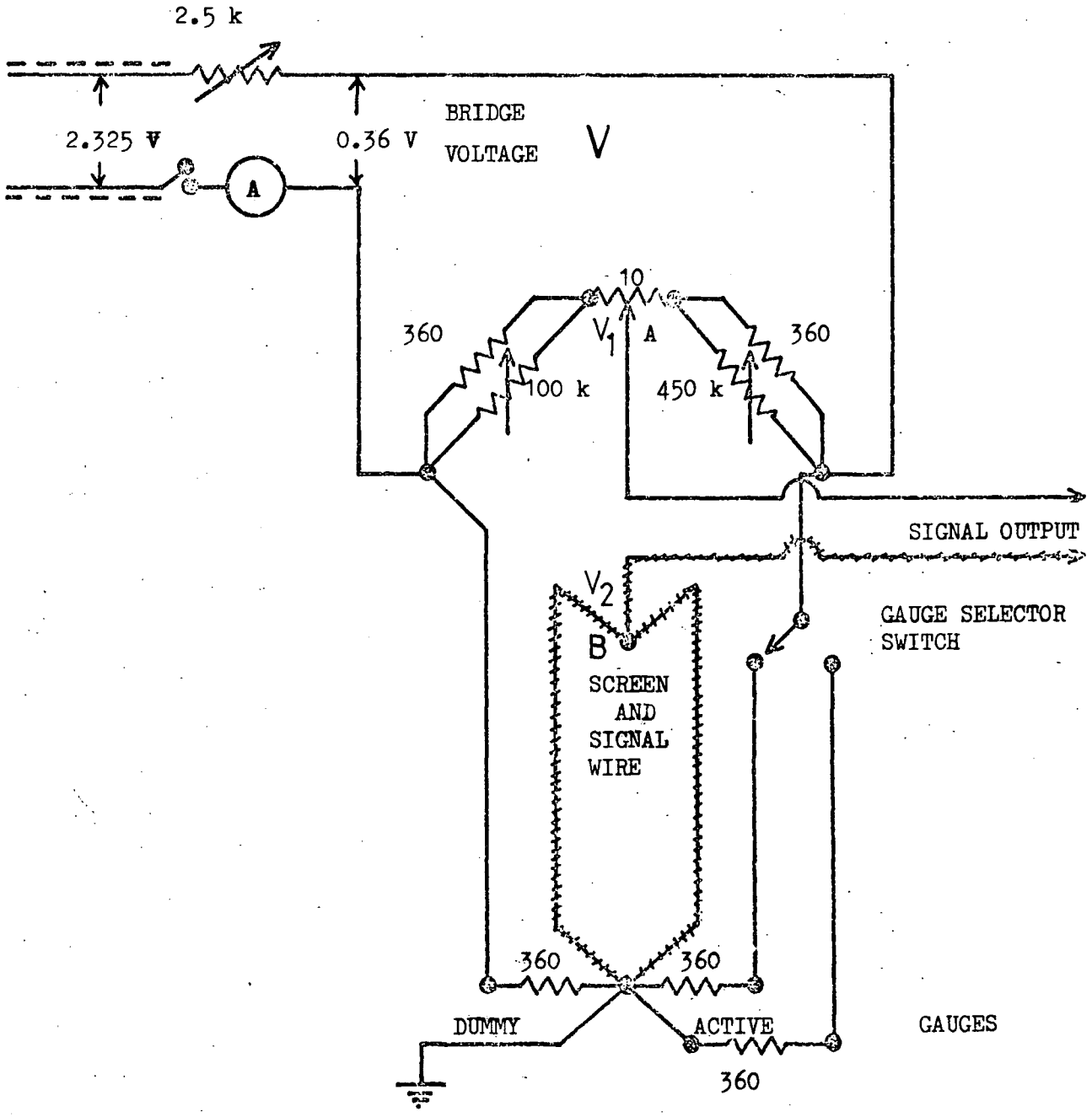

Fig. 6.4 Strain gauge bridge circuit.

$$e = V_2 - V_1 = \frac{V}{4} \cdot \frac{\Delta R}{R}$$

which is related to the strain by gauge factor K

$$e = \frac{V}{4} \quad K \quad \frac{\Delta \ell}{\ell}$$

Hence the strain

$$\frac{\Delta \ell}{\ell} = \frac{4e}{VK} \qquad 6.17$$

The strain deduced from the above expression depends upon bridge supply voltage so a very stable supply voltage was needed. The stabilized supply described by Unvala and Green (1974) and constructed by Joraide was used. Its circuit diagram is shown in Figure 6.5. It consists of two stages. The input voltage of 27 volt d.c. was supplied by a Farnell stabilized power unit. The output voltage of the first A741 integrated circuit was stabilized at about 12V by comparing a fraction of this voltage with that of the reference 5.6 V zener diode, which was used as the power supply for the second i.e. the final output voltage was stabilized by two transistors BFY52 and 479 to 2.85 V. Since (4/VK) is of order unity the output voltage (in volts)is of the same order as the strain and needs to be amplified for recording accurately. A low drift amplifier described by Unvala et al. (1976) consisting of a MAT-01H/308 was initially used. It was found non-linear around zero input voltage. Another amplifier again described by Unvala et al. in the same paper using a 321/308 i.c. operational amplifier was constructed. Later it was found more convenient and reliable to use

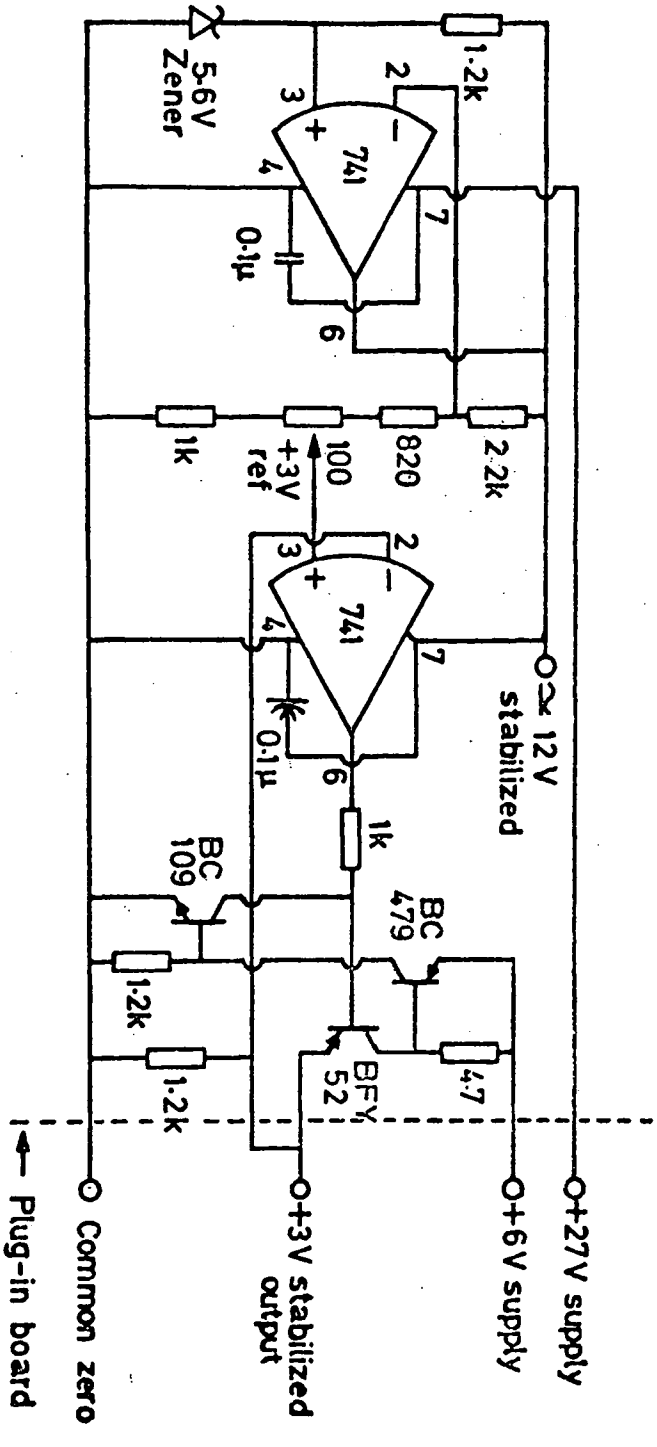

Fig(6·5) Circuit for stabilizer for 3V power supply, after Unvala and Green(1974).

a very stable built-in amplifier of the Datron 1051 Digital Multivoltmeter. This amplified the input voltages 10 times which was sufficient gain in the case of our strongly magnetostrictive Tb alloys.

6.6 Magnetostriction Insert

This consists of two parts connected by a 160cm long stainless steel tube of diameter 19mm and wall thickness ·25mm. At the upper end there is a rotating mechanism consisting of a horizontal shaft bearing a helical pinion. Matching racks are attached to the upper and lower ends of a vertical stainless steel tube referred to as the push rod, passing down through the main stainless steel tube and through a vacuum seal. The push rod can be moved up and down through the upper rack and pinion mechanism by the horizontal shaft. The shaft is driven by a stepping motor through a 100:1 ratio gearbox. Also mounted on the same shaft is a potentiometer to provide a voltage proportional to the movement of the push rod. The top section of the upper driving system is shown in Figure 6.6. The driving system rests on a brass head containing vacuum seals through which the various leads pass. The magnetostriction insert has the disc shaped specimen mounted in the brass measuring assembly (illustrated in Figure 6.7) attached at its lower end. The specimen is contained in a small cylindrical brass box shown in Figure 6.8, being cemented into the box around its edges by Durofix adhesive. Small pads of cotton wool are placed over and under the specimen before the lid is attached.

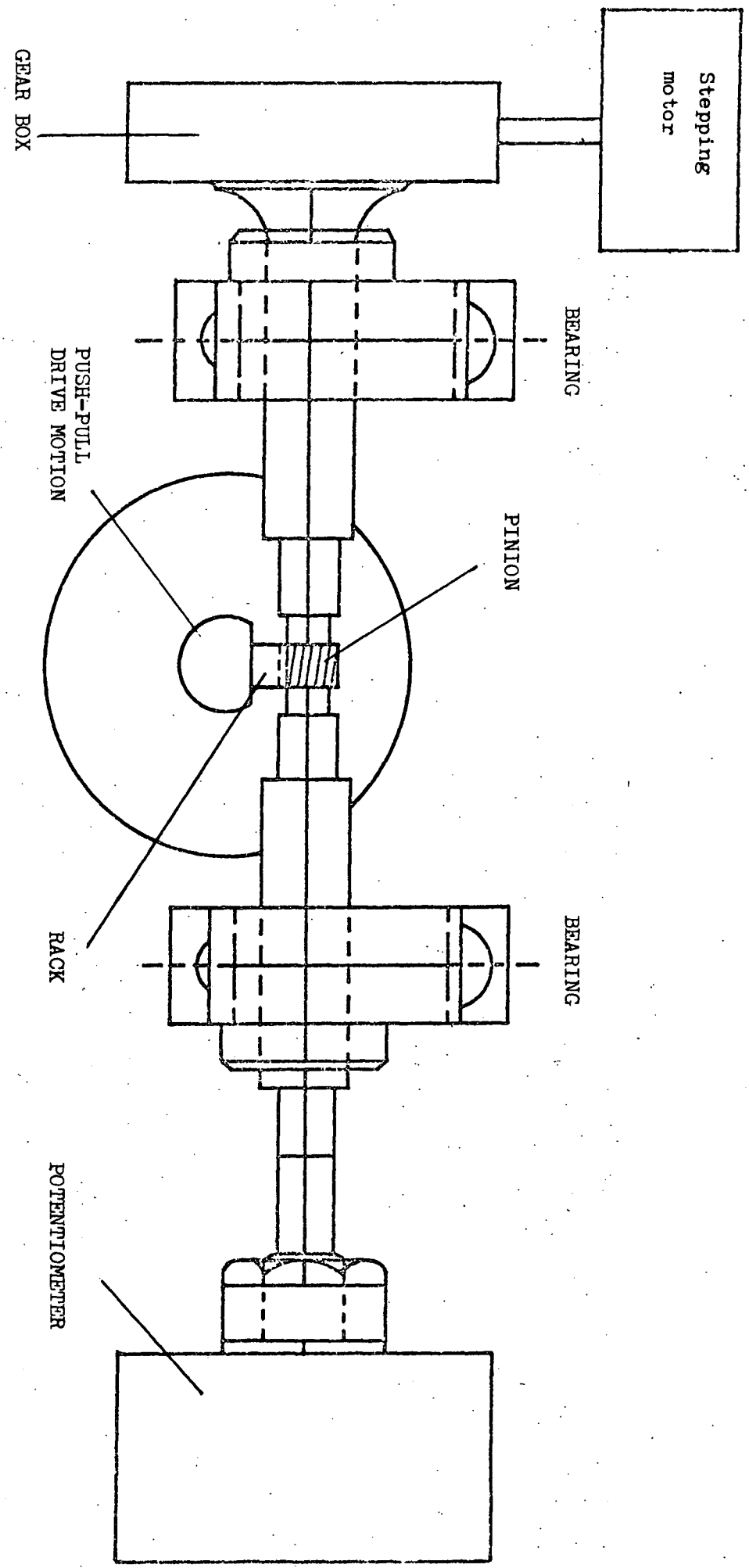

Fig. 6.6 Horizontal section of upper pinion drive assembly.

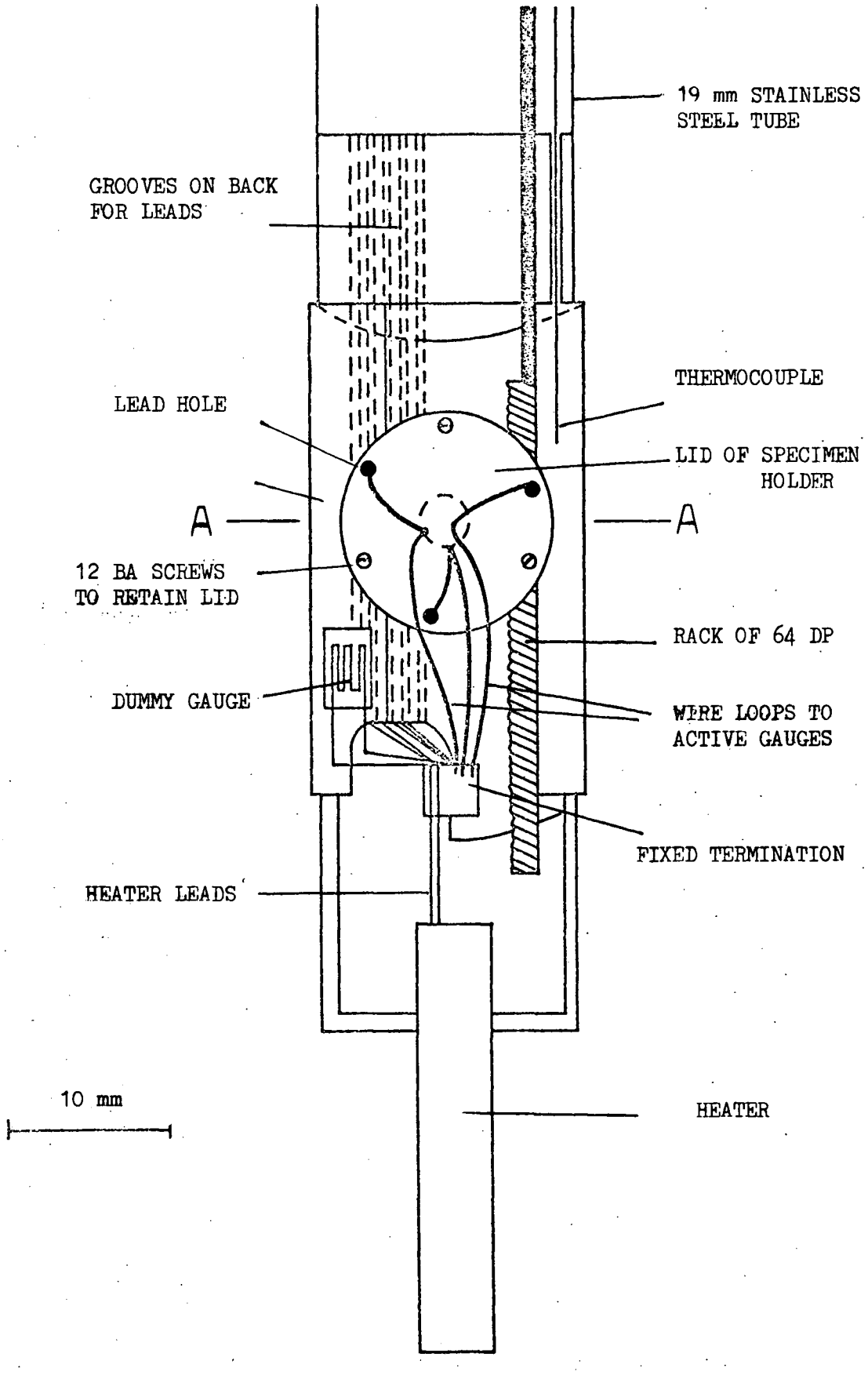

Fig. 6.7 Vertical elevation of measuring assembly.

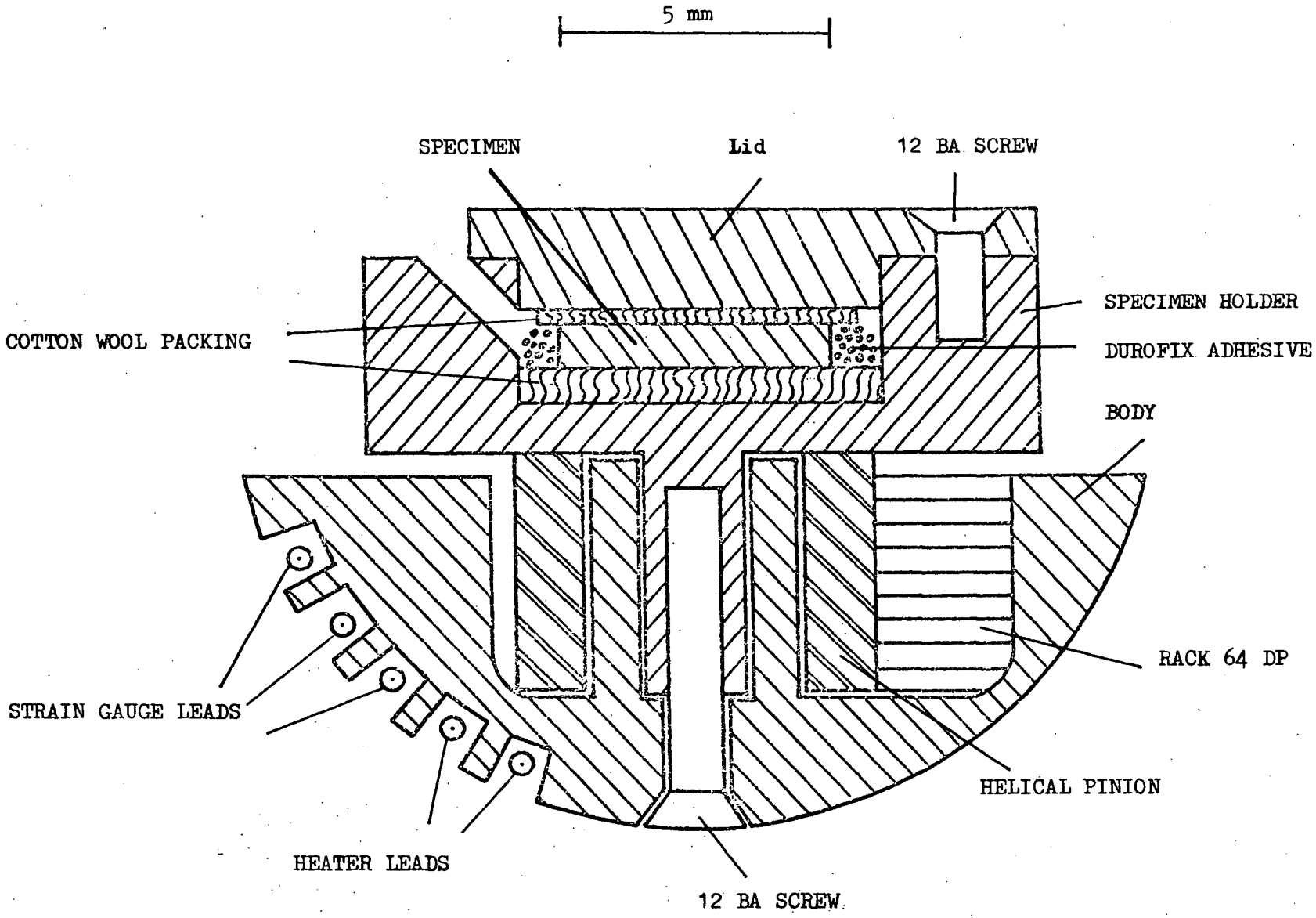

Fig. 6.8 Horizontal section A-A on Fig. 6.7 of helical pinion and crystal holder.

The box is soldered to a brass helical pinion which can be rotated by the vertical movement of the rack at the lower end of the push rod which is actuated from the head of the insert. Thus the specimen may be rotated in a vertical plane which is necessary as the magnetic field is vertical. Leads from the strain gauges are soldered to flexible enamelled copper wires which are brought out of the box and taken to the centre of the lid where they are anchored using Durofix. From there leads are looped to terminal posts on the body of the assembly from which screened leads pass up the tube to which the assembly is attached. A dummy strain gauge cemented on commercial polycrystalline copper is placed near the box. In addition a small auxiliary heater of resistance 40 ohm at 300K is provided below the assembly and a gold/iron (0.03%) with chromel thermocouple is mounted close to the specimen box. The rig so constructed forms an insert to a Thor Cryogenics superconducting solenoid mounted with its axis vertical. The insert fits into a chamber of diameter 24.7mm which can provide temperatures between 4.2K and 300K.

6.7 The Magnet

The Thor Cryogenics super conducting solenoid was used for the measurements of magnetostriction of Gd/Tb alloys. It provides a maximum central field of 14 Tesla and a field uniformity of $\pm$ 5 x 10^{-4} over a cylindrical region of length 30mm and diameter 20mm. The centre of the field is about 150cm down from the top flange of a

chamber of diameter 24.7mm providing access to the field. Various parts of the magnet are shown in Figure 6.9. The solenoid is composed of a number of windings the outer ones being of niobium-titanium alloy while the inner one is of niobium-tin alloy. The solenoid is kept immersed in the liquid helium during the operation to maintain its superconducting state. The liquid helium boil-off rate is reduced to a minimum by a high-vacuum jacket, super insulation consisting of a large number of radiation reflecting mylar sheets, a liquid nitrogen shield and a special copper radiation shield cooled by the liquid helium boil-off. The maximum field attainable in a superconducting solenoid depends upon the critical field of the superconducting material above which the superconducting properties disappear. For the present magnet this limit is 13 Tesla at 4.2K, though fields up to 14 Tesla may be obtained by reducing the pressure over the helium reservoir to reduce the operating temperature to 2K.

The specimen chamber is surrounded by the inner vacuum chamber (I.V.C.) which isolates the specimen space from the liquid helium reservoir and makes the variation of the temperature of the specimen possible without excessive increase in the liquid helium boil-off. The specimen is cooled down by a helium gas flow regulated by a needle valve situated between the sample space and the helium reservoir. A heater and a carbon glass resistor sensor are incorporated in a block at the bottom of the I.V.C. chamber in the path of the gas flow. The temperature

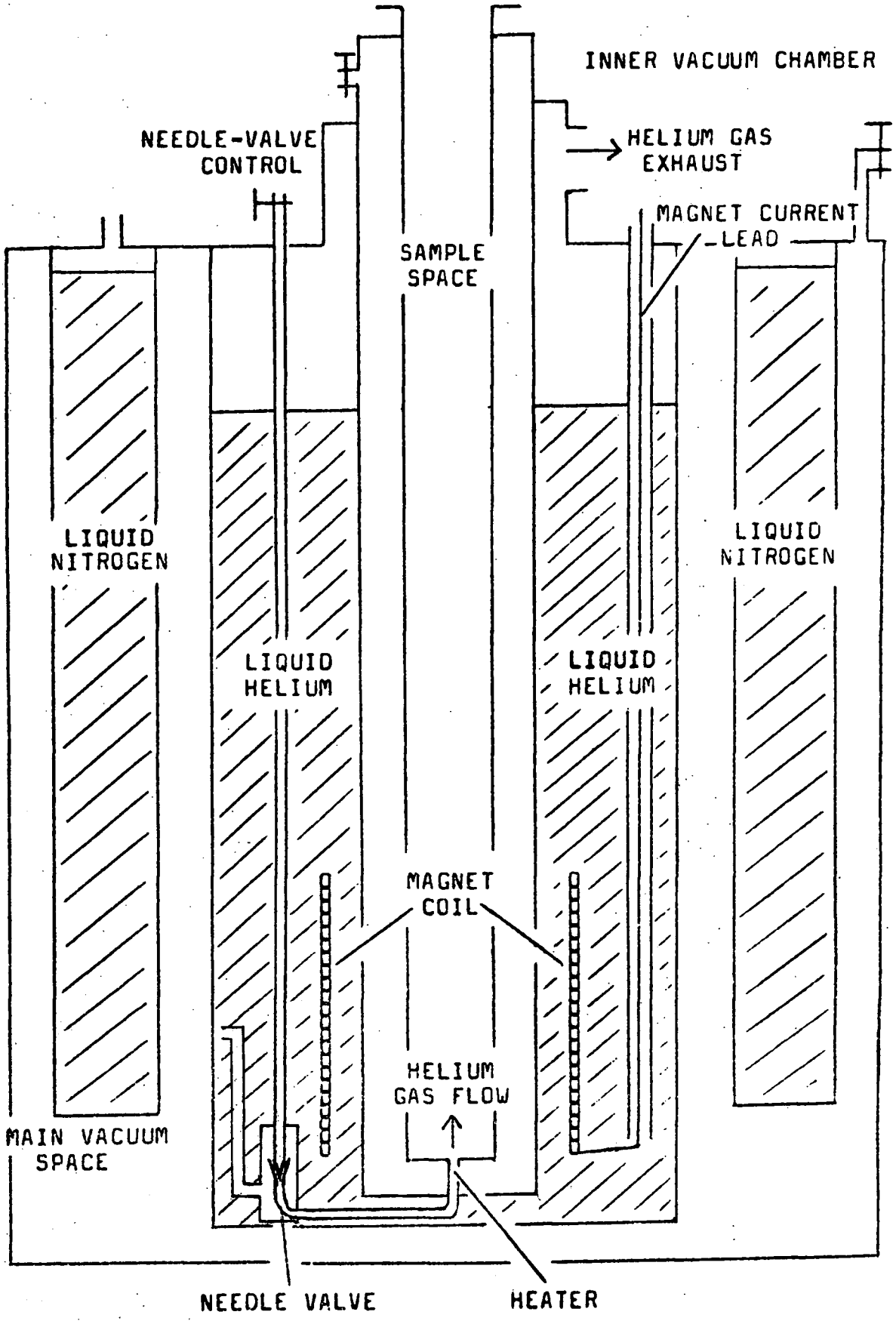

Fig. 6.9 Schematic illustration of the superconducting magnet. The horizontal scale has been increased for the sake of clarity.

of the specimen may be varied and maintained by a Thor temperature controller model 3010 II using either the magnet heater and sensor or the auxiliary heater of the magnetostriction insert and its thermocouple. The temperature of the specimen is varied by changing the flow rate of the helium gas and current in the heater. The gas flow is maintained by creating a pressure difference, maximum 2 lb. per square inch, between helium reservoir and the sample space. In practice the pressure of the sample space was reduced. It was found more convenient to use the auxiliary heater for temperature variation rather than using the magnet heater.

A control board was constructed to evacuate the sample and helium reservoir chambers, fill them with helium gas, flush out any nitrogen or air before liquid helium transfer. This is fitted with vacuum gauges, valves, pressure indicators, non-return pressure release valves and vacuum and gas control valves.

The current to the magnet coil is supplied by a Thor power supply, Model 610. The coil current is varied by an electronic programmer, Model 2020, to the desired level at a suitable rate. If the rate of change of current is too fast, it may result in the magnet becoming normal or resistive and hence generating great heat. Such a reaction is termed as "quenching". The solenoid may be put into persistant mode by making the superconducting switch, within the magnet, superconducting and thus making the solenoid independent of the control unit. The

persistant mode provides greater stability of the field and lower helium boil off as no current is passing through the supply leads which may in fact be removed. The switch may be energised (made resistive) to bring the magnet into active mode by passing 35 to 50 mA current through a built-in heater. The magnet field is directly proportional to the coil current. A current of 4.2A produces a field of 1T. The coil current is measured by sensing the voltage across a shunt resistor in the power supply unit. A Thor liquid helium level meter Model 8020 displays the helium depth in mm sensing regularly at predetermined internals using a superconducting wire probe.

The magnet was precooled with liquid nitrogen. The solenoid was kept immersed in liquid nitrogen for two days prior to the transfer of liquid helium. Cooling down of the magnet and the process of the transfer of liquid helium is described in the magnet handbook.

6.8 Acquisition of Data

A block diagram of the equipment is shown in Figure 6.10. The system is connected to a PET microcomputer via a MINICAM interface. The microcomputer programme provides for the driving of the system by stepping motors at fixed angular intervals, observing the output values of the strain gauge circuit through analogue to digital (A/D) modules at each step, till the crystal is rotated by 185°. The crystal is then turned through 190° in the reverse direction at a constant speed by pushing the rod downward. The crystal is then brought back to the initial

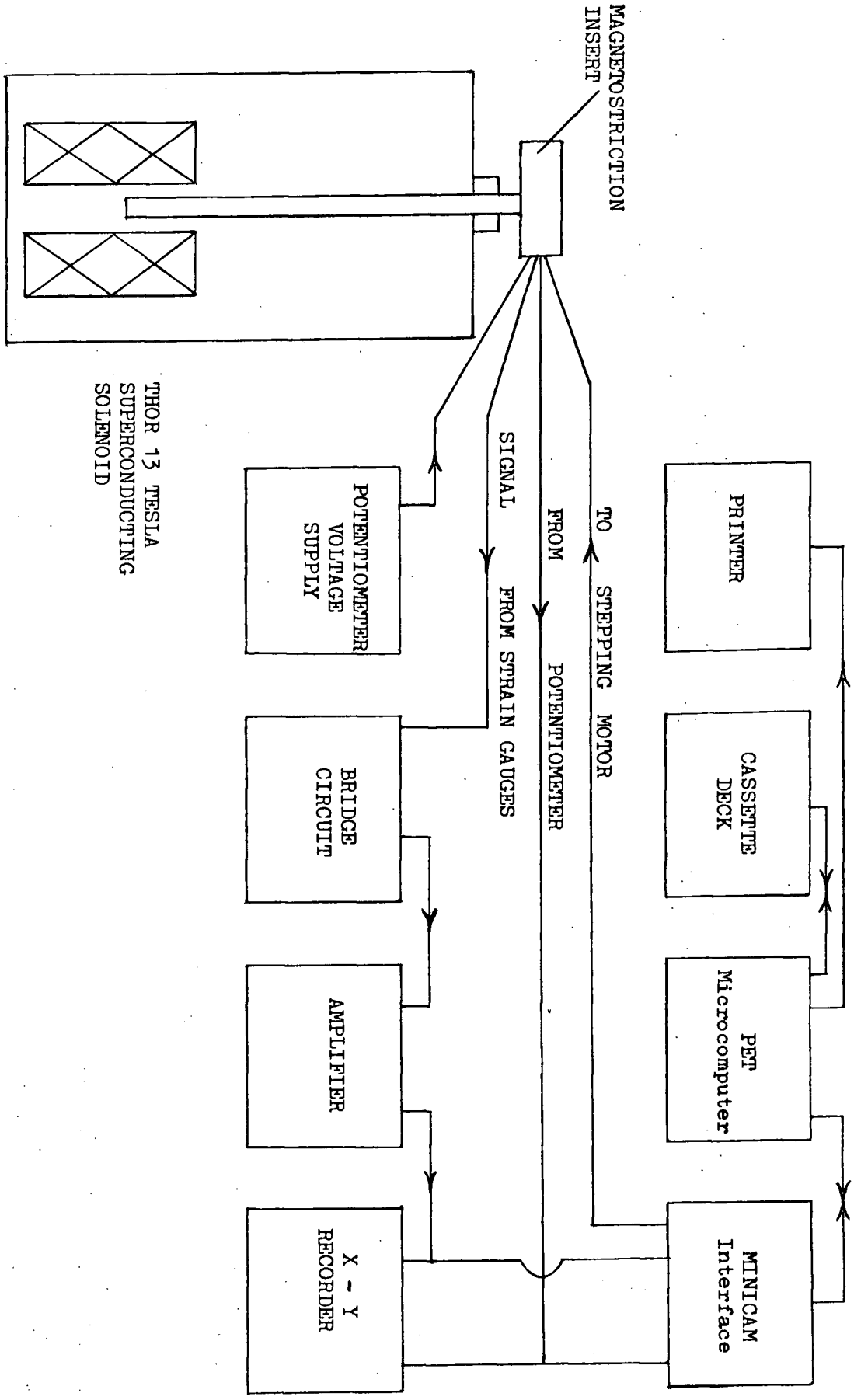

Fig. 6.10 Block diagram of data acquisition system.

zero setting thus eliminating the backlash of the system. The data is recorded while the rod is being pulled up (push rod in tension). This obviates any possible error due to bowing of the push rod, particularly when the magnetization crosses the hard direction, and ensures uniform turning of the crystal in the magnetic field. The intervals may be set at a predetermined level, but usually a half rotation of the specimen is covered by 90 steps. However, any sections of the rotation where the strain is changing rapidly, may be expanded down to a minimum step of 4'. New initial and final limits of the rotation can also be set. At the start of this experiment, the computer programme records the specimen particulars. The time at the start and completion of the rotated is also noted. An additional output to an x-y recorder enables curves of strain versus field angle to be plotted during the specimen rotation in the field. At the completion of the curve, the microcomputer calculates the total strain and then asks for the new settings of the variables (field and temperature) for the trace of the next curve. The screen of the microcomputer displays all the step by step information during data collection. Provision for recording data on cassette tape and also for printed output is included. The curve particulars such as temperature, field, sensitivity of the x-y plotter etc. are recorded with each curve. Audio signals are given at various stages of the data collection and also after any desired pause necessary to alter the

experimental setting.

The computer programme for the automated operation of the experiment is given in Appendix II.

6.9 Calibration of Apparatus

(i) Thermocouple: The e.m.f. of the gold/iron (.03%) with chromel (British Standard) was observed with the junction at room temperature, in iced water, in liquid nitrogen and in liquid helium with the reference junction at liquid nitrogen temperature. The e.m.f. versus temperature curve for the thermocouple is shown in Figure 6.11. The e.m.f. is linear with temperature down to that of liquid nitrogen but between 77K and 4.2K is significantly non-linear. A calibration point at liquid hydrogen temperature would have been desirable to draw the curve between liquid nitrogen and liquid helium temperatures but this was not available. An attempt was made to compare with a gold/iron (.07%) with chromel (American Standard) thermocouple but that also showed similar non linear variation in this region. The maximum error in measurement of the temperature in this region is not thought to be more than three degrees. The changes in the saturation magnetization and in the anisotropy constants at low temperature are not very rapid and this uncertainty in temperature does not cause any significant error.

(ii) Magnetic field of the magnet: A probe, shown in Figure 6.12, was constructed with a search coil at one end to measure the magnetic field of the magnet. The search coil could be moved from the top of the magnet

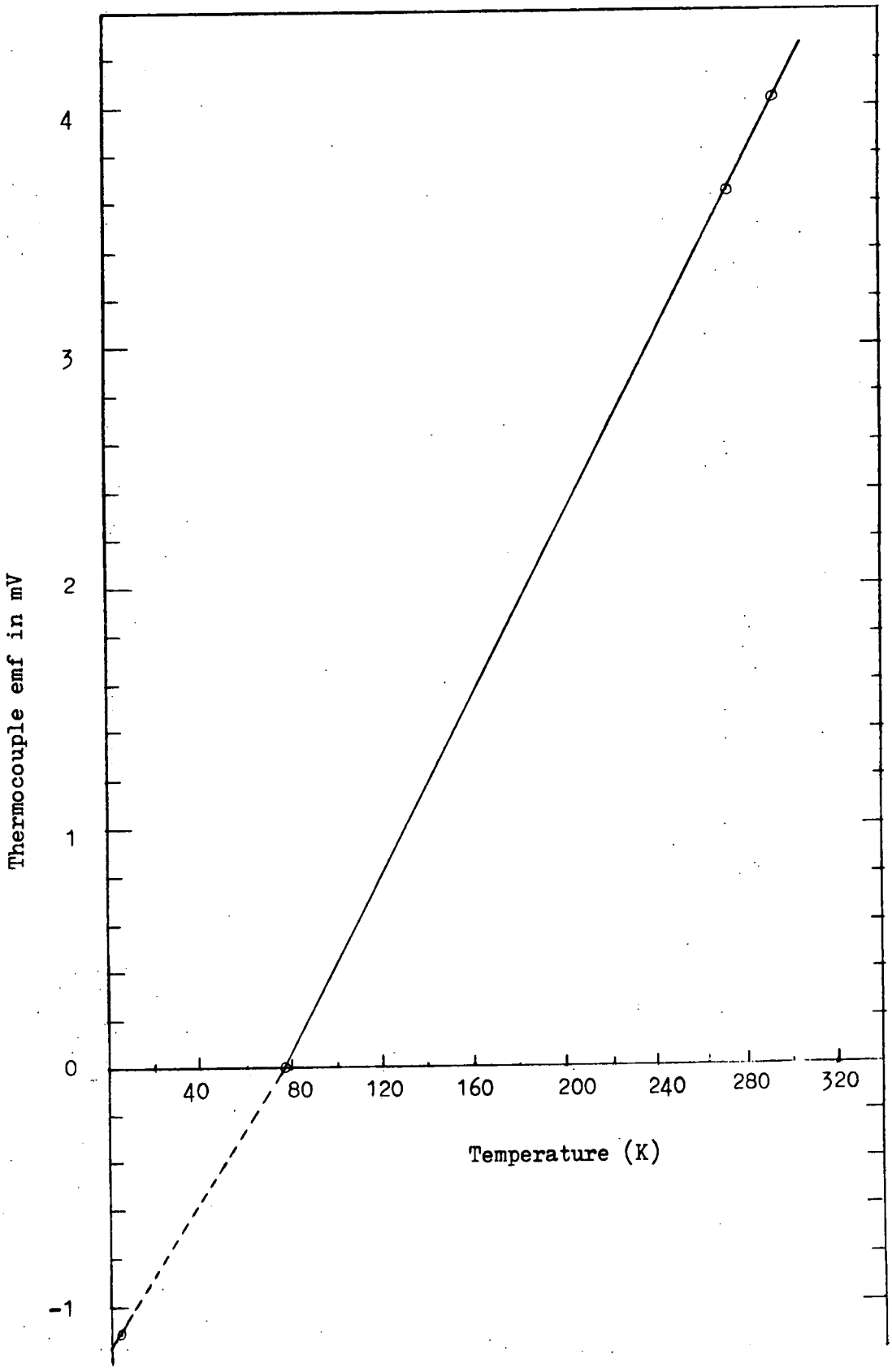

Fig. 6.11 Emf versus temperature curve of the Au-Fe(0.03) with Chromel thermocouple.

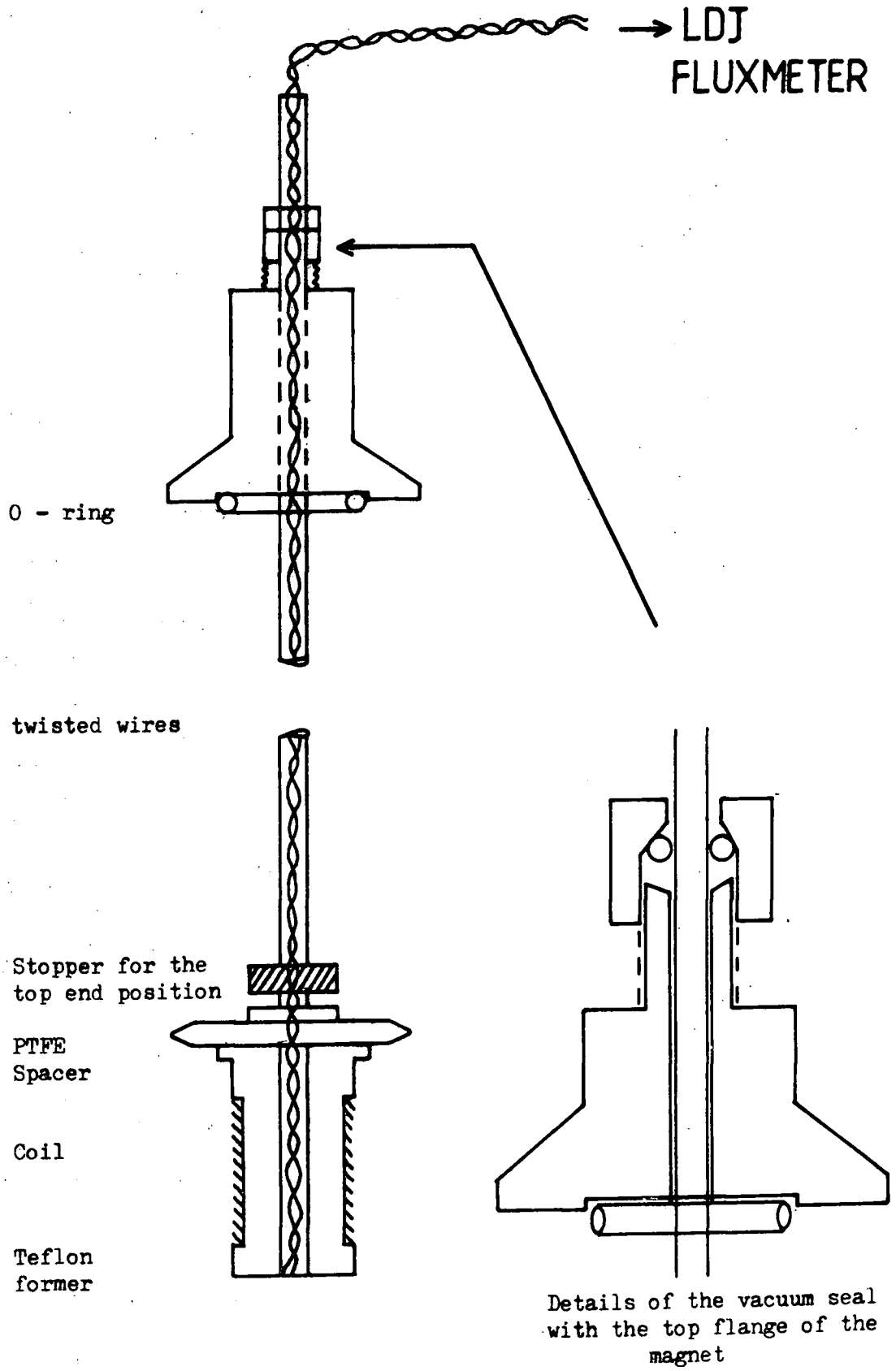

Fig. 6.12 The magnetic field measuring probe.

to the centre of the magnet through a vacuum seal. The coil has 29 turns and the average diameter of the coil is .98cm. The integrated e.m.f. of the search coil was read by the L.D.J flux meter, Model 710, when the coil was moved from the top of the magnet to the centre of the field in a -ve mode only, in 4 and 12 Tesla fields. The meter display is related to the field B by

$$B = \frac{\phi}{NA} = \frac{\text{Display reading x Scale factor}}{\text{No. of turns of the coil x area of the coil}} \quad kG/cm^3$$

where the product of the display reading and the scale factor is a reading of the field in kilomaxwells.

The fields measured in this way never differed by more than 2% from those obtained using the maker's conversion factor (1 T for 4.2A). The actual strength of the current in the superconducting solenoid is difficult to measure because of the unknown induced back e.m.f. of the solenoid, though this dies away with time over a long period. The field measurements of the magnet using the field probe are given in Table 6.1.

(iii) Gauge Factors: The gauge factor had been calibrated by Joraide (1980)by measuring the magnetostriction of a Ni single crystal using the gauge factor value supplied by the manufacturer. The agreement between the observed values of magnetostriction constants and the results of other workers (e.g. Chikazumi, 1964) was reasonable proof of the accuracy of the gauge factor within $\pm$ 1%.

TABLE 6.1

Magnetic field measurements of the solenoid using search coil.

Magnetic field using Manufacturer's current field factor		4 Tesla	12.02 Tesla
Current in the Solenoid		16.866 A	50.68 A
Mean LDJ display of 10 measurements		90.32 $\pm$ 1.7kM	139.51 $\pm$ 2 kM
Scale factor		10	20
Measured field		3.97 $\pm$ .06 T	12.25 $\pm$ .06 T
Difference in fields		- .8%	+ 1.9%
Current to Field Factor	Experimental	4.248 $\pm$ .06AT^{-1}	4.137 $\pm$ .04AT^{-1}
	Average	4.19 $\pm$0.05 AT^{-1}	
	Manufacturer's	4.13 $\pm$0.01 AT^{-1}	

(iv) Bridge Sensitivity: The output voltage of the bridge circuit corresponding to changes in the gauge resistance are related under the condition of equal resistance in each arm of the bridge. The resistances of the gauges change with temperature. The effect of various bridge settings such as starting the curve with zero output voltage of the bridge or in an offset position greater than the normal operational variation were observed on 90% Gd Tb $\hat{b}$-axis crystal at 208K in field of 4 Tesla. Identical magnetostriction curves were produced with no detectable change either in the size or in the shape of the signal. Hence confidence was developed in the sensitivity of the bridge that the changes in the resistance in the experimental variation range cause no appreciable error in the recorded data.

(v) Magnetoresistance of the strain gauges: Magnetoresistance of strain gauges of Karma alloys is claimed to be very small. It was measured by cementing a strain gauge on a polycrystalline copper disc of 5mm diameter and 1mm in the magnetic fields 8 and 12 Tesla at temperatures from liquid helium to about 180K. The maximum average strain observed at 12 Tesla and at liquid helium temperature was 1.5×10^{-5} including all the other experimental errors. The strains at higher temperature and lower field were not detectable. Hence the magnetoresistance effect for most of the data collection was negligibly small.

CHAPTER 7

THE MAGNETOSTRICTION CONSTANT $\lambda^{\gamma,2}$ OF Gd, Tb AND THEIR ALLOYS

7.1 Introduction

The magnetostriction constant $\lambda^{\gamma,2}$ was measured for gadolinium, terbium and their alloys, 90%Gd-10%Tb, 70% Gd-30%Tb, 50%Gd-50%Tb and 10%Gd-90%Tb in the temperature range from liquid helium to about the Curie temperature in magnetic fields of up to 12 Tesla. Variation in strain was measured along the $\hat{b}$-axis of the basal plane crystals corresponding to a 180 degree rotation of the magnetization vector. The constant $\lambda^{\gamma,2}$ was determined using Clark and Callen's expression, equation 4.45, in its simplified form as given in Chapter 6 in equation 6.3 for the particular case of the strain measurements along the $\hat{b}$-axis of the basal plane crystals to yield the constant $\lambda^{\gamma,2}$. The angle θ used in equation 6.3 refers to the angle between the magnetization vector and the $\hat{b}$-axis. The constant $\lambda^{\gamma,2}$ is the total variation in the strain when the magnetization is rotated from the $\hat{a}$-axis to the $\hat{b}$-axis or vice versa. The magnetization vector follows the external field as will be discussed in the next section dealing with data records. In this simple case, $\lambda^{\gamma,2}$ can be determined by measuring the peak to peak amplitude of the curve, a precise knowledge of the exact angle of magnetization is not necessary and so the external field angle may be taken as the angle of magnetization.

7.2 Typical Data Records

According to the equation 6.3 for the constant $\lambda^{\gamma,2}$, the change in the strain follows a cos 2θ variation when the magnetization is rotated in the basal plane. The recorded strain versus field angle curves show good agreement with the theoretical cos 2θ variation. The symmetry, continuity, smoothness and the cos 2θ dependence of the curves are all clear indications that magnetization is actually being rotated in the basal plane of the crystal and closely following the applied field direction. Typical experimental curves recorded by the x-y plotter are shown in Figures 7.1, 7.2 and 7.3. The curve in Figure 7.1 is for 90%Gd-10%Tb taken at liquid helium temperature in a magnetic field of 4 Tesla. The curves other than those for pure Tb show almost no hystersis in their forward and reverse traces which also indicates that the magnetization is following the external magnetic field very closely. The amplitudes of the curves decrease with increase in temperature. Figure 7.2 is the curve for the same crystal in the same field, but at higher temperature 147K with the same sensitivity and bridge setting. The amplitude is a minimum for pure gadolinium and increases with higher terbium concentration in the alloys. The shape of the curves remains the same for all temperatures and for all specimens except for those for pure terbium. These curves showed some hysteresis and were lacking complete symmetry, whereas the curves for 90%Gd-10%Tb crystal show no such hysteresis. A typical curve for pure terbium is shown

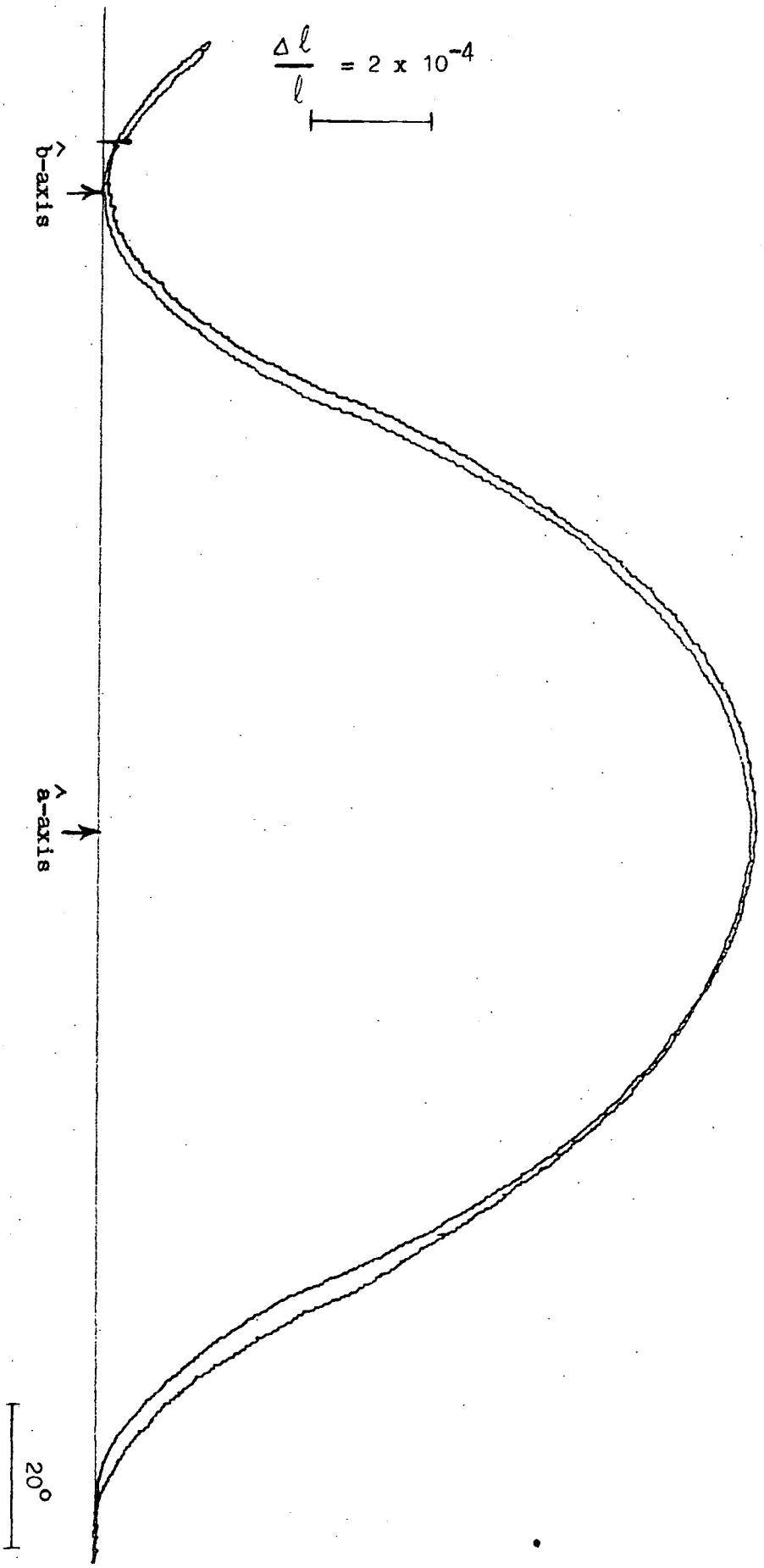

Fig.7.1 A typical basal plane strain versus field angle curve for $Gd_{0.90}Tb_{0.10}$ at 4.2 K and in field of 4 Tesla.

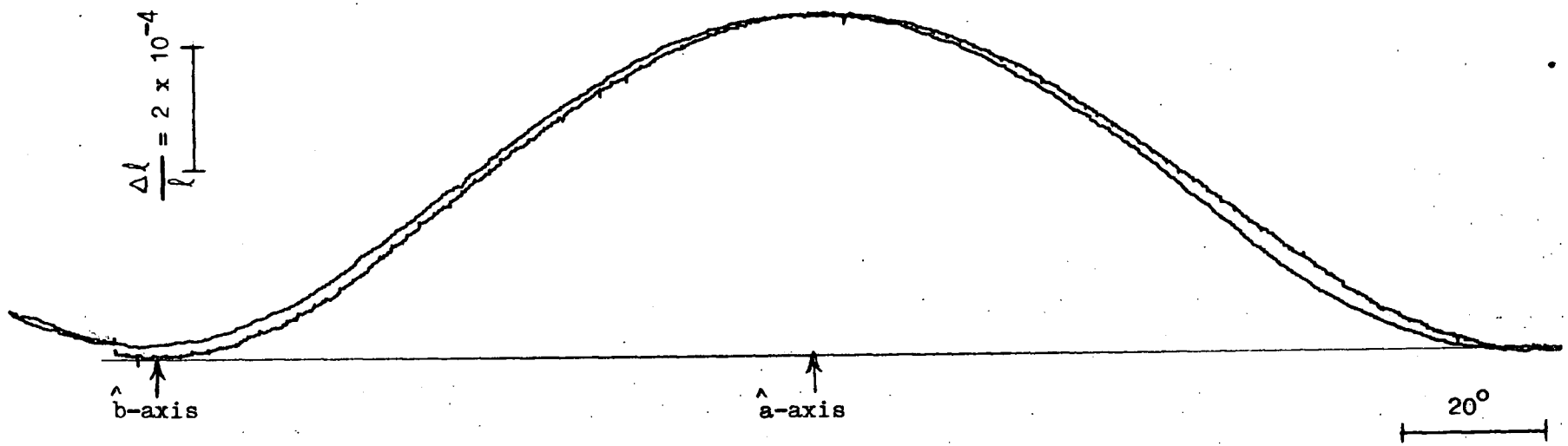

Fig 7.2 A typical basal plane strain versus field angle curve for $Gd_{0.90}Tb_{0.10}$ at 147 K and in field of 4 Tesla.

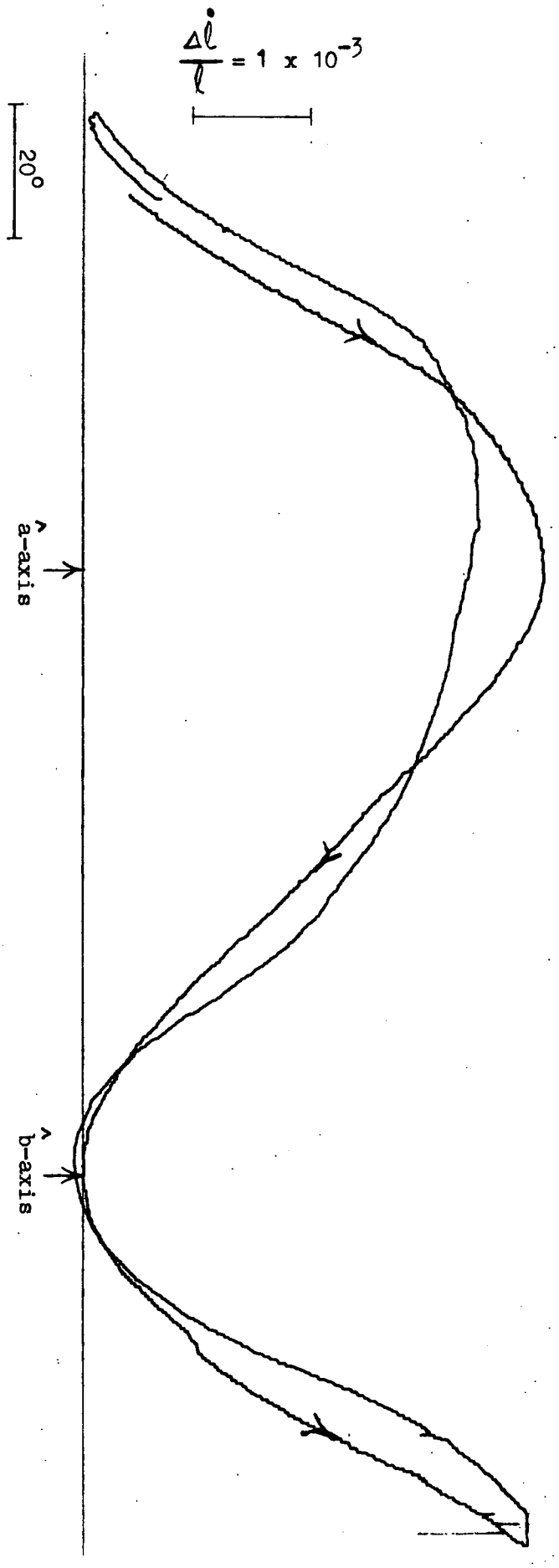

Fig. 7.3 A typical basal plane strain versus field angle curve for pure Tb at 77 K and in field of 12 Tesla.

in Figure 7.3. The terbium curves become symmetrical at higher temperatures.

7.3 Field Dependence of the Strain

The magnetostriction traces were taken in various applied fields increasing to double the previous field in each step up to 12 Tesla. The amplitudes of the curves i.e. $\lambda^{\gamma,2}$ were found to increase slightly with increasing field at the lower field end and to saturate in fields from 4 Tesla to 12 Tesla, except for pure terbium. The increasing field aligns the domains and for the saturation magnetostriction curves makes the specimen a single domain crystal. The field was increased to the strength where no further increase in the $\lambda^{\gamma,2}$ value of the trace was observed whilst the temperature was kept constant at 4.2K. The temperature was then varied while keeping the field constant. The field dependence of the $\lambda^{\gamma,2}$ constant is shown in Figure 7.11 and 7.12 for 50%Gd-50%Tb and 10%Gd-90%Tb specimens respectively.

7.4 Temperature Dependence of the Constant $\lambda^{\gamma,2}$

The variation of the $\lambda^{\gamma,2}$ constant with temperature was observed in magnetic fields producing saturated magnetostriction $\lambda^{\gamma,2}$ signals. To be sure that the field was strong enough to produce single domains in the basal plane and that the measured values of the constants were saturation values, another set of temperature variation was observed at a higher field. The two sets of curves were identical except that slightly higher values of the constants

were found for higher fields at temperatures close to T_c. The most complete account of the theoretical temperature dependence of magnetostriction is given by Callen and Callen (1965) as has been discussed earlier in Section 4.4. Their expression for the temperature dependence using the single-ion model is

$$\lambda(T) = \lambda(o)\,\hat{I}_{(\ell+\frac{1}{2})}\,(\mathcal{L}^{-1}m(T)) = \lambda(o)\hat{I}_{(\ell+\frac{1}{2})}(x) \qquad 7.1$$

where $\hat{I}_{(\ell+\frac{1}{2})}$ is the reduced Bessel function which is the ratio of the hyperbolic Bessel function of order $(\ell+\frac{1}{2})$ to the hyperbolic Bessel function of order $\frac{1}{2}$. The argument of the reduced Bessel function is the inverse of the familiar Langevin function related to reduced magnetization 'm' as

$$\mathcal{L}(x) = \hat{I}_{3/2}(x) = \coth(x) - {}^{1}/x = m \quad . \qquad 7.2$$

An attempt was made earlier to measure the magnetization for the above alloy specimens using the Faraday balance. The values obtained were lower than those measured by Bagguley et al. (1980b) or Corner et al. (1983a). The lower values were mainly due to the available magnetic field being inadequate to produce saturation magnetization and the force of friction between the specimen container and the walls of the measuring insert as the specimen was always pulled towards the sides by the radial field gradiant of the solenoid. Due to the availability of the reliable magnetization values of Corner et al. (1983a) further modifications in the Faraday equipment were not made.

In the calculations of the theoretical temperature dependence, the reduced magnetization values were obtained from the magnetization measurements of Corner et al. (1983a). The argument of the reduced Bessel function was calculated numerically by the microcomputer using Newton's iteration method. The computer programme is listed in Appendix III. The corresponding values of the reduced Bessel functions were obtained from the table of Joraide (1980) adapted after Welford (1975). The observed magnetostriction constant $\lambda^{\gamma,2}$ values versus temperature along with the reduced magnetization and corresponding reduced Bessel function values are given in Tables 7.1, 7.2, 7.3, 7.4, 7.5 and 7.6 for each composition. The theoretical temperature dependence of magnetostriction has been discussed in detail in Chapter 4. The adequacy of various theoretical models for temperature dependence was tested using a least-squares method best fit with the experimental results. The computer programme is listed in Appendix IV. Figures 7.4, 7.5, 7.6, 7.7, 7.8 and 7.9 show the observed temperature dependence of the constant $\lambda^{\gamma,2}$ along with the theoretical dependence curves for each composition of the specimens. The simple square power of reduced magnetization dependence (the two-ion model) did not provide a good fit and was giving higher values of the constant in comparison to the observed ones with increase in temperature. Similarly the fit of the $\hat{I}_{5/2}\hat{I}_{9/2}$ dependence of the Rhyne and Mc Guire (1972) model, which considers magnetoelastic interaction between ions, is also not good. Its dependence falls much more

TABLE 7.1

The temperature variation of the constant $\lambda^{\gamma,2}$ for pure Gd along with the values of reduced magnetization and Bessel functions. $\lambda^{\gamma,2}$ values are in units of 10^{-4}

Field in Tesla	Temp K	$\lambda^{\gamma,2}_{(T)}$	m(T)	$\hat{I}_{5/2}$	$\hat{I}_{9/2}$	$\hat{I}_{13/2}$
0.5	4.2	.95	1	1	1	
1	4.2	1.2	1	1	1	1
2	4.2	1.2	1	1	1	1
4	4.2	1.2	1	1	1	1
4	63	1.0	.965	.8992	.7023	.4770
4	106	.64	.906	.7447	.3790	.1351
4	137	.43	.851	.6237	.2177	.046
4	172	.21	.785	.4974	.1128	.0138
0 K Least squares fit $\lambda(o)$ values			$1\pm.15$ (a)	$1.05\pm.12$ (b)	$1.5\pm.16$ (c)	$1.77\pm.34$ (d)

The values a, b, c, and d are extrapolated 0 K values of the constant $\lambda^{\gamma,2}$ using least squares fit to $m^2(T)$, $\hat{I}_{5/2}$, $\hat{I}_{5/2}\times\hat{I}_{9/2}$ and $\hat{I}_{13/2}$ respectively.

TABLE 7.2

The temperature variation of the constant $\lambda^{\gamma,2}$ in units of 10^{-4} for 90%Gd-10%Tb along with the values of reduced magnetization and Bessel functions.

Field in Tesla	Temp. K	$\lambda^{\gamma,2}(T)$	$m^2(T)$	$\hat{I}_{5/2}$	$\hat{I}_{9/2}$	$\hat{I}_{13/2}$
4	4.2	10.8	1	1	1	1
4	50	9.97	.956	.9364	.8035	.6320
4	82	8.66	.895	.8473	.5769	.3172
4	100	8.16	.848	.783	.4458	.1872
4	120	6.5	.789	.7037	.3164	.0945
4	147	5.4	.702	.5915	.1857	.0342
4	152	5.2	.689	.5776	.1731	.0300
4	178	4.07	.598	.4729	.0981	.0108
4	184	3.86	.575	.4554	.0885	.0090
4	216	2.83	.452	.3289	.0382	.00217
4	258	1.47	.248	.1656	.0078	.00017
4	264	1.26	.213	.1375	.00524	.00009
8	4.2	10.8	1	1	1	1
0 K least squares fit values			9.24 $\pm$.45	10.15 $\pm$.26	17.91 $\pm$2.6	22.65 $\pm$4.7
			(a)	(b)	(c)	(d)

The values a, b, c, and d are extrapolated 0 K values of the constant $\lambda^{\gamma,2}$ using least squares fit to $m^2(T)$, $\hat{I}_{5/2}$, $\hat{I}_{5/2} \times \hat{I}_{9/2}$ and $\hat{I}_{13/2}$ respectively.

TABLE 7.3

The temperature variation of the constant $\lambda^{\gamma,2}$ in units of 10^{-3} for 70%Gd-30%Tb along with the values of reduced magnetization and Bessel functions.

Field in Tesla	Temp. K	$\lambda^{\gamma,2}_{(T)}$	$m^2(T)$	$\hat{I}_{5/2}$	$\hat{I}_{9/2}$	$\hat{I}_{13/8}$
4	4.2	2.13	1	1	1	1
8	4.2	2.13	1	1	1	1
8	35	2.08	.978	.9675	.8957	.7936
8	100	1.63	.846	.7347	.3629	.1239
8	138	1.30	.724	.6191	.2129	.0442
8	162	1.09	.643	.5236	.130	.018
8	180	.939	.573	.446	.084	.0082
8	210	.706	.450	.328	.038	.0022
8	247	.452	.255	.166	.008	.00018
8	274	.306	.049	.031	.0002	0
8	291	.222	0	0	0	0
0 K Least squares fit values			$1.97\pm.08$ (a)	$2.16\pm.05$ (b)	$3.42\pm.07$ (c)	$4.01\pm.1$ (d)

The values a, b, c, and d are extrapolated 0 K values of the constant $\lambda^{\gamma,2}$ using least squares fit to $m^2(T)$, $\hat{I}_{5/2}$, $\hat{I}_{5/2} \times \hat{I}_{9/2}$ and $\hat{I}_{13/2}$ respectively.

TABLE 7.4

The temperature variation of the constant $\lambda^{\gamma,2}$ in units of 10^{-3} for 50%Gd-50%Tb along with the values of reduced magnetization and Bessel functions.

Field in Tesla	Temp. K	$\lambda^{\gamma,2}_{(T)}$	$m^2(T)$	$\hat{I}_{5/2}$	$\hat{I}_{9/2}$	$\hat{I}_{13/2}$
1	4.2	3.41	1	1	1	1
2	4.2	3.46	1	1	1	1
4	4.2	3.41	1	1	1	1
8	4.2	3.41	1	1	1	1
4	43	3.34	.978	.9675	.8957	.7936
4	82	2.91	.895	.8473	.5769	.3172
4	122	2.25	.769	.680	.284	.076
4	.158	1.74	.637	.5199	.1277	.0172
4	204	1.12	.438	.3159	.0347	.0018
4	226	.786	.324	.2222	.0151	.0004
4	260	.421	.057	.0355	.0003	.000001
0 K Least squares fit values			3.21 $\pm$.15 (a)	3.42 $\pm$.06 (b)	5.04 $\pm$.84 (c)	5.87 $\pm$1.3 (d)

The values a, b, c, and d are extrapolated 0 K values of the constant $\lambda^{\gamma,2}$ using least squares fit to $m^2(T)$, $\hat{I}_{5/2}$, $\hat{I}_{5/2} \times \hat{I}_{9/2}$ and $\hat{I}_{13/2}$ respectively.

TABLE 7.5

The temperature variation of the constant $\lambda^{\gamma,2}$ in units of 10^{-3} for 10%Gd-90%Tb along with the values of reduced magnetization and Bessel functions.

Field in Tesla	Temp. K	$\lambda^{\gamma,2}_{(T)}$	$m^2(T)$	$\hat{I}_{5/2}$	$\hat{I}_{9/2}$	$\hat{I}_{13/2}$
1	4.2	6.91	1	1	1	1
2	4.2	7.07	1	1	1	1
4	4.2	7.07	1	1	1	1
8	4.2	7.17	1	1	1	1
4	47	6.83	.953	.929	.784	.601
4	82	5.93	.876	.820	.518	.254
4	122	4.56	.757	.669	.258	.064
4	158	3.48	.608	.482	.103	.012
4	205	1.93	.336	.230	.017	.0006
4	245	.735	0	0	0	0
0 K Least Squares fit values			6.74 $\pm$.28 (a)	7.2×10^{-3} $\pm$.25 (b)	11$\pm$2.1 (c)	13.2 $\pm$3.4 (d)
4	4.2	5.90*				
8	4.2	5.94*				

* For explanation of the different lower value, see text Page 108.

The values a, b, c, and d are extrapolated 0 K values of the constant $\lambda^{\gamma,2}$ using least squares fit to $m^2(T)$, $\hat{I}_{5/2}$, $\hat{I}_{5/2}\times\hat{I}_{9/2}$ and $\hat{I}_{13/2}$ respectively.

TABLE 7.6

The temperature variation of the constant $\lambda^{\gamma,2}$ in units of 10^{-3} for pure Tb along with the values of reduced magnetization and Bessel functions.

Field in Tesla	Temp. K	$\lambda^{\gamma,2}_{(T)}$	$m^2(T)$	$\hat{I}_{5/2}$	$\hat{I}_{9/2}$	$\hat{I}_{13/2}$
12	4.2	6.58	1	1	1	1
12	22	6.02	.982	.9732	.9136	.8272
12	36	5.22	.976	.9644	.8861	.7758
12	71	4.04	.899	.8519	.5872	.3289
12	104	3.35	.815	.7381	.3683	.1276
12	133	2.86	.719	.6143	.2080	.0423
12	146	2.74	.664	.5473	.1479	.0225
12	181	2.49	.484	.3636	.0493	.0033
0 K Least squares fit values			5.38 $\pm$.36	5.67 $\pm$.29	7.83 $\pm$ 1	8.9 $\pm$1.5
			(a)	(b)	(c)	(d)

The values a, b, c, and d are extrapolated 0 K values of the constant $\lambda^{\gamma,2}$ using least squares fit to $m^2(T)$, $\hat{I}_{5/2}$, $\hat{I}_{5/2} \times \hat{I}_{9/2}$ and $\hat{I}_{13/2}$ respectively.

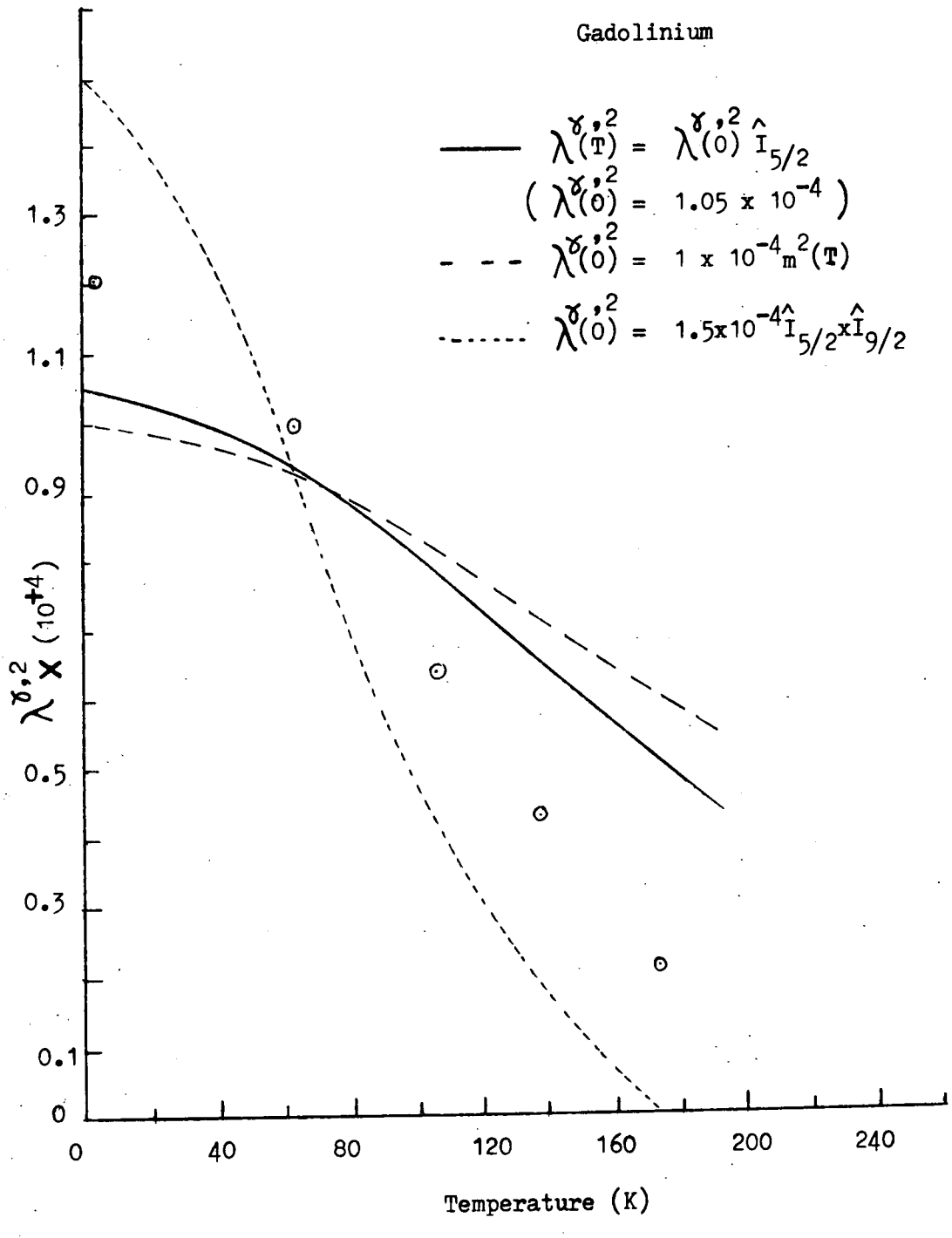

Fig. 7.4 The temperature dependence of $\lambda^{\gamma,2}$ for Gd at 4 Tesla.

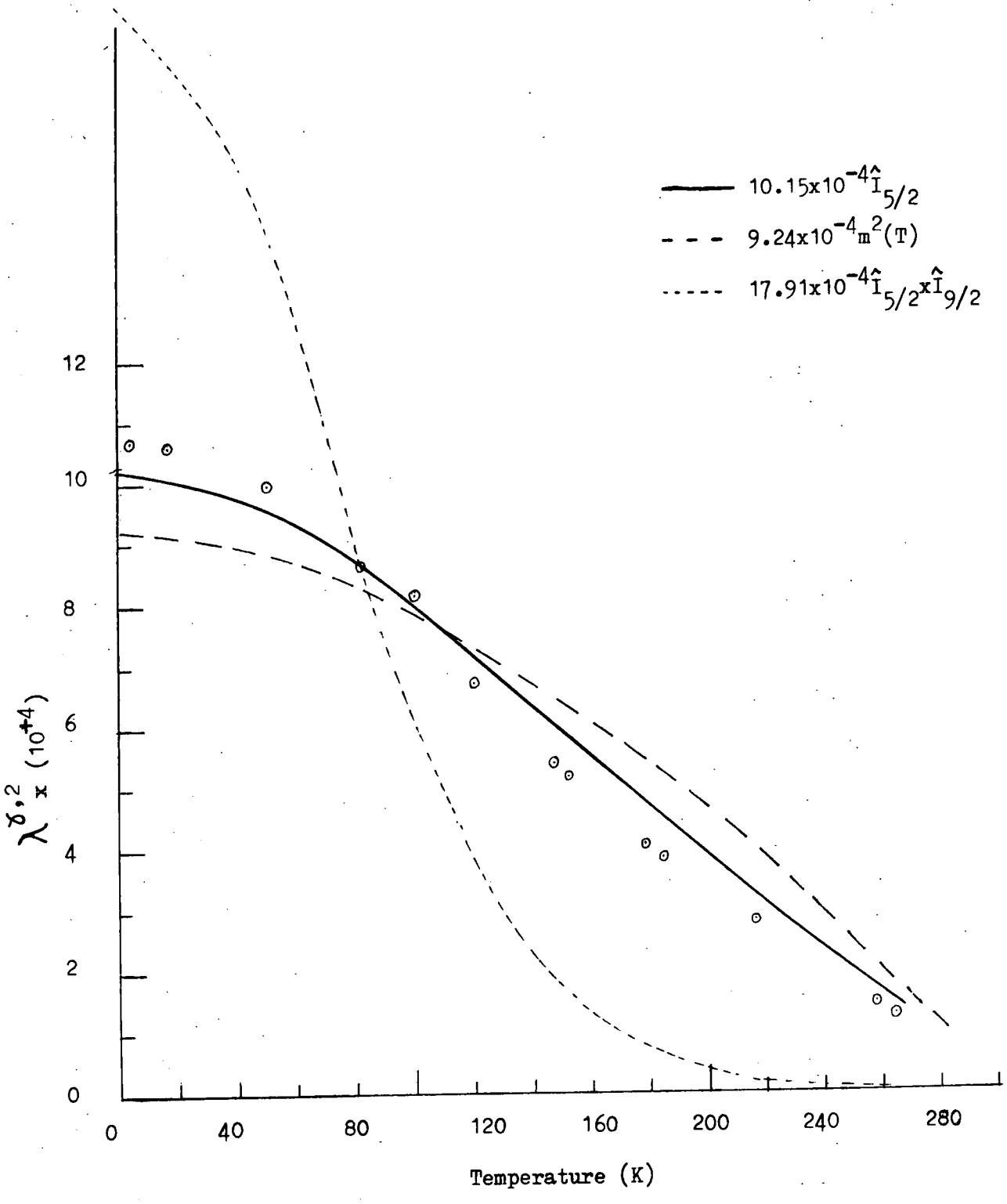

Fig. 7.5 The temperature dependence of $\lambda^{\gamma,2}$ for $Gd_{0.90}Tb_{0.10}$ at 4 Tesla.

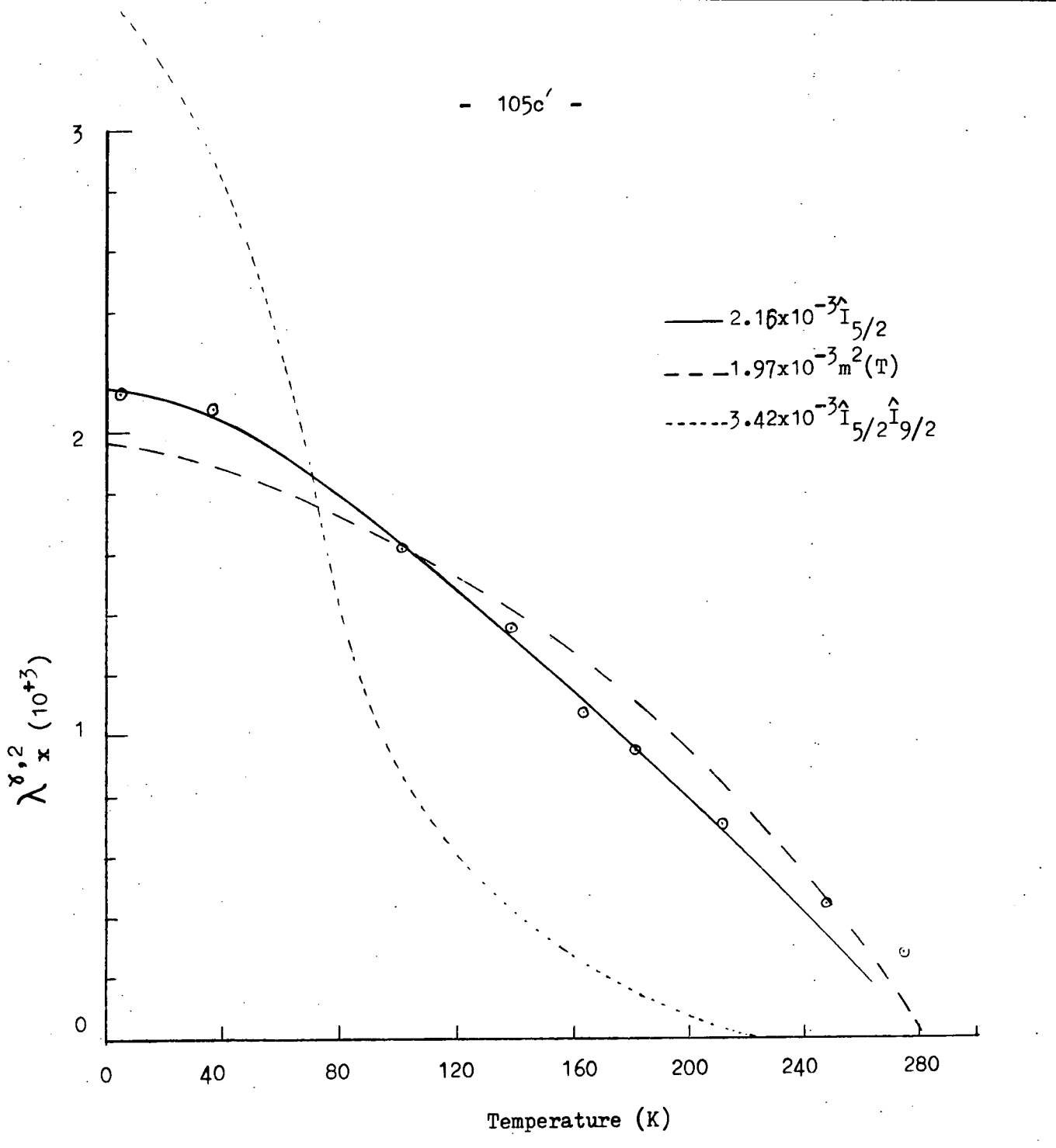

Fig. 7.6 The temperature dependence of $\lambda^{\gamma,2}$ for $Gd_{0.70}Tb_{0.30}$ at 8 Tesla.

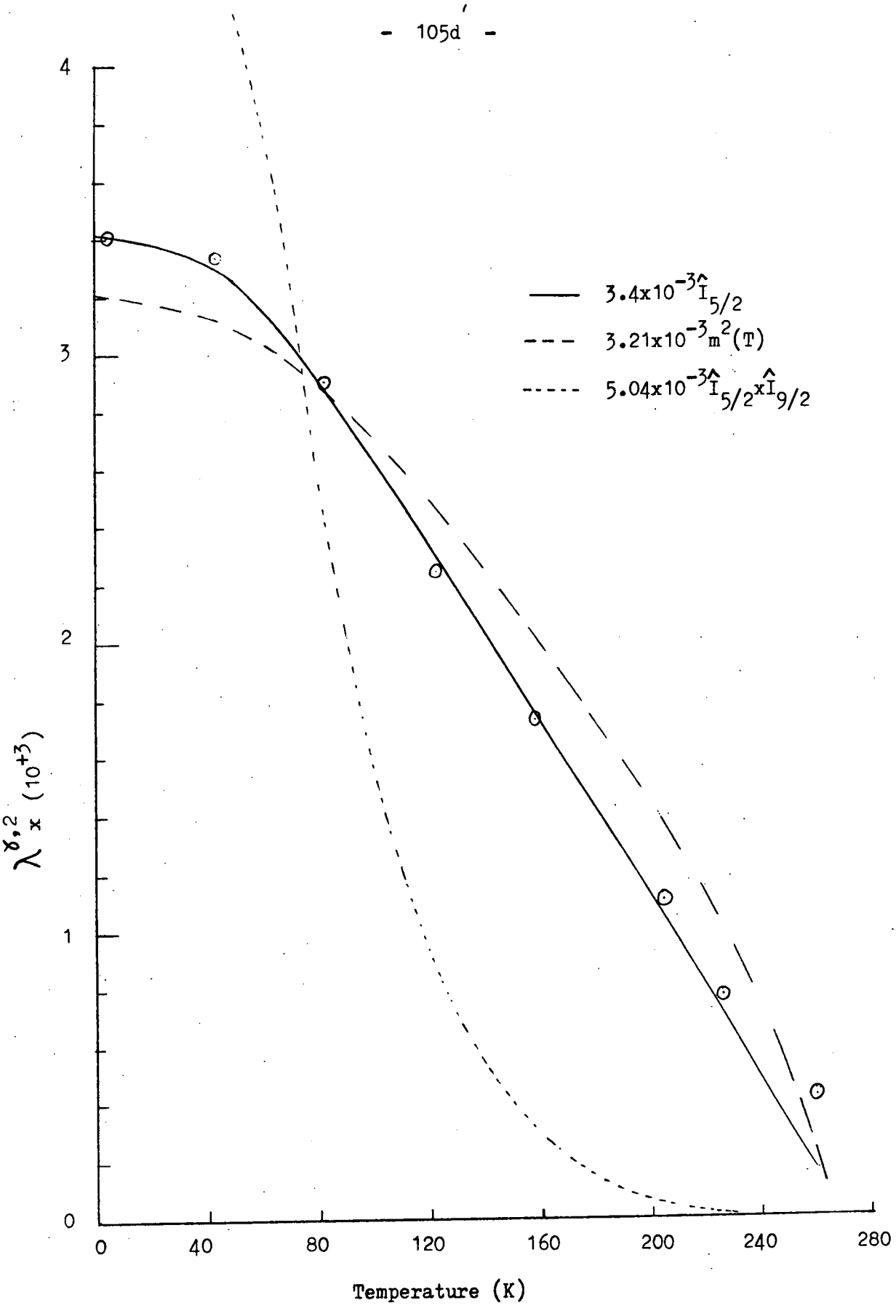

Fig. 7.7 The temaperature dependence of $\lambda^{\gamma,2}$ for $Gd_{0.50}Tb_{0.50}$ at 4 Tesla.

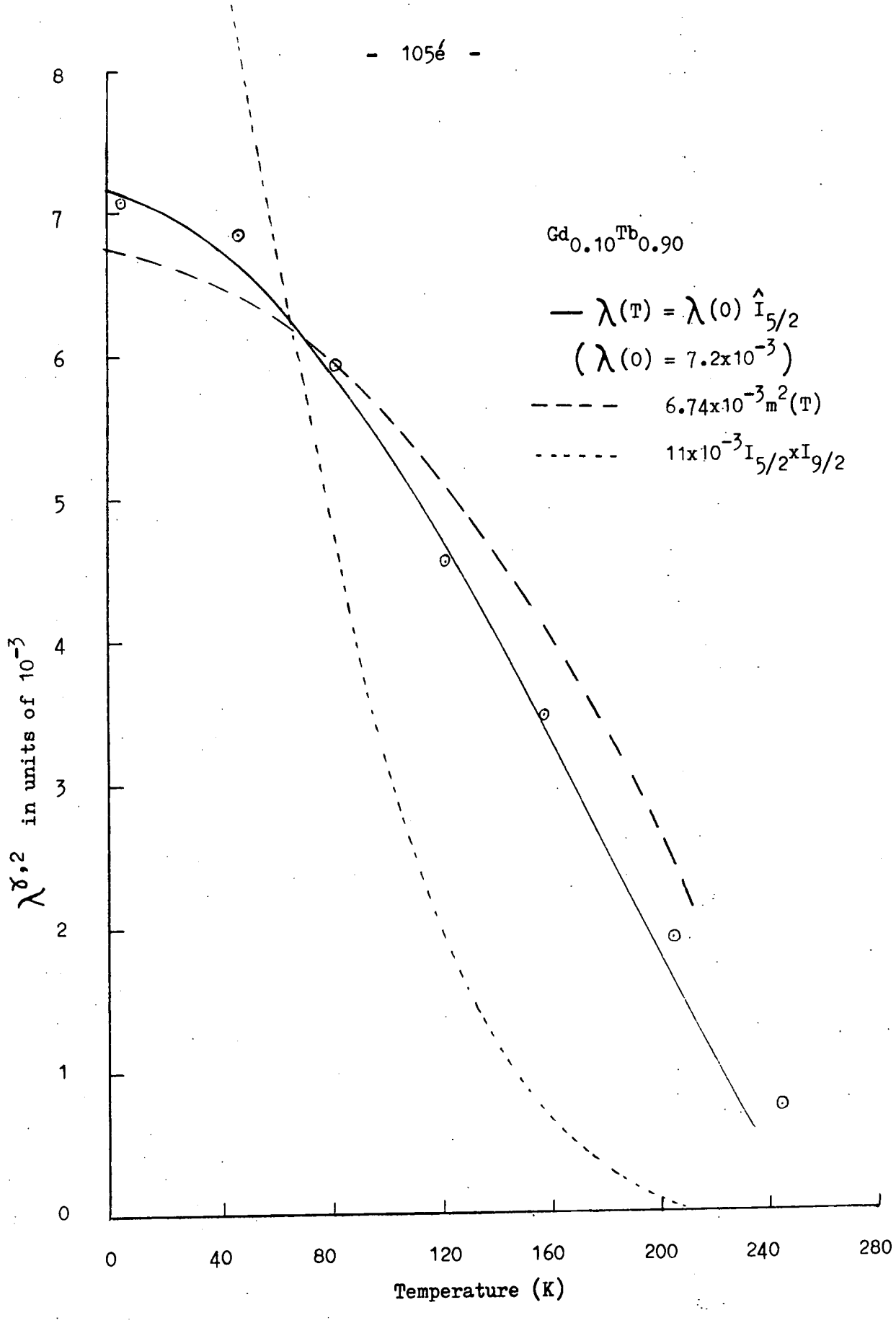

Fig. 7.8 The temperature dependence of $\lambda^{\gamma,2}$ for $Gd_{0.10}Tb_{0.90}$ at 4 Tesla.

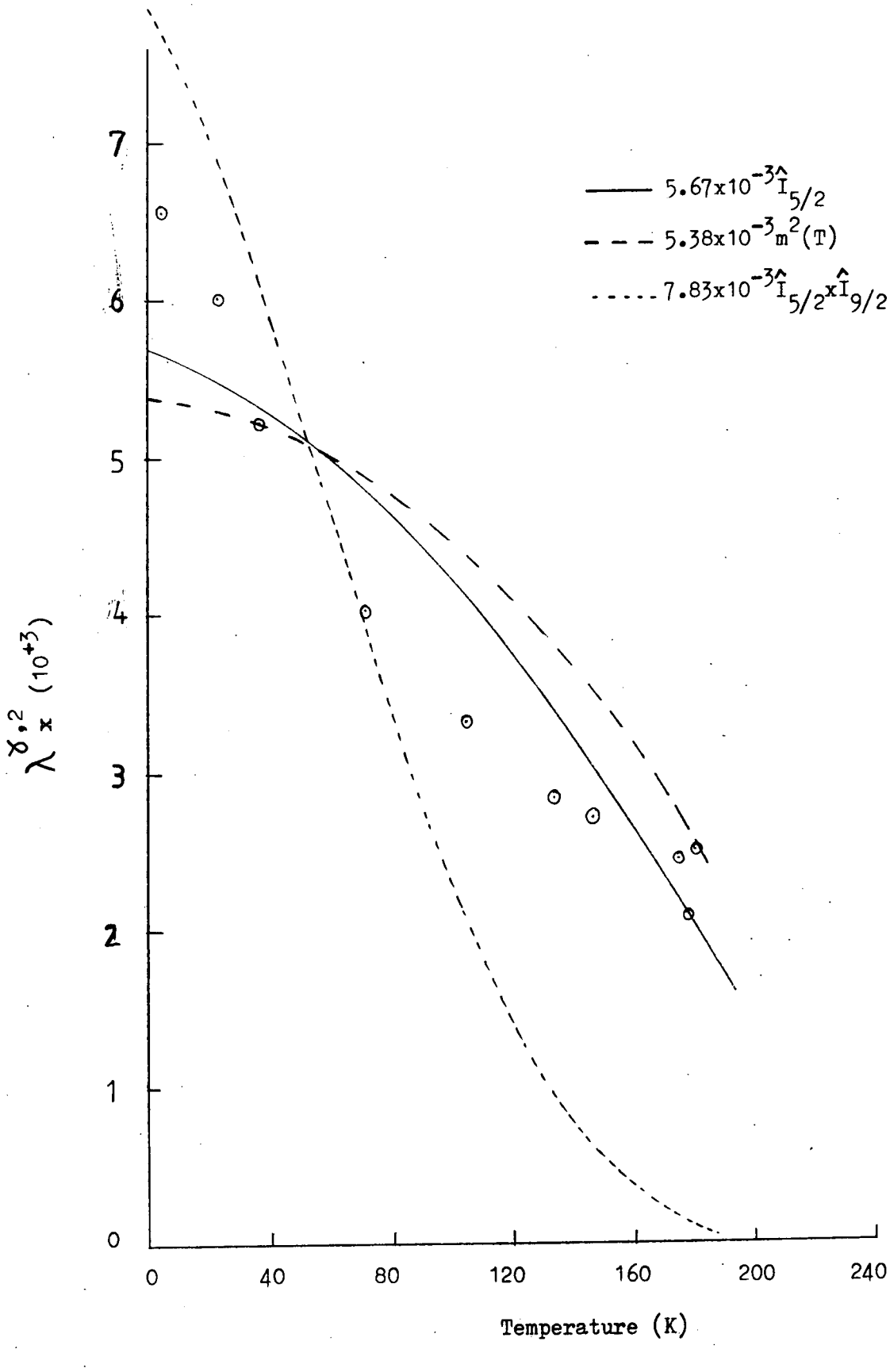

Fig. 7.9 The temperature dependence of $\lambda^{\gamma,2}$ for terbium at 12 Tesla.

sharply than the observed dependence. The $\hat{I}_{5/2}$ dependence model proposed by Callen and Callen (1965) on the basis of single-ion interaction fits very well. The fit with the pure gadolinium is not good but it becomes better for 90%Gd-10%Tb alloys. The agreement is good for 70%Gd-30%Tb, 50%Gd-50%Tb and 10%Gd-90%Tb. Again pure terbium is an exception. The agreement covers almost the entire temperature range. The dgree of best fit can be judged from the percentage error in the values computed using the least-squares method:

Percentage of Gd	100	90	70	50	10	0
Percentage Error	11.4	2.56	2.31	1.75	2.44	5.11

7.5 Composition Dependence of $\lambda^{\gamma,2}$

For each theoretical temperature dependence there corresponds a zero-temperature value of the magnetostriction constant $\lambda^{\gamma,2}_{(o)}$. The best fitting single-ion model curves yielded the best zero temperature values for each composition. These values are very close to the experimentally observed values at the lowest temperature 4.2K. The zero-temperature values $\lambda^{\gamma,2}_{(o)}$ are plotted against alloy composition in Figure 7.10. The variation with composition is seen to be close to a linear one, with the exception of one measurement for 10%Gd-Tb. For comparison the reported values of Joraide (1980) and Nikitin (1977) are also shown in the same figure.

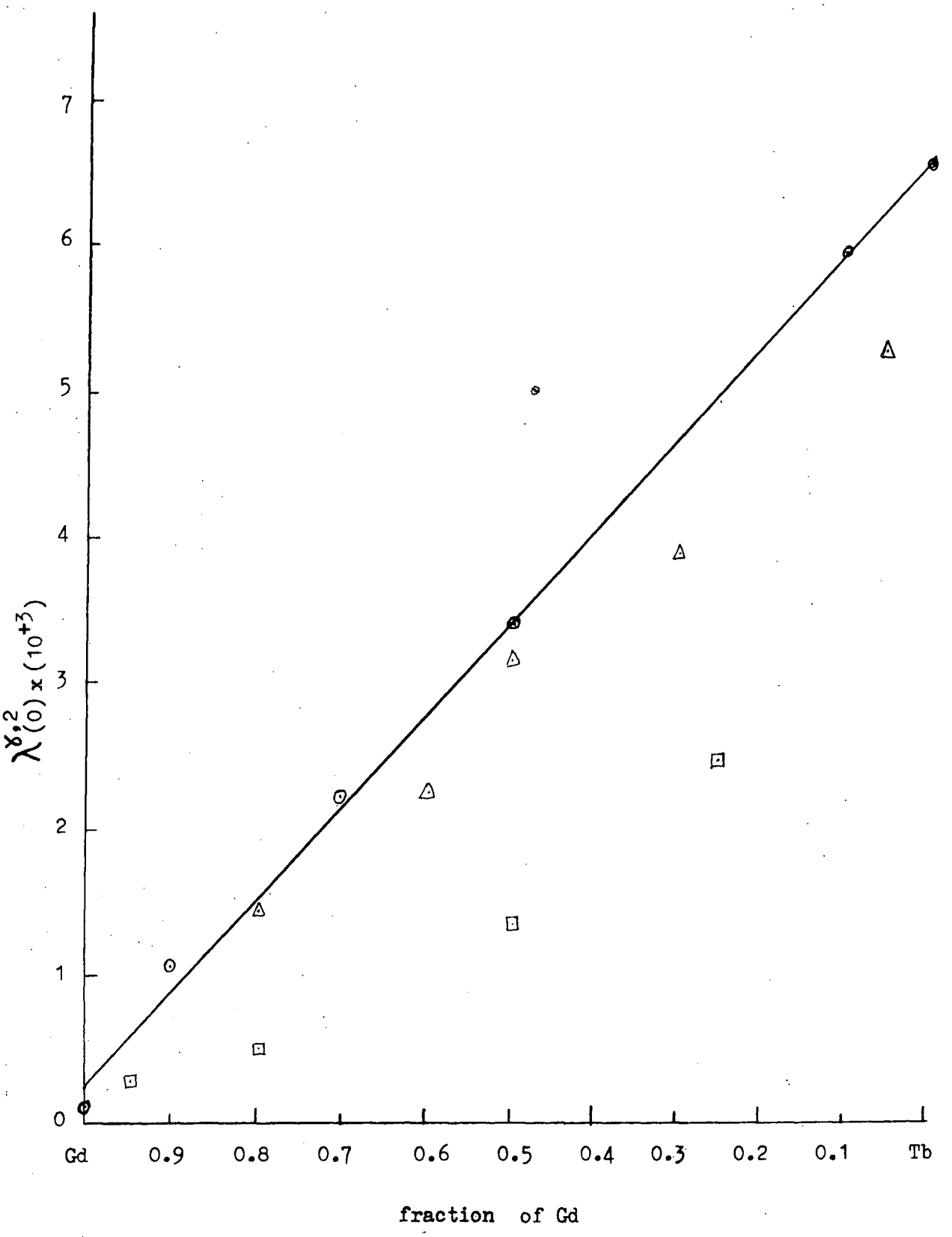

Fig. 7.10 Composition dependence of $\lambda^{\gamma,2}_{(0)}$ for Gd/Tb alloys.

⊡ Joraide, 80 , △ Nikitin, 1977

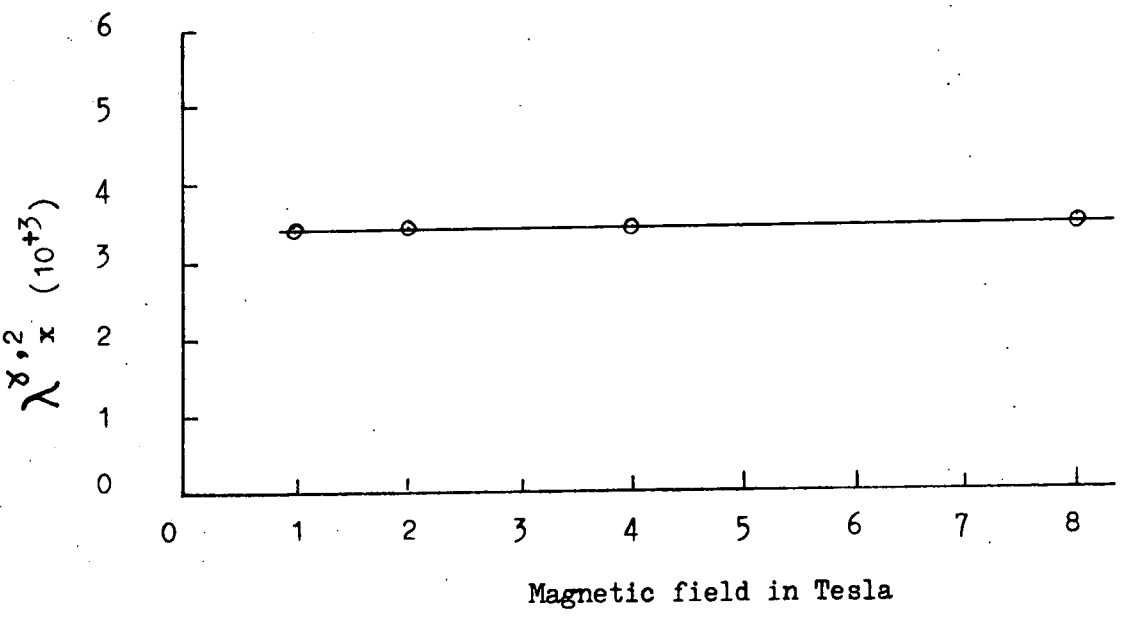

Fig. 7.11 Magnetostrictive strain $\lambda^{\gamma,2}$ for $Gd_{0.50}Tb_{0.50}$ versus field at 4.2 K.

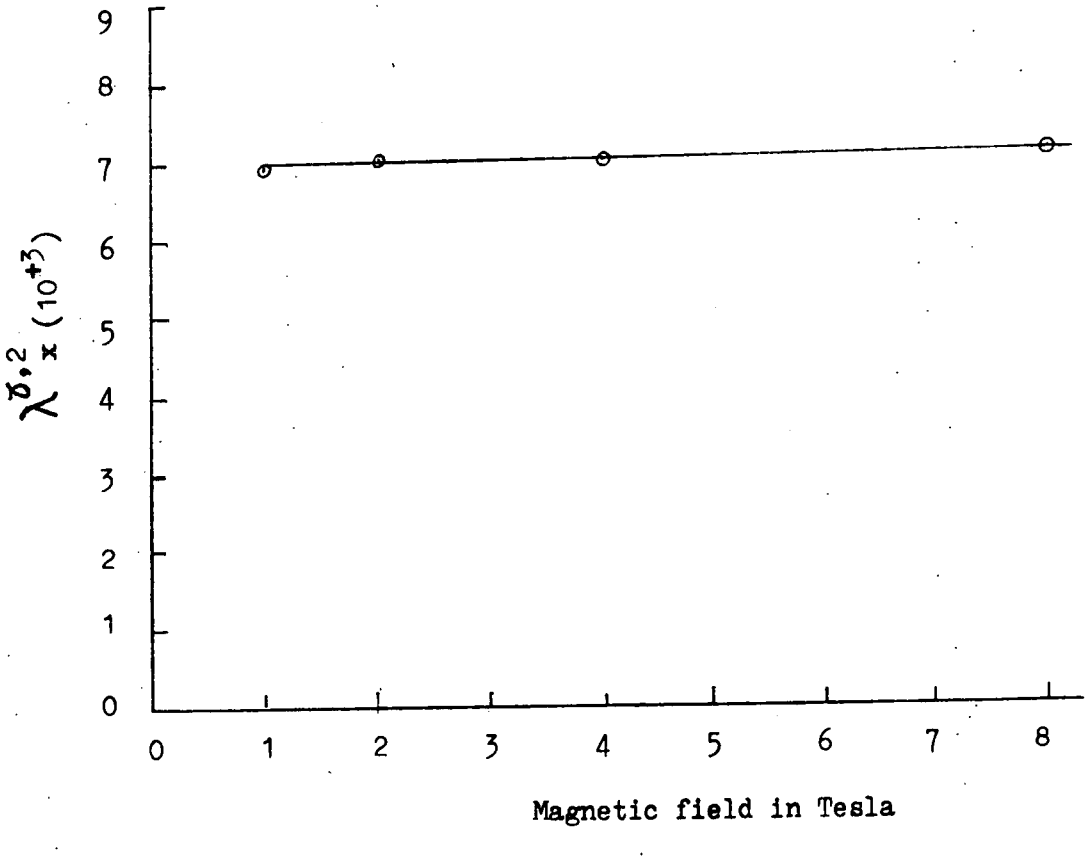

Fig. 7.12 Magnetostrictive strain $\lambda^{\gamma,2}$ for $Gd_{0.10}Tb_{0.90}$ versus field at 4.2 K.

7.6 Discussion of the Results

The zero temperature saturation value of the magnetostriction constant $\lambda^{\gamma,2}_{(o)}$ of pure gadolinium coincides with the value reported by Mishima et al. (1976). The zero temperature values for the other intermediate compositions measured by Joraide (1980) are about half the experimental interpolated values from the present measurement. The lower values of the constant observed by Joraide could be due to some systematic error of the apparatus. According to equation 6.17, the measurements of the strain depend upon the value of bridge voltage. The bridge voltage may vary for each setting of the bridge balancing resistor suitable for the particular case at the time of data recording. He might always have used the value of the bridge voltage recorded during his earlier measurements on a nickel specimen. In the present study the bridge voltage was actually measured throughout for each setting of the experiment. The changes in the resistance of the gauges due to variations in temperature or magnetostrictive strain have little effect on the bridge voltage and cause no detectable error in the measurements. Another reason for lower values could be an unnoticed accidental change in the amplification of the amplifier, but that seems very unlikely.

The values of Joraide do not vary linearly with composition of the alloys, the magnetostriction versus composition curve tends to have an exponential form. The values of the constants measured by Nikitin et al.

(1977) on the other hand, vary linearly with alloy composition. The experimental values in this work are close to those of the Nikitin et al. but are still higher for all compositions. The agreement is close towards the gadolinium rich end, but the difference increases with the increasing terbium concentration.

Two different values of $\lambda^{\gamma,2}$ for the 10%Gd-90%Tb specimen were observed on two different occasions when measurements were repeated. With the later value, all the observed points lie on a straight line with the value of $\lambda^{\gamma,2}$ of pure terbium lying in between those of Nikitin et al. (1977) and Du Plessis (1968). Taking the first value of the $\lambda^{\gamma,2}$ of 10%Gd-90%Tb, the experimental curve does not exhibit such a close approach to linearity, but shows slight curvature. The curve in this case tends towards the du Plessis value for terbium which is considerably larger than the one measured in the present experiment. The attempt to verify the value of the constant for the specimen in question always gave the lower value as expected from the linearly varying curve. The reason for this discrepancy is not known and it is hard to reject any value. A lower value may be explained as due to partially loose bonding of the strain gauge on to the specimen whereas it is hard to get a spurious higher signal. Because the temperature variation of $\lambda^{\gamma,2}$ for pure Tb does not fit well with a simple power law or $\hat{I}_{5/2}$ law extrapolation to 0°K is not so accurate and it is not possible to use the extrapolated value to

differentiate between the values for 10%Gd-Tb with confidence. The other experimental values of the set can accommodate both values though they favour very much the later and repeatable value.

The temperature variation of $\lambda^{\gamma,2}$ was measured for the four compositions (95%Gd-Tb, 80%Gd-Tb, 50%Gd-Tb and 25%Gd-Tb) by Joraide (1980). His temperature dependence has already been discussed in section 5.7 and the variation is shown in Figure 5.14. In general his dependence does not agree with any of the common theoretical models for the whole set of specimens and for the entire range of temperature, though the fit to the single-ion model is not bad in certain cases. Nikitin et al. do not provide the temperature variation of the alloys except for the 50%Gd-50%Tb alloy. The magnetization dependence of $\lambda^{\gamma,2}$ for this alloy has been shown to follow the single-ion model dependence given by equation 7.1. Their technique for measuring the magnetostriction constants is different, thus the field is applied along certain crystallographic directions and the strain is measured along orthogonal $\hat{a}$, $\hat{b}$ and $\hat{c}$ crystallographics axes. The magnetization vector is not rotated in the specimen. The constants are derived by subtracting the phonon part of the strain obtained from the thermal-expansion curves of lutetium.

7.7 Conclusions from the Temperature and the Composition Dependence Results

The temperature dependence of the experimental

results fits the theoretical dependence predicted by the single-ion model extremely well for alloys containing more than 10% Terbium. The agreement is reasonable for 10% terbium concentration, but is not good for pure gadolinium. For this the $\lambda^{\gamma,2}$ constant seems to follow a two-ion dependence but again the fit is not perfect. The composition dependence of $\lambda^{\gamma,2}$ also follows that expected from a single-ion model where the strain is a consequence of interaction of individual Tb ions with the crystal field and a linear variation would be expected on dilution of Tb ions with Gd ions. The conclusion based on the experimental data is in agreement with that of Nikitin et al. based on their magnetostriction and magnetic anisotropy measurements. In the opinion of the author, the entire experimental temperature and composition dependence of the constant $\lambda^{\gamma,2}$ of all the alloy compositions is strongly in favour of the single-ion crystal field mechanism for the origin of the magnetostriction of the terbium-gadolinium alloys.

The situation is simple in the case of $\lambda^{\gamma,2}$ since the basal plane anisotropy of the terbium metal is considerably less than the axial anisotropy. Determination of the other magnetostriction constants is very difficult because of the giant anisotropy of the terbium. A knowledge of the actual angle of magnetization vector is necessary. A detailed discussion of the procedure for determining the other constants and their results will be given in the next chapter.

CHAPTER 8

THE MAGNETOSTRICTION CONSTANTS $\lambda_1^{\alpha,2}$ AND $\lambda_2^{\alpha,2}$ OF Gd AND Gd/Tb ALLOYS

8.1 Introduction

The second order constants $\lambda_1^{\alpha,2}$ and $\lambda_2^{\alpha,2}$ were measured for Gd and Gd/Tb alloys of composition 90%Gd-10%Tb, 70%Gd-30%Tb, 50%Gd-50%Tb and 10%Gd-90%Tb in the temperature range from liquid helium to near their Curie temperatures in magnetic fields of up to 12 Tesla. There were two types of specimen. The pure Gd and the 50%Gd-50%Tb specimens contained $\hat{b}$ and $\hat{c}$ axes in the plane of the disc while all the other specimens were ac plane discs. The measurements of strain along the $\hat{c}$-axis yield the constant $\lambda_2^{\alpha,2}$ and the measurements of strain along $\hat{a}$- or $\hat{b}$-axis of the specimens containing the $\hat{c}$-axis in the plane of the disc yield the constant $\lambda_1^{\alpha,2}$ when the effect of the constant $\lambda^{\gamma,2}$ has been allowed for. Again the Clark and Callen magnetostriction expression given in equation 4.45 was used to represent the magnetostrictive strain. The equation is further simplified for the particular cases to yield expressions for $\lambda_1^{\alpha,2}$ and $\lambda_2^{\alpha,2}$ in equations 6.9 and 6.13 respectively. The early measurements were made using one gauge at a time. The observed curves were not so simple as those for $\lambda^{\alpha,2}$. The strain variations for the full curves were not as expected from their representative equations. Due to the complexity of the curves, it was necessary to measure the strain along both principal axes in the plane of the disc at the same

time. Two strain gauges were cemented at right angles to each other, one on each side of the specimen, and the strain variations along both axes were recorded on a single sheet using the x-y recorder. This revealed more useful information, very helpful in understanding the internal magnetization process. The lack of symmetry of the strain versus field angle curves in general and deviation from a $\cos 2\theta$ theoretical variation in particular for strains along the $\hat{c}$-axis, is a clear indication that magnetization was not following the external magnetic field direction. At low temperatures, terbium has very high magnetocrystalline anisotropy and calculation showed that the magnetization never passes through the hard direction ($\hat{c}$-axis) particularly towards the terbium rich end of the alloy series. The equations 6.9 and 6.13 can be used to determine the magnetostriction constants if the precise direction of magnetization with respect to crystallographic axes is known. This is a completely different situation from that for the constant $\lambda^{\gamma,2}$ where the peak to peak amplitude of the strain variation curve alone was required. The constants represent the magnetostriction due to the rotation of the magnetization in the ac or bc plane.

8.2 Determination of Direction of the Magnetization

If the field is finite, but still strong enough to prevent domain walls from entering the crystal, the magnetocrystalline anisotropy may cause the magnetization vector to be not always parallel to the applied field.

In a simple case when magnetization is rotated completely, this distorts the periodic curve of magnetostriction versus angle of rotation in an infinite field, without changing its amplitude as shown in Figure 8.1. In our particular case the magnetization vector is not rotated completely and so it is necessary to find the direction of magnetization at every point. This can best be done by reference to the free energy function F that must be minimum in the equilibrium state. Let the magnetization lags behind the external field $\underline{B}_0$ by an angle δ when $\underline{B}_0$ makes an angle ψ with the $\hat{c}$-axis as shown in Figure 8.2. The torque L_M experienced due to the angular dependence of the magnetic field energy $F_M = -M_s B_0 \cos\delta$ is given by differentiation with respect to δ as

$$L_M = -\frac{\partial}{\partial\delta}(F_M) = -\frac{\partial}{\partial\delta}(-M_s B_0 \cos\delta)$$
$$= -M_s B_0 \sin\delta. \qquad 8.1$$

The representation of the magnetocrystalline anisotropy energy is given in equation 4.6 for the hexagonal system. The anisotropy constants other than K_1 are comparatively small and can be ignored in the calculation of the angle of magnetization with the $\hat{c}$-axis. Hence the anisotropy energy may be written as

$$F_K = K_1 \sin^2\theta \qquad 8.2$$

where θ is the angle of magnetization with the $\hat{c}$-axis.

The torque L_K can be expressed as

$$L_K = -\frac{\partial F_K}{\partial\theta} = -2 K_1 \sin\theta \cos\theta. \qquad 8.3$$

In the equilibrium state, the total torque L is zero.

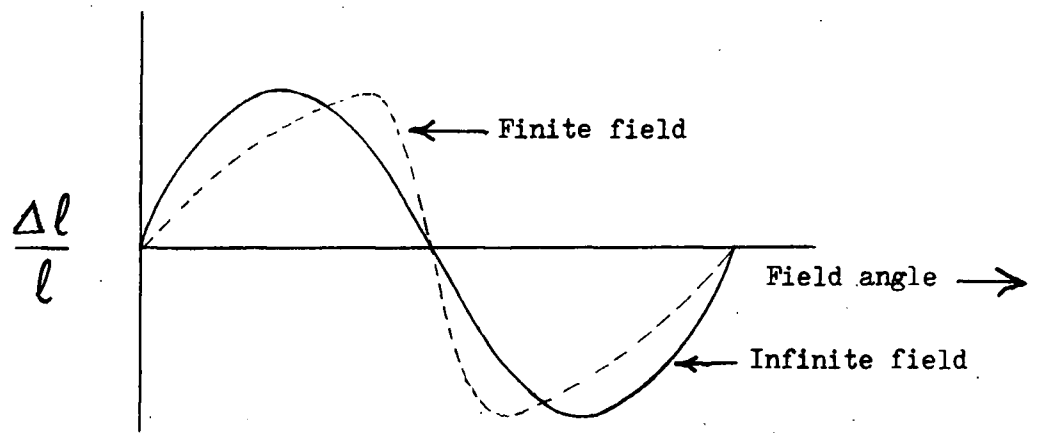

Fig. 8.1 Magnetostriction strain versus field angle

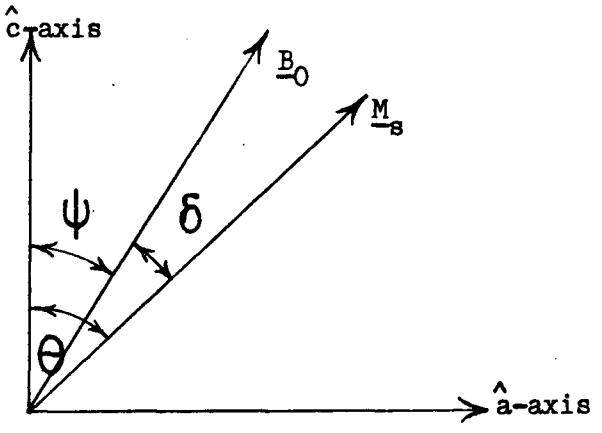

Fig. 8.2 The magnetization and field angles with respect to the c-axis.

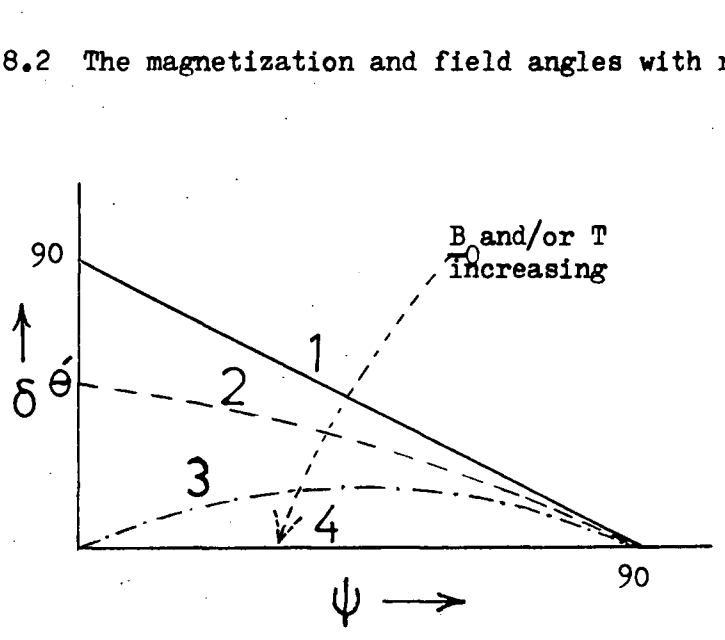

Fig. 8.3 Variation of the angle between field and magnetization due to field and temperature.

(1) Represents no rotation of magnetization at all, the case when $\underline{B}_0 = 0$ or $K_1 = \infty$,

(2) limited rotation of magnetization, part 1 of Fig. 8.4 (b),

(3) full rotation of magnetization, part 2 of Fig. 8.4 (b), and

(4) infinite field case when magnetization closely follows the external field.

Hence

$$L = L_K + L_M = -2K_1 \sin\theta \cos\theta - M_s B_0 \sin\delta = 0 \qquad 8.4$$

or

$$\sin\delta = \frac{-K_1 \sin 2\theta}{B_0 M_s} \qquad 8.5$$

which can be expressed in terms of the angle of the external field as

$$\sin\delta = \frac{-K_1 \sin 2(\psi + \delta)}{B_0 M_s} \qquad 8.6$$

because $\theta = \psi + \delta$.

The general analytical solution of this equation is complicated. However, it can be solved numerically for fixed angle ψ of the external magnetic field. The angle δ between magnetization $\underline{M}$ and the external field $\underline{B}_0$ was calculated for every five degree interval of the angle ψ from 90 to 0 degree by the microcomputer using Newton's iteration method. The computer programme is listed in Appendix V. Hence the angle of magnetization θ with respect to the $\hat{c}$-axis, which is the sum of ψ and δ , is known for all directions of the applied field. There are two cases referred as full or limited rotation of the magnetization. When the external field is along the $\hat{c}$-axis, the angle $\psi = 0$ and the angle δ is equal to the angle of magnetization with the $\hat{c}$-axis. Let this angle be θ'. From equation 8.6, we get

$$\cos\theta' = \frac{-M_s B_0}{2K_1} \qquad 8.7$$

For $\left|\frac{-M_s B_0}{2K_1}\right| < 1$, there is a finite value of θ' and hence magnetization is not rotated completely but stays behind the external field by an angle θ'. This is the case of limited rotation. When magnetic field is increased, or K_1 is decreased by increasing temperature, then $\left|-\frac{M_s B_0}{2K_1}\right|$ may increase to one or greater. For that case $\theta' = 0$ and so there is full rotation of magnetization from the easy axis to the hard axis. The variation of the angles δ and θ' of the magnetization with respect to the external field and the $\hat{c}$-axis is illustrated in Figures 8.3 and 8.4 respectively.

8.3 Typical Data Record

The situation in the case of constants $\lambda_1^{\alpha,2}$ and $\lambda_2^{\alpha,2}$ is not simple and a variety of curves was observed. In the limited rotation case, the magnetization not only stays behind the external field as it attempts to rotate it towards the $\hat{c}$-axis but it also rotates in the basal plane. Let us consider the general case of an ac plane specimen. When the magnetic field is applied along the $\hat{a}$-axis the magnetization will tend to lie along the $\hat{a}$-axis rather than along the $\hat{b}$-axis easy direction. We start with a moderate field sufficient to align the magnetization along the $\hat{a}$-axis, but still too weak to rotate it completely towards the hard direction, the $\hat{c}$-axis. As the applied field is now rotated towards the $\hat{c}$-axis, its component along the $\hat{a}$-axis decreases and the magnetization tends to lie along the easy $\hat{b}$-axis. The specimen is split into two sets of domains in each of which the

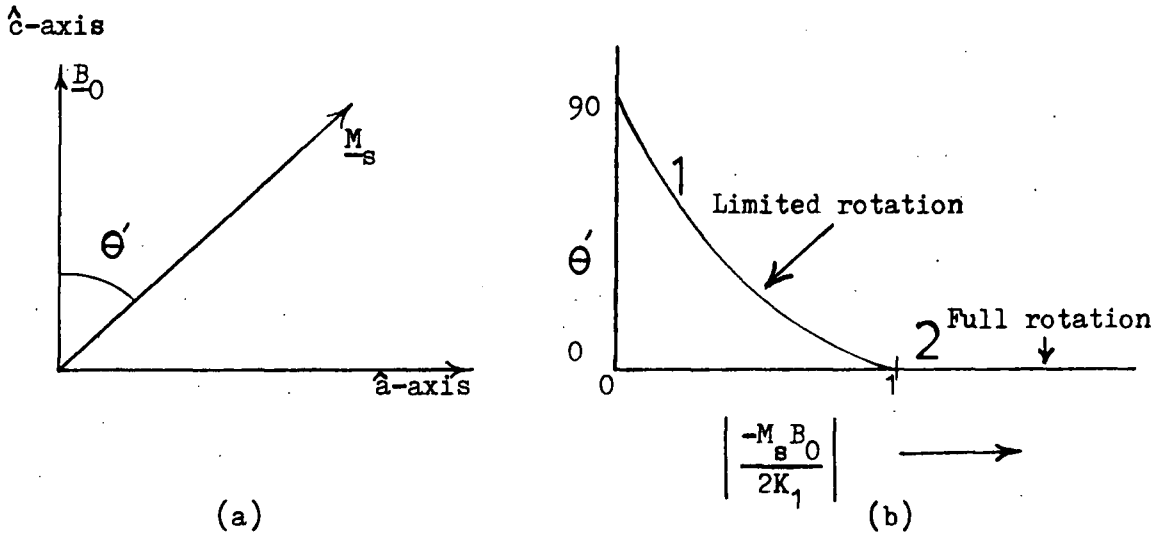

Fig. 8.4a) Maximum rotation of magnetization for field along ĉ-axis,
b) variation of maximum rotation of magnetization.

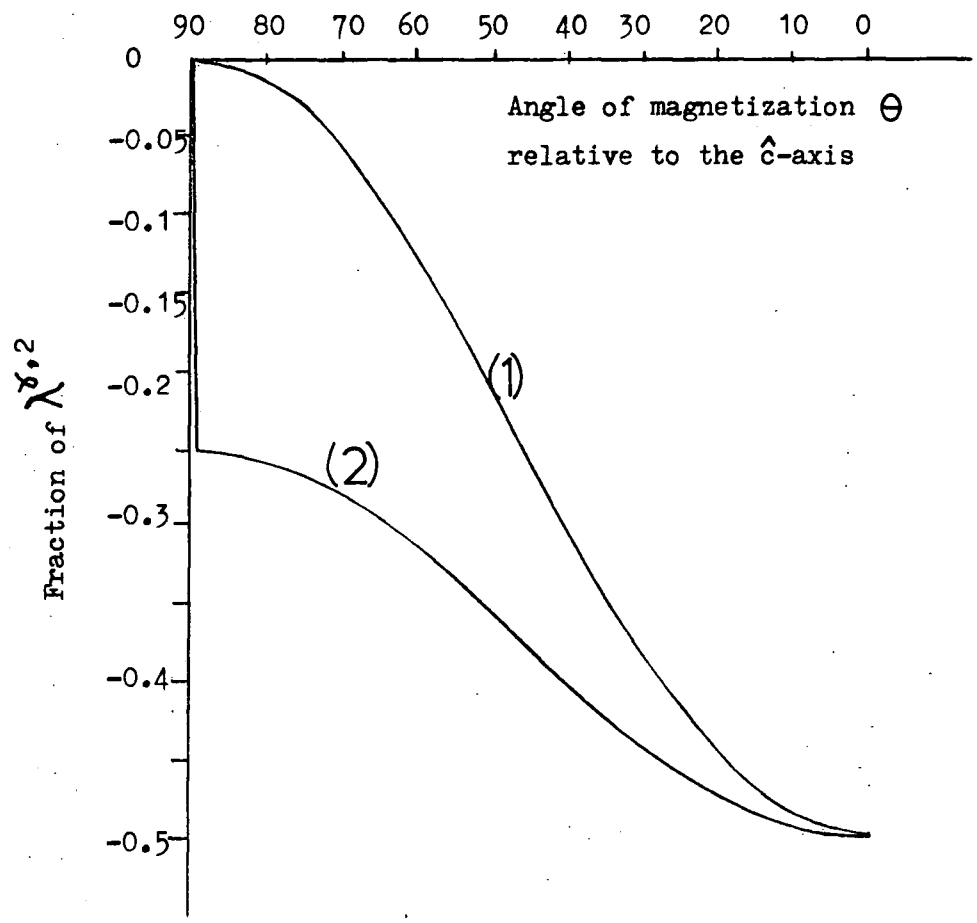

Fig. 8.5 The possible fraction of $\lambda^{\gamma,2}$ involved in the constant $\lambda_1^{\alpha,2}$ for ac plane specimens. For details of curve (1) and (2) see text page 127.

magnetization vector will rotate in the basal plane towards the immediately adjacent $\hat{b}$-axes at 30 degrees on either side of the original $\hat{a}$-axis. It will remain in the basal plane and will not rotate towards the $\hat{c}$-axis because of the giant axial anisotropy of the terbium ions. The rotation of the magnetization in the basal plane causes a strain along the $\hat{a}$-axis due to the $\lambda^{\gamma,2}$ contribution while no appreciable strain occurs along the $\hat{c}$-axis. The strain variation along both $\hat{a}$ and $\hat{c}$ axes for a 70%Gd-30%Tb specimen at 4.2K temperature and in the field of 0.5 Tesla is shown in Figure 8.6. If the field strength is increased, the magnetization stays longer along $\hat{a}$-axis before splitting takes place as can be seen from the curves in Figures 8.7 and 8.8 for the same specimen but in higher fields of 1 and 2 Tesla respectively. It can be seen in Figure 8.8 that the field is beginning to rotate the magnetization towards the $\hat{c}$-axis. Further increase in the field rotates the magnetization more and more towards the $\hat{c}$-axis and causes a flick from one side of the $\hat{c}$-axis to the other as the field passes through the $\hat{c}$-axis, in the case of a limited rotation. During the flicks, sharp changes occur suddenly in a variety of ways. A simple case is shown in Figure 8.9 for the same specimen but in 8 Tesla and at 140K. At higher temperatures, anisotropy decreases and full rotation of magnetization takes place as is shown in Figure 8.10. Further increase in temperature always decreases the amplitude of the strain variations and also the curves become smooth and symmetrical. This is the overall picture

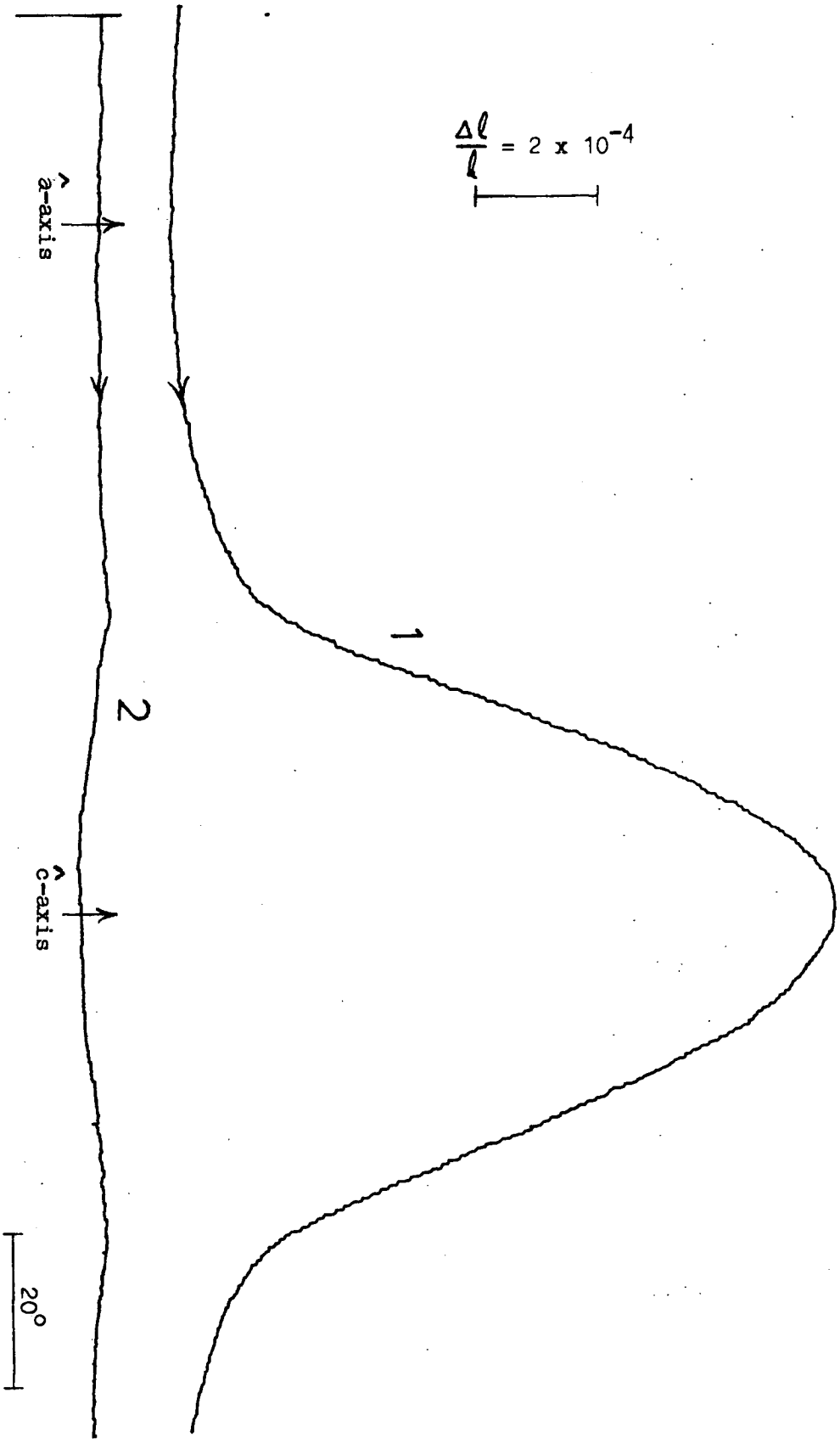

Fig. 8.6 Typical strain versus field angle curves for $Gd_{0.70}Tb_{0.30}$ at 4.2 K and in field of 0.5 Tesla; strains are along â-axis (1) & ĉ-axis (2).

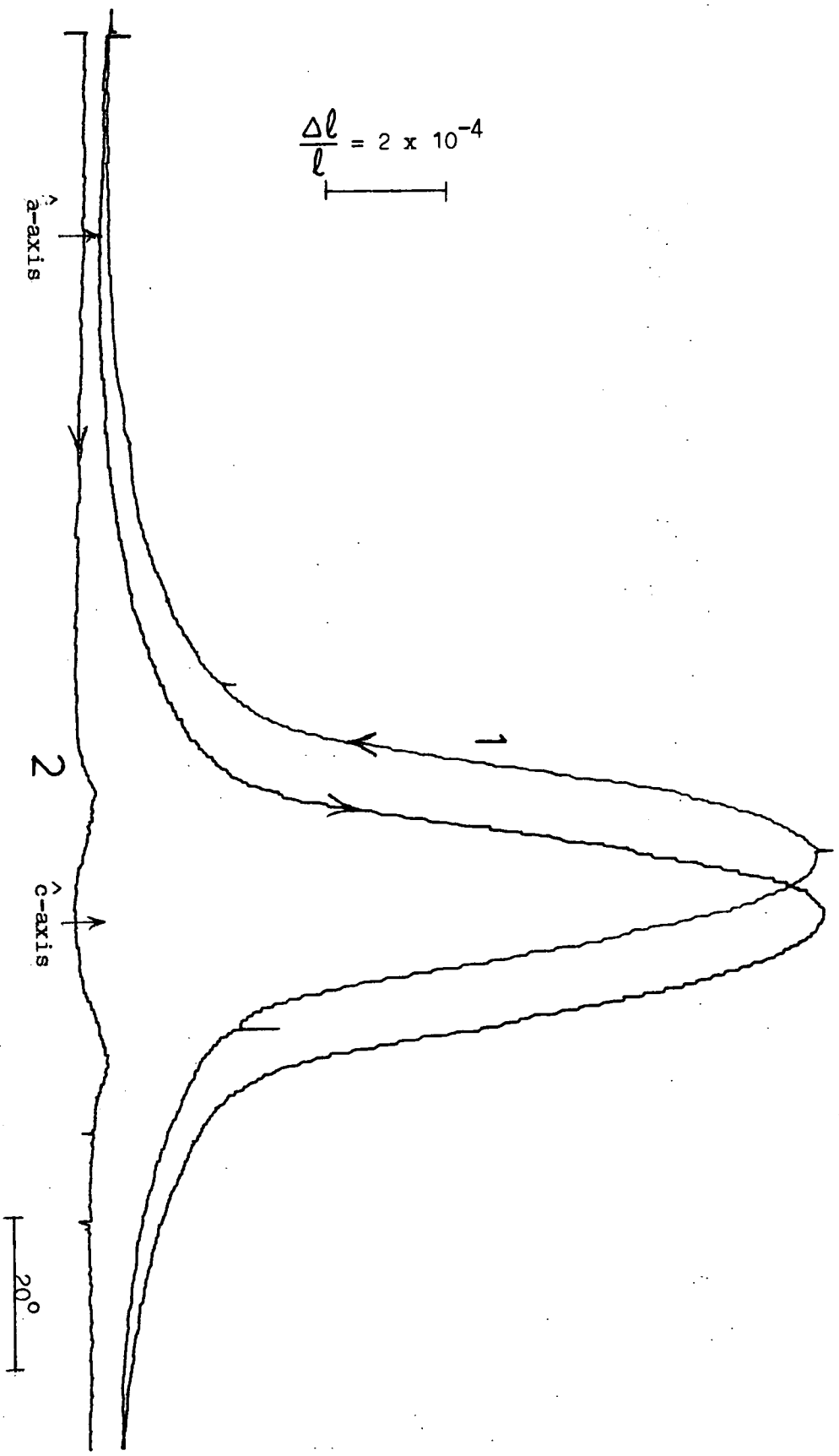

Fig. 8.7 Typical strain versus field angle curves for $Gd_{0.70}Tb_{0.30}$ at 4.2 K and in field of 1 Tesla; strains are along $\hat{a}$-axis (curve 1) and along $\hat{c}$-axis (curve 2).

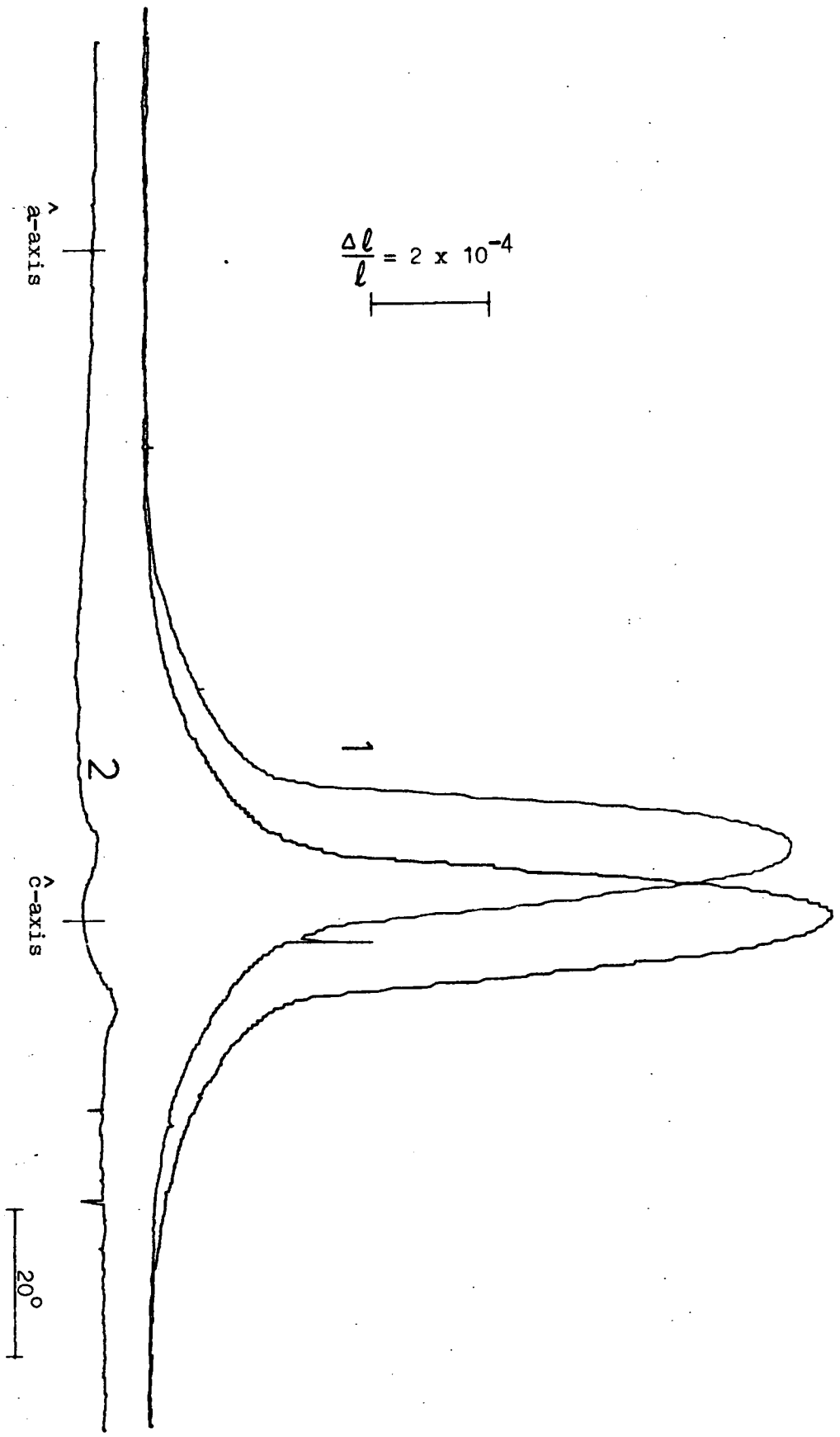

Fig. 8.8 Typical strain versus field angle curves for $Gd_{0.70}Tb_{0.30}$ at 4.2 K and in field of 2 Tesla; strains are along $\hat{a}$-axis (curve 1) and along $\hat{c}$-axis (curve 2).

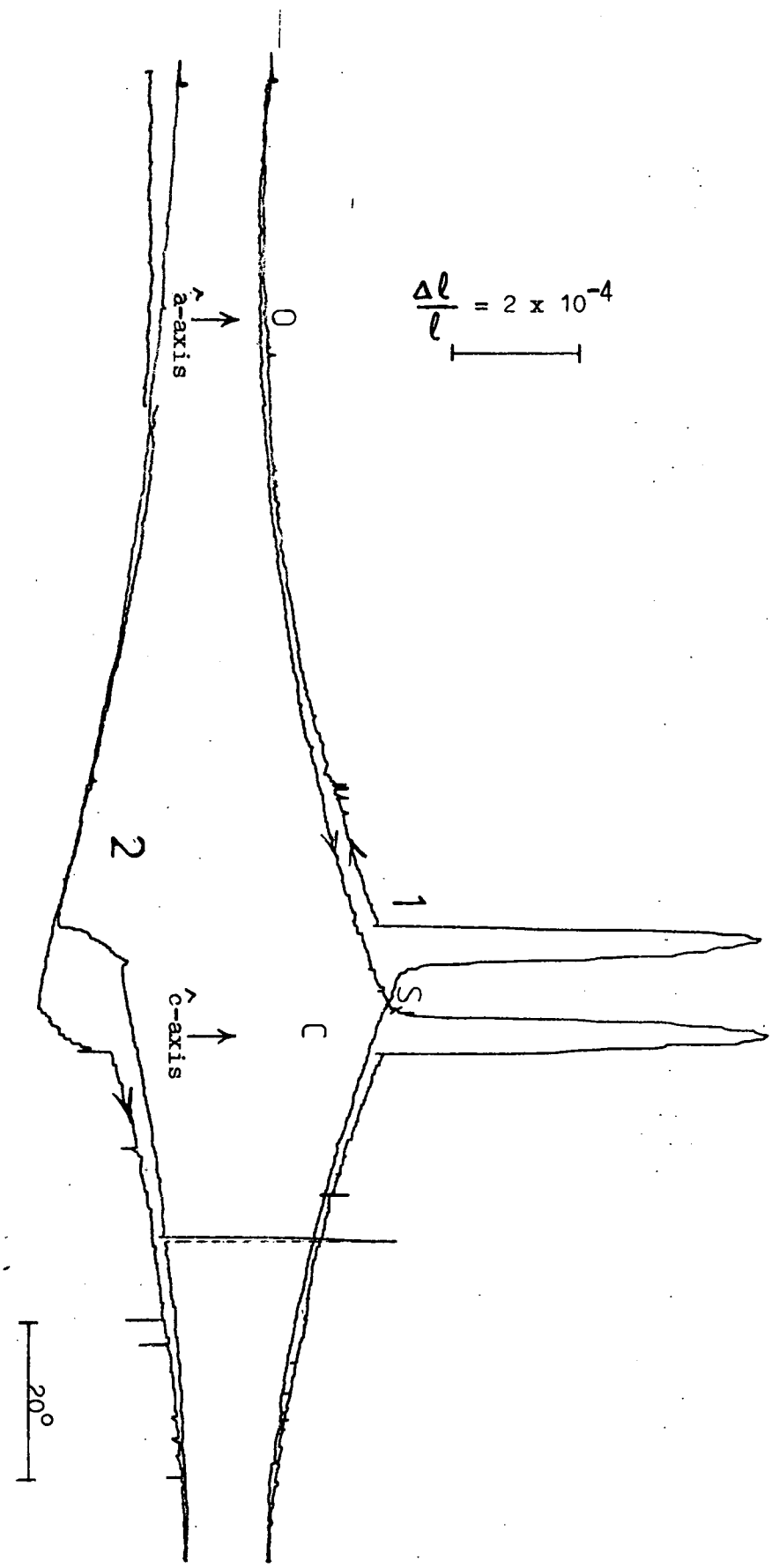

Fig. 8.9 Typical strain versus field angle curves for $Gd_{0.70}Tb_{0.30}$ at 140 K and in field of 8 Tesla; curves 1 and 2 represent strain along $\hat{a}$-axis and $\hat{c}$-axis respectively.

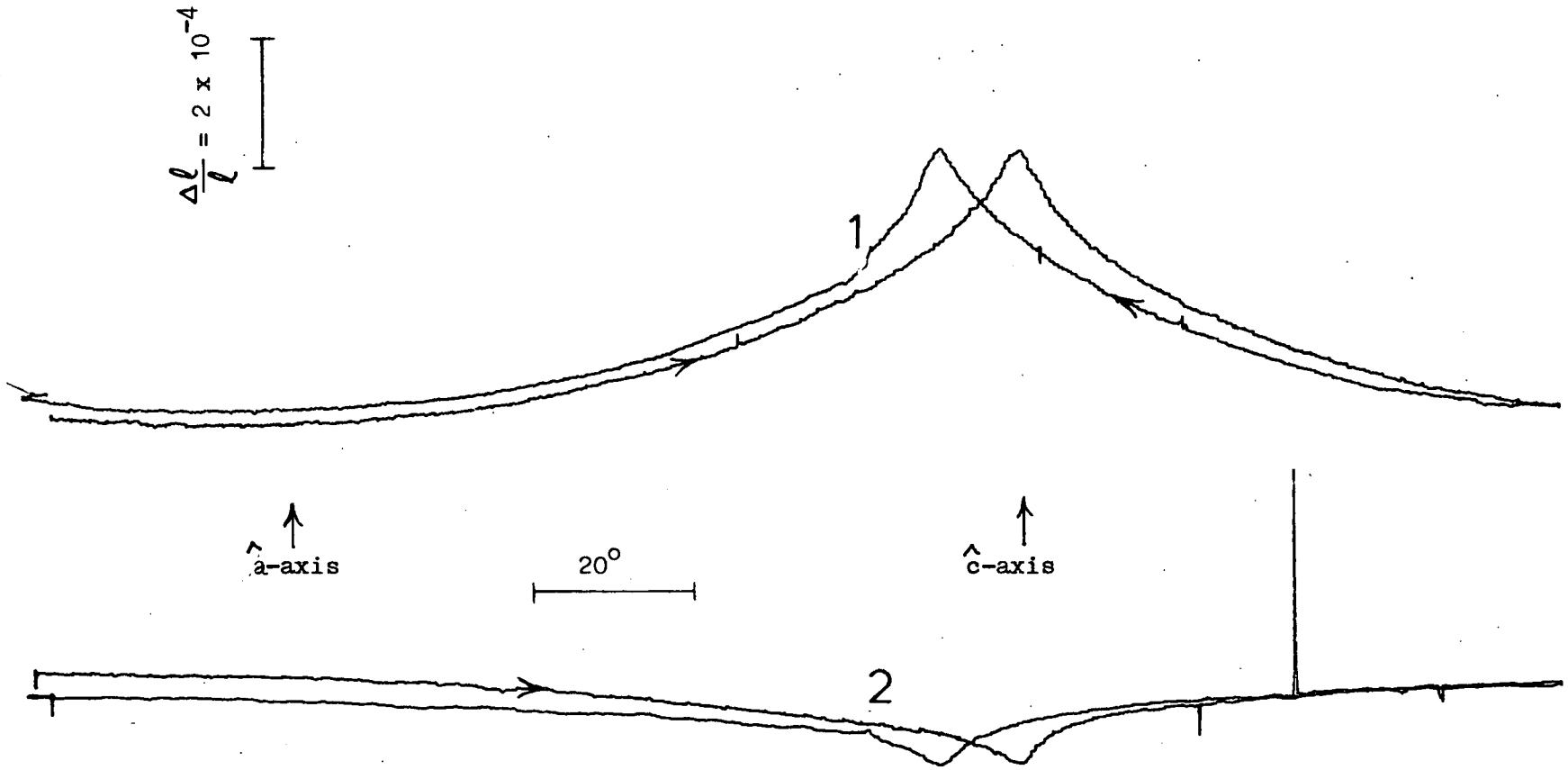

Fig. 8.10 Typical strain versus field angle curves for $Gd_{0.70}Tb_{0.30}$ at 220 K and in field of 8 Tesla; curves 1 and 2 represent strain along $\hat{a}$-axis and along $\hat{c}$-axis respectively.

of all the observed curves. The curves in general represent full rotation of magnetization towards the gadolinium rich end and at higher temperature in high fields. At low temperatures the curves represent limited rotation of magnetization and become very complicated towards the terbium rich end. The typical curve for Gd representing full rotation is given in Figure 8.11. In specimens containing $\hat{b}$ and $\hat{c}$ axes in the plane of the disc, the curves are similar to those described above. The explanation of the form of these curves must however, be slightly different. It is extremely difficult to hold the specimen so that the applied field rotates exactly in the disc plane. If, due to slight misalignment, a component of applied field normal to the disc arose during rotation this could cause the $\hat{b}$-axis directions lying at 60° to the disc plane to be energetically more favourable than those in the plane. This would lead to a strain in the basal plane $\hat{b}$-axis direction due to the rotation of the magnetization vector through 60°.

8.4 The Field Dependence of the Constants

In the majority of the curves recorded to measure the constants $\lambda_1^{\alpha,2}$ and $\lambda_2^{\alpha,2}$, the magnetization was only rotated to a limited angle as discussed in the previous section. The angle of magnetization was calculated from the anisotropy constant to determine the magnetostriction constants. The increase in the field strength mostly resulted in rotating the magnetization to the same angles for a smaller rotation of the applied field than in the

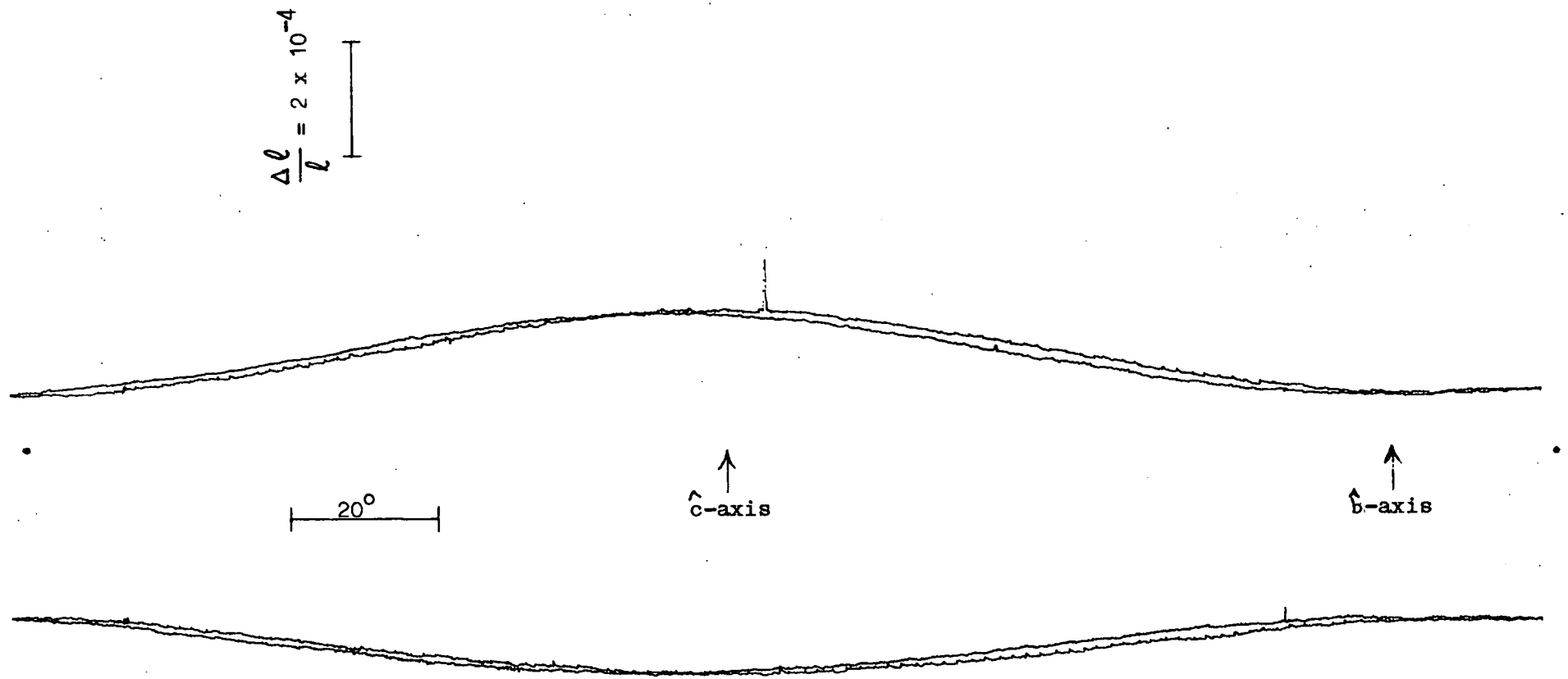

Fig. 8.11 Typical strain versus field angle curves for Gd at 140 K and in field of 4 Tesla; curves 1 and 2 represent strain along $\hat{c}$-axis and along $\hat{\ }$-axis respectively.

weak fields. The maximum variation of the strain of the curve was not changed appreciably except in very weak fields. In fact, the weak fields were insufficient to produce any measurable strain along the $\hat{c}$-axis, except for the pure gadolinium specimen. The high fields of up to 12 Tesla could produce reasonable curves only at higher temperatures for terbium concentration more than 10%. The constants $\lambda_1^{\alpha,2}$ and $\lambda_2^{\alpha,2}$ were determined using the actual angle of magnetization instead of the total variation of the strain for 90° rotation of the magnetization from $\hat{a}$ or $\hat{b}$ axis to the $\hat{c}$-axis. The constants thus obtained are believed to be the saturation magnetostriction constants for their respective temperatures.

At low temperatures for the terbium rich specimens, the magnetization lags more and more behind the applied field as terbium concentration increases because of the very high anisotropy of the terbium ions. In fact the available high fields cannot magnetize terbium rich specimens along the hard direction at low temperatures. The magnetization is rotated towards the $\hat{c}$-axis but stays behind even when the field is along the $\hat{c}$-axis. When the field rotates further and passes on the other side of the $\hat{c}$-axis, then at some stage it becomes energetically favourable for the magnetization vector to lie on the same side as the field. The magnetization vector then suddenly jumps from one side of the $\hat{c}$-axis to the other without actually passing through the $\hat{c}$-axis to occupy a lower energy position, further away from the $\hat{c}$-axis than its previous position. This sudden jumping of the magnetization across

the $\hat{c}$-axis is referred to as a flick. During a flick the information was lost and the strain variations could not be usefully utilized. Attempts were made to rotate the specimen very slowly, 4' per step in the region where a flick occurred, but even that did not improve the situation. At low temperatures, the strain gauges frequently suffered damage due to enormous torque and magnetostrictive strains. The high fields could only be usefully applied at higher temperatures to get maximum information. Most of the data is collected in fields of 12 Tesla.

8.5 Determination of the Constants from Data Records

The angle of magnetization θ was calculated for every ten degree intervals of the applied field angle and corresponding strain variations were measured directly from the curves.

The strain variation changes its sign when the applied field crosses the principal axes. The strain versus the applied field angle curves show sharper turns around the $\hat{c}$-axis than around $\hat{a}$- or $\hat{b}$-axis. Referring to Figure 8.9 the middle point C of the sharp turn was taken as the orientation at which the $\hat{c}$-axis was parallel to the field and from there the position O of the direction of the $\hat{a}$- or $\hat{b}$-axis was fixed 90° back from the potentiometer voltage to the field angle ratio. The position O served as the origin for the measurements and its strain as the reference strain. The strain changes were measured at 10° intervals from the origin O towards the $\hat{c}$-axis

until S where splitting of the magnetization in the basal plane took place. The strain measurements were made only on the forward trace of the curve, taken while the specimen was rotated slowly and the push rod was in tension, with the help of a graticule on a transparent sheet. The merits of taking measurement on forward trace only are given in the description of the acquisition of data in Chapter 6. Knowing the angle Θ of the magnetization and the corresponding strain variation, the constants $\lambda_1^{\alpha,2}$ and $\lambda_2^{\alpha,2}$ are calculated using equation 6.9 and 6.13 respectively.

Two approximations are employed for two extreme cases. Initially the magnetization is assumed to lie along the $\hat{a}$- or $\hat{b}$- axis. The angle ϕ in the basal plane of the magnetization with this axis is thus zero and there is no splitting of the specimen into multidomains. When splitting takes place, the strain variations along $\hat{a}$- or $\hat{b}$-axis are much more rapid than along the $\hat{c}$-axis. The maximum deviation ϕ of the magnetization from the $\hat{a}$-axis for the ac plane specimens in 30 degrees towards the next immediate $\hat{b}$-axes on both sides of the $\hat{a}$-axis. In the case of bc plane specimen, it is 60 degrees towards the other two $\hat{b}$-axes on either side. The magnetization has to cross the intermediate $\hat{a}$-axes to be in the lower energy state along the other $\hat{b}$-axes. This intermediate energy barrier makes the situation further complicated for the bc plane specimens. The variation of the angle ϕ is then non-linear and so is the $\lambda^{\gamma,2}$ contribution towards

the constant $\lambda_1^{\alpha,2}$. The other extreme case is when the field is along the $\hat{c}$-axis i.e. $\psi = 0$. Then ϕ has the maximum value, 30 degrees for the ac plane specimen and may be 60 degrees for the bc plane specimens. In the case of full rotation of magnetization, $\theta = 0$ and the contant $\lambda_1^{\alpha,2}$ and $\lambda_2^{\alpha,2}$ can be calculated from the measurements of the peak heights. For the limited rotation of magnetization the exact strain variation for $\psi = 0$ is not known from the curves and so the constants cannot be derived. However, the situation is simple before the splitting of the magnetization. The constants $\lambda_1^{\alpha,2}$ and $\lambda_2^{\alpha,2}$ were calculated for each angle of magnetization for every 10 degree rotation of the external field from $\theta = 90°$ to the angle where specimen splits into domains using the equations 6.9 and 6.13 respectively. The values of the constant in the set thus obtained were reasonably consistent within 2% for the curves in which some rotation of the magnetization towards the $\hat{c}$-axis took place. Derivation of the constants was restricted mainly to this region in the case of limited rotation. The constants were also determined using the peak height for the full rotation conditions. The $\lambda_2^{\alpha,2}$ values were consistent with the values calculated from the early part of the curve. Further use of the peak height in the case of $\lambda_1^{\alpha,2}$ will be discussed in detail in section 8.7.

8.6 The Constant $\lambda_2^{\alpha,2}$

The measurements of $\lambda_2^{\alpha,2}$ are simpler than those of $\lambda_1^{\alpha,2}$ for the reason that $\lambda^{\gamma,2}$ contribution of the rotation of the magnetization in the basal plane does not affect the constant. The exact rotation in the basal plane is very difficult to find for all the points on the strain versus field angle curve. The uncertain $\lambda^{\gamma,2}$ part in the $\lambda_1^{\alpha,2}$ expression results in a higher error in the $\lambda_1^{\alpha,2}$ values. To determine the constant $\lambda_2^{\alpha,2}$ the strain was measured along the $\hat{c}$-axis and equation 6.13 was used. The sign of the constant $\lambda_2^{\alpha,2}$ for pure gadolinium is negative while for all the alloy specimens it is positive.

8.6.1 The Temperature Dependence of $\lambda_2^{\alpha,2}$

The temperature variation of $\lambda_2^{\alpha,2}$ was studied for Gd, 90%Gd-10%Tb, 70%Gd-30%Tb, 50%Gd-50%Tb and 10%Gd-90%Tb specimens. The curves obtained for the pure gadolinium are simple, smooth and symmetrical. They represent the full rotation of the magnetization and show almost no hysteresis as shown in Figure 8.11. A field of 1 Tesla was enough to produce saturation in strain variation. The temperature was varied at 4 Tesla which was much higher than the field producing saturation values. The observed temperature variation is given in Table 8.1 along with the values of the square of the reduced magnetization and the $\hat{I}_{5/2}$ reduced hyperbolic Bessel functions. The observed temperature variation of the constant was tested with the two theoretical temperature variations arising

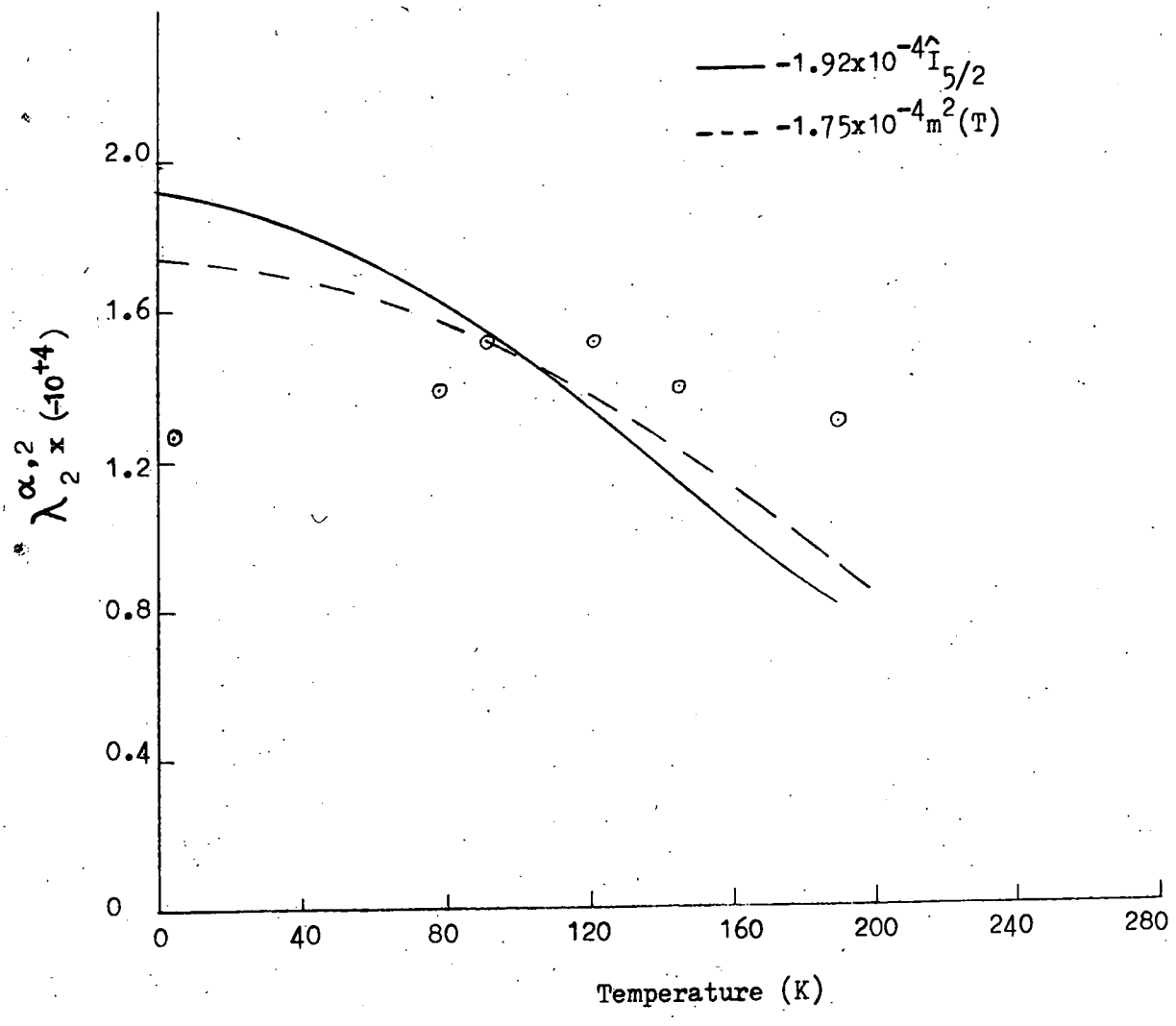

Fig. 8.12 The temperature dependence of $\lambda_2^{\alpha,2}$ for gadolinium at 4 Tesla.

The following paragraph is from page 123, before the description of the 50%Gd-50%Tb specimen.

Temperature variations for 70%Gd-30%Tb were observed in fields of 4 Tesla and 12 Tesla. The values of the constants below liquid nitrogen temperature are the same for both fields but above 120K, 12 Tesla produced higher values. The observed values of the constant are provided in Table 8.3. The agreement with the single-ion model dependence is good above liquid nitrogen temperature but below 80K the experimental points are considerably higher than the theoretical ones. The temperature dependence of the constant for 70%Gd-30%Tb is shown in Figure 8.14.

from the single-ion and the two-ion models. The detailed discussion of these models is provided in section 4 of Chapter 4. The theoretical temperature variation $\hat{I}_{5/2}$ from the single-ion model (equation 4.59) does not fit at all but the two-ion temperature variation $(m(T))^2$ as discussed in equation 4.56 is a little better. The observed data and the theoretical temperature dependences are shown in Figure 8.12.

In the case of 90%Gd-10%Tb, temperature was varied at 4 Tesla and at 12 Tesla. the values of the constant increased with field. With just 10% concentration of terbium, it was very difficult to collect precise information of the constant below liquid nitrogen temperature. The observed temperature variation along with the values of anisotropy constant K_2^o and the other related parameters is given in Table 8.2. The single-ion model temperature variation $\hat{I}_{5/2}$ fits very well with the average of the observed data over the entire range of temperature. The $(m(T))^2$ variation does not fit at all with the experimental results. The temperature dependence, both experimental and theoretical, for 90%Gd-10%Tb is shown in Figure 8.13.

The 50%Gd-50%Tb specimen contained $\hat{b}$ and $\hat{c}$ axes in the disc plane while all other alloy specimens were ac plane discs. Temperature dependence of the constant for this alloy was observed in fields of 8 Tesla and 12 Tesla. The experimental values of the constant produced by 12 Tesla field are about 8% higher than those by the 8 Tesla over the whole range. No value of the constant

* See oposite page

from the single-ion and the two-ion models. The detailed discussion of these models is provided in section 4 of Chapter 4. The theoretical temperature variation $\hat{I}_{5/2}$ from the single-ion model (equation 4.59) does not fit at all but the two-ion temperature variation $(m(T))^2$ as discussed in equation 4.56 is a little better. The observed data and the theoretical temperature dependences are shown in Figure 8.12.

In the case of 90%Gd-10%Tb, temperature was varied at 4 Tesla and at 12 Tesla. the values of the constant increased with field. With just 10% concentration of terbium, it was very difficult to collect precise information of the constant below liquid nitrogen temperature. The observed temperature variation along with the values of anisotropy constant K_2^o and the other related parameters is given in Table 8.2. The single-ion model temperature variation $\hat{I}_{5/2}$ fits very well with the average of the observed data over the entire range of temperature. The $(m(T))^2$ variation does not fit at all with the experimental results. The temperature dependence, both experimental and theoretical, for 90%Gd-10%Tb is shown in Figure 8.13.

The 50%Gd-50%Tb specimen contained $\hat{b}$ and $\hat{c}$ axes in the disc plane while all other alloy specimens were ac plane discs. Temperature dependence of the constant for this alloy was observed in fields of 8 Tesla and 12 Tesla. The experimental values of the constant produced by 12 Tesla field are about 8% higher than those by the 8 Tesla over the whole range. No value of the constant

* See oposite page

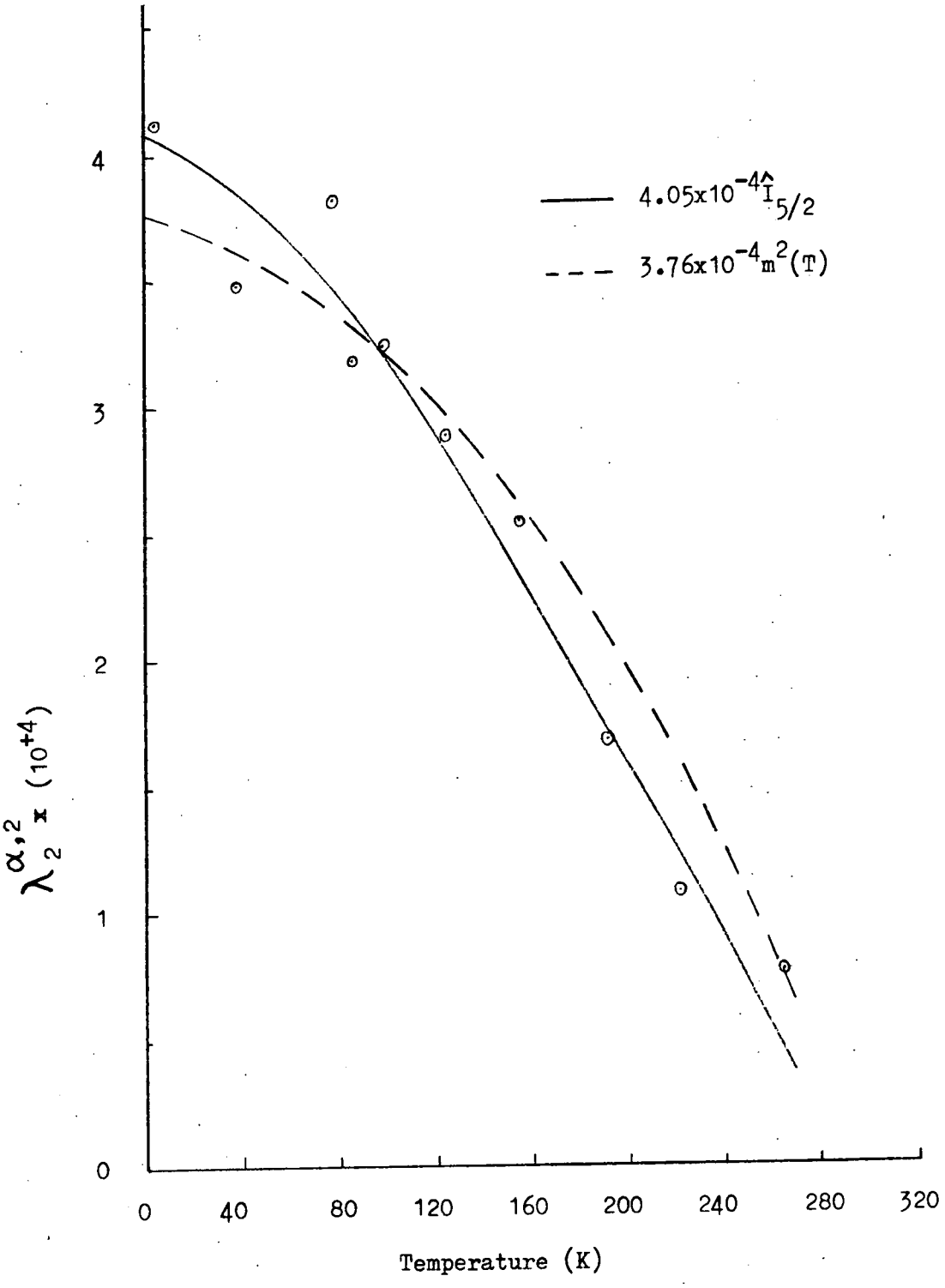

Fig. 8.13 The temperature dependence of $\lambda_2^{\alpha,2}$ for $Gd_{0.90}Tb_{.10}$ at 12 Tesla.

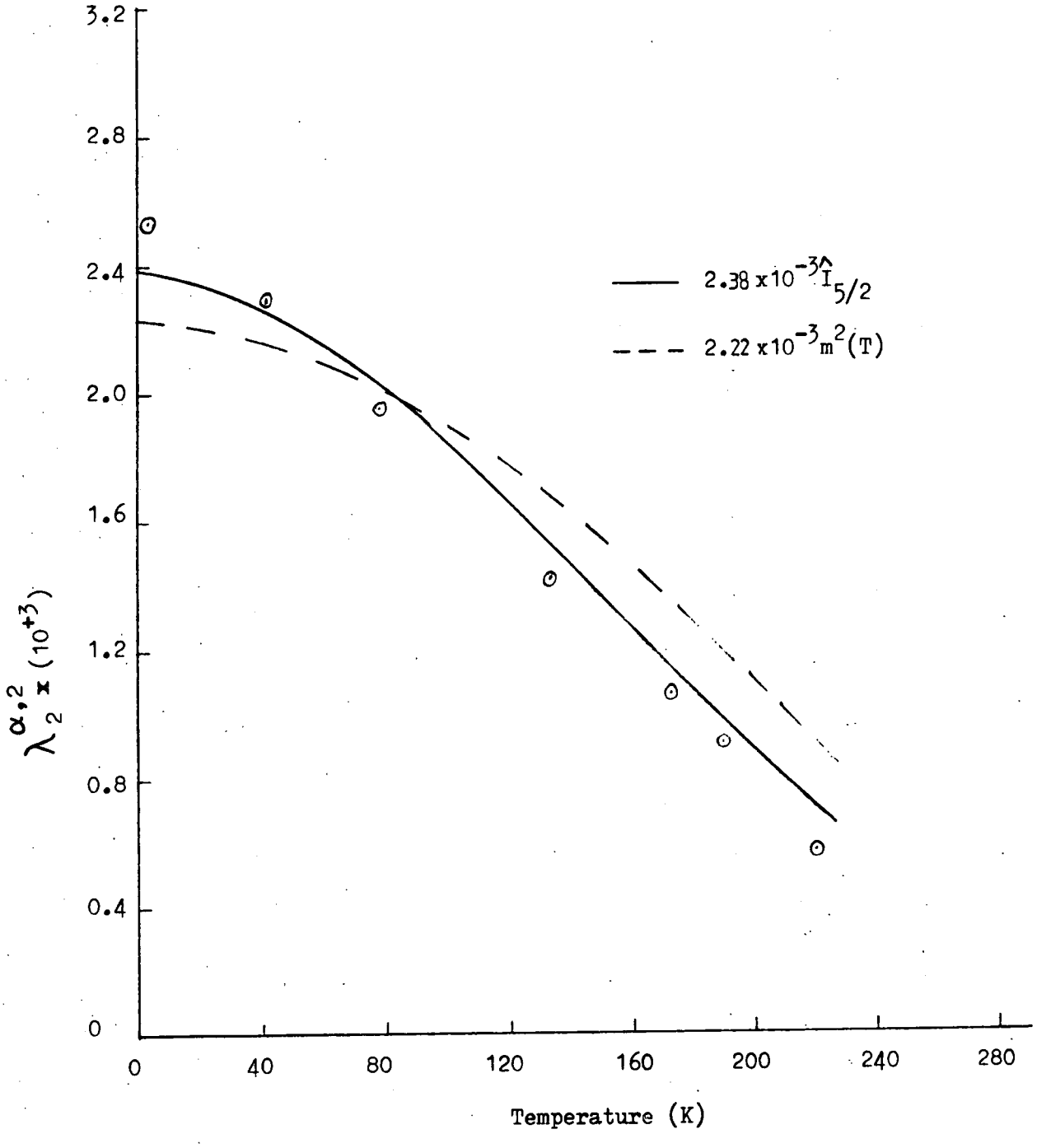

Fig. 8.14 The temperature dependence of $\lambda_2^{\alpha,2}$ for $Gd_{0.70}Tb_{0.30}$ at 12 Tesla.

could be observed below 130 K in the field of 12 Tesla. The strain gauges in this region either damaged or just came off the specimen. The experimental results are given in Table 8.4 while the temperature dependence comparison with theoretical is shown in Figure 8.15. The single-ion model dependence does not fit very well but is better than the two-ion one. The experimental values fall more rapidly with increase in temperature than the theoretical variation. The combination of the contributions from both models does not improve the situation.

The 10%Gd-90%Tb specimen was most tedious to handle and only a few points could be observed in a series of attempts. Due to the limited data available, it was not justifiable to test the adequacy of the temperature dependence predicted by the theoretical models with this specimen. The temperature dependence of the constant $\lambda_2^{\alpha,2}$ observed by Joraide (1980) does not agree well with the single-ion model dependence for three compositions but is good for 25%Gd-75%Tb alloy whose measurements were made in a 13 Tesla field. His other measurements were in much lower fields only up to 3 Tesla which were not strong enough to rotate the magnetization appreciably towards the $\hat{c}$-axis. The strain variations were mainly occurring in the flick region. The measurements made on one alloy 50%Gd-50%Tb by Nikitin (1981) follow the temperature dependence resulting from the single-ion magnetocrystalline interaction.

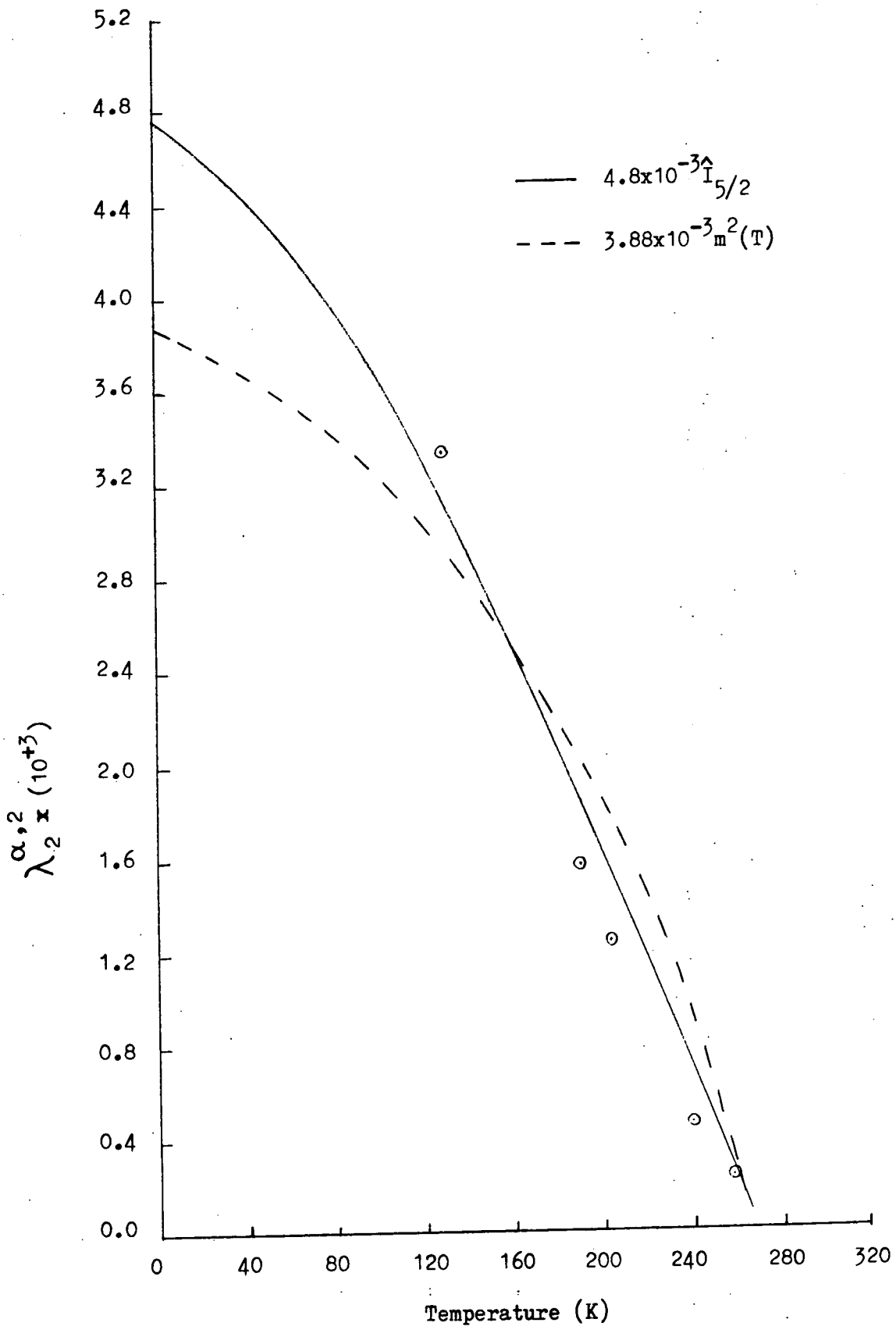

Fig. 8.15 The temperature dependence of $\lambda_2^{\alpha,2}$ for $Gd_{0.50}Tb_{0.50}$ at 12 Tesla.

8.6.2 Composition Dependence of $\lambda_2^{\alpha,2}$

The values of the constant were extrapolated to 0 K. by the least squares method using the single-ion model. The constant $\lambda_{2(o)}^{\alpha,2}$ versus terbium concentration of the alloy is plotted in Figure 8.16. The constant increases with the terbium concentration. The experimental composition dependence of $\lambda_{2(o)}^{\alpha,2}$ has a very nearly linear variation with terbium concentration. The $\lambda_{2(o)}^{\alpha,2}$ value of 50%Gd-50%Tb reported by Nikitin (1981) is much higher than the one obtained in the present study. Direct comparision to find the discrepancy is difficult because of the different techniques of measurements. The values obtained by Joraide (1980) are much lower than the present ones. The fields he applied are believed not strong enough to produce full rotation of the magnetization at low temperatures and so the amplitude of the strain variation was resulting in the lower values of the constant. The composition dependence from his results seems to have an exponential form which is due to the rather lower values of the constant except for 25%Gd-75%Tb. The experimental value of the constant at OK for pure Gd is in agreement with Nikitin (1981) and Joraide (1980). For the rest of the alloy series, the experimental values are significantly higher than Joraide's but lower than those of Nikitin.

8.7 The Constant $\lambda_1^{\alpha,2}$

The constant was measured for Gd and Gd/Tb alloys of composition 90%Gd-10% Tb, 70%Gd-30%Tb, 50%Gd-50%Tb, and 10%Gd-90%Tb in the temperature range from liquid helium

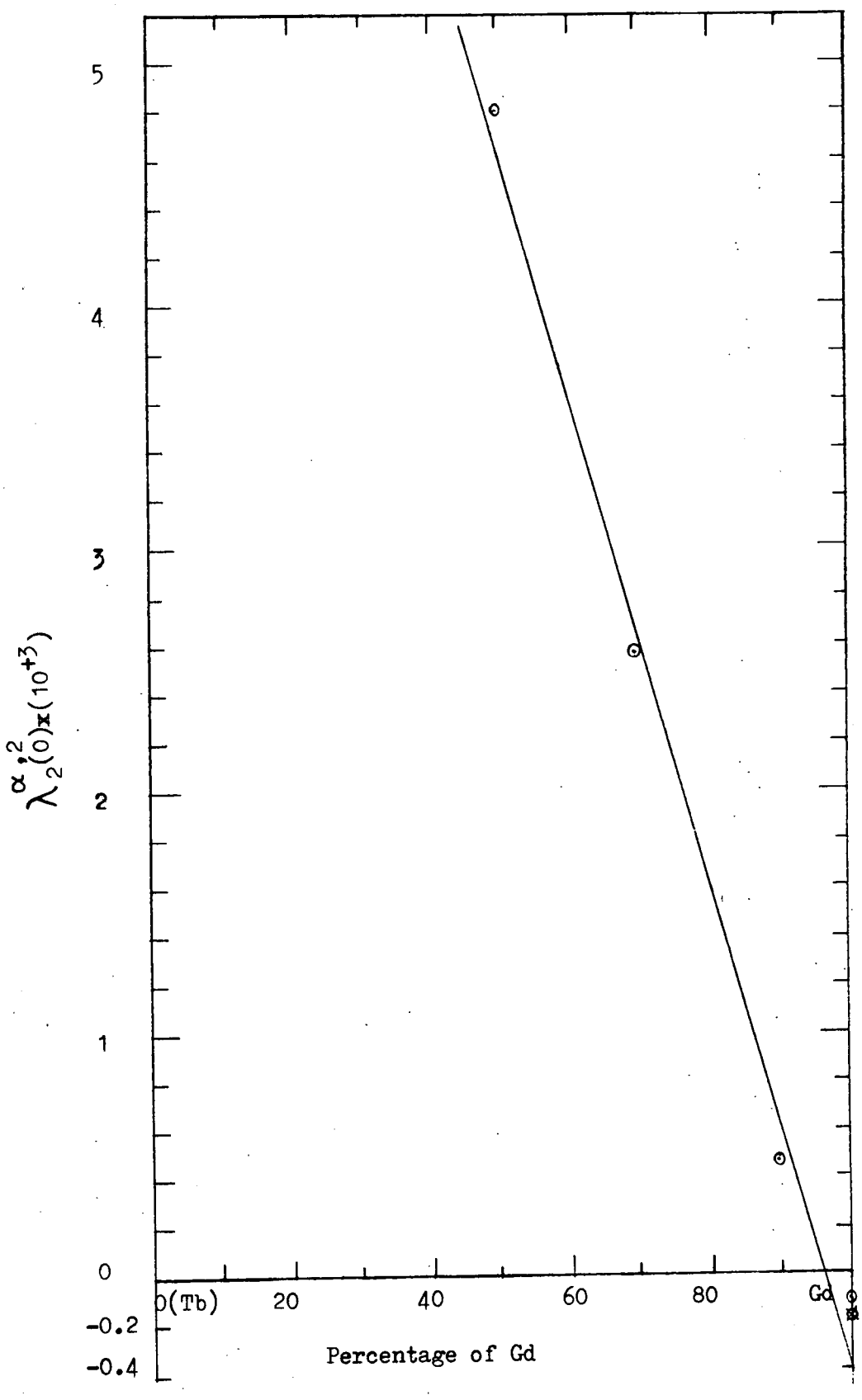

Fig. 8.16 Composition dependence of $\lambda_2^{\alpha,2}(0)$ for Gd/Tb alloys.
⊗ Experimental

to about their Curie temperatures and in magnetic fields of up to 12 Tesla. As discussed earlier in Sections 8.5 and 8.6, the derivation of the constant $\lambda_1^{\alpha,2}$ is very difficult due to the complicated rotation of the magnetization in the basal plane. To determine the constant strain was measured along the $\hat{a}$-axis for the ac plane specimens and along the $\hat{b}$-axis for the bc plane specimens. The Clark and Callen expression for magnetostriction given in Equation 4.45 was further simplified in Chapter 6 to Equation 6.9 for the ac plane specimens. For bc plane specimens the angle ϕ of the magnetization in the basal plane is with respect to the $\hat{b}$-axis. The direction cosines of magnetization and strain are

$$\begin{aligned} \alpha_x &= \sin\theta \sin\phi & \qquad \beta_x &= 0 \\ \alpha_y &= \sin\theta \cos\phi \quad \text{and} & \beta_y &= 1 \\ \alpha_z &= \cos\theta & \beta_z &= 0 \end{aligned} \qquad 8.8$$

instead of those given in equations 6.7 and 6.5 respectively. The equation 6.9 is a special case for $\phi = 30°$. The general solution which is the same for both types of the specimens, is

$$\lambda_1^{\alpha,2} = -\sec^2\theta(\tfrac{1}{2}\lambda^{\gamma,2}(\sin^2\theta \cos 2\phi - 1) + \Delta\lambda_{a \text{ or } b}^{90\rightarrow\theta} \qquad 8.9$$

where $\Delta\lambda_{a \text{ or } b}^{90\rightarrow\theta}$ is the total variation in the strain measured along a or b axis when the magnetization rotates from angle 90° to an angle θ with the $\hat{c}$-axis.

The equation 8.9 shows that the total strain variation measured to determine $\lambda_1^{\alpha,2}$ contains a contribution from

$\lambda^{\gamma,2}$ due to the rotation ϕ of the magnetization in the basal plane. The values of the constant $\lambda^{\gamma,2}$ for the specimens have been obtained and are given in Chapter 7. The expression 6.13 for $\lambda_2^{\alpha,2}$ is independent of ϕ and so of $\lambda^{\gamma,2}$. The values of the constant $\lambda_2^{\alpha,2}$ calculated at various intervals were consistent. This is not true in general for the determination of the constant $\lambda_1^{\alpha,2}$ because the actual value of ϕ is difficult to find. The angle ϕ can be calculated from the basal plane anisotropy constant but the possible existence of an unknown perpendicular component of the applied field makes the calculated values doubtful. The possible ϕ variation and its corresponding effect on the constant $\lambda_1^{\alpha,2}$ is discussed here briefly. The angle ϕ varies fairly uniformly from zero to maximum 30° in the ac plane specimens but in an uncertain way which may lead to a maximum value of 60° in the bc plane specimens. The spread in the values of the fraction of $\lambda^{\gamma,2}$ for the simple case of ac plane specimens is shown in Figure 8.5. In the beginning part of the strain versus temperature curve ϕ is zero which eventually becomes 30° at some stage during the rotation of magnetization from 90° to 0°. The curve (1) represents the fraction of $\lambda^{\gamma,2}$ to be included in the derivation of the constant $\lambda_1^{\alpha,2}$ for one extreme case in which ϕ remains zero while (2) applies to a situation near the other extreme when ϕ becomes 30° after the magnetization has rotated only 2°. In practice the value of the fraction of the $\lambda^{\gamma,2}$ contribution may have some value between those indicated by

the two curves. Thus the values of the constant calculated at regular intervals of θ might show a drift for any fixed value of ϕ unless the calculations were in the region where ϕ had achieved its maximum value or it remained zero when the $\lambda^{\gamma,2}$ contribution followed the curve (2) or (1) respectively. In situations where consistency was not achieved, the derivation of the constant $\lambda_1^{\alpha,2}$ was restricted to the early or the end part of the curve for the limited or full rotation of magnetization case respectively. The values of the constant derived in the later case are more reliable and these were possible only at higher temperatures except for the case of pure gadoliniumm.

8.7.1 The Temperature Dependence of $\lambda_1^{\alpha,2}$

The strain variation versus applied field angle curves for pure gadolinium are simple and represent full rotation of magnetization in the plane containing the $\hat{c}$-axis. The field of 2 Tesla was producing saturation strains. The temperature dependence of the constant for Gd was studied in field of 4 Tesla. The experimental points along with the theoretical variations based on the single-ion $\hat{I}_{5/2}$ and two-ion $m^2(T)$ are shown in Figure 8.17 The agreement of the experimental temperature dependence is not good with either of the models, but it is slightly better with the single-ion $\hat{I}_{5/2}$ variation. This behaviour of Gd is contradictory to that shown in the case of the other constant $\lambda_2^{\alpha,2}$. The sign of the constant is positive and is opposite to that of $\lambda_2^{\alpha,2}$. The constant $\lambda_1^{\alpha,2}$ has negative sign for all the Gd/Tb alloy specimens.

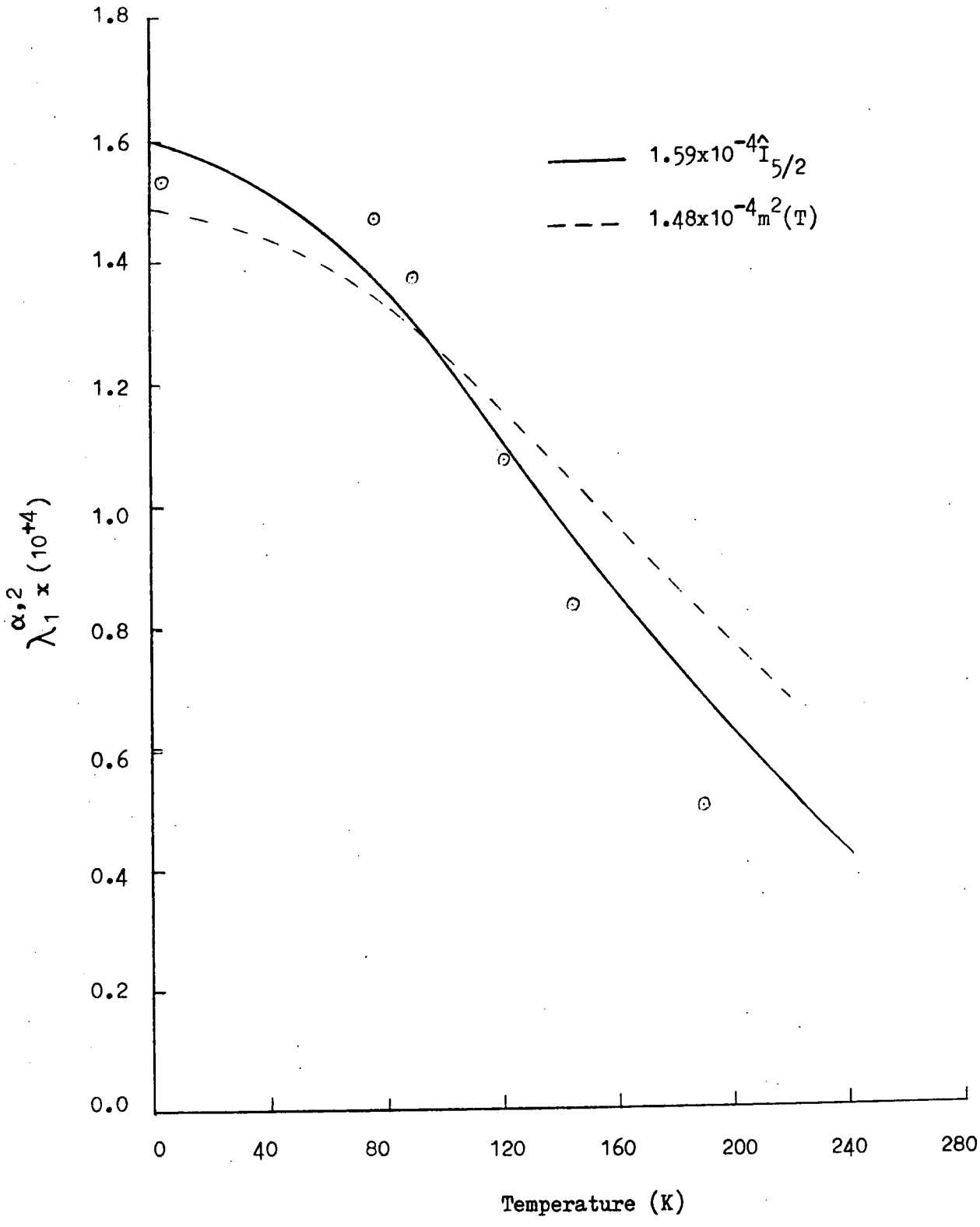

Fig.8.17 The temperature dependence of $\lambda_1^{\alpha,2}$ for Gd at 4 Tesla.

The temperature dependence for 90%Gd-10%Tb alloy was studied in a field of 4 Tesla. The observed temperature variation of the constant is shown in Figure 8.18. The constant does not seem to follow any theoretical temperature variation. The negative value of the constant at low temperatures decreases in magnitude, becomes positive at 95 K and negative again above 140 K. The negative contribution of the terbium ions towards the constant $\lambda_1^{\alpha,2}$ is just dominating the positive contribution of Gd ions at low temperatures. The temperature dependences of individual ions seem to follow different variations; Gd the two-ion $m^2(T)$ variation while Tb the one-ion $\hat{I}_{5/2}$, dropping relatively more quickly at low temperature than at high compared to that of $m^2(T)$.

The values of the constant for 70%Gd-30%Tb could not be experimentally observed below 110 K. The variation of $\lambda_1^{\alpha,2}$ with temperature for 70%Gd-30%Tb along with the theoretical variation is shown in Figure 8.19. The experimental values do not follow very closely any of the two common temperature dependences, but the agreement is better with $\hat{I}_{5/2}$ variation than that of $m^2(T)$. The constant has negative sign over the whole range of temperature variation.

The measurements of the constant become more difficult for the 50%Td-50%Tb specimen. It was not possible to measure the constant below 120 K with fields up to 8 Tesla. The data below this temperature was just possible in the field of 12 Tesla but the risk of damage to the strain

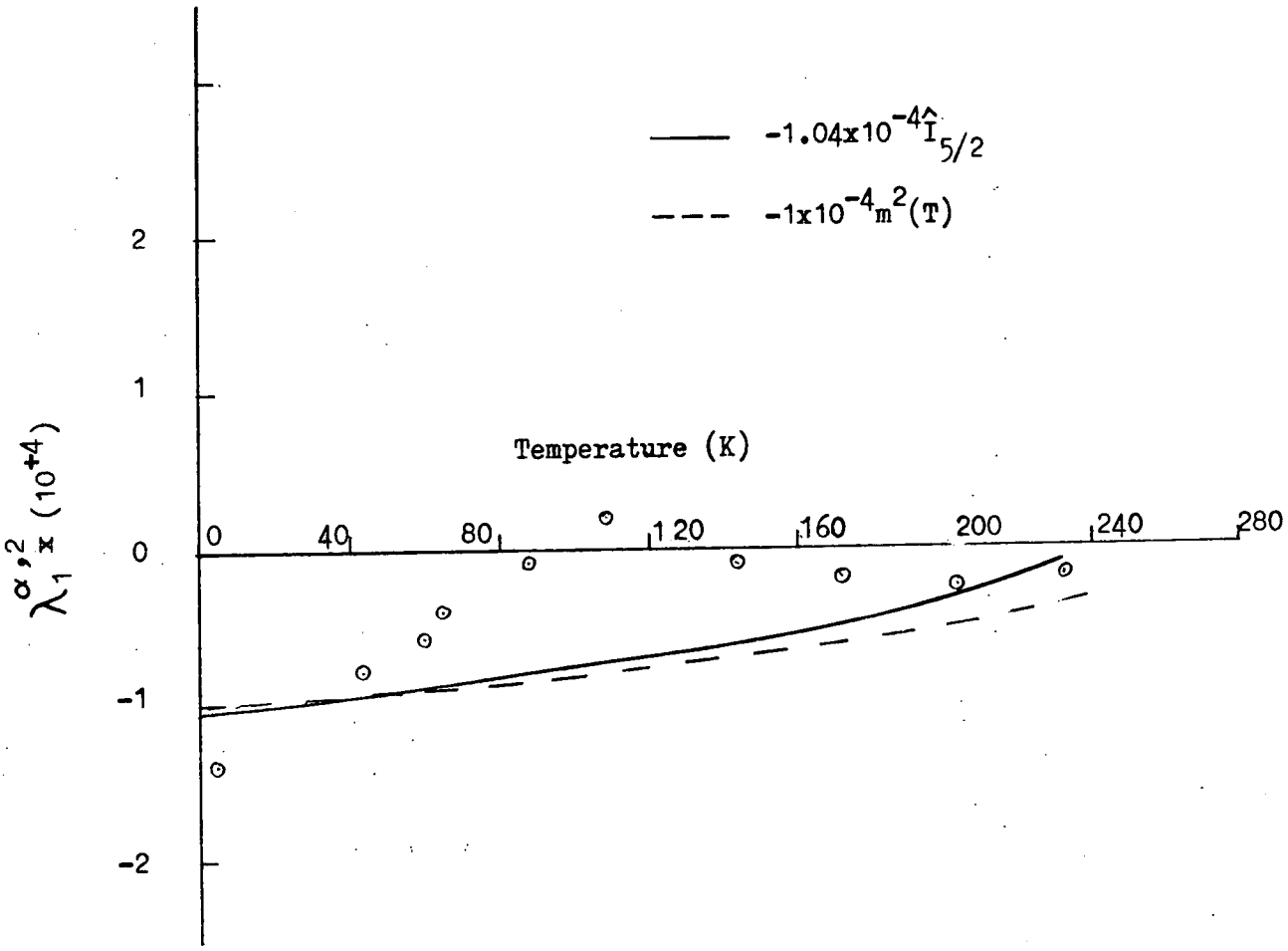

Fig. 8.18 The temperature dependence of $\lambda_1^{\alpha,2}$ for $Gd_{0.90}Tb_{0.10}$ at 4 Tesla.

——— $-8.9\times10^{-4}\hat{I}_{5/2}$

– – – $-7.5\times10^{-4}m^2(T)$

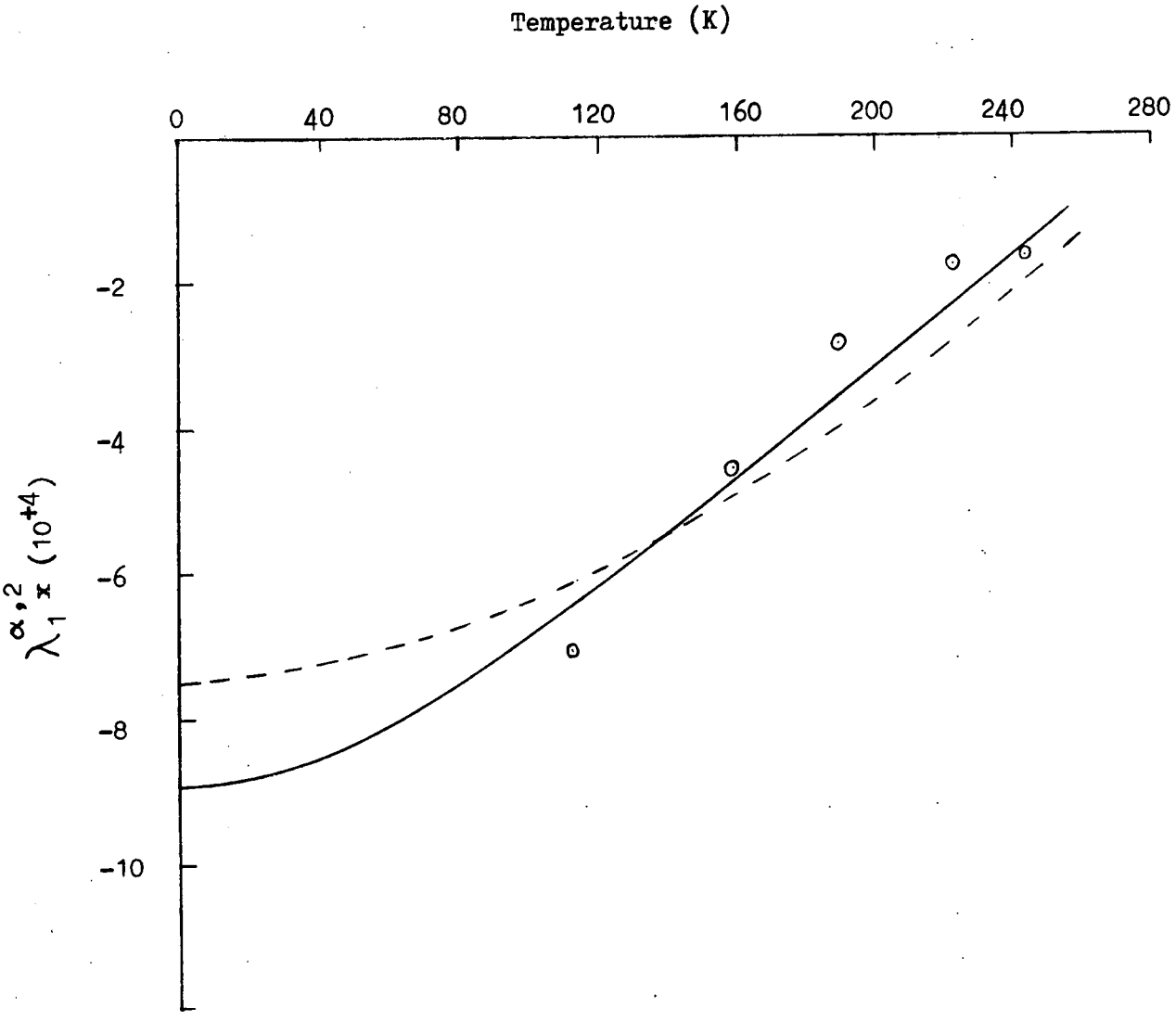

Fig. 8.19 The temperature dependence of $\lambda_1^{\alpha,2}$ for $Gd_{0.70}Tb_{0.30}$ at 8 Tesla.

gauges then becomes very high. Figure 8.20 shows the experimental temperature variation of the constant $\lambda_1^{\alpha,2}$ for 50%Gd-50%Tb specimen along with the temperature variations suggested by two theoretical models. The agreement of the temperature dependence with both models is of the same order. For $\lambda_1^{\alpha,2}(T)$ values see tables 8.1 to 8.4.

The problem of measuring the constant becomes worst for the 10%Gd-90%Tb specimen. The limited number of points available near the Curie temperature with a large spread in the values are really not enough to judge the adequacy of the temperature dependence of the constant with the theoretical one.

The temperature dependence of the constant $\lambda_1^{\alpha,2}$ observed by Joraide (1980) does not fit well with the $\hat{I}_{5/2}$ theoretical dependence resulting from the single-ion mechanism for any of the specimens. The 50%Gd-50%Tb only showed a better fit with the dependence stemming from the two-ion theory. Nikitin (1981) studied the constant only for 50%Gd-50%Tb in the alloy series. He claimed that the temperature dependence of the constant follows the dependence resulting from the single-ion interaction.

8.7.2 Composition Dependence of $\lambda_1^{\alpha,2}$

The extrapolated values of the constant $\lambda_1^{\alpha,2}(o)$ to 0 K. were obtained using $\hat{I}_{5/2}$ single-ion and $m^2(T)$ two-ion theoretical temperature variations by the least squares method for each composition of the alloy. The variation of $\lambda_1^{\alpha,2}(o)$ with the terbium concentration is shown in Figure 8.21. The values seem to lie along a straight

TABLE 8.1

The temperature variation of the constants $\lambda_2^{\alpha,2}$ and $\lambda_1^{\alpha,2}$ in units of 10^{-4} for pure Gd.

Field in Tesla	Temp. K	$\lambda_{2(T)}^{\alpha,2}$	$m^2(T)$	$\hat{I}_{5/2}$
4	4.2	-1.27	1	1
4	78	-1.38	.899	.849
4	91	-1.51	.862	.800
4	121	-1.50	.776	.685
4	145	-1.39	.700	.589
4	189	-1.29	.560	.433
0 K Least squares fit values			-1.75 $\pm$.2	-1.92 $\pm$ .3

Field in Tesla	Temp. K	$\lambda_{1(T)}^{\alpha,2}$	$m^2(T)$	$\hat{I}_{5/2}$
4	4.2	1.53	1	1
4	78	1.47	.90	.850
4	91	1.37	.86	.802
4	121	1.07	.78	.685
4	145	.83	.70	.589
4	190	.5	.55	.427
0 K Least squares fit values			1.48 $\pm$.09	1.59 $\pm$.06

TABLE 8.2

The temperature variation of the constants $\lambda_2^{\alpha,2}$ and $\lambda_1^{\alpha,2}$ in units of 10^{-4} for 90%Gd-10%Tb

Field in Tesla	Temp. K	$\lambda_2^{\alpha,2}(T)$	K_2^o $10^{+7}Jm^{-3}$	$m^2(T)$	$\hat{I}_{5/2}$
12	4.2	4.13	.258	1	1
12	39	3.49	.249	.964	.947
12	77	3.82	.218	.903	.856
12	86	3.18	.208	.882	.827
12	99	3.24	.197	.854	.790
12	124	2.88	.172	.776	.685
12	156	2.14	.140	.677	.565
12	191	1.58	.104	.554	.427
12	221	1.08	.073	.426	.309
12	265	.76	.033	.203	.013
0 K Least Squares fit values				3.76 $\pm$.74	4.06 $\pm$.13
		$\lambda_1^{\alpha,2}(T)$			
4	4.2	-1.4	.259	1	1
4	44	-0.8	.247	.964	.947
4	60	-0.6	.234	.936	.907
4	64	-0.4	.230	.929	.893
4	108	+0.2	.188	.828	.754
4	141	-0.1	.157	.726	.623
4	171	-0.2	.126	.619	.497
4	203	-0.3	.092	.506	.380
4	232	-0.2	.062	.377	.090
0 K Least Squares fit values				1×10^{-4} $\pm$ .3 "	-1.04×10^{-4} $\pm$ .3 "

TABLE 8.3

The temperature variation of the constants $\lambda_2^{\alpha,2}$ and $\lambda_1^{\alpha,2}$ in units of 10^{-3} for 70%Gd-10%Tb, (the values of K_2^o are the average of Corner (1983b) and Hawkins (1982)/ Paige (1983)).

Field in Tesla	Temp. K	$\lambda_2^{\alpha,2}(T)$	K_2^o $10^{-2}Jm^{-3}$	$m^2(T)$	$\hat{I}_{5/2}$
12	4.2	2.538	1.100	1	1
12	41	2.288	1.030	.964	.947
12	78	1.950	0.900	.897	.849
12	133	1.417	.625	.736	.634
12	172	1.060	.435	.601	.480
12	189	0.912	.360	.537	.412
12	220	0.570	.235	.405	.290
0 K Least squares fit values				2.22 ±.13	2.38 ±0.05
		$\lambda_1^{\alpha,2}(T)$			
8	112	-.71	.73	.81	.730
8	159	-.46	.50	.66	.537
8	190	-.29	.355	.53	.407
8	223	-.18	.22	.39	.273
8	245	-.17	.14	.27	.179
0 K Least squares fit values				-.75 ±.07	-.89 ±.05

TABLE 8.4

The temperature variation of the constants $\lambda_2^{\alpha,2}$ and $\lambda_1^{\alpha,2}$ in units of 10^{-3} for 50%Gd-50%Tb.

Field in Tesla	Temp. K	$\lambda_2^{\alpha,2}(T)$	K_2^o $10^7 Jm^{-3}$	$m^2(T)$	$\hat{I}_{5/2}$
12	131	3.344	1.20	.735	.632
12	190	1.574	.62	.506	.376
12	203	1.260	.50	.452	.329
12	240	0.470	.16	.240	.158
12	242	0.383	.15	.224	.145
12	258	0.242	.04	.077	.05
0 K Least squares fit values				3.88 $\pm$.42	4.8 $\pm$.3
		$\lambda_1^{\alpha,2}(T)$			
12	130	-1.45	1.21	.74	.637
12	158	-1.36	.94	.64	.513
12	188	- .71	.64	.51	.385
12	229	- .50	.28	.31	.210
12	255	- .38	.07	.12	.073
0 K Least squares fit values				-1.936 $\pm$.14	-2.393 $\pm$.16

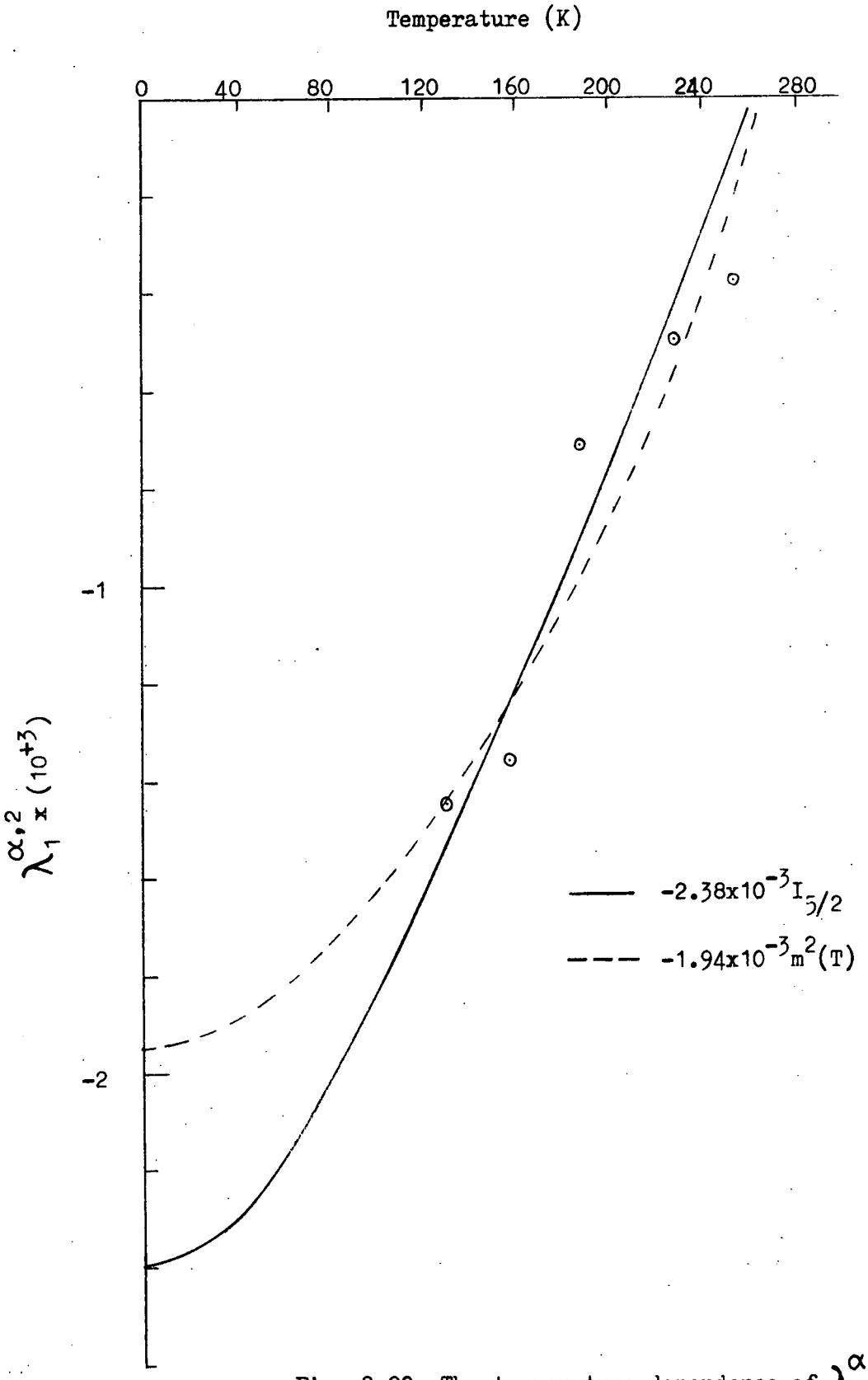

Fig. 8.20 The temperature dependence of $\lambda_1^{\alpha,2}$ for $Gd_{0.50}Tb_{0.50}$ at 12 Tesla.

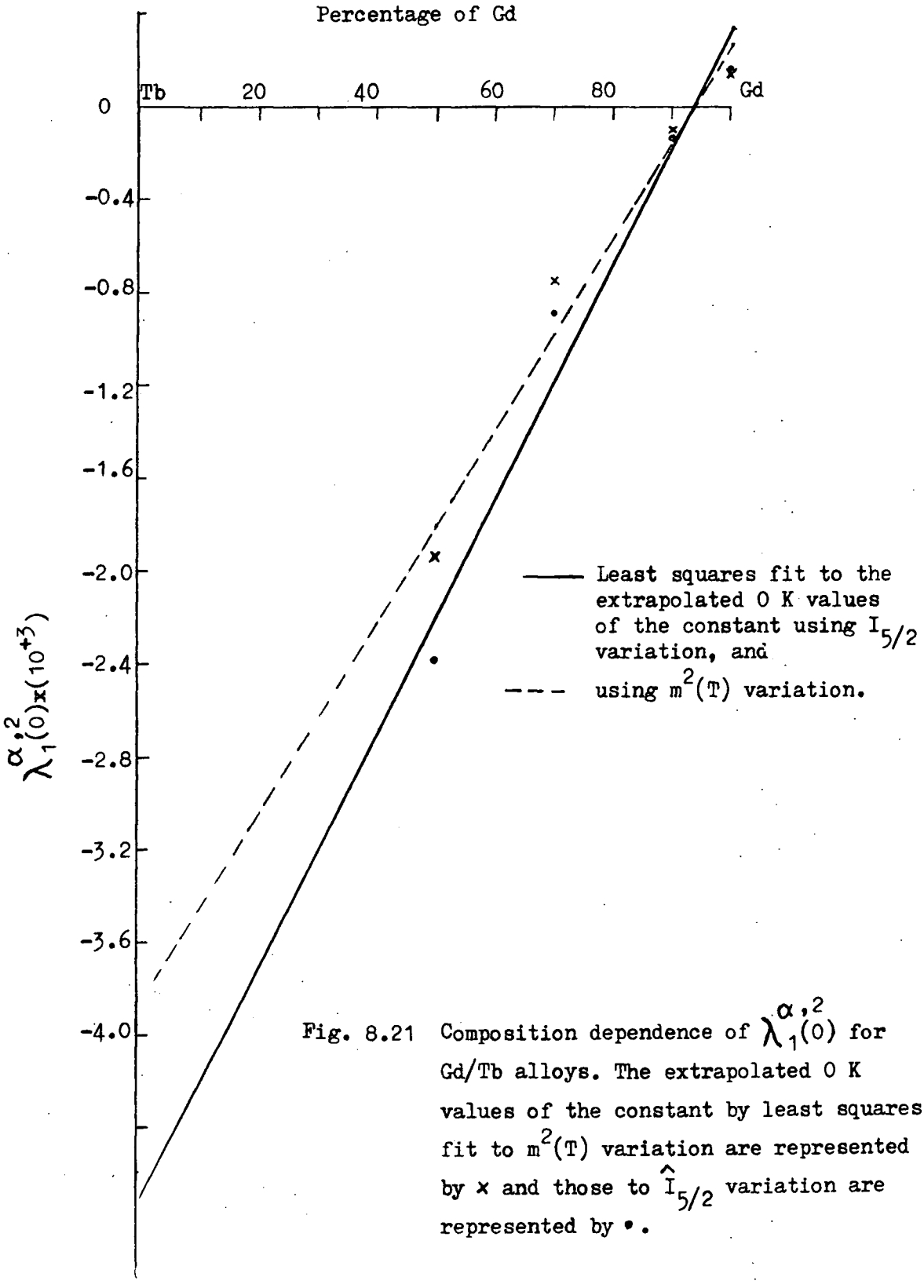

Fig. 8.21 Composition dependence of $\lambda_1^{\alpha,2}(0)$ for Gd/Tb alloys. The extrapolated 0 K values of the constant by least squares fit to $m^2(T)$ variation are represented by × and those to $\hat{I}_{5/2}$ variation are represented by •.

line. The linear behaviour of the constant with the alloy composition is not very good but is more conclusive than its temperature dependence. The experimental values of the constant at 0 K. fall in between those of Joraide (1980) and Nikitin (1981). In general the difference between the values decreases towards the gadolinium end of the series. The composition dependence observed by Joraide (1980) despite his unsatisfactory analysis of the strain curves for this constant, has an excellent linear variation.

CHAPTER 9

DISCUSSION, CONCLUSIONS AND SUGGESTIONS

9.1 Introduction

The results of the measurements of the magnetostriction constants $\lambda^{\gamma,2}$, $\lambda_1^{\alpha,2}$ and $\lambda_2^{\alpha,2}$ of order $\ell = 2$ of single crystals of Gd, Tb and their alloys have been presented in Chapters 7 and 8. The study of the temperature dependence and composition dependence of these constants provide a powerful tool to understand qualitatively the nature of the giant magnetostriction exhibited by terbium metal. The temperature dependence of the magnetostriction constants was compared with those predicted by the theories based on two-ion interactions and single-ion magnetocrystalline interactions.

9.2 Results and Discussion

The value of the constant $\lambda^{\gamma,2}(o)$ of Gd at zero temperature is in agreement with that of Mishima (1976). The constant $\lambda^{\gamma,2}$ drops very sharply with increase in temperature. It has positive sign in the observed temperature range from 4.2K to 170K. The temperature dependence of $\lambda^{\gamma,2}$ for Gd does not follow that expected from the single-ion theory and the agreement with a simple two-ion model is not good either. The temperature dependences of $\lambda^{\gamma,2}$ for the other Gd/Tb alloys follow an $\hat{I}_{5/2}$ temperature variation as proposed by Callen and Callen (1965). The agreement is very good for alloys containing more than 10% Tb. The composition dependence of Gd/Tb alloys is found linear with terbium concentration as is expected

from the single-ion model. The dilution of terbium ions with gadolinium results in separating terbium ions from each other without affecting the crystal field. So, the linear decline in the magnetostriction with the loss of terbium ions is the direct consequence of the single-ion crystalline field interaction.

The value of the constant $\lambda_2^{\alpha,2}(o)$ of pure gadolinium observed has the same value as reported by Mishima (1976), and is very close to that of Nikitin (1981), but is higher than Alstad and Legvold (1964). The constant $\lambda_2^{\alpha,2}$ is negative and shows decrease in the value with temperature and has minimum around 120K. Similar minima were observed by Mishima (1976) around 120K and around 140K by Alstad and Legvold (1964). The temperature dependence of the constant for Gd cannot be explained by any simple theory. The sign of the constant becomes positive for all the alloy specimens. The $\lambda_2^{\alpha,2}$ constant for 90%Gd-10%Tb shows reasonable agreement with a temperature dependence resulting from the single-ion model. The variation of the constant with temperature for 70%Gd-30%Tb is also in good agreement with an $\hat{I}_{5/2}$ variation. The fit of the temperature dependence of the constant is not so good for the 50%Gd-50%Tb specimen. The composition dependence of the constant shows a linear variation with terbium concentration but the measurements do not extend over the full range of composition so that the result is not so convincing as that for $\lambda^{\gamma,2}$.

The experimental value of $\lambda_1^{\alpha,2}(o)$* is very close to that of Mishima (1976) and the same as that of Alstad and Legvold (1964), but higher than that of Nikitin (1981). The constant has a positive sign which changes to negative for the other alloy specimens. Representation of the constant by the single-ion function $\hat{I}_{5/2}$ is not very good but this is still better than an $m^2(T)$ dependence. In the case of 90%Gd-10%Tb the gadolinium ions produce a positive strain while the terbium ions produce a negative one of similar magnitude. These strains however follow different temperature dependences so that the constant is negative at low temperatures, becomes positive around 90K and has maximum at 110K. the temperature dependence cannot be represented by any one theory. The fit of the temperature dependence of the constant for 70%Gd-30%Tb and 50%Gd-50%Tb with an $\hat{I}_{5/2}$ single-ion variation is not perfect but better than an $m^2(T)$ two-ion variation. Since the temperature dependence of $\lambda_1^{\alpha,2}$ for all the specimens was not very well represented by $\hat{I}_{5/2}$ single-ion variation, the extrapolated zero temperature values of the constant for each specimen were calculated by the least squares method using $\hat{I}_{5/2}$ and $m^2(T)$ variations. Neither set of values thus obtained seems to vary linearly with composition.

The anomalous behaviour of the constant $\lambda_2^{\alpha,2}$ for 80%Gd-20%Tb reported by Joraide (1980) was not observed for the intermediate alloy 90%Gd-10%Tb specimen. Instead,

* for Gd

the temperature variation of $\lambda_1^{\alpha,2}$ for 90%Gd-10%Tb showed a behaviour similar to the anomalous one. But this can be understood on account of the comparable but opposing contributions towards $\lambda_1^{\alpha,2}$ made by a large number of Gd ions against a small number of Tb ions. The contributions towards $\lambda_2^{\alpha,2}$ are again opposing each other but the one made by Tb ions is dominant.

9.2.1 Conclusions

The study of the temperature dependence of the magnetostriction constant $\lambda^{\gamma,2}$ for the entire range of Gd/Tb alloy compositions and the composition dependence of the constant is decisively in the favour of the single-ion magnetocrystalline interaction responsible for the giant magnetostriction exhibited by terbium metal. The temperature and composition variations of the constant $\lambda_2^{\alpha,2}$ also show reasonable agreement with the single-ion model. The results of the measurements of the temperature and composition dependence of the constant $\lambda_1^{\alpha,2}$ do not inspire a similar degree of confidence in making a decision about the nature of the interactions on their own, but at the same time do not discard the single-ion nature of the interaction. On the basis of the present study, the dependence of the giant magnetostriction in the basal plane on the temperature can be described by the relation 7.1 predicted by the single-ion magnetocrystalline interaction theory. The very small magnetostriction of spherically symmetric s-state gadolinium compared to the

giant magnetostriction shown by the terbium is a clear indication that the origin of large values of the magnetostriction of terbium or heavy rare earths in general is due to the interaction of the anisotropic 4f electronic charge distribution with the crystalline field. The conclusion is in agreement with the recent studies of magnetocrystalline anisotropy of Gd/Tb alloys by Hawkins (1982), Paige (1983) and Corner (1983b). It is also consistent with the results established by Belov et al. (1968), Nikitin et al. (1976, 1977a and 1977b) and Nikitin (1981) on the basis of their anisotropy and magnetostriction studies on the single crystal heavy rare earth alloys. The less strongly supporting $\lambda_2^{\alpha,2}$ results and weak support or neutral behaviour of the $\lambda_1^{\alpha,2}$ measurements to the conclusion is due to the assumptions made. Though the fermi surface of gadolinium is very close to that of terbium yet it is not idential (Keeton and Loucks, 1966). It results in a non-linear deformation of the Fermi surface in the alloys. The exchange magnetostriction in the rare earths, depends on the singularities of the Fermi surfaces (Tonegawa, 1964). Therefore, one may expect non-linear change in the magnetostriction constants of exchange origin. Moreover, in the derivation of magnetostrictive strains the constants of order higher than $\ell = 2$ are ignored. It is therefore, naturally difficult to expect a perfect fit of the experimental results with only one simple theory. On top of these, there are some

limitations of the technique of the measurements leading to errors in the results. These are discussed in the following section.

9.2.2. Sources of Error and Limitations of the Technique

The analysis involved in the derivation of the constants $\lambda_2^{\alpha,2}$ and $\lambda_1^{\alpha,2}$ is based on a knowledge of the anisotropy constants of the alloys of the specimens. Thus any error in the anisotropy constants will be incorporated in the derived magnetostriction constants. The effect of uncertainty in the values of the anisotropy constants was investigated by recalculating the magnetostriction constants using 20% lower and higher values of the anisotropy constant. It was found that the strain constants are quite sensitive to a change in the value of the anisotropy. The percentage error resulting in the strain constants was not linear and also varied with temperature and composition of the alloy. The resultant percentage error varied between half to twice as that of anisotropy.

The values of the constant $\lambda_2^{\alpha,2}$ and $\lambda_1^{\alpha,2}$ depend on the angle of magnetization θ and particularly $\lambda_1^{\alpha,2}$ is very sensitive to the angle in the case of limited rotation. The angle θ is calculated using anistropy constant values as described in section 8.2. The determination of the origin of the angle is discussed in section 8.5. The sharp peak around the $\hat{c}$-axis was taken as reference. The reference is reasonable in case of full rotation or

nearly full rotation of magnetization. But, in the case of a limited rotation of magnetization it may shift because the magnetization may not jump immediately the field crosses the $\hat{c}$-axis. This could result in a considerable error in the values of the constant $\lambda_1^{\alpha,2}$.

The strain gauge is an indirect method of measuring strains. The strain measurements depend upon the bond of the strain gauge. Though the bond M-610 is recommended for the present experimental conditions yet it frequently suffered damage when working in high fields and with the strongly magnetostrictive alloys in the terbium rich end of the series. The strain gauge may be suffering gradual loss of bond with the specimen before actually becoming detached. This could result in a decline in the values of the constant.

The specimens are held in magnetic fields using Durafix adhesive. To leave the specimens free to deform according to magnetostrictive strains, cotton wool pads were placed on both sides of the specimens. But, the small amount of the adhesive round the edges of the specimen may spread around and at low temperatures could cause considerable constraint to the free deformation of the specimen.

The possibility of the existence of a component of magnetic field normal to the plane of the specimen is another source of error for calculating angle ϕ and hence affects the strain constants involving the contribution from $\lambda^{\gamma,2}$.

9.3 Suggestions for Future Work

The present model for analysis of experimental data to derive magnetostriction constants takes into account the angle of overall magnetization resulting from the magnetic moments of Gd and Tb ions. The easy direction for Tb is the $\hat{b}$-axis while that for Gd is inclined at an angle to the $\hat{c}$-axis which varies with temperature. The magnetic moments of Gd ions will obviously rotate more easily towards the field direction than Tb due to the relatively very small anisotropy. The overall angle of magnetization thus may not be representing the true rotation of the moments of terbium ions. The analysis should be improved to include the true rotation of the magnetization due to terbium ions. Let us consider the magnetizations due to individual ions as illustrated in Figure 9.1. The total magnetization of the alloy then can be expressed as

$$M = (M_{Gd} \cos \delta_1 + M_{Tb} \cos \delta_2) / \cos \delta \qquad 9.1$$

where M_{Gd} and M_{Tb} are the saturation magnetizations of Gd and Tb respectively and interactions between those moments are not taken into account. If the interaction is of single-ion nature, the M_{Gd} and M_{Tb} can be expressed by the simple relation to the numbers of ions. Hence

$$M = \mu_{Gd} \, xN \cos \delta_1 + \mu_{Tb} \, (1-x) \, N \cos \delta_2 \qquad 9.2$$

where μ_{Gd} and μ_{Tb} are the magnetic moments of the Gd and Tb ions respectively (the contribution of conduction electrons being included), x is the percentage concentration

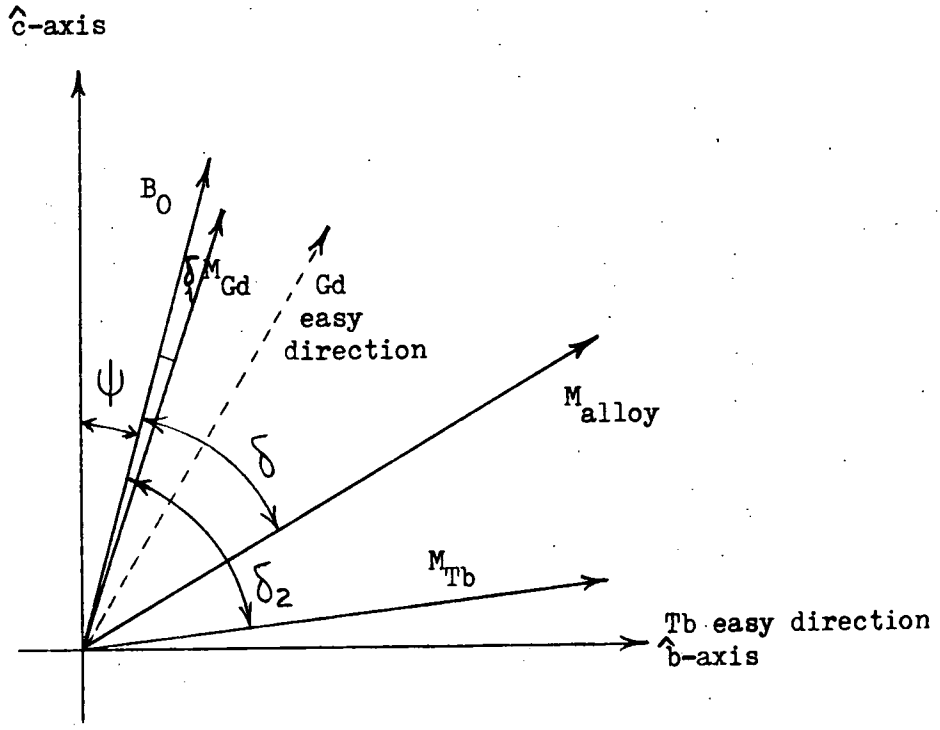

Fig 9.1 Direction of magnetizations due to individual alloy components relative to applied field and crystal axes.

of Gd and N is the total number of ions.

For a given alloy composition in a fixed field applied along a direction specified by ψ, δ_1 can be calculated from a knowledge of the anisotropy constants for Gd as described in Section 8.2. So δ_2 can be calculated using Equation 9.2. δ_2 can also be obtained like δ_1 using the anisotropy constants of pure Tb. The degree of agreement between the two δ_2 calculated values of Tb would be another test of the single-ion nature of the interaction of the Tb ions. If the correlation proved to be good then it would indicate that changes should be made in the technique for analysis of $\lambda_1^{\alpha,2}$ and $\lambda_2^{\alpha,2}$ constants. Instead of using the bulk anisotropy constants for the alloy to determine the derivation of the Tb ionic moment and hence the value of θ, the anisotropy constants for pure Tb should be used. A theoretical treatment would then be required to calculate the bulk strain for a crystal in which Gd and Tb ionic moments are not colinear.

Other systems of alloys should also be studied for example, Gd/Tm. Thulium exhibits the $\hat{c}$-axis modulated ferromagnetic ordering. The results of the competition between the non-colinear moments for various magnetic ordering like CAM, cone plus helix, CAM plus helix, ferro and ferri for different temperature and composition conditions would reveal more useful information to understand the complicated magnetic properties of the rare earths.

The technique to determine the constants certainly needs improvements to obtain the constant $\lambda^{\varepsilon,2}$ and

possibly other higher order constants. This would require improvements in analysis techniques and in the equipment used for strain measurement.

The latter might be brought about either by improvements to the existing equipment or by another approach to strain measurement. The mounting of the specimen should be such that the field always remains in the specimen plane. The rotation of the principal axes of the specimen with respect to applied field needs to be most accurate. The axes from the x-ray measurements should be correlated to the rotation of the angle sensing potentiometer so that the absolute knowledge of directions relative to the field were available rather than inferring those directions from the recorded curves. Alternatively, the rotation of the specimen should be measured directly by fixing a small coil on the specimen box in between two other fixed coils. The central coil fed by an AC signal, will generate a pick-up signal in the outer coils. From the phase and amplitude of this the angle may be inferred.

Alternatively an X-ray technique which measures the lattice parameters directly may be tried. This would require considerable design genius to produce apparatus capable of using X-rays in the small space normally available at low temperatures with high magnetic fields. Such methods might involve the determination of the constants from the spontaneous magnetostriction which appears on cooling through the Curie point along with a knowledge of the thermal expansion on the lines of Nikitin et al. (1977b).

The fact that magnetization causes mechanical strains implies that mechanical stress will affect the magnetization. The study of magnetization of the samples subjected to hydrostatic or uniaxial pressures is another way of estimating magnetostriction.

As a further alternative a dilatometer similar to that described by de Lacheisserie (1975 and 1977), which would also require major redesigning of the magnetostriction insert, could be employed.

APPENDIX I

Relation between the Anisotropy Constants and Coefficients

The magnetocrystalline anisotropy is most commonly represented using Legendre polynomials. The Legendre polynomials occurring in Equation 4.11 can further be expanded in terms of cosines of even-multiplied angles as

$$P_2 (\cos\theta) = \tfrac{1}{4} (1 + 3\cos 2\theta) \qquad A1$$

$$P_4 (\cos\theta) = \frac{1}{64} (9 + 20\cos 2\theta + 35\cos 4\theta) \qquad A2$$

$$P_6 (\cos\theta) = \frac{1}{512} (50 + 105\cos 2\theta + 126\cos 4\theta + 231\cos 6\theta) \qquad A3$$

These equations can be rewritten involving powers of sines:

$$P_2(\theta) = 1 - \frac{3}{2}\sin^2\theta \qquad A4$$

$$P_4(\theta) = 1 - 5\sin^2\theta + \frac{35}{8}\sin^4\theta \qquad A5$$

$$P_6(\theta) = 1 - \frac{21}{21}\sin^2\theta + \frac{189}{8}\sin^4\theta - \frac{231}{16}\sin^6\theta \qquad A6$$

Thus equation 4.11 can also be expressed in terms of powers of sines. The comparison of the new co-efficients with those of equation 4.6, yields relations between the anisotropy constants of different representations given as

$$K_1 = -\frac{3}{2}K_2^o - 5K_4^o - \frac{21}{2}K_6^o - \qquad A.7$$

$$K_2 = \frac{35}{8}K_4^o + \frac{189}{8}K_6^o + \qquad A.8$$

$$K_3 = -\frac{231}{16}K_6^o - \qquad A.9$$

$$K_4 = K_6^6 \ , \qquad A.10$$

and correspondingly,

$$K_2^o = \frac{2}{3} K_1 - \frac{16}{21} K_2 - \frac{176}{231} K_3 - \qquad A.11$$

$$K_4^o = \frac{8}{35} K_2 + \frac{144}{385} K_3 + \qquad A.12$$

$$K_6^o = - \frac{16}{231} K_3 - \qquad A.13$$

$$K_6^6 = K_4 \ . \qquad A.14$$

In a similar way the co-efficients K'^0 can be related to K_ℓ^o as

$$K_2'^o = \sqrt{\frac{4\pi}{5}} \ K_2^o \qquad A.15$$

$$K_4'^o = \sqrt{\frac{4\pi}{9}} \ K_4^o \qquad A.16$$

$$K_6'^o = \sqrt{\frac{4\pi}{13}} \ K_6^o \qquad A.17$$

$$K_6'^6 = \sqrt{\frac{4\pi}{13}} \ K_6^6 \ . \qquad A.18$$

APPENDIX II

Computer programme for the automated operation of the experiment.

The following programme written in BASIC for Commodore PET was used to collect the magnetostriction data in conjunction with a tractor printer 4022. In this particular programme A% = 10 is the address for the position potentiometer analogue to digital module while A% = 11 is for strain gauge signals, and A% = 32 is of the module for the stepping motor to turn the specimen in the forward direction while A% = 33 is for the reverse direction, of the MINICAM interface.

```
10 rem magnetostriction data collection  & analysis : ma127
20 poke1,0:poke2,148:a%=1:n%=1:t%=1
26 dimx(200):dimy(200):dimk(100)
28 dima(20):dimb(100):dimth(100):dimlm(100):dimk6(100)
30 dimmt(100):dimdt(100):dimms(100):dimm(100):dimt(100):dimq$(100)
32 dimgd(10):dimro(100)
34 open1,4:print#1,chr$(147):close1
36 fi=+180: z=+2710
40 gosub 1000
50 print""
55 print"press the appropriate key to:"
60 print"":print"record the particulars----------p"
62 print"":print"read current values of a/d------v"
65 print"":print"run from present position-------r"
68 print"":print"run with temp. & field values---o"
70 print"":print"set new rotation limits---------c"
72 print"":print"load the data from tape---------l"
74 print"":print"know programme sections---------s"
76 print"":print"or for analysis/calculations ---a"
80 getw$:ifw$="" then 80
82 ifw$="a"then gosub 3000:goto 50
84 ifw$="r"then 130
86 ifw$="c"then 1500
88 ifw$="o"then 130
90 ifw$="l"then 2000
92 ifw$="s"then 5200
94 ifw$="i"then 1300
96 ifw$="v"then 1400
97 ifw$="p"then 1100
98 gosub 5990:goto 50
```

```
100 fors1=1tosn:sys57386:next s1
102 sb=sb-1:if sb=0 then return
104 fors1=1to sp*600:next s1
106 geta$:ifa$<>""then return
108 goto100
110 sn=3:sb=1:gosub100
112 print"hit any key to continue"
116 geta$:ifa$=""then 116
118 print"ok":return
120 gosub 110
121 goto130
122 t2=ti:sn=5:sb=10:sp=3:input"minutes *";t1:ift1=0then t1=20
123 printnd$;:print""t1"minute interval from":print""ti$
124 if ti-t2<3600*t1 then 124
126 gosub100:print""nd$;nd$:return
130 print""
131 da = 18 : mo = 8
132 rem  --         --
134 rem day   &   month
136 rem
138 gd =70  :ax$ = "b": no = 1 :bo$="h"
139 rem  --          -        -       -
140 rem gd% , perp. axis  &  no     box
142 v=.3615:rem bridge voltage in volt
144 ga$ = "c"
145 rem    -
146 rem strain gauge is along ga$
148 rem
150 y$=" 5 mv/cm":x$=".2 v/cm":c$="1-13b"
151 rem --            --          ----
152 rem senstivity y , x & cassette
153 rem
154 ag$="10 of datron 1051"
155 rem  -----------------
156 rem gain = ag$
157 ifw$="o"then 1200
158 ifw$="o"then w$="r":gosub 110
159 print"";
160 print"date:"da"-"mo"- 83     &    time = "ti$
164 print"crystal:"gd"%gd"(100-gd)"%tb; perp."ax$"-axis ("no")"
168 print"strain gauge is along "ga$"-axis  in box  "bo$
170 print"x sens.="x$" & b.voltage ="v
172 print"gain ="ag$
174 print"recorded on cassette : "c$
180 print"rotation limits: from "z" to "fi :print""
190 pp=0:print"curve no"q", f="f$" & y="y$
200 print"temp.="t$" or t="t"&v= "v
210 print"step     rotation   signal    x:a/d"
220 print""
490 xl=5000:xh=-5000
500 yl=5000:yh=-5000
510 at$=ti$:p=0:nn=32:es=0:q1=0
512 r=1:rr=97
```

```
520 for i=r to rr
530 a%=10:d=usr(5):x(i)=((z-d)/(z-fi))*
540 x(i)=int(x(i)*1000+.5)/1000
550 if xh  <x(i) then xh  =x(i)
560 if xl  >x(i) then xl =x(i)
570 a%=11:y(i)=usr(5)
590 if yh  <y(i) then yh =y(i)
600 if yl  >y(i) then yl  =y(i)
610 r=xh-xl:am=yh-yl
620 printnd$;:print i,x(i),y(i),d
624 pp=pp+1:if pp>3 then pp=0:print"";
630 l=i
640 ifx(i)>(+.04)then684
642 getnn$:ifnn$<>""thenq1=q1+1:ifq1=1thenprint"turning slowly steps=";:pp=pp+
644 ifq1=1then nn=val(nn$):q1=q1+1:goto652
645 ifq1=2then654
646 ifq1>2thennn=32:printnd$;"back to normal with steps="nn"      ":pp=pp+1
647 ifq1>2thenq1=0
648 goto670
652 printnn:ifnn=0thenprintnd$;:input"steps,please*";nn
654 es=es+1
670 a%=32:n%=nn:t%=10:a=usr(1):a=usr(3)
674 a%=67:c=usr(2)
675 ifi=97thenr=97+1:rr=(97+es):goto520list685
680 next i
682 printnd$;:input"need further rotation*";a$
683 ifa$="y"thenr=i:rr=i+es/4:goto520
684 ed$=ti$
685 for s1=pp to 3 :print"":next s1
686 n8=(i-1)*32-es*28 :printn8,"no. of short steps"es
687 sn=3:sp=1  :sb=1 :gosub100
690 print"rotation="r"amplitude="am"  at"ed$
700 a%=33:n%=n8:t%=10:a=usr(1):a=usr(3)
702 a%=67:c=usr(2)
710 a%=10:f=usr(5):printf;
720 if f>z+100 thenprint"*";:goto 750
730 a%=33:n%= 40:t%=10:a=usr(1):a=usr(3)
740 goto710
750 a%=32:n%=170:t%=10:a=usr(1):a=usr(3)
752 a%=10:f=usr(5):
754 iff=z or f < z then printf:print"":goto757
756 a%=32:n%=4:t%=10:a=usr(1):a=usr(3):goto752
757 ift$<>""then770
758 sn=5:sp=2  :sb=10:gosub100
760 input"q,temp,field, v & ys*";q,t$,f$,g2,ys$
761 ift$="n"then 50
762 t=53*val(t$)+77
764 if g2<>0 then v=g2
766 ifys$<>""theny$=ys$ :print"y senstivity is now = "y$
770 rem print "curve no "q
776 rem printnd$;
780 open1,4:open2,4,1:open3,4,2:open4,4
782 g$="999    s9.999       s9999           999    s9.999       s9999"
```

```
786 print£1,"curve  no."q" , temp.= "t$" or ="t"k    &    mag field = "f$
796 print£1,"crystal:"gd"%gd"(100-gd)"%tb; perp."ax$"-axis("no")";
798 print£1," recorded during ("at$" to "ed$")"
800 print£1,"senstivity y ="y$", gain ="ag$"& bridge voltage ="v"volt"
801 rem print£1," & strain gauge is along "ga$"-axis
804 print£1,"":print£1," no"tab(4)"radians"tab(6)"sg.o/p";
806 print£1,tab(11)"no"tab(4)"radians"tab(6)"sg.o/p"
808 print£1,""
810 for i=1 to 1 step 20
812 print£3,g$:print£2,i,x(i),y(i),i+1,x(i+1),y(i+1)
813 p=p+1:ifp=5thenp=0:print£1
815 nexti
820 print£1,"peak to peak amplitude ="am",   rotation through "r"radions"
840 print£1,"":print£1,"":print£1,""
850 close1 :close2 :close3 :close4
855 print"saving data on tape "
856 ift$=""then input"q,temp,field*"q,t$,f$:print""
860 open1,1,1,"data"
865 print£1,da;",";mo
870 print£1,gd;",";ax$;",";ga$
880 print£1,q;",";t$;",";f$
885 print£1,1
890 fori=1to 1
900 print£1, i;",";x(i);",";y(i)
910 next i
914 close 1,1,1
916 q=q+1
918 print"";:printnd$;
920 print"saved on tape"
922 sn=3:sp=3:sb=2:gosub 100
923 input"need total strain*";a$
924 ifa$="y"thengosub9200
925 if v$="f"then gosub 4000
928 if a$="w"thent1=20:gosub 122:goto923
930 print"":printnd$:input" temp. , field , v & ys *";t$,f$,g2,ys$
931 ift$="n"then 50
932 ifys$<>""theny$=ys$ :print""
934 t=53*val(t$)+77
936 ifg2<>0 then v=g2
940 printnd$;
960 print"":go to 190
970 stop
1000 nc=40
1050 r$="":nl$="":nf$="":nc$="":nb$="":if nc=0 then nc=40
1052 ifnf<>0then for s1=1tonf:nf$=nf$+"":nexts1
1054 ifnl<>0then r$="":for s1=1tonl:nl$=nl$+"":nexts1
1058 for s1=1tonc:nc$=nc$+" ":nexts1
1064 for s1=1tonc:nb$=nb$+"":nexts1
1070 nd$=r$+nl$+nf$+nc$+nb$
1074 return
```

APPENDIX III

Computer programme for calculating the argument of the reduced Bessel function from the reduced magnetization.

```
3200 print" langevin fn. argument x from reducd     magnetization m"
3210 print"         by newton's method"
3220 input"reduced magnetization*";m,sx
3225 if m=0 then return
3230 x=sx: if sx=0 then x=.05
3250 x1=((exp(x)+exp(-x))/(exp(x)-exp(-x))-(1/x)-m)
3255 ifabs(x1)<0.0001 then3320
3260 a=1.01*x
3270 x2=((exp(a)+exp(-a))/(exp(a)-exp(-a))-(1/a)-m)
3290 x=x-.01*x*x1/(x2-x1):print x
3300 goto 3250
3310 x=int(x*1000+.5)/1000
3320 print"": print""x,x1:print""
3330 print"need further x  (y) ?"
3340 get a$  :ifa$="" then3340
3350 ifa$="y"then 3220
3390 return
```

APPENDIX IV

Computer programme for least squares fit.

```
4500 print""
4510 print" least squares curve fitting
4520 print""
4530 print"programme will fit data to one of the   followings ";
4531 print"& gives their errors"
4532 print"press lp for linear ------"chr$(34)"y=k.x "chr$(34):print""
4540 print"      l  for linear ------"chr$(34)"y=m.x+c "chr$(34):print""
4550 print"      e  for exponential -"chr$(34)"y=a.exp(b.x)"chr$(34):print""
4560 print"      p  for power law ---"chr$(34)"y=e.x↑f "chr$(34)
4580 input"lp,l,e or p*";k$
4590 print""
4600 if k$="l" then print" fitting to  a linear function   y=m.x+c":c$="o"
4604 if k$="lp" then print" fitting to  a linear function   y=k.x":c$="o"
4610 if k$="e" then print"fitting to exponential fn.  y=a.exp(b.x)":c$="o"
4620 if k$="p" then print" fitting to a power law function y=e.x↑f":c$="o"
4630 if k$="n" thenprint" ok":return
4640 if c$<>"o" then 4540
4650 rem
4660 input"curve no.  &  number of points  *";q$,n
4664 print""
4670 for m=1 to n
4690 input"pair of values, first x & then y *";x,y
4700 printm" x="x"  & y="y
4710 print"press any key to proceed, r to retype   this value"
4720 get b$:if b$="" then4720
4730 if b$="r"then print"retype":goto  4690
4740 x(m)=x:y(m)=y
4750 print"next":next m
4752 nn=n
4754 print"goto4760"
4760 print"set of values is as follows"
4764 print"curve n0. "q$
4770 rem print"     x-value      y-value"
4780 for m= 1 to n
4790 rem printm"  "x(m)"    ",y(m)
4794 print"x("m")="x(m),":y("m")="y(m)
4800 next m
4810 print"press any key to proceed   or    r            to retype the set"
4812 get b$:if b$="" then4812
4814 if b$="r"then print"start again":goto 4660
4830 rem for n=3 to nn
4832 sx=0:sy=0:x2=0:y2=0:xy=0:d1=0
4834 print"no   x-value      y-value"
4836 for m=1 to n
4838 printm"  "x(m)"    ",y(m):nextm
4840 if k$="e" then for m=1 to n :y(m)=log(y(m)):next m
4850 if k$="p" then for m=1 to n :y(m)=log(y(m)):x(m)=log(x(m)):next m
```

```
4860 for m=1 to n
4870 sx=sx+x(m):sy=sy+y(m)
4880 x2=x2+x(m)↑2:y2=y2+y(m)↑2
4890 xy=xy+x(m)*y(m):next m
4900 d=n*x2-sx↑2
4902 k=y2/xy: v=(x2-xy/k)/n
4906 vk=(v*k↑4/y2)↑.5
4910 c=(x2*sy-sx*xy)/d
4920 mm=(n*xy-sx*sy)/d
4930 for m=1 to n :d1=d1+(y(m)-mm*x(m)-c)↑2:next m
4940 sm=n/(n-1)*(d1/d)↑0.5
4950 sc=sm*(x2/n)↑0.5
4954 if k$="p" then 5150
4960 if k$="e" then 5050
4962 if k$="l" then 4980
4964 print" fit to y=k.x has following values"
4966 print"k="k"with error=+-"vk
4968 rem input"next set*";a$:ifa$="n" then 3000
4969 k(n)=k:k(10+n)=vk: rem goto 4650
4970 print"and"
4980 print"fit to y=m.x+c has following values"
4990 print"m="mm"with error=+-"sm
5000 print"c="c"with error=+-"sc""
5002 rem print"press any key to continue"
5004 rem get a$ :if a$="" then 5004
5006 fori=1tow*100:nexti
5008 return
5010 next n
5011 print"curve no."q$
5012 for i=3 to n-1 :print"n="i" k="k(i)" error="k(10+i):next i
5014 open1,4:print£1,"curve no."q$
5015 print£1,"n.pt.    k              error"
5016 fori=3to n-1 :print£1,i" "k(i)"  "k(i+10):next i
5017 print£1,"m="mm"error ="sm" and c="c"  +-"sc:print£1:print£1:close1
5018 input"next set*";a$:ifa$="n" then 3000
5020 goto 4650
5050 print"fit to y=a.exp(b.x) has following values"
5060 a=exp(c):sa=a*(exp(sc)-1)
5070 print"b="mm" with error=+- "sm""
5080 print"a="a" with error=+- "sa""
5090 next n: input"next set*";a$:ifa$="n" then 3000
5100 goto 4650
5150 print" fit to y=e.x↑f has following values"
5160 e=exp(c):se=e*(exp(sc)-1)
5170 print"f="mm" with error=+- "sm""
5180 print"e="e" with error=+- "se""
5187 return
5190 input"next set*";a$:ifa$="n" then 3000
5194 goto 4650
```

APPENDIX V

Computer programme for calculating angle of magnetization relative to the $\hat{c}$-axis.

```
3600 print"lagging angle   between magnetization and magnetic field"
3602 print"sin(lag)=(-3/2*k2)/(b0*ms*ro)*sin(2(sai+lag))"
3605 print"iteration by newtons method"
3610 j$="":j=0:jj=0 :l$=""
3620 print"press any key to continue but to end e"
3625 get a$ : if a$="" then 3625
3627 if a$="e" then 3000
3630 jj=jj+1:j=j+1
3632 input"crystal gd% & density *"; gd,ro
3634 ifgd=0 then gd=gd(j-1)
3636 ifro=0 then ro=ro(j-1)
3638 gd(j)=gd:ro(j)=ro
3640 input"curve & temp(emf)*";q$,t
3642 if t<>0 then t=53*t+77
3644 ift=0 then t=t(j-1)
3646 t(j)=t:q$(j)=q$
3650 input"k2(10↑-7),field,ms,k6(10↑-5) & d.theta*";k ,b0,ms,m6,dt
3652 if k<>0 then k=k*10↑-7
3670 if k=0 then k=k(j-1)
3674 k(j)=k
3680 mt=90:k6=m6*10↑-5:if m6=0 then k6=k6(j-1)
3682 if dt=0  then dt=5
3684 k6(j)=k6:dt(j)=dt
3690 if b0=0 then b0=b(j-1)
3694 b(j)=b0
3700 if ms=0 then ms=ms(j-1)
3704 ms(j)=ms: m(j)=ms(j)*ro
3706 print"curve no."q$
3708 print"":printgd"%gd-tb, b0="b0", temp="t"k"
3710 print"k2="k", ms="ms" & ro="ro
3711 print"k6="k6
3712 rem print"sai decreases from"mt"by "dt"degrees"
3714 print"type  r to retype ,   l for last curve  & any for next curve"
3716 get a$ :if a$="" then 3716
3717 if a$="r" then j=j-1:jj=jj-1:goto3630
3718 if a$<>"l" then 3630
3720 for j=1 to jj
3730 k2=k(j):dt=dt(j):ms=ms(j):k6=k6(j)
3732 q$=q$(j):t=t(j):gd=gd(j):ro=ro(j)
3734 m=m(j) :b=b(j):a1=.1:a1=0:a2=0
3740 ll=36*k6/(b*m)
3742 if (ll↑-2-1)<0 then print"could not calculate spiiting angle":goto3750
3744 lt=atn(sqr(ll↑-2-1)):ss=int(lt*180/)
```

```
3750 for i= mt to 0 step -dt
3752 print"curve no."q$(j)
3754 print"basal plane spliting starts at"(90-ss)
3760 c=int(1000*(-3/2*k2)/b/m+.5)/1000
3762 print"(-3/2.k2)/b/m="c", b0="b"& k2="k2:la=al:ifla=0 then la=.2
3765 print"sai="i"& ms*ro="m""
3770 d1=sin(la)+c*sin(2*(i*/180+la))
3780 print"lag= "int(1000*la+.5)/1000"   &  dif="int(d1*10^5+.5)/10^5
3790 if abs(d1)<.0001 then 3850
3794 a1=a1+1: if a1=6 then a1=0 : a2=a2+1:la=.2+.1*a2
3800 a=1.001*la
3810 d2=sin(a)+c*sin(2*(i*/180+a))
3815 d=d2-d1:print,,d:if d=0 then la=al:goto 3770
3820 la=la-.001*la*d1/d:if la=0 then la=.01
3830 ifabs(la)>/2 then print"ff"la:la=al
3840 goto 3770
3850 lm=la*180/ :a1=0 :a2=0
3870 print""i,la:al=la
3900 print"sai="i"degree &  lag ="lm:th=i+lm:printth
3902 lm(i)=int(10000*cos(th*/180)^2+.5)/10000:th(i)=th
3905 for aa=1 to 99 :next aa:geta$
3907 if a$="n"then 3600
3910 next i
```

REFERENCES

Abraham, A., and Bleaney, B. (1970), Electron Paramagnetic Resonance, Clarendon Press, Oxford.

Akulov, N.S. (1931), Z. Phys. 57, 249.

Akulov, N.S. (1936), Z. Phys. 100, 197.

Alstad, J.K., and Legvold, S. (1964), J. Appl. Phys. 35, 1752.

Anderson, P.W. (1951), Phys. Rev. 83, 1260.

Bagguley, D.M.S., Liesegang, J., and Robinson, K. (1974), J. Phys. F4, 594.

Bagguley, D.M.S., Partington, J.P., Robertson, J.A., and Woods, R.C. (1980a), J. Mag. Mag. Mat. 20, 56.

Bagguley, D.M.S., Partington, J.P., Robertson, J.A., and Woods, R.C. (1980b), J. Phys. F10, 967.

Banister, J.R., Legvold, S., and Spedding, F.H. (1954), Phys. Rev. 94, 1140.

Bartholin, H. (1970), Thesis, Grenoble, France.

Bartholin, H., and Bloch, D. (1969), Phys. Rev. 188, 845.

Bartholin, H., Beille, J., Bloch, D., Boutron, P., and Feron, J.L. (1971), J. Appl. Phys. 42, 1679.

Bartholin, H., Bloch, D., and Georges, R. (1969), Colloque. CNRS No. 188, Grenoble, P.301.

Beaudry, B.J., and Gshneidner, K.A. (1978), Ch. 2 of Handb. on the Phy. & Chem. of R.E. (eds. Gschneidner and Eyring), North-Holland.

Belov, K.P., Levitin, R.Z., Nikitin, S.A., and Ped'ko, A.V. (1961), Zh. Eksperin. Teor. Fiz. 40, 1562.

Belov, K.P., Levitin, R.Z., and Ponomarjov, B.K. (1968), J. Appl. Phys. 39, 3285.

Belov, K.P. (1971), Sov. Phys. JETP 33, 1187.

Bethe, H. (1933), Handb. d. Physik 24, 595.

Birss, R.R. (1959), Advances in Physics, 8, 252.

Birss, R.R., and Keeler, G.J. (1974) Phys. Stat. Sol. B 64, 357.

Birss, R.R., Keeler, G.J., and Leo, P.D. (1981), J. Mag. Mag. Mat. 25, 1.

Birss, R.R., Keeler, G.J., and Shepherd, C.H. (1977a), Physica B 86, 47.

Birss, R.R., Keeler, G.J., and Shepherd, C.H. (1977b), J. Phys. F 7, 1669.

Birss, R.R., and Wallis, P.M. (1964), Proc. Int. Conf. on Magnetism, Nottingham, p.744.

Birss, R.R., and Wallis, P.M. (1968), J. Appl. Phys. 39, 1347.

Bitter, F. (1931), Phys. Rev. 38, 1903.

Bloch, F. (1932), Phys. Z. 74, 295.

Bly, P.H., Corner, W.D., Taylor, K.N.R., and Darby, M.I., (1968), J. Appl. Phys. 39, 1338.

Bozorth, R.M. (1954), Phys. Rev. 96, 311.

Bozorth, R.M. (1967), J. Appl. Phys. 38, 1366.

Bozorth, R.M., and Gambino, R.J. (1966), Phys. Rev. 147, 487.

Bozorth, R.M., and Suits, J.C. (1964), J. Appl. Phys. 35, 1039.

Bozorth, R.M., and Wakiyama, T. (1963), J. Phys. Soc. Japan 18, 97.

Brenner, R. (1957), Phys. Rev. 107, 1539.

Brillouin, L. (1931), Die Quanten statistik, Springer, Berlin.

Brooks, M.S.S. (1969), J. Phys. C 2, 1016.

Brooks, M.S.S., and Egami, T. (1973), J. Phys. C 6, 513, and 3719.

Brooks, M.S.S., and Egami, T. (1974), J. Phys. C 7, 979.

Brophy, J.J. (1977), Basic electronics for Scientists, McGraw-Hill, London.

Burgardt, P. (1976), Ph.D. Thesis, Iowa State University, U.S.A.

Burgardt, P., and Legvold, S. (1975), AIP Conf. Proc. 24, 418.

Cable, J.W., and Wollan, E.O. (1968), Phys. Rev. 165, 733.

Cable, J.W., Wollen, E.O., Koehler, W.C., and Wilkinson, M.K. (1965), Phys. Rev. A 140, 1896.

Cahn, R.W. (1980), Contemp. Phys. 21, 43.

Callen, E. (1968), J. Appl. Phys. 39, 519.

Callen, E.R., and Callen, H.B. (1963), Phys. Rev. 129, 578.

Callen, E.R., and Callen, H.B. (1965), Phys. Rev. A 139, 455.

Callen, E.R., and Callen, H.B. (1966), J. Phys. Chem. Solids, 27, 1271.

Callen, H.B., and Strikman, S. (1965), Solid State Commun. 3, 5.

Carlson, O.N., Schmidt, F.A., and Peterson, D.T. (1975), J. Less-Common Metals 39, 277.

Carr, W.J. (1958), Phys. Rev. 109, 1971.

Chikazumi, S. (1964), Physics of Magnetism, J. Wiley & Sons, London.

Child, H.R., and Cable, J.W. (1969), J. Appl. Phys. 40, 1003.

Child, H.R., and Koehler, W.C. (1966), J. Appl. Phys. 37, 1353.

Child, H.R., Koehler, W.C., Wollan, E.O., and Cable, J.W., (1965), Phys. Rev. A 138, 1655.

Clark, A.E., Desavage, B.F., and Bozorth, R. (1965), Phys. Rev. A 138, 216.

Coleman, W.E., (1964), Ph.D. Thesis, West Virginia University, U.S.A.

Coleman, W.E., and Pavlovic, A.S. (1965), J. Phys. Chem. Solids, 26, 691.

Colvin, R.V., Legvold, S., and Spedding, F.H. (1960), Phys. Rev. 117 953.

Cooper, B.R. (1968), Solid State Physics 21, 393.

Coqblin, B. (1977), The Electronic Structure of Rare Earth Metals and Alloys : The Magnetic Heavy Rare Earths, Academic Press.

Coqblin, B., Iglesias-ricardi, J.R., and Jullien, R., (1978), Contemp. Phys. 19, 327.

Corner, W.D. (1983b), Private communication.

Corner, W.D., Bareham, H., Smith, R.L., Tanner, B.K., Farrant, S., Jones, D.W., Beaudry, B.J., and Gschneidner, K.A., Jr., (1980), J. Mag. Mag. Mat. 15-18, 1488.

Corner, W.D., Roe, W.C., and Taylor, K.N.R. (1962), Proc. Phys. Soc. 80, 927.

Corner, W.D., Szpunar, B., Fort, D., and Jones, D.W. (1983a), J. Mag. Mag. Mat., in press.

Corner, W.D., and Tanner, B.K. (1976), J. Phys. C 9, 627.

Crangle, J., (1977), The Magnetic Properties of Solids, Edward Arnold, London.

Crangle, J., and Goodman, G.M. (1971), Proc. Roy. Soc. Lond. A 321, 477.

Cullity, B.D. (1972), Introduction to Magnetic Materials, Addison-Wesley.

Curry, R.G., and Taylor, K.N.R. (1976), Phys. Rev. B 14, 4219.

Darby, M.I., and Issac, E.D. (1974), IEEE Trans. on Mag. 10, 259.

Darby, M.I., and Taylor, K.N.R. (1964), Proc. Int. Conf. on Magnetism, Nottingham, 742.

Darnell, F.J. (1963a), Phys. Rev. 130, 1825.

Darnell, F.J. (1963b), Phys. Rev. 132, 1098.

Darnell, F.J. (1963c), Phys. Rev. 132, 128.

Darnell, F.J., and Cloud, W.H. (1969), J. Appl. Phys. 35, 935.

De Lacheisserie, E. Du Tremolet (1975), Revue de Physique Appliqué Tome 10, 169.

De Lacheisserie, E. Du Tremolet (1977), Revue Francaise de Mechanique 64, 19.

Deniszezyk, J., and Kozarzewski, B. (1983), J. Mag. Mag. Mat. 37, 217.

Dimmock, J.O., and Freeman, A.J. (1964), Phys. Rev. Lett. 13, 750.

Dreyfus, B., Mickel, J.C., and Thoalouze, D. (1967), Phys. Lett. A 24, 457.

Du Plessis, P. Dev. (1968), Phil. Mag. 18, 145.

Du Plessis, P. Dev. (1969), Physica 41, 379.

Du Plessis, P. Dev., and Alberts, L., (1965) Solid State Commun. 3, 251.

Egami, T. (1972), J. Phys. C 5, L85.

Elliot, J.F., Legvold, S., and Spedding, F.H., (1953), Phys. Rev. 91, 28.

Elliott, J.R., and Stevens, K.W.H. (1953), Proc. Roy. Soc. A 219, 387.

Elliott, J.R, (1972), Magnetic Properties of Rare Earth Metals, Plenum, U.S.A.

Erickson, R.A. (1953), Phys. Rev. 90, 779.

Feron, J. -L., (1969), C.R. Acad. Sci. B 269, 611.

Feron, J. -L., Huy, G., and Pauthenet, R. (1970a), Coll. Int. du C.N.R.S. 180, Vol II, 17.

Feron, J. -L., Huy, G., and Pauthenet, R. (1970b), Z. Angew. Phys. 30, 61.

Feron, J. -L., and Pauthenet, R. (1969), C.R. Acad. Sci. B 269, 549.

Finkel, V.A., and Belov, V.S. (1973), Sov. Phys. JETP, 37, 90.

Finkel, V.A., and Belov, V.S. (1974), Sov. Phys. JETP, 38, 963.

Flippen, R.B., (1963), J. Appl. Phys. 7, 2026.

Fuji, H., (1969), J. Sci. Hiroshima University, A-II 33, 43.

Fujiwara, H., Fujii, H., Hidaka, Y., Ito, T., Hashimoto, Y., and Okamoto, T. (1977), J. Phys. Soc. Japan 42, 1194.

Gamari, S.H., and Bredimas, V. (1983), J. Mag. Mag. Mat. 36, 131.

Goldman, J.E., (1947), Phys. Rev. 72, 529.

Graham, C.D., (1962), J. Phys. Soc. Japan, 17, 1310.

Graham, C.D. (1963), J. Appl. Phys. 34, 1341.

Graham, C.D. (1967), J. Appl. Phys. 38, 1375.

Greenough, R.D., and Underhill, C. (1976), J. Phys. E 9, 451.

Gribanore, I.F., and Zavadskii, E.A., (1983), J. Mag. Mag. Mat. 37, 51.

Griffel, M., Skochdopole, R.E., and Spedding, F.H., (1954), Phys. Rev. 93, 657.

Gschneidner, K.A. Jr., and Eyring, L., (eds.), (1978), Handbook of the Physics and Chemistry of Rare Earths, Vol. 1., North Holland.

Hansen, P., and Lebech, B., (1976), J. Phys. F 6, 2179.

Hausmann, K. (1970), Phys. Stat. Sol. 38, 809.

Houman, J.G., Jensen, J., and Touborg, P., (1975), Phys. Rev. B 12, 332.

Hawkins, R.D., (1982), Ph.D. Thesis, Durham University.

Hegland, D.E., Legvold, S., and Spedding, F.H., (1963), Phys. Rev. 131, 151.

Heisenberg, W., (1926), Z. Phys. 38, 411.

Heisenberg, W. (1928), Z. Phys. 49, 619.

Honda, K., and Kaya, S., (1926), Sci. Rep. Tohoku Imp. University, 15, 721.

Hukin, D.A., and Jones, D.W., (1976), J. Crystal Growth.

Hurd, C.M., (1975), Contemp. Phys. 16, 517.

Hurd, C.M., (1982), Contemp. Phys. 23, 469.

Inone, J., and Shimizu, M., (1980), J. Appl. Phys. F 10, 721.

Jennings, L.D., Miller, R.E., and Spedding, F.H. (1960), J. Chem. Phys. 33, 1849.

Jennings, L.D., Stanton, R.M., and Spedding, F.H., (1957), J. Chem.l Phys. 27, 909.

Jensen, J. (1974), Phys. Rev. Let. 37, 951.

Joraide, A.A. (1980), Ph.D. thesis, Durham University.

Jordan, R.G., (1974), Contemp. Phys. 15, 375.

Jordan, R.G., and Jones, D.W., (1973), J. Less-Common Metals, 31, 125.

Jordan, R.G., Jones, D.W., and Hems, V.J., (1975), J. Less-Common Metals 42, 101.

Karpenko, V.P., and Irkhin, Yu.P., (1973), Sov. Phys. JETP, 37, 383.

Kasuya, T., (1956), Progr. Theor. Phys. 16, 45.

Kasuya, T., (1966), Magnetism Vol. II B. (eds. Rado, G.T., Suhl, H.), Academic Press.

Keeler, G.L., and Pearson, P. (1978), Ref. of Beaudry and Gschneidner (1978), 464.

Keeton, S.C., and Loucks, T., (1966), Phys. Rev. 146, 429.

Keffer, F., (1955), Phys. Rev. 100, 1692.

Kirchner, H., (1936), Ann. Phys. Lpz. 27, 49.

Kittel, C., (1976), Introduction to Solid State Physics, John Wiley & Sons.

Kittel, C., and Galt, J.K., (1956), Solid State Physics, 3, 437.

Koehler, W.C., (1965), J. Appl. Phys. 36, 1078.

Koehler, W.C., (1972), Ch. 3 of Magnetic Properties of Rare Earth Metals, (ed. Elliott, R.J.) Plenum Press.

Koehler, W.C., Cable, J.W., Wilkinson, M.K., and Wollan, E.O. (1966), Phys. Rev. 151, 414.

Langevin, P., (1905), Annls. Chim. Phys. 5, 70.

Legvold, S., (1980), Ch.3 of Ferromagnetic Materials (ed. Wohlfarth, E.P.,) North Holland.

Legvold, S., Green, R.W., Ostenson, J.E., and Beaudry, B.J. (1978a), Phys. Rev. B 18, 1162.

Legvold, S., Queen, J., Beaudry, B.J., and Harmon, B.N., (1979a), J. Mag. Mag. Mat. Proc. Int. Conf. on Magnetism 15-18, 1221, (Jan. 80).

Legvold, S., Harmon, B.N., Beaudry, B.J., Burgardt, P., Younkin, D.R., and White, H.W. (1977a), Phys. Rev. B 16, 4986.

Legvold, S., Beaudry, B.J., Ostenson, J.E., and Harmon, B.N. (1977b), Solid State Common. 21, 1061.

Legvold, S., Spedding, F.H., Barson, F., and Elliot, J.F. (1953), Rev. Mod. Phys. 25, 129.

Lewis, E.A.S. (1970), Phys. Rev. B 1, 4368.

Lifshitz, E., and Laudau, L., (1935), Phys. Zeits. d. Sowjetunion 8.2, 153.

Lindgard, P.-A., (1977), Phys. Rev. B 16, 2168.

Mackintosh, A.R., and Smidt, F.A., (1962), Phys. Lett. 2, 107.

Makenna, T.J., Campbell, S.J., Chaplin, D.H., and Wilson, V.H., (1980), J. Mag. Mag. Mat. 20, 207.

Malik, S.K., Sankar, S.G., Rao, V.U.S., and Wallace, W.E., (1977), Mag. Lett. 1, 57.

Marshall, W., (1955), Proc. Roy. Soc. A 232, 48.

Martin, D.J., and Rhyne, J.J., (1977), J. Phys. C 10, 4123.

Mason, W.P., (1951), Phys. Rev. 82, 715.

Mason, W.P., (1954), Phys. Rev. 96, 302.

Mihai, V., and Franse, J.J.M., (1976), Rev. Roum. Phys. 21, 1041.

Mishima, A., (1976), See Mishima et al. (1976).

Mishima, A., Fujii, H., and Okamoto, T., 91976), Phys. Soc. Jap. 40, 962.

Morrish, A.H., (1965), The Physical Principles of Magnetism, John Wiley & Sons, N.Y.

Néel, L., (1948), Ann. Phys. 12-3, 137.

Nellis, W.J., and Legvold, S., (1969), Phys. Rev. 180, 581.

Nigh, H.E., Legvold, S., and Spedding, F.H., (1963), Phys. Rev. 132, 1092.

Nigh, H.E., Legvold, S., Spedding, F.H., and Beaudry, B.J. (1964), J. Chem. Phys. 41, 3799.

Nikitin, S.A., (1962), Zh. Eksperim Teor. Fiz. 43, 31.

Nikitin, S.A., (1979), Sov. Phys. JETP 50, 176.

Nikitin, S.A., (1981), Sov. Phys. JETP 53, 104.

Nikitin, S.A., Sheludko, N.A., Posyado, V.P., and Chuprikov, G.E., (1977 or 1977a), Sov. Phys. JETP 46, 530.

Nikitin, S.A., Andreenko, A.S., Poyado, V.P., and Chuprikov, G.E., (1977b), Fiz. Tverd. Tela (Leningrad) 19, 1792.

Nikitin, S.A., Andreenko, A.S., Zvezdin, A.K., and Popkov, A.F., (1979), Sov. Phys. JETP 49, 1090.

Nikitin, S.A., and Arutyunian, N.P., (1979), Sov. Phys. JETP 50, 962.

Nikitin, S.A., Kim, D., and Christyakov, O.D., (1976), Sov. Phys. JETP 44, 843.

Nikitin, S.A., Talalaeva, E.V., Chernikova, L.A., Chuprikov, G.E., Ivanova, T.I., Kaxakov, G.V., and Yarkho, G.A., (1978), Sov. Phys. JETP 47, 105.

Paige, D.M., (1983), Ph.D. Thesis, University of Durham.

Pal, L., (1954), Some remarks on the quantum theory of energy anisotropy of ferromagnetic crystals, Phy. Abs., 9744.

Palmer, S.B., and Islam, M.N., (1974), Proc. R. Soc. London A 338, 341.

Pauli, W., (1920), Z. Physik 2, 201.

Pearson, R.F., (1979), Ch. 3 of Experimental Magnetism Vol. 1 (ed. Kalvius, G.M., and Tebble, R.S., J. Wiley & Sons).

Peterson, D.T., (1971), Verlag der Zeitschrift fur Naturforschung, Tubingen, P.104.

Peterson, D.T., and Schmidt, F.A., (1972), J. Less-Common Metals, 29, 321.

Potton, R.J., and Keeler, G.J., (1980), J. Mag. Mag. Mat. 20, 258.

Preisach, F., (1929), Ann. Phys., Lpz. 3, 737.

Rado, T.G., and Suhl, H., (1963), eds. Magnetism, Academic Press.

Rhyne, J.J., (1972), Ch. 4 of Magnetic Properties of Rare Earth Metals (ed. Elliott, R.J.,), Plenum Press.

Rhyne, J.J., and Clark, A.E., (1967), J. Appl. Phys. 38, 1379

Rhyne, J.J., Foner, S., McNiff, E.J. Jr., and Doclo, R., (1968), J. Appl. Phys. 39, 892.

Rhyne, J.J., and Legvold, S., (1965), Phys. Rev. 138, A 507.

Rhyne, J.J., and McGuire, T.R., (1968), J. Appl. Phys. 39, 892.

Roeland, L.W., Cock, G.J.,,and Lindgard, P.-A., (1975), J. Phys. C 8, 3427.

Roeland, L.W., Cock, G.T., Mueller, F.A., Moleman, A.C., McEwen, K.A., Jordan, R.G., and Jones, D.W., (1975a), J. Phys. F 5, L233.

Rudermann,M.A., and Kittel, C., (1954) Phys. Rev. 96, 99.

Shepherd, C.H., (1976), Ph.D. thesis, University of Salford.

Shull, C.G., Strauser, W.A., and Wollan, E.O., (1951), Phys. Rev. 83, 333.

Shull, C.G., Strauser, W.A., and Wollan, E.O., (1951), Phys. Rev. 83, 333.

Simons, D.S., and Salamon, M.B., (1974), Phys. Rev. B 10, 4680.

Slater, J.C., (1965), Quantum Theory of Molecules and Solids Vol. 2, McGraw-Hill.

Slater, J.C., (1967), Quantum Theory of Molecules and Solids Vol. 3, McGraw-Hill.

Smit, J., and Wijn, H.P.J., (1959), Ferrites, John Wiley & Sons.

Smith, R.L., Tanner, B.K., and Corner, W.D., (1977), J. Phys. F 7, 1229.

Smith, R.L., Corner, W.D., Tanner, B.K., Jordan, R.G., and Jones, D.W., (1978), IOP Conf. on Rare earths and Actinides, 37, 215.

Smith, R.L., Corner, W.D., and Tanner, B.K., (1980) J. of Mag. Mag. Mat. 20, 265.

Stevens, K.W.H., (1952), Proc. Phys.Soc. (London), A 65, 209.

Stryjewski, E., and Giordano, N., (1977), Adv. Phys. 26, 487.

Sze, H.H., Rao, K.V., and Meaden, G.T., (1969), J. Low Temp. Phys. 1, 563.

Tajima, K., (1971), J. Phys. Soc. Japan 31, 441.

Tajima, K., and Chikazumi, S., (1967a), Japan J. Appl. Phys. 6, 897.

Tajima, K., and Chikazumi, S., (1967b), J. Phys. Soc. Japan, 23, 1175.

Tanner, B.K., (1976), X-Ray Diffraction Topography, Pergamon Press, London.

Tanner, B.K., (1979) Contemp. Phys. 20, 187.

Taylor, K.N.R., and Darby, M.I. (1972) Physics of Rare Earth Solids, Chapman & Hall.

Thoburn, W.C., Legvold, S., and Spedding, F.H. (1958), Phys. Rev. 110, 1298.

Tohyama, K., and Chikazumi, S., (1973), J. Phys. Soc. Japan 35, 47.

Tonegawa, T., (1964), J. Phys. Soc. Japan 19, 1168.

Turov, E.A., and Mitsek, I., (1960), Sov. Phys. JETP 37, 801.

Unvala, B.A., and Green, A.K., (1974), J. Strain Analysis 9, 88.

Van Vleck, J.H.,(1932), The Theory of Electronic and Magnetic Susceptibilities, Oxford University Press.

Van Vleck, J.H., (1937), Phys. Rev. 52, 1178.

Van Vleck, J.H., (1945), Rev. Mod. Phys. 17, 27.

Van Vleck, J.H., (1962), Rev. Mod. Phys. 34, 681.

Volkov, V.M., Kustov, E.F., Makietov, T.K., and Steczko, G., (1981), Phys. Stat, Sol. B 104, 649.

Vonsovskii, S.V., (1974), Magnetism, John Wiley & Sons.

Voronel, A.V., Garber, S.R., Sinkina, A.P., and Charkina, I.A., (1966), Sov. Phys. JETP 22, 301.

Wagner, T.K., and Stanford, J.L. (1969), Phys. Rev. 184, 505.

Weiss, P., (1907), J. Phys. Theor. 6, 661.

Welford, J., (1975), Ph.D. Thesis, University of Durham.

Wells, P., Lanchester, P.C., Jones, D.W., and Jordan, R.G., (1975), J. Phys. F 4, 1729.

White, H.W., Beaudry, B.J., Burgardt, P.,Legvold, S., and Harmon, B.J., (1975), AIP Conf. Proc. 29, 329.

White, R.M., and Geballe, T.H., (1979), Long rang order in Solids, Suppl. 15 to Solid State physics, Academic Press.

Wilkinson, M.K., Koehler, W.C., Wollan, E.O., and Cable, J.W., (1961), J. Appl. Phys. 32, 48S.

William, H.J., Bozorth, R.M., and Shockley, W., (1949) Phys. Rev. 75, 155.

Wohlfarth, E.P., Ed. (1980), Ferromagnetic Materials, North-Holland Pub. Co.

Yafet, Y., and Kittel, C., (1952), Phys. Rev. 87, 290.

Yang, J.J.H., (1971), Ph.D. Thesis, University of California.

Yosida, K., (1957), Phys. Rev. 106, 893.

Yosida, K., (1968), J. Appl. Phys. 39, 511.

Yosida, K., and Watabe, A., (1962), Prog. Theor. Phys. 28, 351.